ABSTRACT

Title of dissertation: RESOLUTION IMPROVEMENT OF PHOTOLITHOGRAPHIC TECHNIQUES BASED ON VISIBLE LIGHT

Zuleykhan Tomova, Doctor of Philosophy, 2017

Dissertation directed by: Professor John Fourkas
Department of of Chemistry and Biochemistry

The semiconductor industry is planning to use Extreme Ultraviolet lithography as its next-generation patterning technique. However, this technique has run into many roadblocks due to its cost and complexity. An alternative approach employs light in the near-UV. A 2-color photolithographic technique based on combination of two colors on the near-UV or visible light has shown promising results in creating structures with sizes at a fraction of the excitation light wavelength. One color of light excites photoinitiator molecules to a chemically active state that leads initiation of polymerization. A second color of light deactivates photoinitiator molecules before they form radicals, inhibiting polymerization.

In this thesis we show how extending 2-color lithography to include a third color (3CL) can achieve super-resolution for applications requiring fabrication of closely packed structures. The advantage of the 3CL process is in its separation of polymerization initiation and deactivation steps by involving different chemical states that allow for more efficient deactivation and for increased resolution.

Some of the crucial elements needed to achieve an optimized scheme for 3CL are the determination of the intramolecular transitions that participate in the process, the lifetimes of the photoinitiators, and the exposure parameters. Several photoinitiators were studied to determine the optimal exposure conditions. Polymerization action spectra and deactivation action spectra were used to determine the combinations of excitation and deactivation parameters resulting in the most efficient deactivation. The 2-beam initiation threshold (2-BIT) method was introduced for *in situ* measurement of the order of effective nonlinearity of photoresists. The order of the effective nonlinearity was determined for a series of photoinitiators under various excitation wavelengths and fabrication velocities.

Additionally, a photoinitiator with a proportional velocity (PROVE) dependence, in which feature size increases with the velocity, was found to undergo efficient self-deactivation at increased temperatures. This dependence was demonstrated by gradually heating the sample and analyzing the fabricated feature sizes. Spot heating with a laser beam was also used to locally prevent polymerization. The correlation between polymerization rate and temperature opens opportunities for high speed fabrication that uses temperature gradients to create finer structures.

RESOLUTION IMPROVEMENT OF PHOTOLITHOGRAPHIC TECHNIQUES BASED ON VISIBLE LIGHT

by

Zuleykhan Tomova

Dissertation submitted to the Faculty of the Graduate School of the
University of Maryland, College Park in partial fulfillment
of the requirements for the degree of
Doctor of Philosophy
2017

Advisory Committee:
Professor John T. Fourkas, Chair/Advisor
Professor Daniel E. Falvey
Professor Amy S. Mullin
Professor Gottlieb S. Oehrlein
Professor Raymond J. Phaneuf

Dedication

This work is dedicated to my parents, Tomov Mukhmat and Leyla, and my teachers and lifelong mentors, Dzaurova Aza and Bazorkin Akhmet, for their unconditional suppport and believe in me.

Acknowledgments

I am extremely lucky to have met amazing people in my life and I am deeply grateful to all the people who have been with me on this journey. You made this work possible and I will cherish your support forever.

First, I would like to thank my graduate adviser, Professor John Fourkas. I am very fortunate to have had the opportunity to work under his guidance on such interesting and challenging problems. Throughout these years, I have been constantly amazed at how easily he can find elegant solutions to any problem that I have faced. His creative ideas and always positive, uplifting mood were a source of inspiration for me. I could not wish for a more supportive and kind adviser.

I would like to thank my committee members; Professor Daniel Falvey, Professor Amy Mullin, and Professor Gottlieb Oehrlein for helpful discussions about the three-color lithography project and much valuable advice. I am incredibly grateful to John Petersen for sharing his knowledge and experience in optical lithography. So many times, his advice and feedback have helped me to overcome difficulties with my experiments. I would like to thank our collaborators Robert Devoe and Brian Gates at 3M for helpful discussions and feedback on the KL68 project.

I am so thankful to all the members of the Fourkas group. First, I would like to thank Dr. Sanghee Nah and Dr. Michael Stocker for taking me under their wings when I first joined the group, and for teaching me so much about MAP, RAPID and MAIL and experimental procedure. Their breadth of knowledge and patience during training made me feel very welcome in the group.

Of course, I am incredibly grateful to everyone I had the privilege to work with the last several years, especially Dr. Nikolaos Liaros, Sandra Abigail Gutierrez Razo, and Samuel Cohen. Projects described in this thesis were as interesting as they were big, and without our team's help I would still be collecting data. I am thankful to Dr. Liaros for helping me with 2-BIT, 3-color, and KL68 experiments. When Dr. Liaros joined our group as a postdoctoral fellow, his broad knowledge of optics and experience in performing z-scan measurements helped me to gain new skills. Sandra Abigail Gutierrez Razo helped me tremendously with sample preparation. I did not realize how much time preparing the samples was taking out of my work day until Sandra took it over. I would like to thank Samuel Cohen for writing the Matlab code for 2-BIT data fitting. Samuel is a Matlab genius and I hope to be half as good at coding in the future. I am very thankful to Amanda Souna and Dr. John Bender for their help with KL68 experiments, for performing and analyzing SEM images of fabricated voxels.

I would like to thank Dr. Christopher Rivera for teaching me how to align cavities of the Ti:Sapphire lasers, and for his encouraging "don't worry, it took me couple weeks when I did for the first time too. Now I finish in a day". DC's humidity gave me enough practice to hit my goal. I am fortunate to have worked with Dr. Rivera for few weeks before he left the group. His deep knowledge in wide range of optics and incredible teaching skills rapidly boosted my experimental skills.

I also would like to thank my partners in laser alignment "assignments", Dr. Alison Sikorsky and Dr. Farah Dawood. Their positive attitude turned a tedious work task into a fun activity. I would like to thank Matthew Hourwitz for being a

good friend all these years. His constant jokes made me look at the bigger picture no matter how long or hard my day was. My warmest thanks are to Dr. Carlos Toro, Dr. Xiaoxiao He, Dr. Sijia Qin, Dr. Xiaoyu Sun, Dr. Samrat Dutta, Floyd Bates II, and Dr. Jarrett Leeds for being good friends all these years.

I would like to thank our collaborators Steven Wolf and Matthew Thum for their help with the UV-visible and transient absorption measurements of our photoinitiators.

I am deeply grateful to everyone who helped editing this work. I can never repay hours of help from Shirl Phelps. Her feedback tremendously improved my writing skills. I am grateful to Daniel Bragason, Justine DeCamillis, Dr. Nikolaos Liaros, Sandra Abigail Gutierrez Razo for reading my chapters and for giving me so much support during this writing period. You made this process much less painful.

I would like to thank my family for their constant support and encouragement. I know how hard it was for my parents to let their only child move across the ocean to a new county to attend graduate school. They knew better than I all the hardships I would face, starting with separation from my family. Yet, they have only encouraged me in pursuing my dreams and have not doubted me even for a second. I cannot express with words how grateful I am for everything.

I would like to thank my first teacher, and my "second mom", Aunt Aza and my physics teacher, Bazorkin Akhmet Sergeevich. I would not have made it this far without their guidance. I remember every evening Aunt Aza spent patiently giving me math lessons under the light of a lit candle after teaching all day at school. I am forever indebted to you, Aunt Aza.

I would like to take this chance to thank Bazorkin Akhmet Sergeevich. He made me fall in love with physics with one simple question in the seventh grade. His wisdom, kindness and guidance inspired me to become a better person, never stop learning, and to constantly challenge myself. I am proud to call myself a student of Galaeva Marem, our school principle. During one of the hardest moments of my life, she taught me, a crushed 13-year-old, not to pay attention to other peoples opinions and to follow my goals regardless of what anyone might think. Every time I felt tired and uninspired, I thought of her and Bazorkin Akhmet and it helped to get through the toughest times in graduate school.

Lastly, I would like to thank all my friends for their support. The length of this work will not allow me to thank everyone personally, but I cherish the support and friendship from them all. I would like to thank Brooke Hester for introducing me to the Chemical Physics Program, and for helping me through my application process. Yanina Shevchenko was with me every step from the moment I was thinking about getting my PhD abroad. Her constant guidance to this day makes me deeply treasure our friendship. I am very glad Mena Issler decided to study in Russia as an exchange student. I am happy to call her my friend for the last 10 years. I miss you and look forward to our next trip.

Table of Contents

List of Tables

List of Figures

List of Abbreviations

2-BIT	2-beam initiation threshold
2CL	2-color lithography
2PA	2-photon absorption
3CL	3-color lithography
3D	three-dimensional
AR5	mixture of trimethylolpropane triacrylate and tetrahydrofurfuryl acrylate
CW	continuous wave
DETC	7- diethylamino-3-thenoylcoumarin
EUV	extreme ultraviolet
HWP	half-wave plate
ISC	intersystem crossing
ITX	isopropyl thioxantone
KL-68	bis-[4-(diphenylamino) stryl]-1-(2-ethylhexyloxy),4-(methoxy)benzene
LRdB	Lissamine Rhodamine B Sulfonyl Chloride
MACS	multiphoton absorption cross sections
MAIL	multiphoton absorption-induced luminescence
MAP	multiphoton absorption polymerization
MEMS	microelectromechanical systems
MGC - HCl	malachite green carbinol hydrochloride
MGCB	malachite green carbinol base
ML	modelocked
MPA	multiphoton absorption
NA	numerical aperture
NFE	nonlinear fluorescence excitation
PAG	photoacid generator
Pol	polarizer
PROVE	proportional velocity
PSF	point spread funcion
RAPID	resolution augmentation through photo-induced deactivation
RISC	reverse intersystem crossing
SEM	scanning electron microscope
SR285	tetrahydrofurfuryl acrylate
SR351	trimethylolpropane triacrylate
SR368	tris(2-hydroxy ethyl) isocyanurate triacrylate
SR444	pentaerythritol triacrylate
SR499	ethoxylated trimethylolpropanetriacrylate
SRd101	Sulphorhodamine 101
SRdB	Sulphorhodamine B
STED	stimulated emission depletion
TEA	triethylamine
TPA	two-photon absorption
TPO-L	Ethyl (2,4,6-trimethylbenzoyl) phenylphosphinate

TREPR	time-resolved electron paramagnetic resonance
TTA	triplet-triplet annihilation
UV	ultraviolet
Voxel	volume element

Chapter 1

Background

1.1 Introduction

Moore's law states that the number of electronic elements that can fit in a given area on a chip doubles approximately every 18 months [1, 2]. With the ongoing need in the semiconductor industry to reduce feature sizes further, researchers have developed novel techniques, based on the application of high-energy photons or charged particles. However, achieving nanoscale features (isolated fabricated elements) as well as nanoscale resolution (the minimum distance at which the features can be distinguished) is quite challenging. According to Abbe's criterion, the diffraction limit of a microscope is given by the formula $d = \frac{\lambda}{2n \sin \alpha}$, where λ is the wavelength of the light, n is the refractive index of the medium, α is the half-angle of the imaging aperture, and the quantity $n \sin \alpha$ is called the numerical aperture (NA). As a point of reference, for a high-magnification microscope objective, the value of the NA is about 1.4, which corresponds to a resolution of approximately one-third of the wavelength of light used.

Conventional approaches to improve resolution employ short-wavelength light, such as ultraviolet (UV) or extreme ultraviolet (EUV). When the light is used to write a pattern in the photoresist sample, it first passes through a mask. The resultant patterned light then changes the chemical composition of the exposed areas of

the sample. Afterwards, during the development stage, either the exposed material or the non-exposed material is removed, depending on the type of photoresist being used.

Although it can lead to a reduction in feature sizes, EUV light is expensive to generate and not easy to control. In comparison, photolithography based on the visible or near-IR light is more efficient, as light in the visible spectrum requires less expensive sources, and is easier to produce and manipulate. For these reasons, techniques using visible light wavelength for nanoscale lithography have garnered a great deal of interest and enthusiasm.

A new approach towards fabricating superresolved structures employs combination of two lasers at wavelengths in the near-UV, visible or near-IR regions [3–6]. In this approach, one color is used to initiate a polymerization reaction. The second color selectively deactivates polymerization in the desired regions of the sample, leading to the formation of structures with sizes below the diffraction limit. Even though 2-color lithography allows for the creation of lines as narrow as 11 nm using 800 nm light [5], maintaining the same size when fabricating closely-packed structures has proven to be challenging. Writing lines close to one another leads to a decrease in resolution and widening of the created lines as compared to isolated ones.

This challenge can be overcome using 3-color lithography, in which polymerization is initiated via two steps. One color pre-activates the photoinitiator molecules in the resist sample to a chemically inert metastable state, and a second color deactivates the molecules from this state. The third color brings the remaining pre-

deactivated molecules to a chemically active state that leads to polymerization. The two-step initiation process allows us to avoid the exposure build-up that typically takes place during 2-color lithography and to improve the resolution of the resultant structures.

The 3-color lithography technique can be realized using a linear absorption in thin films for applications in the semiconductor industry. The thickness of the thin films will limit the height of the fabricated structures, while phase masks can be used to change intensity distribution of the lasers in the plane of the thin films.

As a first step towards creating superresolved structures in thin films, we are developing 3-color lithography in thick films using multiphoton absorption. Multiphoton absorption polymerization (MAP) has attracted interest from in a wide range of academic and industrial fields for its ability to create three-dimensional (3D) structures with feature sizes below the diffraction limit. It is a versatile fabrication technique based on multiphoton absorption, in which a polymerization reaction is triggered by the absorption of multiple photons of light in the visible part of the electromagnetic spectrum.

MAP allows for rapid screening of photoresists for their potential use in thin film photolithography. Once appropriate materials are identified using MAP in thick films, processes can be developed to spin-coat these materials as thin films to be used with linear polymerization. This thesis focuses on developing new approaches to test photoresists and to characterize potential photoinitiators for achieving superresolution with multi-color lithographic techniques.

1.2 Multiphoton absorption theory

Absorption is typically a linear process, in which a photon whose energy matches the energy gap between a ground state and an excited state causes a transition. In multiphoton absorption (MPA), this process is instead driven by the simultaneous absorption of two or more photons, the energies of which sum to the transition energy. This nonlinear process was predicted theoretically in 1931 by Maria Göppert-Mayer [7, 8]. Even though it was first predicted in 1931, MPA was not experimentally demonstrated until the invention of the laser. Because two or more photons need to be absorbed simultaneously to cause a transition between energy states, an ultrafast pulsed laser is generally required to drive MPA processes.

In MPA, the absorption rate is proportional to the intensity of the light source to the power of the number of photons being absorbed. In the case of two-photon absorption (2PA), for instance, this relationship is quadratic.

The differences between one-photon and two-photon absorption, as well as the potential for MPA to be used in 3D fabrication, can be demonstrated through exposure of a solution of homogeneously distributed fluorescent molecules, as shown in Fig. 1.1. In the case of single-photon absorption, the absorption rate is directly proportional to the intensity of the light. Because the molecules in the sample are distributed uniformly, the intensity distribution through the sample is constant in each transverse plane, exciting the same number of molecules in each such plane throughout the entire path length of the laser beam.

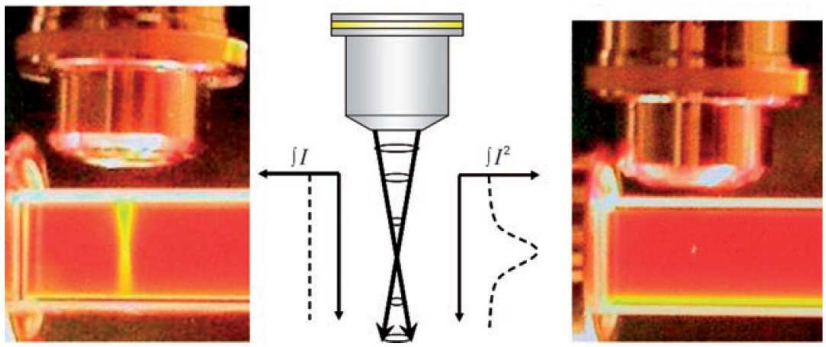

Figure 1.1: One-photon (left) and two-photon (right) absorption causing fluorescence in a Rhodamine B solution. The integrated intensity is the same in each transverse plane in the case of single-photon absorption, and is maximized within the tight focal of the microscope objective for two-photon absorption [9].

The intensity profile for 2PA shows different behavior, because the absorption rate is proportional to the *square* of the intensity. Therefore, the transverse integral of the intensity squared is at a maximum where the beam is most tightly focused. By using an objective with high NA, the laser beam can be focused to a tight focal volume and, as presented in Fig. 1.1, 2PA excites molecules only in a small region. Such a nonlinear ratio between the light intensity and the absorption rate opens the potential for applications such as 3D microfabrication [10,11], optical data storage [12–14], and 3D fluorescence imaging [15–19].

In 2PA molecules are typically excited from the ground state S_0 to the first excited S_1 by absorbing two or more photons with a collective energy E that is equal to the energy difference between S_0 and S_1. The first photon excites a molecule from S_0 to a virtual intermediate state with a lifetime τ_i, and a second photon further excites the molecule to the S_1 state. The lifetime of the intermediate state can

be determined from the uncertainty principle via $\Delta E \tau_i \geq \hbar$, where ΔE represents the uncertainty of the energy after the photon excites the photoinitiator molecule [20]. Assuming the energy of the intermediate state is close to that of S_1, for a transition caused by an absorption of a photon with an energy in the visible light range $\tau_i \approx 10^{-15} - 10^{-16}$ sec. The lifetime τ_i defines the time period within which the two photons must arrive to excite the molecule to the S_1. The absorbed photons can be of equivalent energies $E_1 = E_2$ (degenerate 2PA), where E_1 is the energy of the first absorbed photon and E_2 is the energy of the second photon. In this case, the transition energy $E = E_1 + E_2 = 2E_1 = 2E_2$. In the non-degenerate case, $E_1 \neq E_2$, but $E = E_1 + E_2$.

Even though the majority of research on 2PA has focused on the degenerate case, non-degenerate 2PA has been demonstrated in some cases to have a higher absorption cross-section [21, 22]. Non-degenerate 2PA has been achieved by using a pump-probe, two-beam configuration in which the pump beam wavelength was in the near-IR and the probe beam consisted of white-light continuum [23, 24].

1.3 Multiphoton absorption polymerization (MAP)

1.3.1 MAP mechanism

For MAP, the laser used to initiate polymerization is typically in the near-infrared region, with a wavelength of ∼800 nm, a pulse duration of ∼100 fs, and a repetition rate of ∼80 MHz. The light is focused into the photoresist through a high-NA objective, resulting in a high probability of multiple photons being absorbed

simultaneously in the focal region. A typical MAP photoresist consists of monomers or oligomers and photoinitiator molecules.

In most photoresists, a similar transition from the ground state to an excited state can be achieved through linear absorption at a shorter wavelength. As was the case for fluorescence excitation in Fig. 1.1, in contrast to linear photopolymerization with UV light, MAP takes place only within the focal region of the laser beam, following common mechanisms for photopolymerization, such as radical and cationic.

1.3.2 Radical Photopolymerization

Typically, MAP is performed using a negative-tone photoresist, meaning that a cross-linking reaction occurs in the regions that are exposed to laser light [25–27]. Afterwards, insufficiently crosslinked regions are washed away by a solvent during the development stage.

In radical photopolymerization, photoinitiator molecules excited to S_1 typically undergo intersystem crossing (ISC) to a triplet state T_1 that produces free radicals. The radicals initiate a polymerization chain reaction (Fig. 1.2).

Equations 1.1-1.4 show schematically the mechanism of the radical crosslinking process [28,29]. Here the photoinitiator molecule I transitions to an excited state I^*, from which it produces free radicals $R\cdot$ (Eq. 1.1). After the radical formation step, a chain reaction between radicals $R\cdot$ and monomers M produces radical monomers

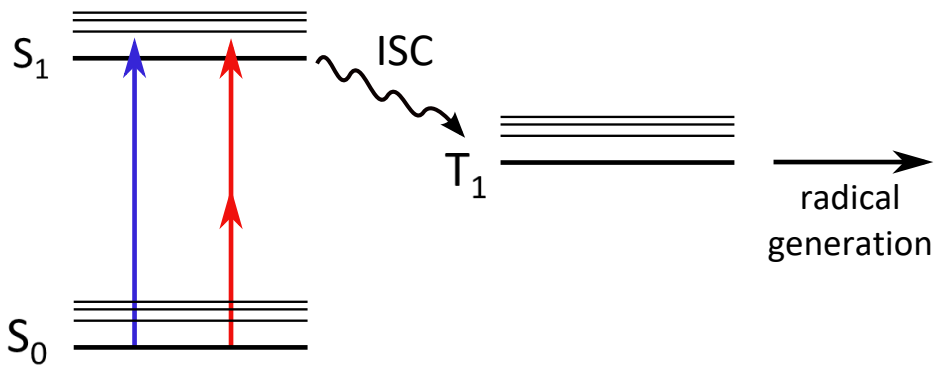

Figure 1.2: Jablonski diagram showing an electronic transition between the ground state S_0 and an excited state S_1 caused by linear absorption (blue) or two-photon absorption (red). After the transition, the molecule undergoes intersystem crossing (ISC) to a triplet state T_1, creating radicals and initiating a polymerization chain reaction.

$RM\cdot$ (Eq. 1.2). This process continues, expanding and growing oligomer radicals, until two radicals meet and terminate the reaction (Eq. 1.3,1.4).

$$\begin{aligned}
&\textit{Initiation} && I \xrightarrow{h\nu} I^* \rightarrow R\cdot && (1.1)\\
&\textit{Propagation} && R\cdot + M \rightarrow RM\cdot \xrightarrow{M} RMM\cdot \quad \cdots \rightarrow RM_n && (1.2)\\
&\textit{Termination} && RM_n\cdot + RM_m\cdot \rightarrow RM_{n+m}R && (1.3)\\
& && RM_n\cdot + RM_m\cdot \rightarrow RM_n + RM_m && (1.4)
\end{aligned}$$

An alternative path for radical formation may occur in systems with a co-initiator, in which radicals are formed by abstraction of a hydrogen atom from the co-initiator. Among other components, the pre-polymer sample may also contain polymerization inhibitors that act to terminate the polymerization reaction to enhance shelf life.

1.3.3 Cationic Photopolymerization

Cationic photopolymerization involves the formation of an acid, which is usually a Brønsted acid, using a photoacid generator (PAG). In radical photopolymerization, crosslinking occurs during the exposure. In cationic photopolymerization, exposure causes acid generation, but the polymerization reaction takes place during a post-bake process. One of the most common epoxy-based, negative-tone, cationic photoresists is SU-8. SU-8 is widely used in the semiconductor industry for the fabrication of various microelectromechanical systems (MEMS) elements and microfluidic devices, and in biological applications, due to its good biocompatibility [30–35]. One of the important physical properties of SU-8 is its high viscosity, which allows for spin-coating of photoresist films with thicknesses of up to hundreds micrometers. Normally, SU-8 resin contains cyclopentanone as a solvent and a triarylsulfonium salt that is used as the PAG. Some PAGs [36–38] make it possible to use linear exposure wavelengths in the visible, whereas others are active in the near UV. Good adhesion and high chemical resistance make SU-8 a popular candidate for the fabrication of complex three-dimensional structures with high aspect ratios.

1.3.4 MAP Applications

One of the appealing applications of MAP is in the field of fabrication of three-dimensional (3D) structures. The ability of MAP to fabricate complex structures has led to a wide range of various applications in fields such as 3D structure fabrication

[29, 39–43], microfluidics [44–46], optical data storage [47, 48], microelectronics [49–52], and microbiology [53, 54].

Here I will discuss some representitave examples. Because MAP is a rapid and flexible technique for fabricating complex structures by simply moving the laser's focal point, MAP has been used in the fabrication of a wide range of optical devices, such as lenses, waveguides [49, 55–57], and "Y-splitter" waveguides [58, 59], as well as in the creation of optical devices combining refractive and diffractive properties, such as Fresnel lenses, axicon lenses and gratings (Fig. 1.3) [60, 61].

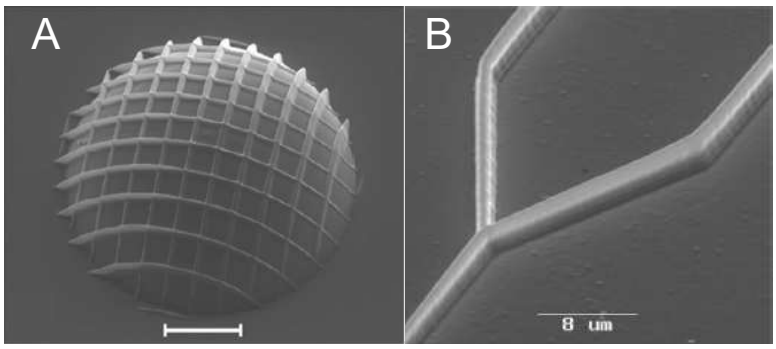

Figure 1.3: SEM images of A) a lens with a 2D grating combining diffractive and refractive properties; the scale bar is 10 μm [62]; and B) a Y-splitter waveguide fabricated by MAP [58].

Structures can be fabricated on the side of an optical fiber. For instance, Sherwood *et al.* demonstrated fabrication of a ring microresonator on the side of the polished fiber using MAP [63]. In another experiment, high coupling efficiency and low power loss were achieved in a microring resonator system [64], as shown in Fig. 1.4. Employing MAP in the fabrication of these devices allows for the easy tuning of system parameters such as coupling distance, the radius of curvature, and

the width of the gaps in the coupling regions to obtain the best coupling efficiency with minimal power loss.

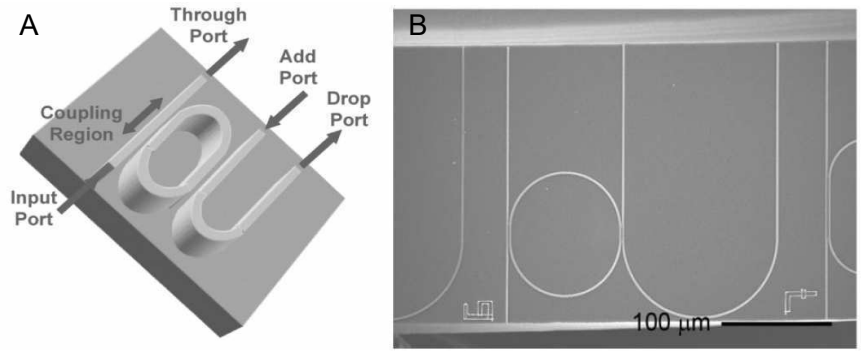

Figure 1.4: A) Diagram of a microring resonator with input and output ports. B) Electron micrograph of a microring resonator device. The straight waveguide directs the light into the microring, whereas the output port has a shape of a "U" [64].

Malinauskas *et al.* demonstrated the fabrication of micro-optical elements on glass slides and optical fiber tips [60], with combined refractive and diffractive properties due to matching the refractive indices of the optical elements and the substrate. Photonic crystals, interferometers and Y-connectors are other optical structures that can be created using MAP. Photonic crystals, as periodic dielectric structures, have optical properties that are in some way analogous to the electronic properties of semiconductors. A photonic bandgap in the near-infrared frequencies makes these structures great candidates for waveguides, microlenses and filters. Photonic crystals with lattice constants in the sub-wavelength range are used in telecommunications applications. One of the first photonic crystals fabricated with MAP had a bandgap at approximately 4 μm [65]. More recently reported crys-

tals have had the bandgaps of 1.9 μm [66] and in the range of 1.3 to 1.7 μm [67], corresponding to telecommunication wavelengths (Fig. 1.5A).

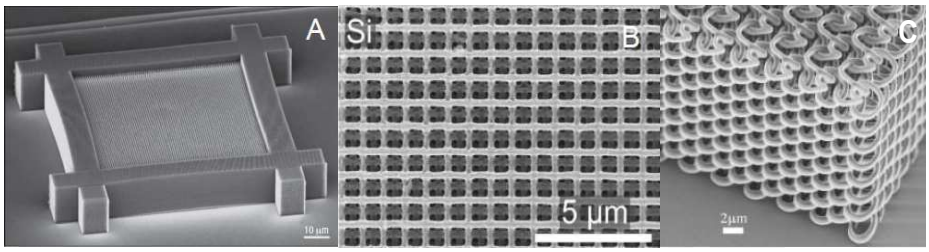

Figure 1.5: SEM images of photonic crystals fabricated by MAP. A) SU-8 photonic crystal with 40 layers and a band gap in the near-infrared [67]. B) Silicon photonic crystal fabricated by double inversion [68]. C) Circular-spiral crystal, with an 180° phase shift between adjacent spirals [69].

Chichkov *et al.* reported fabrication of woodpile photonic crystal structures in organic-inorganic hybrid polymers and SU-8 resin that were used as templates for the fabrication of highly refractive TiO_2 replicas [70]. The difference in the refractive index of the polymerized structure and air was not high enough to provide a full photonic bandgap. More complex shapes were achieved by the double inversion of a periodic matrix [68]. Fig. 1.5B shows a crystal fabricated by the double-inversion of the SU-8 matrix that was first filled with SiO_2, after which the SU-8 was removed, and then the remaining structure was infiltrated by Si vapor deposition. Subsequent chemical etching removed the SiO_2 matrix, so that the resulting silicon photonic crystal replicated the SU-8 structure.

Traditionally, the periodic elements that form a photonic crystal have a logpile structure. However, using MAP, more complex unit shapes have been demonstrated,

such as diamond and spiral unit cells. Fig. 1.5C shows a photonic crystal matrix with spiral periodic elements with different transmission coefficients for different polarizations of light [71, 72].

Even though MAP allows for the fabrication of polymeric structures with a range of architectures, many applications in electronics require electrically conductive structures. This requirement, in turn, requires incorporation of metals such as gold, copper or silver into the polymer structures [51, 73]. Selective functionalization of polymer microstructures may be performed if different types of polymers are used [74].

1.3.5 Nonlinear processes

MPA allows for the excitation of photoinitiator molecules in a tight volume within the focal region of the laser beam, strongly limiting the reaction volume in which polymerization takes place. The polymerized feature formed when the laser focus is held at a single point is called a volume element, or voxel. The nonlinear dependence of the absorption probability on the exposure intensity allows for voxel sizes smaller than the Abbe limit.

Chemical nonlinearity also plays a significant role in the fabrication of small features. The nonlinear chemical nature of the photoresist includes processes such as self-quenching, and results in a certain exposure threshold that must be exceeded to render the resist insoluble. The size of the excited volume can be further reduced by adjusting the laser intensity such that only the center of the beam is above the

intensity threshold. Such laser power adjustment effectively reduces the number of excited molecules and the size of the polymerized structures.

Even though it is possible to cause two-photon absorption using a continuous wave (CW) laser, the average power required to initiate a transition in this case is typically quite high. In most cases, MAP is performed by using a femtosecond pulsed laser with a high repetition rate to deliver enough energy per pulse to allow MPA to occur at low average power. Focusing a laser beam through a microscope objective into a photoresist and translating the focal region allows for the creation of complex structures with a resolution much smaller than the wavelength of the light employed. In 2001, Kawata *et al.* demonstrated fabrication of 120 nm features in the transverse direction using an 800 nm beam [50]. Even smaller features of 80 nm were subsequently fabricated using 800 nm light [75]. Employing a shorter wavelength of 520 nm, nanoscale features as small as 65 nm were fabricated by Tan *et al.* [43].

1.3.6 Resolution challenges of MAP

MAP is a versatile tool for the fabrication of 3D structures with features at a sub-micron scale. It is possible to create structures of arbitrary complexity by using a single laser beam that is focused into a tight volume. The process of fabrication is performed by moving the sample relative to the laser beam focus, and is controlled by a computer program directing coordinates to form a 3D structure. This fabrication process does not require repeated exposure through a mask. The laser beam can

be focused within the sample depth to initiate polymerization, under the condition that the laser beam's focus creates parts of the structure at the substrate surface, so that final structure is attached to the substrate and does not wash away during the development step.

It is challenging to fabricate structures with transverse feature sizes below 80 nm using MAP. Furthermore, due to the manner in which the laser beam is focused by an objective, feature sizes in the axial direction (along the direction of beam propagation) are three to five times larger than those in the transverse direction [76]. No matter how small the intensity in the center of the laser beam, focusing it through the objective lens results in an elongated intensity distribution, resulting in the voxel looking like a *cucumber* (Fig. 1.6).

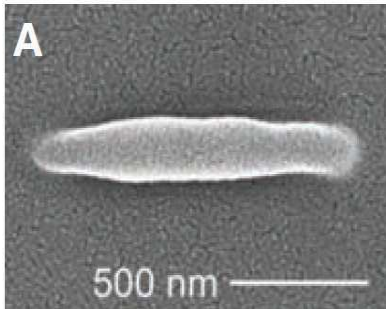

Figure 1.6: Scanning electron micrograph of a voxel created using MAP [3].

The limitations of a laser beam focusing in both axial and transverse directions makes it challenging to use MAP for fabrication of structures with reproducible feature sizes below 100 nm. A number of research groups have directed their efforts to advancing MAP technology to reduce feature size in both the axial and transverse directions.

1.4 2-color lithography: Optical deactivation of photopolymerization

1.4.1 Stimulated emission depletion

MAP is a powerful tool for creating 3D structures with linewidths that are much smaller than the wavelength of the light involved. However, the resolution of these features is still limited by diffraction. Recent 2-color improvements in MAP, allowing for the fabrication of even smaller features, were inspired by a super-resolved fluorescence microscopy technique called stimulated emission depletion (STED) [77–79]. In STED, two pulsed laser beams at different wavelengths are focused at the same spot in a fluorescent sample. The first laser beam excites fluorophores, after which the second beam causes them to undergo a stimulated emission transition back to the ground state, such that they do not fluoresce (Fig. 1.7).

By passing the second beam through a spatial phase element, it is possible to create a dark area in the center of the second laser beam. When the two beams are then overlapped, only the molecules in the dark central area of the second beam fluoresce. The molecules that are outside of the dark circle are excited by the first beam and undergo stimulated emission by the second beam. The effective diameter of dark region of the second beam can be decreased by increasing the second beam's intensity, creating saturation. The size of the fluorescent region, and therefore the resolution, can be far below the diffraction limit.

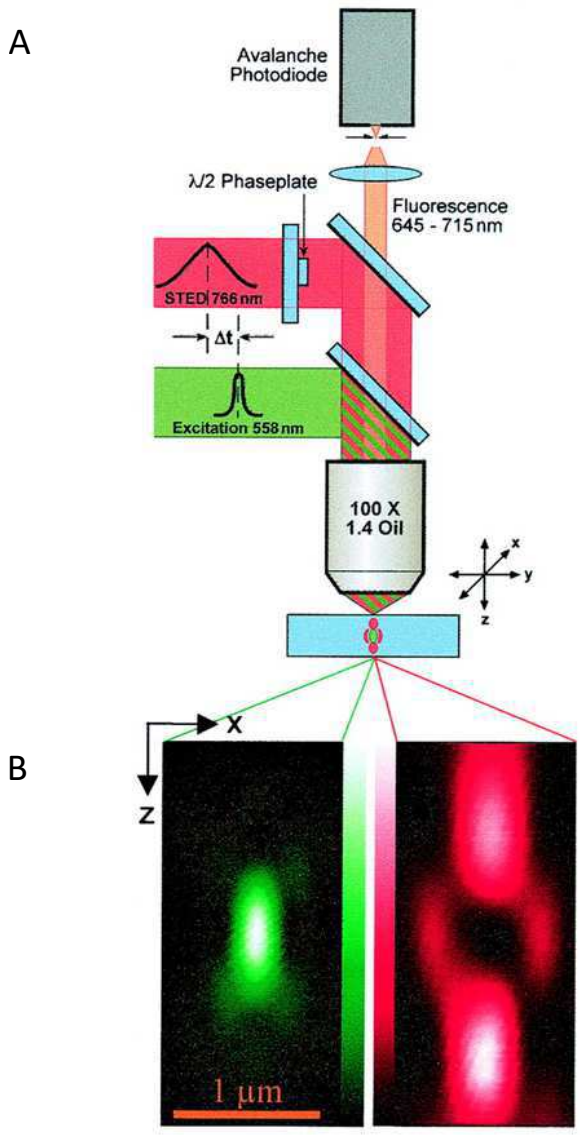

Figure 1.7: A) Combination of excitation pulses and stimulated emission depletion pulses for fluorescence inhibition. B) Measured excitation point spread funcion (PSF) and STED-beam PSF. The STED-beam PSF has a local minimum at the center and intense maxima above and below the focal plane [79].

1.4.2 RAPID lithography

To achieve superior resolution, an approach similar to STED can be used for deactivating photoinitiator molecules. In analogy with STED, one laser beam is

employed to excite photoinitiator molecules and a second beam is used to deactivate molecules selectively so that they will not participate in the reaction.

Contrary to the fluorescent molecules used in STED, most radical photoiniators have only a small oscillator strength between the ground and first excited states, which means that absorption from the first excited state to higher-energy states can dominate over stimulated emission. Thus, the deactivation laser beam will transfer photoinitiator molecules to a higher energy state and enhance polymerization, rather than inhibiting it.

This issue can overcome by employing a photoinitiator with a large absorption cross-section (from the ground state to the first excited state). One common dye molecule that was found to fulfill this requirement is malachite green carbinol base (MGCB) [3]. MGCB has a large absorption cross-section and can generate free radicals through multiphoton absorption.

Two tunable, synchronized Ti:Sapphire lasers were employed to demonstatate deactivation of MGCB molecules. The first laser, called the excitation laser, produced pulses with a duration of 200 fs at 800 nm and excited molecules through MPA. Pulses from the second, deactivation beam were stretched to 50 ps and deactivated the MGCB molecules, thus inhibiting polymerization. This process is known as resolution augmentation through photo-induced deactivation (RAPID). Fig. 1.8A shows lines created using the RAPID technique with two beams with an offset. Varying the time delay between excitation and deactivation pulses showed no effect on the deactivation efficiency, thus implying that MGCB molecules go to

an intermediate state with a long lifetime. A continuous wave (CW) deactivation laser was also able to turn the polymerization off (Fig. 1.8B).

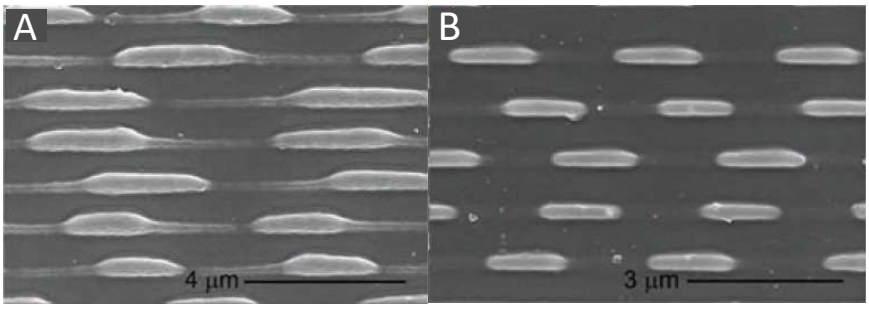

Figure 1.8: Scanning electron micrographs (SEM) of lines fabricated with RAPID lithography using two 800 nm laser beams. A) Lines created using 200 fs pulsed laser beam and an offset deactivation beam with 50 ps pulse duration. B) Lines written using coincident excitation beam with a 200 fs pulse duration and a CW deactivation beam. The deactivation beam was chopped in both cases [3].

To create a "doughnut" mode, the deactivation beam was sent through a phase mask, creating a half-wave delay in the beam center. Fig. 1.9 (left) demonstrates the multiphoton-absorption-induced luminescence signal from gold nanoparticles caused by the excitation and deactivation beams, to measure PSFs and ensure overlap of the beams.

Employing the phase mask in the deactivation beam path allowed for reduction of the axial dimension of the fabricated features down to 40 nm ($\lambda/20$) and the transverse dimension down to 80 nm ($\lambda/10$) using an 800 nm beam. As shown in Fig. 1.10, the voxel height changed from 600 nm without a deactivation beam to 40 nm when the power of the deactivation beam increased to 93 mW, corresponding to a change of aspect ratio from 3.5 to 0.5.

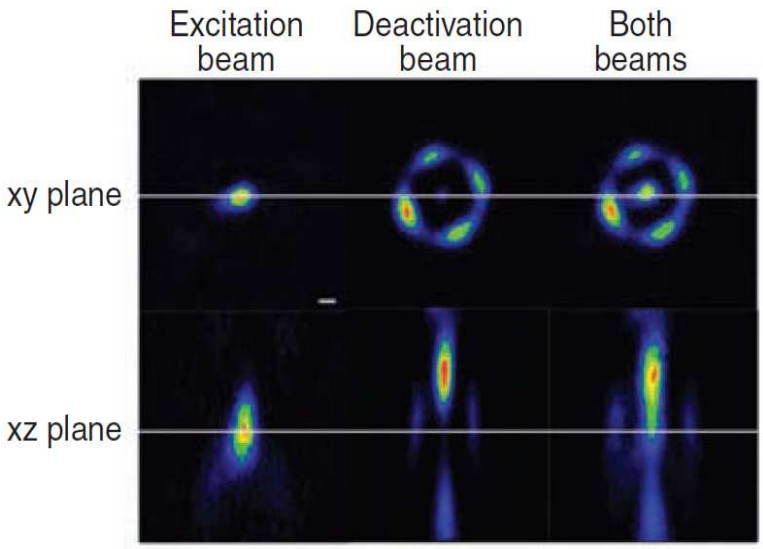

Figure 1.9: Point-spread functions of the RAPID excitation beam, the deactivation beam, and both beams overlapped, using multiphoton-absorption-induced luminescence. The scale bar at the bottom of the left top image is 200 nm. [3]

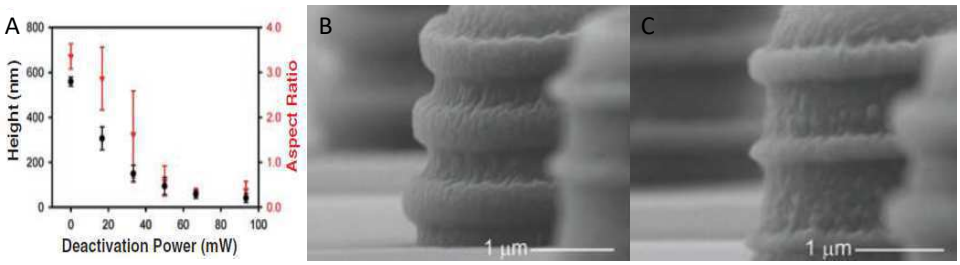

Figure 1.10: A) Height and aspect ratio of voxels fabricated at different deactivation beam powers. Error bars represent one standard deviation from four voxel measurements. B) The SEM image of a tower fabricated without deactivation beam by MAP. C) The SEM image of a tower created by RAPID. Reproduced from [3].

Other groups have developed new 2-color lithographic systems using different deactivation mechanisms. The group of McLeod at CU Boulder used a chemical system for a 2-color excitation/deactivation scheme, based on a photoexcitable

polymerization inhibitor [4]. For this demonstration, the negative-tone photoresist contained a photoinitiator system – a combination of camphorquinone and ethyl 4-(dimethylamino)benzene – that was excited by one wavelength, and an inhibitor – tetraethylthiuram disulfide – that terminated polymerization upon excitation at a shorter wavelength. In contrast to the previous mechanism, the photoinitiator in this scheme generates free radicals upon linear excitation at 473 nm and the inhibitor is activated by one-photon excitation at 364 nm. As follows from Fig. 1.11A, the polymerization rate slows down by approximately a factor of 5 when the photoresist is exposed to both wavelengths, compared to exposure to 473 nm alone. This reaction resulted in features with dimensions of 200 nm with 473 nm light using a lens with NA = 0.45.

Fig. 1.11B shows the inverse dependence of the voxel size on the power of the UV laser. With increasing power and photoinhibition rate, the voxel size was reduced from 3.6 μm to 200 nm. Incorporating a lens with NA = 1.3 allowed for the fabrication of 110 nm voxels with 473 nm light.

This technique was later employed in a modified chemical system [80] using a different monomer with higher viscosity, which increased the photosensitivity of the photoresist as well as the stability of the fabricated lines. The photoinitiator camphorquinone, coinitiator ethyl 4-(dimethylamino)benzoate, and photoinhibitor tetraethylthiuram disulfide were mixed with the photoresin BPE-100. A linearly polarized CW laser operating at 488 nm was used to initiate polymerization and a circularly polarized CW laser beam at 375 nm inhibited polymerization. The size of the voxel was predicted by a non-steady-state kinetic model and confirmed by fab-

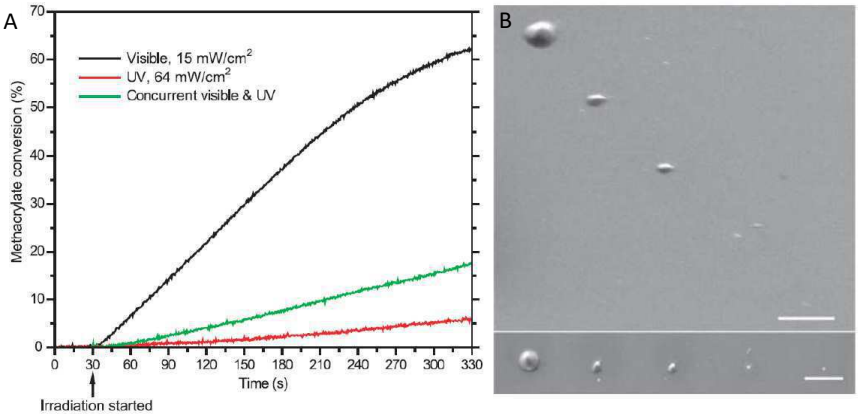

Figure 1.11: A) Polymerization rate for a methacrylate photoresist containing a radical photoinitiator and photoinhibitor, as measured by using time-resolved Fourier transform infrared spectroscopy. The highest polymerization rate corresponds to visible light exposure (black curve), that excites photoinitiator molecules. Concurrent visible light and and UV exposure (green curve) excites both photoinitiator and inhibitor molecules, while exposure to UV only (red curve) excites the inhibitor only. B) SEM image of the voxels fabricated at different UV powers, showing the inverse dependence of the voxel size on the deactivation light power. The scale bar is 10 μm [4].

rication of dots. As shown in Fig. 1.12, the lateral size of the voxels decreased from 1200 nm to 330 nm with increasing deactivation power. By adjusting the inhibiting laser beam, the size could be further reduced to 40 nm. During a continuous line exposure, the linewidth could be reduced from 400 nm to 130 nm. The size of the dots fabricated under various exposure duration was plotted as a function of the deactivation laser (Fig. 1.12C), where the color of the dot represents the size.

Another two-color polymerization depletion scheme was demonstrated recently [81, 82]. Using a doughnut-shaped deactivation beam, the lateral widths of the fabricated features were reduced from 155 nm to 65 nm in a photoresist containing pentaerythritol triacrylate (SR444) and isopropyl thioxantone (ITX) as the pho-

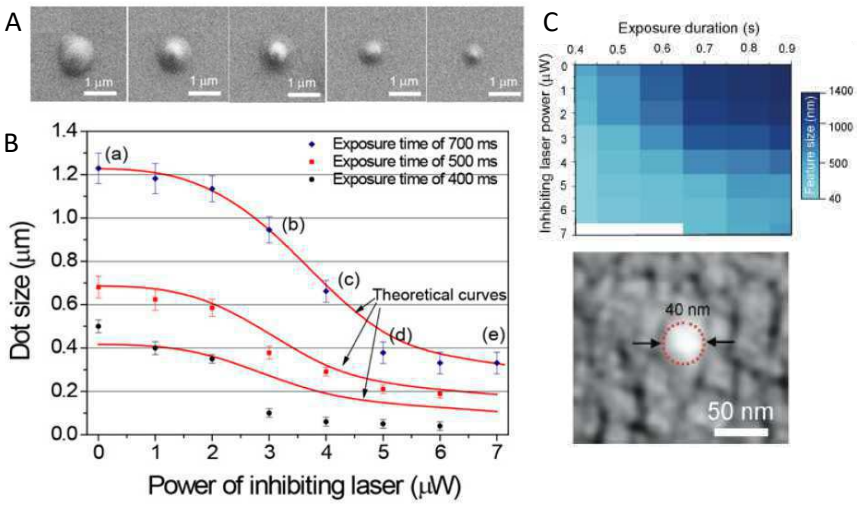

Figure 1.12: A) SEM images of dots fabricated with constant 488 nm exposure at different powers of a 375 nm inhibition laser in the ethoxylated bis-phenol-A-dimethacrylate-based photoresin, BPE-100. The 488 nm excitation power was 200 nW and the exposure time was 0.7 s. B) The dot sizes plotted as a function of the inhibition laser power. The curves represent simulated predictions. C) The dot size plotted as a function of the inhibition laser power and exposure time (top) and an SEM image of the smallest voxel fabricated [80].

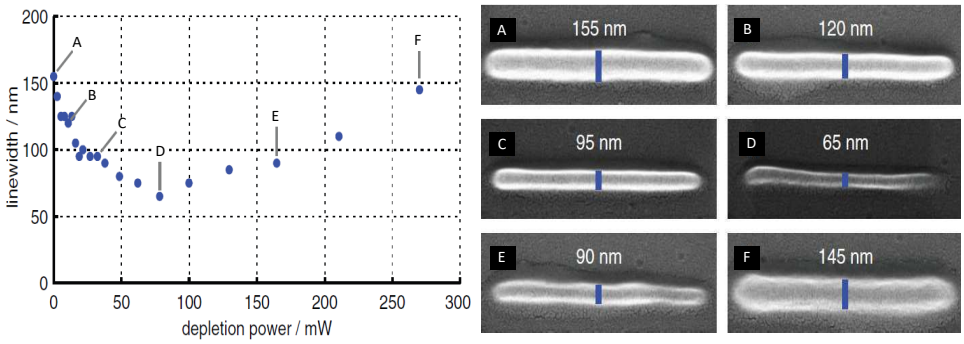

Figure 1.13: Width of the lines fabricated in an ITX based photoresist with 13.5 mW of mode-locked, 810 nm exposure as a function of phase-shaped 532 nm CW deactivation power [81].

toinitiator (Fig. 1.13). Similarly, different photoresists based on SR444 and 7-diethylamino-3-thenoylcoumarin (DETC) were used to demonstrate fabrication of gratings through a stimulated-emission depletion scheme [82]. Using a CW depletion beam with a "doughnut" mode, gratings with 200 nm and 175 nm periods were demonstrated.

1.4.3 Self-deactivation of proportional velocity (PROVE) dependence photoinitiators

Further investigation of RAPID showed that for a class of molecules, deactivation can be so efficient that it is driven by the ultrafast excitation pulses themselves [83]. Typically in radical photopolymerization, faster fabrication velocities lead to the fabrication of narrower lines (Fig. 1.14A). At a constant velocity the linewidth remains constant. The linewidth can be changed by altering the laser beam's power or by adjusting the fabrication velocity. At constant laser power, higher velocities result in a lower exposure dose at any given point, and, consequently, thinner lines.

For certain molecules, such as, malachite green carbinol hydrochloride (MGC - HCl), the linewidth is proportional to the fabrication velocity [83]. In other words, the faster the laser beam is scanned across the photoresist, the wider are the lines (Fig. 1.15A). In an MGC - HCl resin, higher exposure doses, or slower fabrication velocities, produce finer lines. This polymerization behavior, known as a proportional velocity (PROVE) dependence, was demonstrated by fabricating sets of pyramids

(Fig. 1.14B, Fig. 1.15B). For conventional MAP photoinitiators, the polymerization is increased at the turning points, when the stage slows down and the exposure dose increases (Fig. 1.14C). In MGC-HCl photoresist, the turning points show little to no polymerization due to the PROVE behavior (Fig. 1.15C).

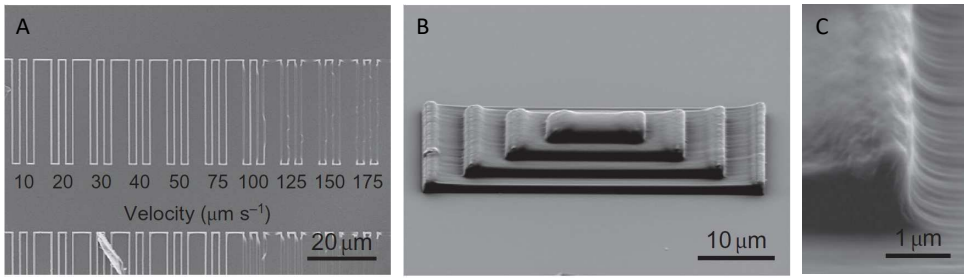

Figure 1.14: A) Lines fabricated at different velocities in a photoresist containing Lucirin TPO-L; B) 60° view of a pyramid fabricated with this photoresist; C) image of the turning points of the pyramid, corresponding to the points where fabrication velocity decreases, resulting in increased polymerization. Successive levels of the pyramid (from bottom to top) were created with velocities of 100, 75, 50, and 25 m/s [83].

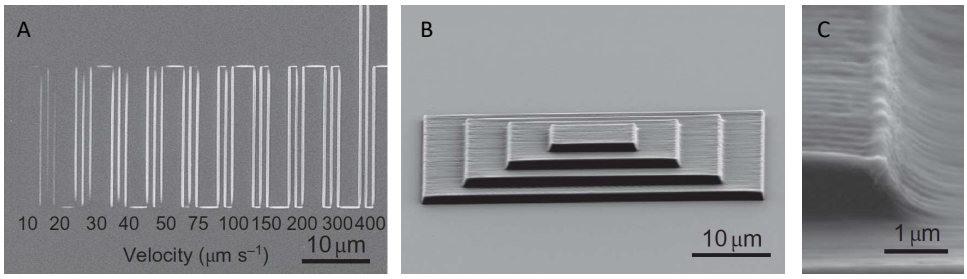

Figure 1.15: A) Lines fabricated at different velocities in a photoresist containing MGC-HCl; B) 60° view of the pyramid fabricated with this photoresist; C) image of the turning points of the pyramid, corresponding to the points where fabrication velocity decreases, resulting in decreased polymerization. Successive levels of the pyramid (from bottom to top) were created with velocities of 100, 75, 50, and 25 m/s [83].

PROVE behavior can be understood based on a model developed for the original RAPID experiments. In this model, following the two-photon absorption of 800 nm light, the photoinitiator molecule transitions to an intermediate state that can be deactivated by the absorption of another 800 nm photon. Thus, MGCB is deactivated by light of the same wavelength used for excitation, resulting in a competition between these two processes. It was predicted that if the deactivation process is more efficient than excitation, then a PROVE dependence will be observed. Because at slower fabrication velocities the exposure dose increases, molecules are more efficiently deactivated from the intermediate state by a subsequent laser pulse. When the fabrication velocity increases, more excited molecules are left in the intermediate state, leading to the formation of wider lines. PROVE behavior was observed for a wide range of related dyes. It was also demonstrated that by combining a traditional MAP photoinitiator (with inverse linewidth dependence on fabrication velocity) and a PROVE photoinitiator, the polymerization rate and linewidth could be made to be independent of the fabrication velocity over a wide range of velocities.

1.5 Thesis outline

Visible-light photolithography, based on multiphoton absorption polymerization, is a promising technique for the fabrication of structures with feature sizes less than 100 nm. This thesis focuses on further development of photopolymerization deactivation mechanisms and the study of potential new photoinitiator molecules. The experimental approach to testing these mechanisms is described in Chapter 2.

Knowledge of photoinitiator molecule properties is desirable for developing resists with more efficient deactivation. Discussed in Chapter 3, the 2-beam initiation threshold (2-BIT) technique allows for the measurement of the order of effective nonlinear absorption directly in the photoresist, helping to identify relevant parameters for the experimental approach to deactivation. Chapter 4 examines the self-deactivating photoinitiatior KL68.

As an alternative to the 2-color photolithography (2CPL), 3-color photolithography facilitates additional resolution improvement. This method involves three different energy states, thus avoiding competition between deactivation and initiation. Several molecules have been tested as possible photoinitiators to demonstrate this approach. Chapter 5 discusses the study of the molecular properties of biacetyl and its potential used as a 3-color photoinitiator.

To further expore the possilities of this method, Chapter 6 reviews the experimental data from 2-BIT measurements, polymerization and deactivation action spectra of benzil, α-naphthil, β-naphthil and pyridil in an acrylic resin. An overview of this work's results and future directions are presented in Chapter 7.

Chapter 2

Experimental methods

2.1 Experimental setup

Polymerization initiation was performed with a tunable Ti:sapphire oscillator (Coherent Mira 900-F) with a pulse duration of ∼150 fs and a repetition rate of 76 MHz. The laser is tunable between ∼700 nm and 900 nm. The laser beam was collimated with a set of lenses and a pinhole, and expanded to 8 mm to fill the back aperture of a microscope objective. The power was controlled with a polarizer and a half-wave plate. The laser beam was directed into an inverted microscope (Zeiss Axiovert 100) by scanning galvanometric mirrors, and reflected into a microscope objective by a dichroic mirror. A 1.45 NA, 100×, oil-immersion objective (Zeiss α Plan-Fluar) was used used to focus the laser beam in the photoresist.

The photoresist sample was mounted on a sample holder and placed on a 3-axis piezoelectric stage (Physik Instrumente). The piezoelectric stage was used for a fine sample positioning, as it moves in a 250 μm range in three dimensions with sub-nanometer resolution. The piezo stage was attached to a translation stage (Ludl), which was used for coarse sample positioning in the xy plane and for fast fabrication, as it can move with velocities up to cm/sec.

The laser beam position within the photoresist was changed either by moving the scanning mirrors or by moving the sample stage. In the first case the sample

position was fixed and the laser focal point was moved relative to the sample. In the second case, the laser focal point was fixed and a LabView program was used to move the sample stage in the X, Y and Z directions, allowing for 3D fabrication. Polymerization was monitored through a CCD camera attached to the microscope.

For polymerization deactivation experiments employing two laser beams in the wavelength range 700-900 nm, a beam from a second tunable Ti:sapphire oscillator (Coherent Mira 900-F) was set at a desired wavelength and directed to the inverted microscope. The power of the second beam was also controlled by a polarizer and a half-wave plate. The polarization of the second beam was orthogonal to that of the first laser beam, and the two beams were combined by a polarizing beam cube before entering the microscope (Fig. 2.1).

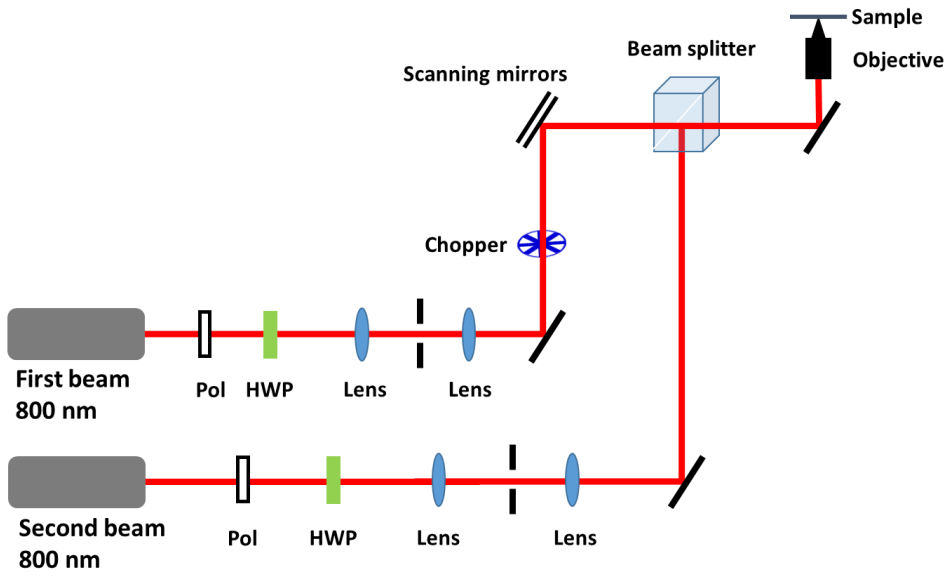

Figure 2.1: Diagram of the experimental setup for the polymerization deacivation experiments using two Ti:sapphire laser beams

Precise overlap of the two laser focal spots is essential for two-beam experiments. To assure that the two beams were overlapped completely, multiphoton-absorption-induced luminescence (MAIL) from gold nanoparticles was used to measure the laser beams' point spread functions (PSFs) [84]. Gold nanoparticles were placed on a glass slide that was mounted above the objective. Back-scattered MAIL from each beam was collected by single-photon-counting avalanche photodiode detectors below the microscope. The excitation light was separated from the luminescence signal using a filter below the objective. Due to the high efficiency of MAIL and the high sensitivity of the photodiodes, a laser intensity of $\sim$1 mW at the sample surface was used.

A radial polarization converter (ARCoptix) was used to change the spatial intensity distribution of the first beam and selectively deactivate photoinitiator molecules, leading to a decrease in the feature size. A linearly polarized light was sent through a liquid crystal (LC) cell of a polarization converter [85]. Depending on the orientation of LC molecules, the refractive index of the cell changes and the electric field vector rotates, resulting in the transmitted beam having a radial or azimuthal polarization (Fig. 2.2). The polarization is changed by applying a bias voltage between electrodes attached to the liquid crystal cell, Fig. 2.3A.

The deactivation beam was sent through a polarizing beam cube to select the beam's polarization along one of the axis and change it from the doughnut shape to resemble a TEM10 mode. A diagram for overlapping two laser beams is shown in Fig. 2.3B. Here, the centers of the two beams were aligned, so that the peak intensities of the deactivation beam were aligned with the side edges of the

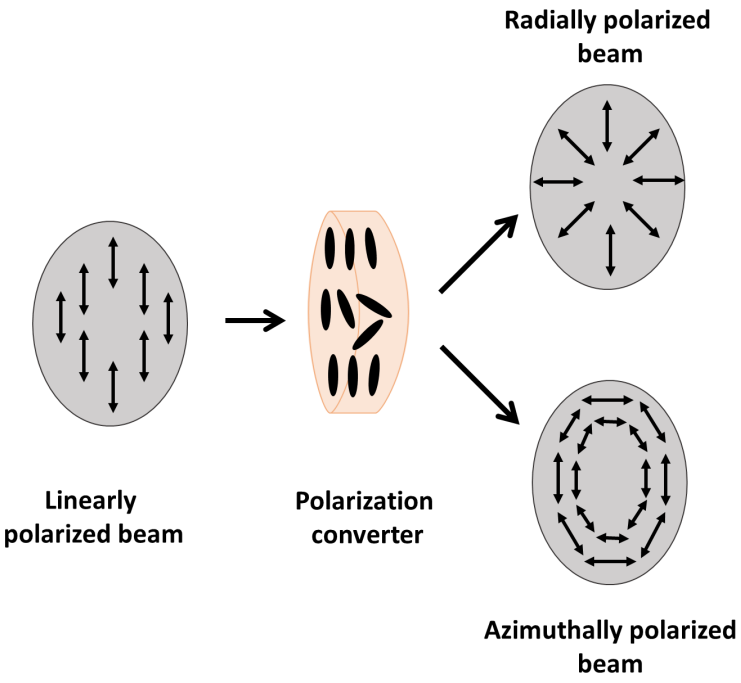

Figure 2.2: Schematics of radiation polarization change using a radial polarization converter based on liquid crystal cell. Reproduced from www.arcoptix.com

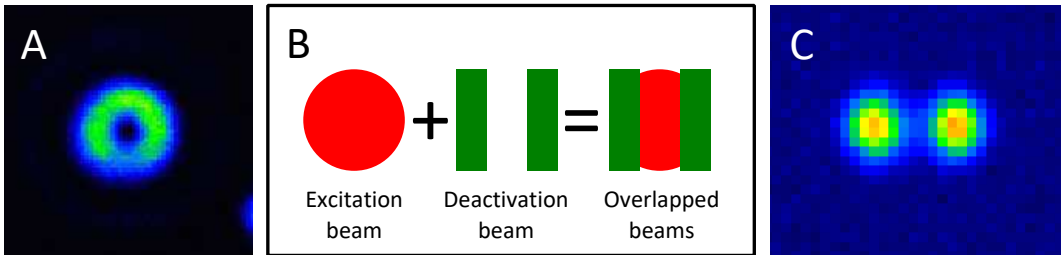

Figure 2.3: A) Typical MAIL signal generated from gold nanoparticles by a doughnut-shaped laser beam, produced by a radial polarization converter. B) Experimental scheme of overlapping two beams for polymerization deactivation studies. C) Y-axis intensity distribution of the doughnut-shaped laser beam.

excitation beam. In this case, molecules in the center region of the excitation beam initiated polymerization. Simultaneously, molecules along the sides of the excitation beam were deactivated, preventing the formation of free radicals in this region, and thereby creating thinner lines.

The two laser beams were roughly aligned before entering microscope objective. For a finer overlapping, the luminescence signal was collected by scanning an area across a gold nanoparticle by moving the deactivation beam with scanning mirrors. This procedure allows for optimization of the radial polarizer parameters for the deactivation beam (Fig. 2.4). Because only the deactivation beam was reflected from the scanning mirrors, the MAIL image of gold nanoparticles from the excitation beam was measured by moving the piezo stage relative to the fixed excitation beam. Once the signal was collected, the scanning mirrors' position was changed to overlay the first beam with the second in XY plane and along the Z (propagation) axis.

2.2 Sample preparation

Unless specified otherwise, all photoinitiators were dissolved in a monomer solution composed of tris(2-hydroxy ethyl) isocyanurate triacrylate (SR368) and ethoxylated trimethylolpropanetriacrylate (SR499). First, the two monomers were mixed in a 1:1 wt ratio (1:1 SR368/499). The mixture was then heated to 80 °C, until the SR368 was melted, and thoroughly mixed using a vortex mixer. The photoinitiator was added to a monomer mixture at a desired wt% and placed in an

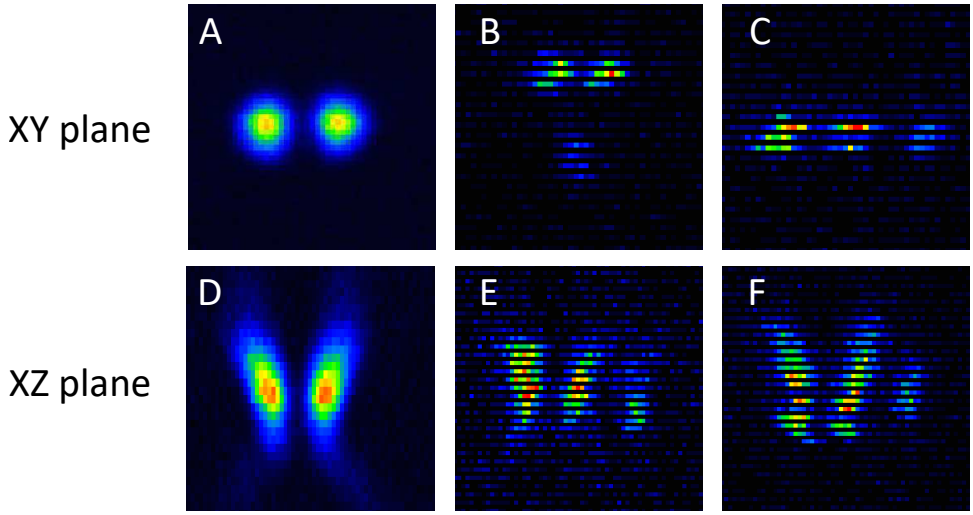

Figure 2.4: Overlapping two laser focal points in the X, Y, and Z directions by collecting MAIL from gold nanoparticles. A) MAIL from the gold nanoparticles is generated by moving the deactivation laser beam using scanning mirrors. B) MAIL from the gold nanoparticles is generated by two laser beams with an offset along the Y-axis. The excitation beam is positioned between the lobes of the deactivation beam, and an offset is introduced to demonstrate the accuracy of laser beam alignment along the X-axis. C) MAIL from gold nanoparticles generated by two laser beams with an offset in the X-axis. The excitation beam is positioned on the side of the deactivation beam at an offset to demonstrate alignment along the Y-axis. D) - F) Corresponding MAIL images from gold nanoparticles scanned in the XZ plane.

oven at 90 °C for three minutes, then mixed using the vortex mixer for thirty seconds, and put on a mechanical rotator for five minutes. These steps were repeated three times. Afterwards, the photoresist was left on the mechanical rotator overnight. After at least 12 hours of rotation the sample was placed in an oven at 90 °C for three minutes and then filtered using a 18G $1\frac{1}{2}$ needle and 0.2 μm or 0.4 μm Nylon filters. After filtering, the sample was placed in an oven at 90 °C and centrifuged at 3400 rpm/min for five minutes to get rid of any air bubbles.

Once centrifuged, a drop of the photoresist was placed on a functionalized #1 glass coverslip from Corning, which was used as a substrate for MAP experiments. Coverslips were functionalized to promote adhesion of the polymerized structures. The first step in functionalization was cleaning in an oxygen plasma for 4 mins. Afterwards, coverslips were immersed in a solution of 93% ethanol, 5% distilled water and 2% (3-acryloxypropyl) trimethoxysilane by volume for 14 hours, followed by rinsing in ethanol for 1 hour and drying at 95 °C for 1 hour. After drying, a coverslip was taped on a microscope slide. A drop of the filtered photoresist was placed on the coverslip. The photoresist was covered with another coverslip that was also taped to the microscope slide. A piece of tape approximately 600 μm thick acts as a spacer between the two coverslips and determines a thickness of the photoresist film.

Afterwards, a prepared sample was mounted on a microscope glass holder and placed above the microscope objective for the MAP experiments. After polymerization, unexposed photoresist was removed by rinsing twice in ethanol for 2 minutes and once in water for 2 minutes. After development, samples were left to dry at room temperature. For examination with a scanning electron microscope (SEM), a coverslip was attached to SEM mount with carbon tape and covered with a $\sim$20 nm thick platinum/palladium layer in a sputter coater.

Chapter 3

2-Beam initiation threshold: A technique for the *in situ* measurement of the order of effective nonlinear absorption in multiphoton photoresists

Based on "Zuleykhan Tomova, Nikolaos Liaros, Sandra A. Gutierrez Razo, Steven M. Wolf, and John T. Fourkas, Laser Photonics Rev. 2016, 10, 849854" Contributions: 2-BIT measurements were performed by Z.T. and N.L.; samples were prepared by S.G.R.; absorption spectra were collected by S.W.

3.1 Introduction

The ever-increasing applications of MAP have driven the sustained development of new materials for this technology. One focus has been on the creation of photoinitiators that have improved multiphoton absorption cross sections (MACS) [14]. However, the measurement of MACS to states that undergo irreversible photochemistry is challenging. Early attempts worked under the assumption that the MACS for fluorescence mirrors that for photochemistry [86].

A number of techniques have been developed to characterize the order of nonlinear absorption. In the nonlinear transmission technique, a beam passes through a sample and its energy is measured before and after the sample. The transmittance

depends on the incident beam energy, and is measured at varying intensities. If the nonlinear transmittance is affected only by 2PA, then assuming that the incident beam has Gaussian intensity distribution and is focused near the sample, the transmitted intensity I can be expressed as

$$I = \frac{I_0 \ln(1 + I_0 L\beta)}{I_0 L\beta} = \frac{\ln(1 + I_0 L\beta)}{L\beta}, \tag{3.1}$$

where I_0 if the intensity of the incident light, L is the thickness of a sample, and β is the nonlinear absorption coefficient of the material [87–89]. The nonlinear absorption coefficient β is measured as a function of I_0. If no other nonlinear processes are involved, such as excited-state absorption, three-photon absorption, or beam profile changes, then the coefficient β is independent of the incident intensity I_0. The 2PA cross-section σ_2 can be determined using

$$\sigma_2 = \frac{\hbar\omega\beta}{N_0} = \frac{\hbar\omega\beta}{N_A c \times 10^{-3}}, \tag{3.2}$$

where N_0 is the molecular density of the sample, N_A is the Avogadro constant, and c is the sample concentration.

In the z-scan technique, measurements are performed by passing a focused Gaussian beam through a cuvette with a solution of interest [90, 91]. The transmittance is measured as a function of the cuvette position along the beam propagation direction and is collected in the far field. If the transmittance is measured through a finite aperture the technique is called close aperture z-scan. In the absence of the aperture the total transmittance is measure and the method is distinguished as open aperture z-scan.

The third-order nonlinear susceptibility $\chi^{(3)}$ in the case of 2PA is

$$\chi^{(3)} = \chi_R^{(3)} + i\chi_I^{(3)} \tag{3.3}$$

where the imaginary part is related to the nonlinear absorption coefficient β by the expression

$$\chi_I^{(3)} = \frac{n_0^2 \epsilon_0 c^2}{\omega} \beta \tag{3.4}$$

and the total absorption α of the medium is a sum of the linear absorption and 2PA:

$$\alpha(I) = \alpha + \beta I, \tag{3.5}$$

where I is the intensity of the incident beam.

For a Gaussian beam with waist w_0, the transmittance obtained through the z-scan technique can be expressed as

$$T(z) = \sum_{n=1}^{\infty} \frac{(-q_0(z,o))^m}{(m+1)^{3/2}}, \tag{3.6}$$

where $q_0(z,t) = \beta I_0(t) L_{eff}/(1 + z^2/z_0^2)$, z is position of the sample, $z_0 = kw_0^2/2$ is the diffraction length of the beam, $k = 2\pi/\lambda$ is the wave vector, I_0 is the maximum intensity in the focus, $L_{eff} = (1 - e^{-\alpha L})/\alpha$, L is the length of the sample and α is the linear absorption.

For small third-order nonlinear loss the normalized transmittance can be described as [92]

$$T(z) = 1 - \frac{\beta I_0 L_{eff}}{2\sqrt{2}} \frac{1}{1 + z^2/z_0^2}. \tag{3.7}$$

The coefficient β can be determined experimentally by fitting z-scan data to Eq. 3.7 and the 2PA cross-section can be obtained using Eq. 3.2.

In the case of close aperture z-scan the sign and magnitude of the nonlinear refractive index can be obtained by collecting light after the sample through an aperture in front of the detector. For the third-order nonlinear materials, the refractive index n can be expressed as

$$n = n_0 + \frac{n_2}{2}|E|^2 = n_0 + n_2 I \tag{3.8}$$

where n_0 is the linear index of refraction, E is the peak electric field, and n_2 is nonlinear refractive index. The n_2 can be determined from the normalized transmittance for the far-field condition

$$T(z, \Delta\phi_0) = 1 - \frac{4\Delta\phi_0 x}{(x^2+9)(x^2+1)} \tag{3.9}$$

where $x = z/z_0$, $\Delta\phi_0 = kn_2 I_0 L_{eff}$ is the phase change. The real part of the third-order optical susceptibility can be obtained using following expression

$$\chi_R^{(3)} = 2n_0^2 \epsilon_0 c n_2. \tag{3.10}$$

The nonlinear fluorescence excitation (NFE) method determines the 2PA cross section by measuring the intensity of fluorescence emission as a function of excitation intensity [93–95]. The 2PA cross-section σ_2 is proportional to the NFE action cross section σ_{NFE} through the expression

$$\sigma_{NFE} = \eta_2 \sigma_2, \tag{3.11}$$

where η_2 is the fluorescence quantum efficiency of the material and σ_{NFE} is determined from the NFE. 2PA spectra can be obtained by performing NFE measurements as a function of excitation wavelength. A related technique determines the

order of nonlinear absorption based on the measurements of multiphoton-induced phosphorescence intensity [96, 97].

The thermal lensing technique measures optical effects generated by heat dissipation during the radiationless decay of molecules from an excited state to the ground state [98–100]. During such a decay, the released energy locally increases temperature, changing the refractive index and effectively creating a lens in the sample.

Although the assumption that the MACS measured for fluorescence mirrors that for photochemistry is often reasonable, there is no guarantee that it is correct in any given system. Even if the excitation of fluorescence is a 2-photon process at a given wavelength, initiation of photochemistry need not be, as has been demonstrated recently for 7-diethylamino-3-thenoylcoumarin [101]. More generally, at a given wavelength, the order of the effective nonlinear optical absorption for MAP, i.e. the nonlinear absorption process that leads to polymerization, need not match the dominant order of nonlinear absorption at the same wavelength as measured with techniques such as the z-scan [102]. It is therefore essential to know the effective order of nonlinear absorption if one wishes to determine the effective MACS corresponding to a MAP process.

With this problem in mind, a number of recent studies have focused on determining the effective order of the nonlinear absorption of photoinitiators *in situ* by measuring the initiation of photopolymerization. In one commonly used technique, the feature size is measured as a function of fabrication velocity for a range of different average laser powers [43, 62]. However, Fischer *et al.* pointed out that this

method cannot unambiguously determine the order of nonlinear absorption in a photoresist [6], and developed an alternative technique in which the exposure threshold is measured as a function of pulse energy at different pulse repetition rates [6]. Their method can provide detailed information on the processes that contribute to MAP at different pulse intensities. The same group also introduced a technique in which the effective order of nonlinear absorption is determined by measuring the polymerization threshold at a fixed repetition rate but different exposure times [103]. However, both of these techniques require fast, nonmechanical shutters and high-power (multiwatt) oscillators, which are not available in many laboratories in which MAP is performed.

Here, we introduce a simple and complementary method for determining the effective order of nonlinear absorption processes in photoresists. The 2-beam initiation threshold (2-BIT) technique can be implemented with the addition of a few simple optics, can be performed with a single, low-power ultrafast oscillator, and allows for the determination of the order of the effective nonlinear absorption using only a single repetition rate. 2-BIT is therefore amenable to use in virtually any laboratory that performs MAP.

3.2 Theory

In MAP, multiphoton excitation of a photoinitiator leads to local crosslinking of a negative-tone photoresist. Photoresists have highly nonlinear exposure curves, such that they become insoluble above a threshold exposure dose. In principle,

this threshold is reached when a specific density of photoinitiators has been excited. However, the use of ultrafast pulses in MAP brings other time scales into play. On the one hand, ultrafast pulses are typically much shorter than the time scales on which photoinitiators undergo photochemistry [104]. On the other hand, due to the small size of the region irradiated at any given time in MAP, the diffusion of heat or species such as radicals or quenchers can play an important role in determining the threshold exposure. Diffusive effects leading to termination become important when, due either to a low pulse intensity or a low repetition rate, the exposure time at a given spot is relatively long [103]. Because of these effects and others, it is often desirable to be able to determine the order of the effective nonlinear absorption of a photoresist at a fixed repetition rate.

If the exposure conditions are comfortably between these two extremes, then overcoming the exposure threshold can safely be equated with generating a specific density of photoinitiators that have been excited at some time in the exposure window. This condition is generally met at a typical oscillator repetition rate at a reasonable fabrication velocity (e.g., tens to hundreds of μm/s). It is essential that the repetition time be much longer than the excited state lifetime of the photoinitiator, to prevent any effects of excited-state absorption. Typical radical photoinitiators generate radicals on a 100 ps time scale [104], which is two orders of magnitude faster than a typical repetition rate.

The radicals that are formed do not absorb the laser light, and so are unaffected by subsequent pulses. It is also important that the repetition period be much shorter than the termination time scale, so that the effects of the laser pulses are cumulative.

In a typical photoresist, termination becomes important on time scales of 100 ms or more [103], which is much longer than the typical dwell time on a given spot. If a fixed duration for the exposure window (t_w) and a fixed repetition rate for the ultrafast pulses (ν_{pulse}) are chosen, then the minimum average power for which crosslinking is observed can be defined as $P_{th}(t_w, \nu_{pulse})$.

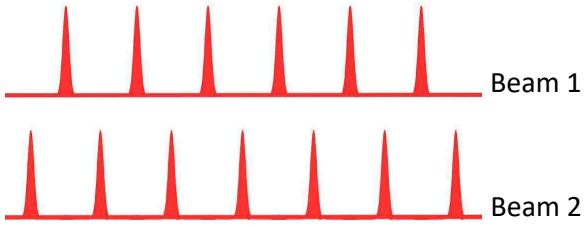

Figure 3.1: Pulse trains of two beams.

Consider the case in which exposure occurs via two independent trains of pulses that are identical in wavelength, duration, and repetition rate, but not in intensity. For simplicity, assume that these pulse trains are timed such that pulses arrive at the sample at repetition rate $2\nu_{pulse}$. Shown in Fig. 3.1 are two pulse trains with a time delay such that pulses are equally spaced in time.

So long as ν_{pulse} and $2\nu_{pulse}$ are (1) small enough that there is plenty of time for excited photoinitiators to undergo chemistry between pulses and (2) large enough that diffusive effects are unimportant between pulses, the exposure threshold will be reached when

$$P_1^n + P_2^n = P_{th}^n. \tag{3.12}$$

Here, the subscript denotes the pulse train and n denotes the number of photons involved in the transition to the excited state that is the gateway to crosslinking. This equation can be recast in terms of normalized powers $\bar{P}_i = P_i/P_{th}$ as

$$\bar{P}_2 = \sqrt[n]{1 - \bar{P}_1^n} \tag{3.13}$$

Thus, by measuring the value of $\bar{P}_2$ required to reach the threshold exposure for different values of $\bar{P}_1$, n can be determined directly. In practice, the power of each beam is normalized to the threshold power for polymerization using that beam, to correct for any minor differences in properties such as beam size, pulse length, or focal volume.

3.3 Methods and materials

3.3.1 2-BIT experimental setup

A tunable, femtosecond Ti:sapphire oscillator (CoherentMira 900-F) was used as the excitation source. The repetition rate of the laser was 76 MHz, and the pulse duration was approximately 150 fs. The beam was spatially filtered and then split into two roughly equal parts. Each beam was passed through a separate variable beam expander to allow for adjustment of the beam size at the back aperture of the microscope objective, Fig. 3.2.

The average power of each beam was adjusted using a motorized half-wave plate and a Glan-Taylor polarizer. To increase the accuracy of the laser power measurement, a small portion of each beam was reflected using a 95:5 beam splitter

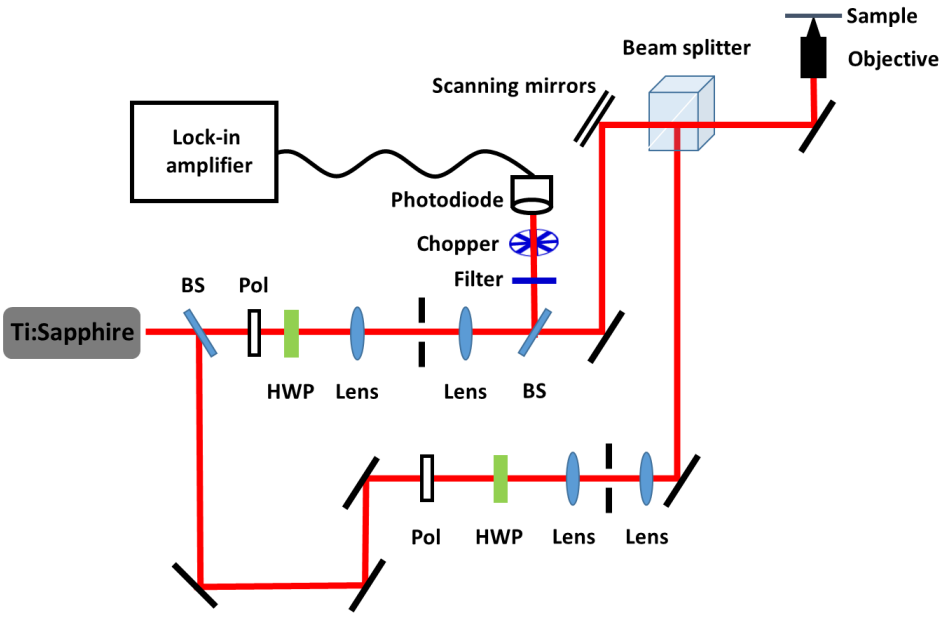

Figure 3.2: Experimental setup for 2-BIT measurements.

and then passed through colibrated neutral-density filters to lower its intensity. The beam was chopped, and its power was measured using a calibrated Si photodiode, the output of which was sent to a lock-in amplifier.

The two beams were combined through a polarizing beam cube and made collinear. The lengths of the two beam paths were adjusted so that consecutive pulses arrived at the sample with roughly equally spaced timings, giving an effective repetition rate of 152 MHz. The timing between the pulse trains was adjusted using a fast photodiode and an oscilloscope, which is sufficiently precise for performing 2-BIT experiments. The beams were sent through the reflected-light illumination port of an inverted microscope and were focused through a 100×, 1.45 NA oil-immersion objective, the back aperture of which was overfilled. Samples were mounted on a 3-axis piezoelectric stage for fine sample positioning in all dimensions. The piezo stage

was attached to a motor-driven stage for coarse sample positioning. The movement of the sample stage was controlled using LabVIEW programs, and fabrication was followed in real time using a CCD camera and a monitor. To ensure that the two focused beams had identical focal volumes that were completely overlapped at the sample, gold nanoparticles were deposited on a cover slip and multiphoton absorption induced luminescence (MAIL) was used to determine the position and shape of the point-spread function of each beam, as described in Section 2.1. Special attention was paid to ensure that the two beams had exactly the same diameter and that the divergence at the entrance pupil of the microscope objective, such that beams of the same average power would also have the same on-axis intensity. However, we note that due to the normalization of the power thresholds, 2-BIT measurements are tolerant to modest misalignments of the beams.

3.3.2 Sample preparation

The photoresist samples studied were created by adding 0.1 - 2.0 wt% photoinitiator to a base resist composed of 45 wt% tris (2-hydroxy ethyl) isocyanurate triacrylate and 55 wt% dipentaerythritol pentaacrylate. The photoinitiators examined are shown in Fig. 3.3, and included Lucirin TPO-L, Irgacure 369, Irgacure 651, Irgacure 819, and crystal violet lactone.

All samples were blended at 2500 rpm for 5 min using a vortex mixer. After mixing, a drop of the photoresist was placed on a functionalized, #1 glass coverslip. The functionalized coverslips were prepared by exposure to oxygen plasma for about

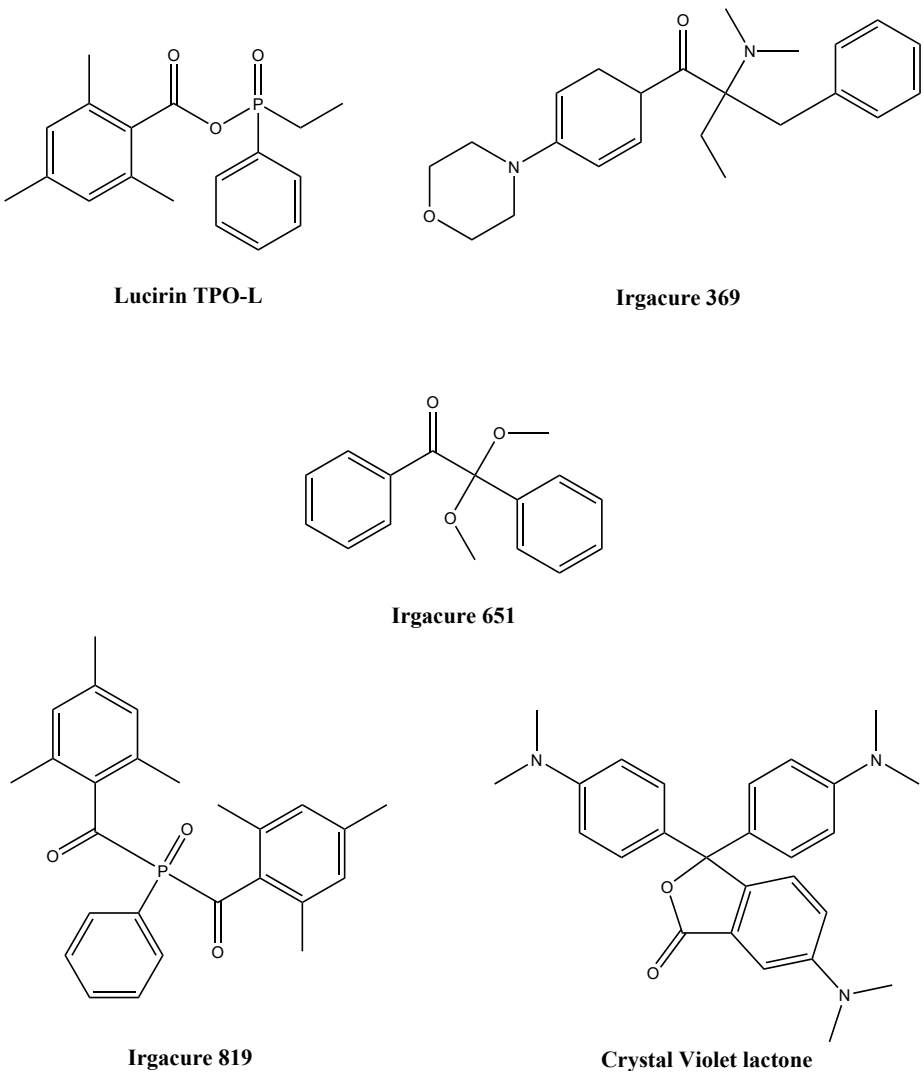

Figure 3.3: Structures of the photoinitiators studied.

4 min, immersion in a solution of 93 vol% ethanol, 5 vol% distilled water and 2 wt% (3-acryloxypropyl) trimethoxysilane (Gelest) for 14 h, rinsing in ethanol for 1 h, and drying at 95 °C for 1 h.

Samples for MAIL were prepared by placing a drop of solution containing 50 nm gold nanoparticles with a diameter of about 50 nm on a #1 cover slip. The the cover slip with the solution was left to dry at room temperature overnight. After

the solvent was evaporated the coverslip was placed in the microscope for MAIL imaging and alignment of the two laser focal points.

3.3.3 2-BIT measurements

The first step in a 2-BIT measurement is determination of the polymerization threshold powers of each laser beam independently. Fig. 3.4A shows the pulse train of the beam 1 only at the polymerization threshold, and Fig. 3.4E shows pulse train of beam 2 only at the polymerization threshold. These thresholds were measured

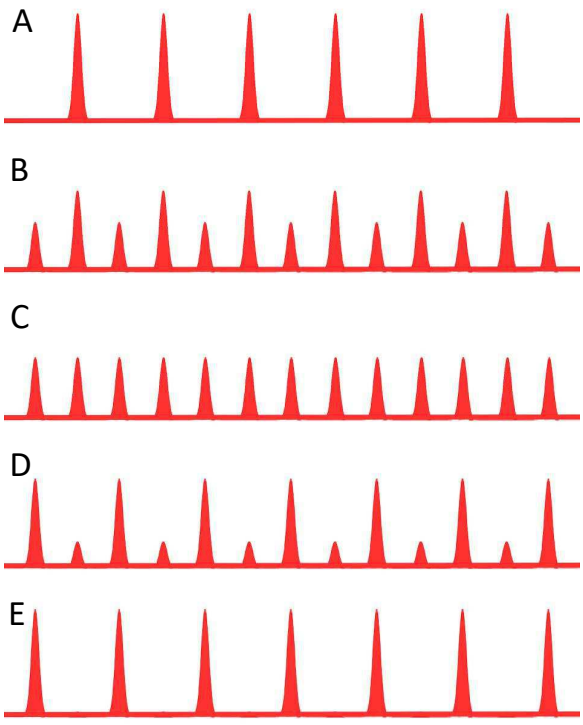

Figure 3.4: Schematics of laser power in 2-BIT measurements. A) Beam 1 at threshold power, beam 2 blocked. B) - D) Beam 1 set at lower power with beam 2 set at the corresponding intensity to reach threshold. E) Beam 1 blocked, beam 2 at threshold.

by creating sets of lines at a constant distance above the coverslip surface at a stage velocity of 20 μm/s. The minimum average power at which fabricated lines were observed was then determined visually on the monitor. This is a well established, robust and reliable method of determining the threshold for MAP [25, 101] that we employ here due to its ease of use, but 2-BIT can be used in concert with any method of measuring the threshold exposure. Although the threshold exposure measured may differ for different optical systems, the normalization procedure described above corrects for any such differences.

The power of the first laser beam is then lowered to a set of fixed values below the threshold. For each of the fixed values of P_1, the corresponding minimum value of the power of the second beam, P_2, for which polymerization is observed at the same stage velocity was determined (Fig. 3.4B - D). The values of P_1 were chosen so that a representative range of values of P_2 was measured, such that a plot of $\bar{P}_2$ vs. $\bar{P}_1$ could be fit reliably. At least five measurements were made for each value of P_1 so that reproducibility could be quantified.

3.4 Results and discussion

Lucirin TPO-L and Irgacure 369 are two commercial photoinitiators that are known to be effective materials for MAP [25, 105]. Shown in Figs. 3.5A and 3.6A are 2-BIT data for photoresists containing Lucirin TPO-L and Irgacure 369. In each case the laser was tuned to a center wavelength of 800 nm. The best-fit exponential

was determined in each case by nonlinear least-squares fitting of the 2-BIT data to Eq. 3.13.

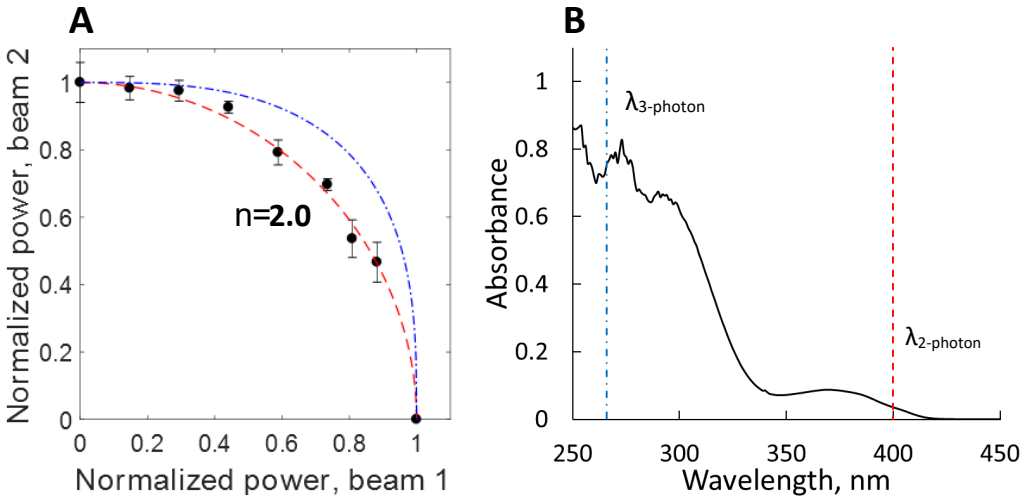

Figure 3.5: A) 2-BIT data for photoresists containing 1.0 wt% Lucirin TPO-L. The dashed lines are the best fits to Eq. 3.13. The dashed-dotted lines are the result that would be expected for 3-photon absorption as a reference. B) The absorption spectra of TPO-L in methanol, with the effective wavelengths for 2-photon and 3-photon absorption indicated as dashed and dashed-dotted lines, respectively. The error bars in this and the ensuing figure are based on standard deviations from multiple measurements.

Although the absorption spectra of the initiators may be slightly different in the photoresist, spectra obtained in methanol give a semiquantitative measure of the positions of the absorption bands. Lucirin TPO-L has modest absorption at 400 nm, and strong absorption at 267 nm (Fig. 3.5B). The single-beam threshold power for this initiator was 5.9 ± 0.2 mW, and the best-fit exponent to the 2-BIT data is 2.0 ± 0.1. Despite the strong linear absorption at the effective 3-photon wavelength, this material acts quadratically at 800 nm, as has been suggested previously [25, 106]. Irgacure 369 has a weak absorption tail at 400 nm and considerably stronger

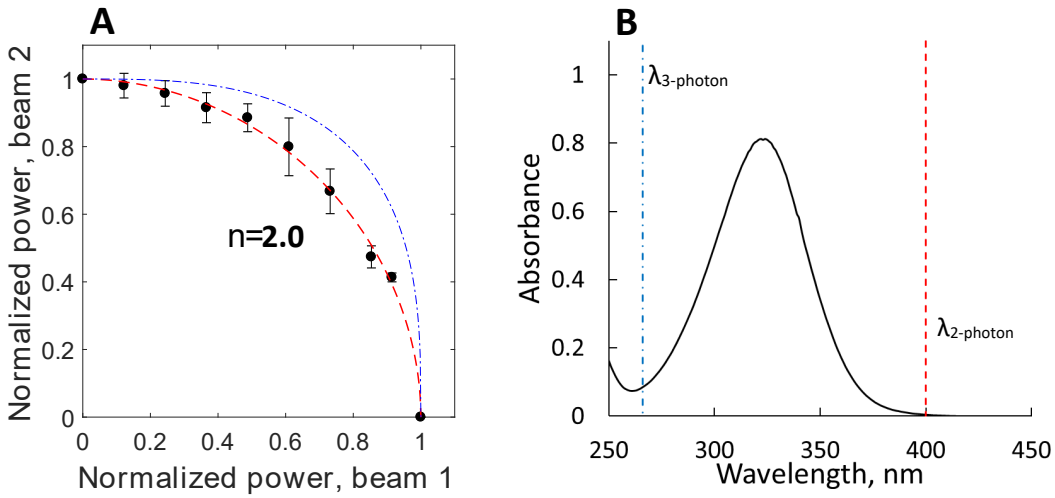

Figure 3.6: A) 2-BIT data for photoresists containing 0.1 wt% Irgacure 369. The dashed lines are the best fits to Eq. 3.13. The dashed-dotted lines are the result that would be expected for 3-photon absorption as a reference. B) The absorption spectra of Irgacure 369 photoinitiator in methanol, with the effective wavelengths for 2-photon and 3-photon absorption indicated as dashed and dashed-dotted lines, respectively.

absorption at 267 nm (Fig. 3.6B). The single-beam threshold power for this initiator was 6.6 ± 0.4 mW, and the best fit 2-BIT exponent for this material is 2.0 ± 0.2 at 800 nm. It is evident from the 2-BIT data that the effective nonlinearity in this material is primarily a 2-photon absorption at 800 nm, in agreement with previous measurements [6, 86, 107]. Thus, as expected, both materials form radicals via 2-photon absorption at 800 nm. It is difficult to predict the nonlinearity in these materials from the absorption spectrum alone, due to the different orders of nonlinearity for 2- and 3-photon absorption in conjunction with the potential influence of selection rules in multiphoton transitions.

Irgacure 651 is another commercial photoinitiator that has also been used for MAP [108]. The 2-BIT data for this initiator are shown in Fig. 3.7A for excitation

at a center wavelength of 830 nm. As can be seen from the inset in Fig. 3.7, this

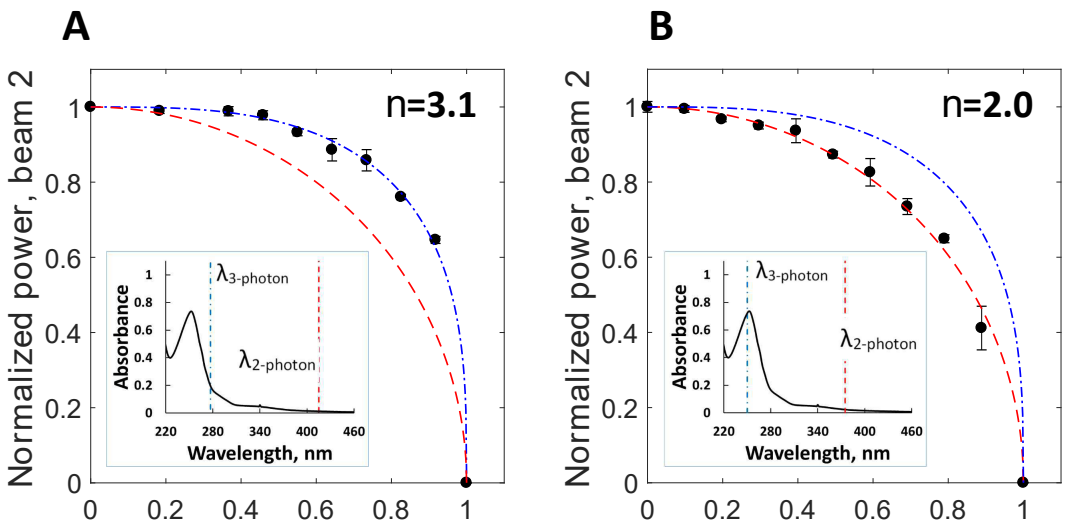

Figure 3.7: A) 2-BIT data for photoresists containing 1.0 wt% Irgacure 651 measured with excitation beam at 830 nm. The dashed-dotted lines are the best fits to Eq. 3.13. The dashed lines are the results that would be expected for 2-photon absorption as a reference. The inset show the absorption spectra of photoinitiator in methanol, with the effective wavelengths for 2-photon and 3-photon absorption indicated as dashed and dashed-dotted lines, respectively. B) 2-BIT data for photoresist containing 0.1 wt% Irgacure 651 and measured with an excitation beam at 750 nm. The dashed lines are the best fits to Eq. 3.13. The dashed-dotted lines are the results that would be expected for 3-photon absorption as a reference.

material has weak absorption at 415 nm and stronger absorption at 277 nm. The single-beam threshold power for this initiator was 17.6 ± 0.9 mW, and the best fit exponent for the 2-BIT data is 3.1 ± 0.1, indicating that polymerization is a 3-photon process for this initiator at this wavelength. This result again underscores the fact that the order of the effective nonlinear absorption cannot be determined readily from the linear absorption spectrum alone. It is possible, for instance, that there is significant 2-photon absorption to the origin of the lowest singlet excited

state in this molecule, but that this state does not generate radicals. Additional measurements performed with 750 nm wavelength indicate that at shorter wavelengths, this initiator does transition to initiating via 2-photon absorption (Fig. 3.7B. The single-beam threshold of the 750 nm beam was 10.6 ± 0.2 mW and the best fit to the 2-BIT data is 2.0 ± 0.1.

Crystal violet lactone is not typically used as a photoinitiator, but is one of many common dyes [83] that can produce radicals, and therefore act as a photoinitiator, under multiphoton excitation. The 2-BIT data for a photoresist containing this material for 800 nm excitation are shown in Fig. 3.8A. As can be seen from the absorption spectrum in the inset of Fig. 3.8A, this material has weak absorption at 400 nm and strong absorption at 267 nm. In this case, the single-beam threshold power was 5.2 ± 0.4 mW. The 2-BIT data are best fit with an exponent of 3.0 ± 0.1, indicating that the dominant effective nonlinear absorption is 3-photon at 800 nm.

Irgacure 819 also has been used as a two-photon radical photoinitiator [86]. Its absorption spectrum, shown in inset of Fig. 3.8B, has strong absorption band around 300 nm and a weaker peak at 400 nm, suggesting that there might be a dominant 3-photon absorption process for 800 nm excitation. 2-BIT data for a photoresist containing Irgacure 819 measured at 800 nm are shown in Fig. 3.8B. The single-beam threshold power for the 2-BIT measurements was 7.4 ± 0.3 mW. The exponent of the best fit to the 2-BIT measurements is 2.0 ± 0.1, indicating that the dominant effective nonlinear absorption is 2-photon at 800 nm. Again we find

that the absorption spectrum alone is not sufficient to predict the order of effective nonlinear absorption for initiating polymerization.

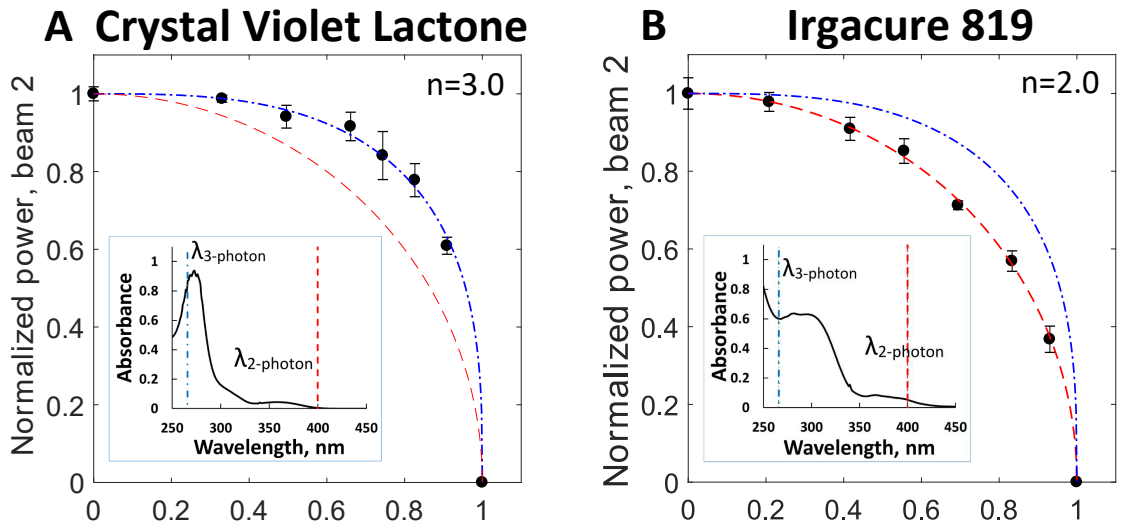

Figure 3.8: 2-BIT data for photoresists containing (A) 2 wt% crystal violet lactone and (B) 0.3 wt% Irgacure 819. The dashed-dotted lines in the panel A are the best fits to Eq. 3.13. The dashed lines are the results that would be expected for 2-photon absorption as a reference. The dashed lines in the panel B are the best fits to Eq. 3.13. The dashed-dotted lines are the results that would be expected for 3-photon absorption as a reference. The insets have the same meaning as in Fig. 3.7.

Even when the 2-photon absorption spectrum has been measured using another technique, such as fluorescence, it may not match the polymerization action spectrum. Furthermore, MAP photoinitiators that have been assumed to operate via 2-photon absorption near 800 nm may actually operate via 3-photon absorption. Identification of such photoinitiators may make it possible to improve the resolution of MAP.

3.5 Conclusions

2-BIT is a simple and effective method for the *in situ* measurement of the order of effective nonlinear absorption in multiphoton photoresists, and as such can be an important element of the development of new materials that extend the capabilities of MAP. 2-BIT relies on the use of a single oscillator at a fixed repetition rate, and so can be set up easily in virtually any laboratory in which MAP is performed. This technique can be used with any type of MAP photoresist, and can be implemented with any of a wide range of means for determining the initiation threshold of a photoresist, including monitoring of lines or voxels during fabrication using optical or spectroscopic methods, or postfabrication using methods such as optical, electron, and atomic force microscopy. 2-BIT allows the order of the effective nonlinear absorption of a photoresist to be determined without having to use devices for rapid beam modulation, and measurements can be performed at any desired repetition rate. Variations of this technique can be used to make *in situ* measurements of the order of the effective optical nonlinearity (and therefore the multiphoton action cross section, as opposed to the multiphoton absorption cross section) not just in photoresists, but in any sort of system in which nonlinear absorption causes a property to reach a measureable threshold. With knowledge of the other relevant parameters, it will further be possible to use 2-BIT data to convert the multiphoton action cross section into a multiphoton absorption cross section. 2-BIT therefore promises to be a powerful means of elucidating the photochemical

and photophysical details of complex multiphoton processes through, for instance, comparison with nonlinear absorption data.

Chapter 4

Deactivation in PROVE dependence photoinitiator

Contributors: Zuleykhan Tomova, Nikolaos Liaros, Sandra A. Gutierrez Razo, Samuel Cohen, Amanda Souna, John Bender. Contributions: 2-BIT measurements, polymeriztion initiation and deactivation experiments were performed by Z.T. and N.L.; samples were prepared by Z.T. and S.G.R.; SEM measurements were performed by Z.T.; matlab code for the best-fit exponential to 2-bIT data was written by S.C.; absorption spectra were collected by S.W.

4.1 Introduction

Multiphoton absorption polymerization (MAP) [15] is an effective technique for fabrication of densely packed structures with features that can be on the sub-100 nm scale [10, 11, 42, 43, 50, 52]. The typical material for MAP is a negative-tone photoresist consisting of a monomer mixture and a photoinitiator [25–27]. Upon absorption of two or more photons, photoinitiator molecules are excited to a higher singlet state, usually followed by intersystem crossing and radical formation, initiating a polymerization chain reaction [28].

Common photoinitiators exhibit positive contrast, meaning that the size of the fabricated features increases with increasing exposure. However, recently several photoinitiators have been shown to exhibit negative contrast, i.e. the size of fabricated features decreases with exposure [83, 109]. Negative-contrast materials open the door for new opportunities for various applications. Here, we present a study of one of these photoinitiators, KL-68.

4.2 Experimental section

4.2.1 Sample preparation

The photoinitiators examined included bis-[4-(diphenylamino) stryl]-1-(2-ethylhexyloxy), 4-(methoxy)benzene (KL-68), Lucirin TPO-L and malachite green carbinol base (MGCB). The structures of these photoinitiators are shown in Fig. 4.1.

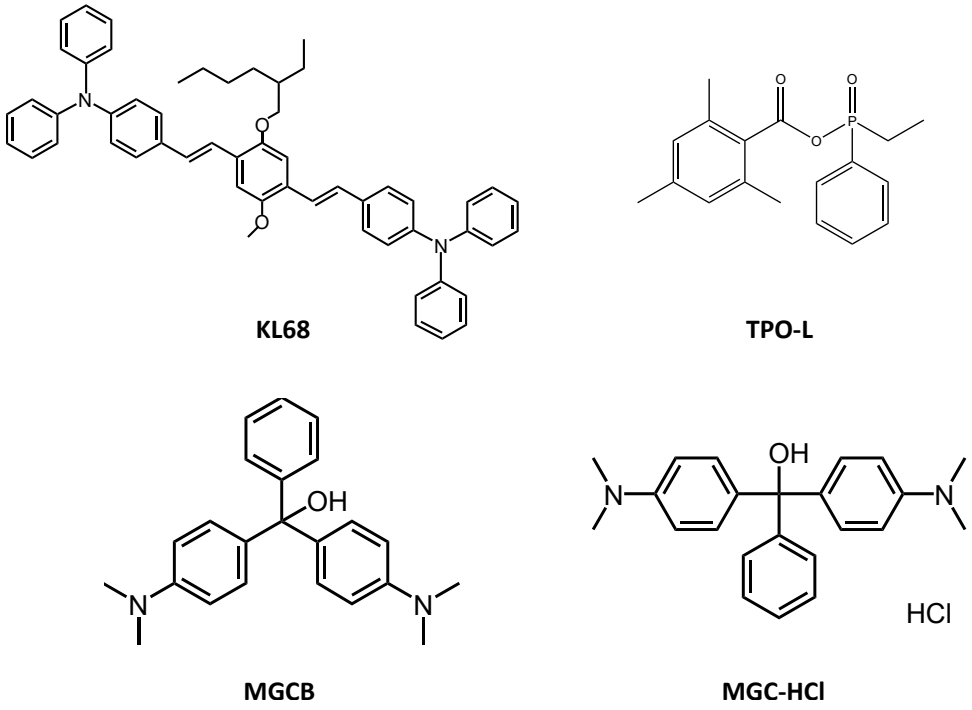

Figure 4.1: Structures of the photoinitiators KL68, TPO-L, MGCB, and MGC-HCl.

For single- and dual-beam exposure experiments photoinitiators were added to a mixture of SR368 and SR499 monomers and samples were prepared as described in Section 2.2.

Samples denoted F2.5 and F3.0, which were obtained from 3M, were composed of KL68 in a mixture of trimethylolpropane triacrylate (SR351) and tetrahydrofurfuryl acrylate (SR285), referred to as AR5 resin. Diaryliodonium hexauroantimonate (iodonium salt) was also obtained from 3M.

4.2.2 Optical setup

Polymerization was performed with a tunable Ti:sapphire oscillator (Coherent Mira 900-F) with a center wavelength of 800 nm, a pulse duration of ∼150 fs, and a repetition rate of 76 MHz. A solid-state, diode-pumped laser (Coherent Verdi V10) was used as the 532 nm, CW source. The beams were combined by a polarizing beam cube and directed to a sample by a dichroic mirror through a 100×, 1.45 NA, oil-immersion objective (Zeiss R Plan-FLUAR) mounted on an inverted microscope (Zeiss Axiovert 100). Cover slips with resin samples were mounted on a 3-axis piezoelectric stage for fine sample positioning in all dimensions. The piezo stage was attached to a motor-driven stage for coarse sample positioning. The movement of the sample stage was controlled using LabVIEW programs, and fabrication was followed in real time using a CCD camera and a monitor. To ensure alignment of the two laser focal spots within the sample, the laser beams were scanned over gold nanoparticles deposited on a cover slip. Multiphoton absorption induced luminescence, which was collected using single-photon-counting avalanche photodiodes, was used to determine the position and shape of the point-spread function of each beam [84].

4.3 Results and discussion

4.3.1 KL68 characterization

The UV-visible absorption spectrum of KL68 in toluene (Fig. 4.2) shows an absorption band centered at 430 nm and a weaker band at 300 nm. To determine the polymerization rate and fabrication velocity dependence, both samples F2.5 and F3.0 were exposed to a single 800 nm ML beam at various powers and velocities.

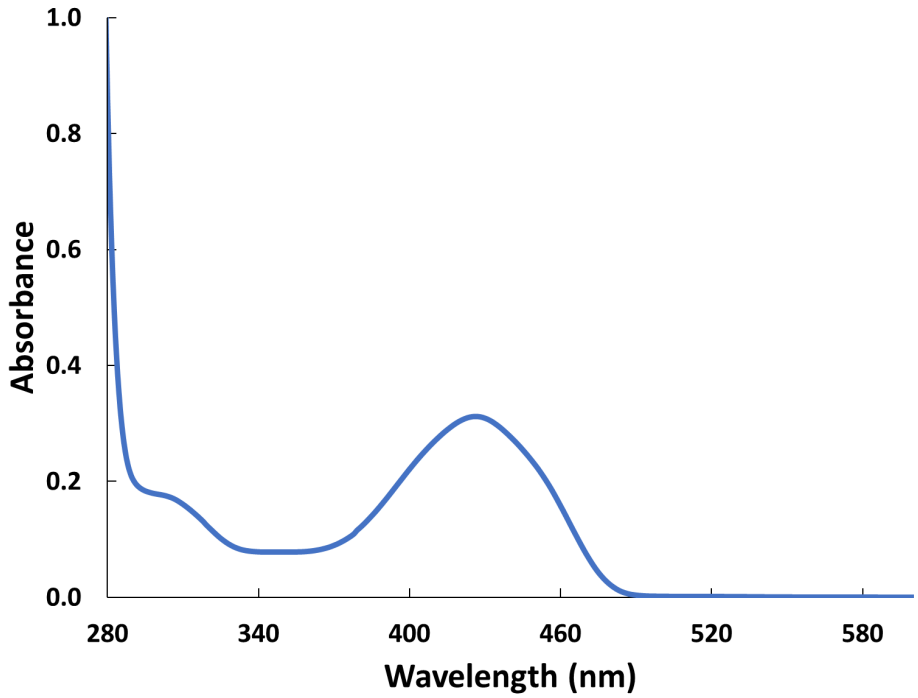

Figure 4.2: Absorption spectrum of KL68 in toluene.

The fabrication velocity for sample F3.0 ranged from 70 μm/sec to 240 μm/sec in 10 μm/sec steps, and from 200 μm/sec to 300 μm/sec in 20 μm/sec steps. At powers above 14 mW, the sample was overexposed, resulting in burns in the focal

region of the laser beam. Therefore, the exposure experiments were performed with laser power set at 9 mW at the sample plane.

At this power no polymerization was observed at velocities lower than 80 μm/sec and fabricated lines were observed at velocities of 100 μm/sec or more. No decrease of linewidth was observed with increasing velocity in the range from 100 μm/sec to 300 μm/sec.

Sample F2.5 was exposed at powers of 16 mW, 14.5 mW, and 12 mW. Because F2.5 also exhibits negative contrast behavior [109], polymerization was initiated at velocities from 30 μm/sec to 400 μm/sec. At 16 mW and 14.5 mW exposure beam powers, the photoresist burned within the laser focus at velocities from 350 μm/sec to 400 μm/sec. To cover a wider range of velocities, the power of the fabrication beam was set to 12 mW. At this power, no polymerization was observed below a velocity of 200 μm/sec.

To understand the relationship between the fabrication velocity and initiation, reciprocity curves were measured in a photoresist containing 0.0075 wt% KL68 in a 1:1 SR368/499 mixture. For this sample, polymerization was initiated with a single 800 nm ML beam. The minimum laser power required to initiate polymerization (the polymerization threshold) was measured at fabrication velocities ranging from 0 μm/sec to 400 μm/sec.

As shown in Fig. 4.3, the polymerization threshold power decreases significantly as the fabrication velocity is increased from 5 μm/sec to 150 μm/sec, and remains roughly constant in the range of fabrication velocities from 150 μm/sec to 400 μm/sec.

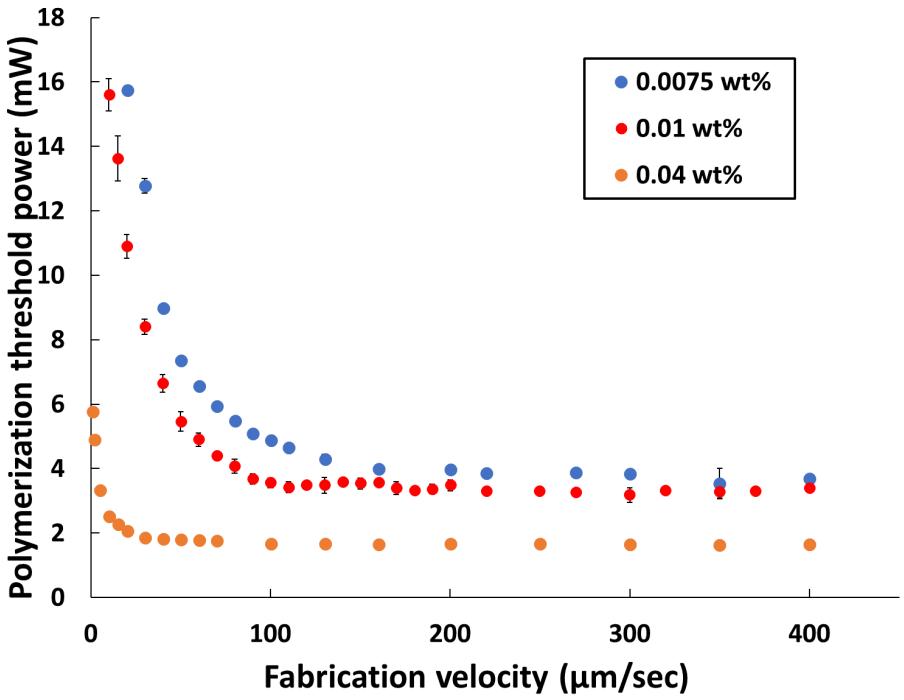

Figure 4.3: Polymerization threshold power for 800 nm initiation at various fabrication velocities for resins with three different KL68 concentrations.

The trend was similar for resists with 0.01 wt% and 0.04 wt% KL68 as well. As the concentration of KL68 in the photoresist increases, the polymerization threshold decreases for every given velocity, becoming constant at a lower power value for each higher KL68 concentration. For example, at 20 μm/sec the polymerization threshold power decreases from about 16 mW to 2 mW as the concentration of KL68 is increased from 0.0075 wt% to 0.04 wt%.

Other photoinitiators that were tested, such as TPO-L and MGCB, exhibit the opposite behavior (positive contrast): increasing the fabrication velocity increases the polymerization threshold. Because higher velocities correspond to shorter ex-

posure times, a higher laser intensity is required to initiate polymerization when fabricating more rapidly. For negative-contrast photoresists such as the one in Fig. 4.3, longer exposure times lead to finer features or even the complete absence of polymerization unless the laser power is increased. This effect may be due to a self-deactivation process. As has been shown before [3], polymerization deactivation in some photoresists can be achieved by addition of a second CW beam. For other photoresists [83], deactivation is more efficient, so that the excitation laser pulses can drive deactivation. This phenomenon can cause longer exposure times to lead to thinner structures.

4.3.2 2-BIT study of KL68

To investigate the negative-contrast behavior, the order of effective nonlinear absorption was measured through 2-BIT (2-beam initiation threshold) experiments at different fabrication velocities as described in Chapter 3. Each laser power value was normalized to the polymerization threshold and the best-fit exponential was determined by nonlinear least-squares fitting of the recorded data to Eq. 3.13. Each data point is an average of at least 5 measurements, and the error bars in figures with 2-BIT data represent plus or minus one standard deviation.

Fabrication velocities for 2-BIT measurements were chosen from a reciprocity curve. Fig. 4.4 shows a representative reciprocity curve for sample of photoresist containing 0.1 wt% KL68.

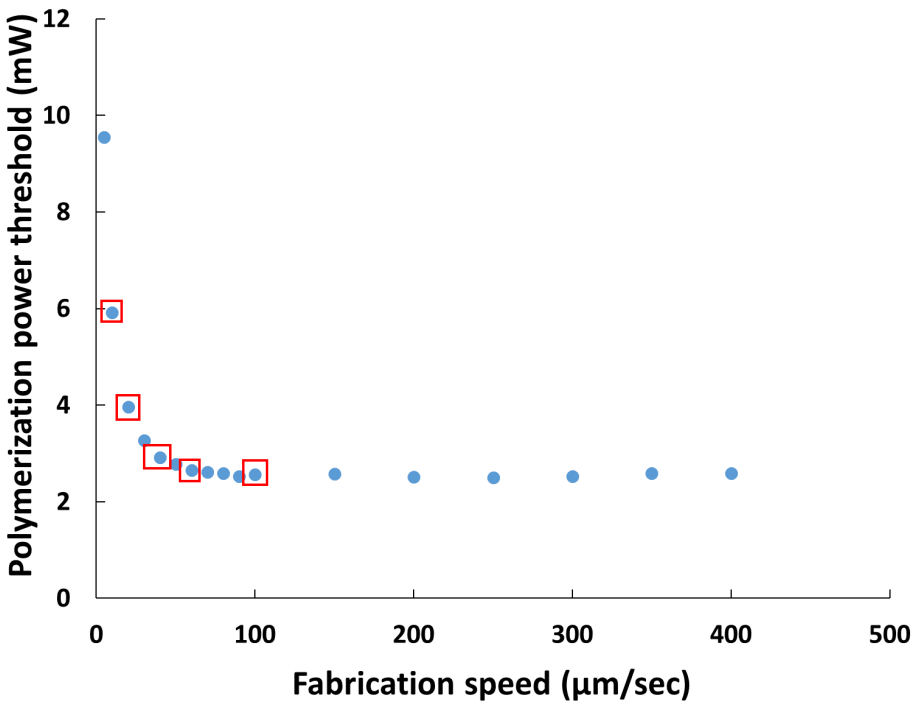

Figure 4.4: Power threshold as a function of fabrication speed in 0.1 wt% KL68 in 1:1 SR368/499. Red squares represent fabrication velocities for which 2-BIT measurements were performed: 10, 20, 40, 60, and 100 μm/sec.

Several fabrication velocities within the region of the nonlinear relationship between power threshold and fabrication velocity (10 μm/sec, 20 μm/sec, and 40μm/sec) were chosen for 2-BIT measurements, as were two fabrication velocities in the region in which the polymerization threshold becomes independent of the fabrication speed (60 μm/sec and 100 μm/sec). The 2-BIT data are shown in Fig. 4.5. The exponents were extracted from each 2-BIT data set, and are summarized in Table 4.1. With the exception of 20 μm/sec, as fabrication speed increases, the order of effective nonlinear absorption increases as well.

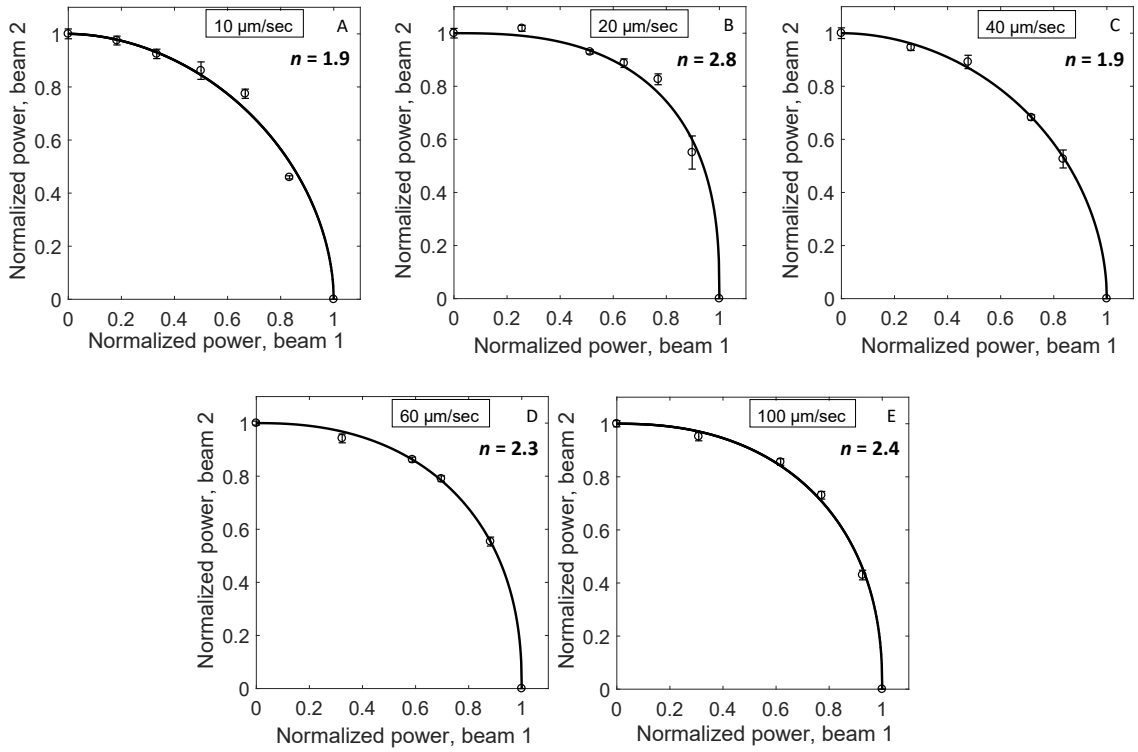

Figure 4.5: 2-BIT data measured using 800 nm, ML excitation in a resist containing 0.1 wt% KL68 at various fabrication velocities: A) 10 μm/sec; B) 20 μm/sec; C) 40 μm/sec; D) 60 μm/sec; and E) 100 μm/sec.

Although the exponent is $\sim$2 under some conditions, which is indicative of a conventional 2-photon absorption process, at most of the velocities the exponent is greater than 2. These data indicate that processes other than 2-photon absorption affect the exponent, including some sort of deactivation process. It is likely that at all velocities the exponent reflects some sort of a balance between 2-photon absorption and other phenomena.

Fabrication velocity, μm/sec	n
10	1.9 ± 0.2
20	2.8 ± 0.4
40	1.9 ± 0.1
60	2.3 ± 0.1
100	2.4 ± 0.2

Table 4.1: Order of effective nonlinear absorption of photoresist containing 0.1 wt% KL68 measured at different velocities.

4.3.3 KL68 power threshold with iodonium salt

It has been shown previously that the presence of an iodonium salt affects the shape and size of polymerized structures and voxels [109,110]. To study the effect of iodonium salts on polymerization efficiency, iodonium salt (diaryliodonium hexauroantimonate) was added to photoresists containing KL68 at various concentrations. Reciprocity curves were measured for samples with two concentrations of KL68 and sets of iodonuim salt for each KL68 concentration in 1:1 SR368/499. Samples measured included 0.1 wt% of KL68 with 0.5, 0.3, 0.1, 0.05, or 0 wt% iodonium salt, and 0.01 wt% of KL68 with 0.03, 0.01, 0.005, 0.001, or 0 wt% iodonium salt.

As shown in Fig. 4.6, the presence of salt at a low concentration strongly increases the polymerization threshold. A further increase of the salt concentration either decreases the threshold slightly or has no effect. To compare the effect of salt

on the polymerization efficiency, the polymerization threshold value was plotted as s function of salt concentration at each fabrication velocity.

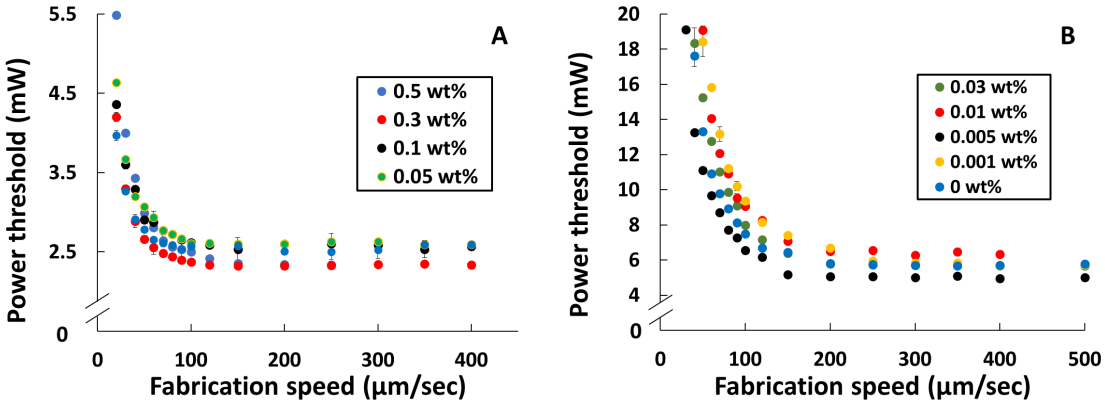

Figure 4.6: Reciprocity curves for two different concentrations of KL68 in the resin mix of 1:1 SR368/499: A) 0.1 wt% KL68; B) 0.01 wt% KL68. Each curve corresponds to a different iodonium salt concentration. The salt concentrations tested ranged from 0.005 wt% to 0.5 wt%.

As can be seen in Fig. 4.7, for a 50 μm/sec fabrication speed, the dependence of the power threshold on the salt concentration is complex. An oscillating ratio between the power threshold and the salt concentration is observed. The ratio between the polymerization threshold and the salt concentration becomes more linear as the fabrication speed is increased. The strongest effect of salt on the polymerization efficiency was observed for the slowest fabrication speeds.

Several effects could play a significant role in this phenomenon, including local thermal heating from longer laser exposure. To study thermal effects on polymerization efficiency, an objective heater was used to heat the oil-immersion objective and, consequently, heat the sample. Reciprocity curves were measured in a sample containing 0.01 wt% KL68 in 1:1 SR368/499 with 0.01 wt% iodonium salt at three

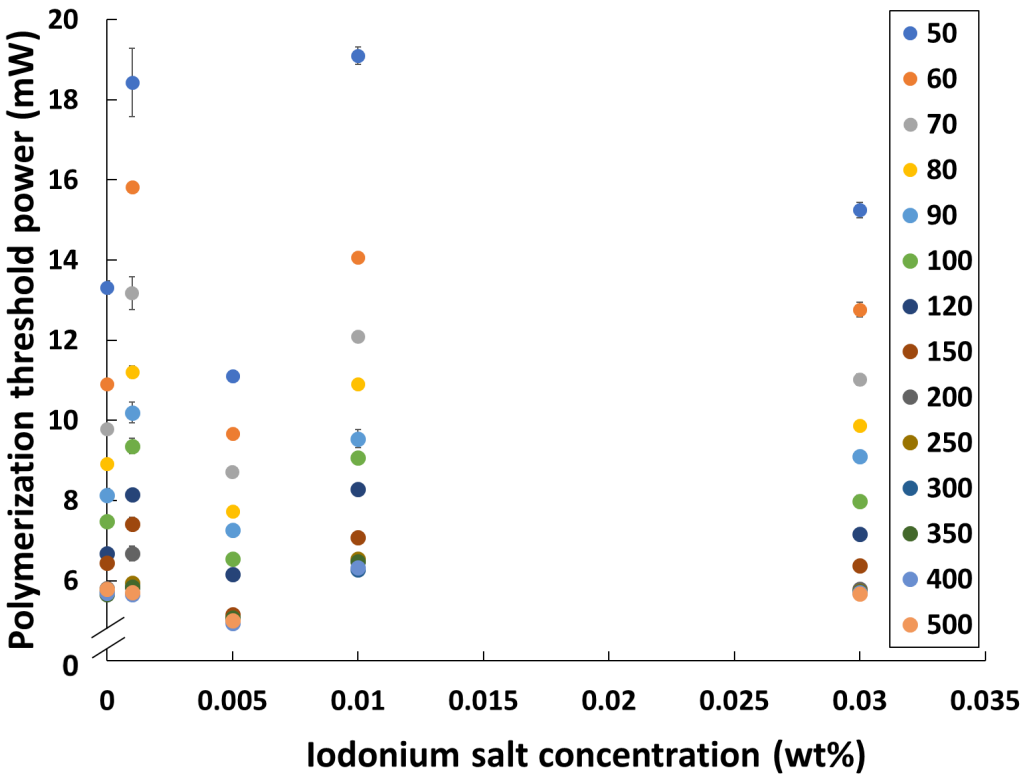

Figure 4.7: Polymerization threshold power values for different salt concentrations extracted from reciprocity curves for 0.01 wt% KL68 in 1:1 SR368/499. Each data point in the legend corresponds to a different fabrication velocity in μm/sec.

different temperatures: 23.7 °C (room temperature), 27 °C, and 30 °C. The data presented in Fig. 4.8 demonstrate that there is an increase in the polymerization threshold by a factor of 2 for a temperature increase between 23.7 °C and 30 °C. At all temperatures, the polymerization threshold decreases significantly when the fabrication speed increases from 20 μm/sec to 300 μm/sec, and remains independent of the fabrication speed in the range from 300 μm/sec to 1 cm/sec.

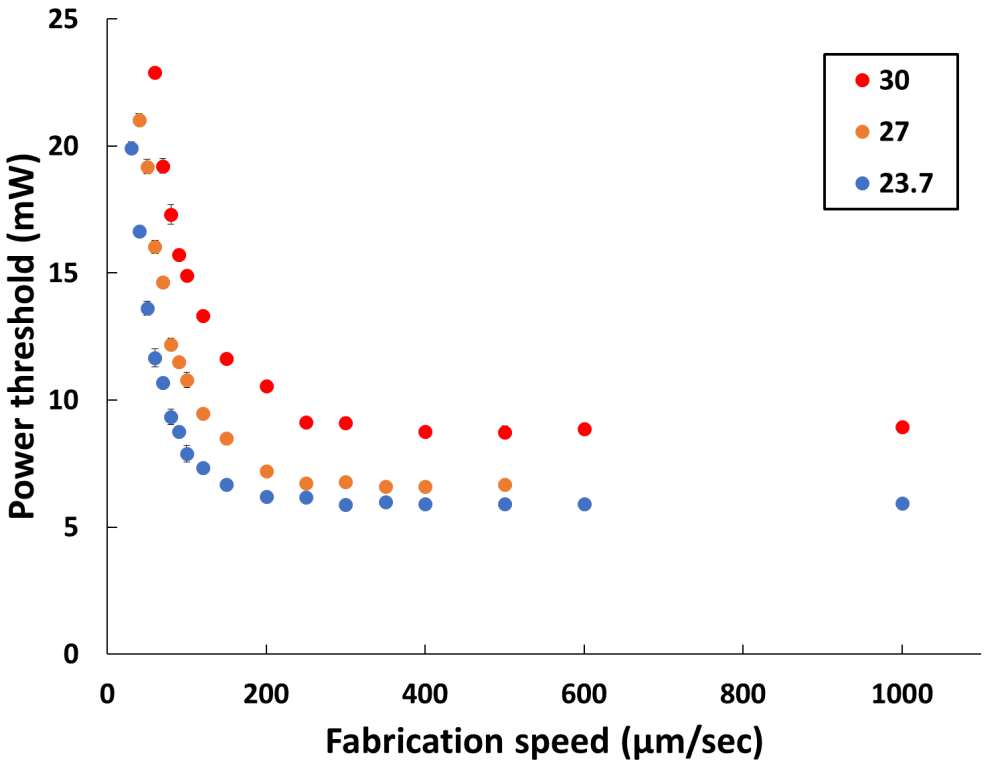

Figure 4.8: Reciprocity curve for 0.01 wt% KL68 in 1:1 SR368/499 with 0.01 wt% iodonium salt at three different temperatures: 23.7 °C (room temperature), 27 °C, and 30 °C.

4.3.4 Temperature effects

The effects of temperature on polymerization efficiency were studied further in photoresist samples containing KL68, MGCB, MGC-HCl and TPO-L. The temperature of each sample was increased from room temperature to 33 °C with an objective heater.

Sets of rows were fabricated for each sample and temperature. Each row had 20 cells with dimensions of 5 μm×10 μm. A spot in the center of each cell was exposed for 0.5 sec with the 800 nm ML beam. The focal height varied by

100 nm between adjacent cells, and ranged from 0 to 2 μm above the surface. At lower heights no features were fabricated, because the focus was inside the substrate and the intensity exposing photoresist was below threshold. As the focal point moves into the photoresist, the laser exposes a greater volume of the photoresist, creating larger volume elements (voxels). At some height, the voxels are barely attached to the substrate and fall over. Fallen voxels are ideal for imaging [9]. All measurements within each sample were performed at a constant laser power, and 10 to 15 measurements were made for each height.

After developing samples, the height and width of fallen voxels were measured using SEM. A representative fallen voxel is shown in Fig. 4.9.

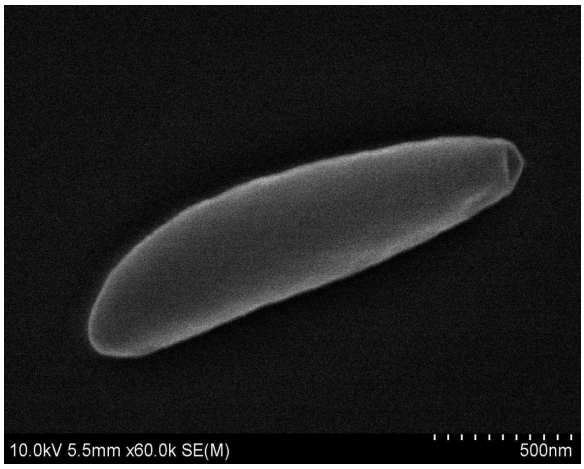

Figure 4.9: Scanning electron micrograph of a fallen voxel.

For samples containing MGCB, TPO-L or MGCB in 1:1 SR368/499, sample heating either had no effect on polymerization or caused an increase in voxel size over the measured temperature range. For a sample containing 1.5 wt% MGCB at 24.4 °C, 27 °C, 30 °C, and 33 °C, polymerization was initiated by an 800 nm ML beam

set at 16 mW at the sample plane. An analysis of SEM measurements, presented in Fig. 4.10, shows that the average widths of the fallen voxels ranged between 520 nm to 560 nm, with no statistically significant temperature dependence. The change in the average height with increasing temperature was slightly more pronounced, varying from 2.08 μm at 23.7 °C to 2.00 μm at 33 °C. It is not clear if the change in height is statistically significant.

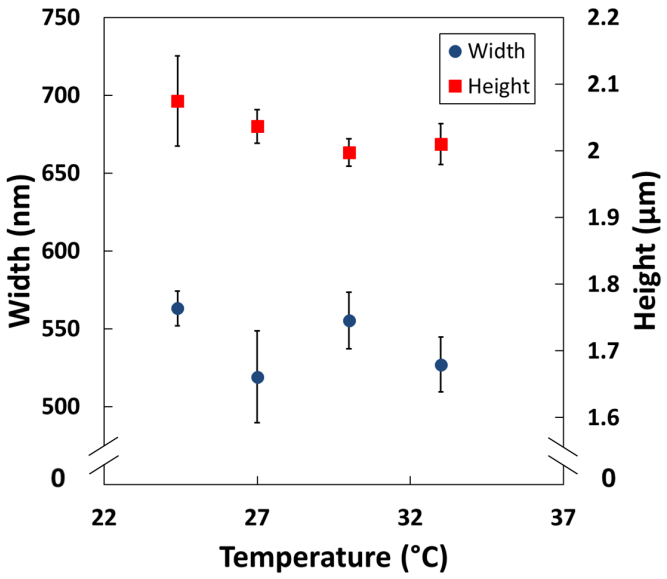

Figure 4.10: Voxel size temperature dependence for sample 1.5 wt% MGCB in 1:1 SR368/499.

A similar tendency was observed for 3 wt% TPO-L in 1:1 SR368/499. As shown in Fig. 4.11, the average dimensions of the voxels decreased from 1.84 μm to 1.66 μm with a temperature increase of 8.4 °C. The average voxel width was nearly constant throughout this temperature range. However the shape of some of

the voxels was deformed, resulting in a larger deviation from the average of over 20 measured voxels at each temperature point. Again, it is not clear that any changes in voxel size with temperature are statistically significant.

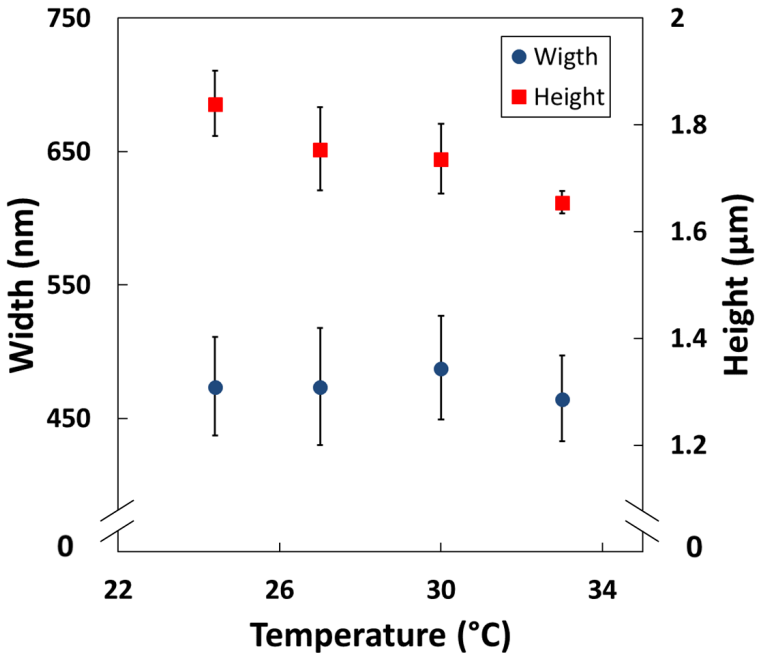

Figure 4.11: Voxel size temperature dependence for a sample of 3 wt% TPO-L in 1:1 SR368/499.

The thermal effect on voxel dimensions was the strongest in samples containing KL68. This photoinitiator was studied in both photoresist AR5 from 3M (sample noted F2.5) and a typical monomer mixture of 1:1 SR368/499. Both samples were measured over a smaller temperature range, as the voxels disappeared at higher temperatures. At room temperature (24 °C) the laser power was set to a value above the polymerization threshold for which exposure for 0.5 sec did not cause

sample damage and polymerized lines of the reference rows were visible. This power was used for all measurements. With increasing temperature, reference lines and voxels became less visible, indicating a slower polymerization rate. At 30 °C, no lines were observed and voxels were barely noticeable. Increasing the temperature more resulted in the complete absence of polymerization.

The data in Fig. 4.12 show that raising the temperature by 6 °C causes the average voxel height to decrease from ∼800 nm to ∼400 nm and the average width to decrease from ∼220 nm to ∼160 nm. These measurements were repeated several times in different samples, and the results were comparable each time.

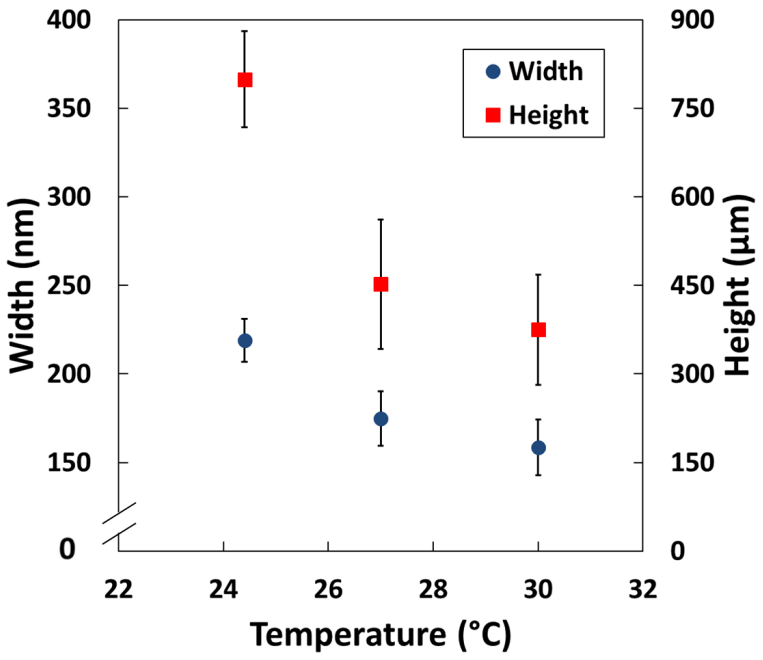

Figure 4.12: Voxel size temperature dependence for sample F2.5.

For samples containing 0.05 wt% KL68 in 1:1 SR368/499, both the average voxel height and the average voxel width decreased with increasing temperature. Polymerization was not observed for a temperature increase over 3 °C. As shown in Fig. 4.13, over this temperatures range the average voxel height decreased from 1150 nm to 980 nm and the average voxel width decreased from ∼310 nm to ∼270 nm.

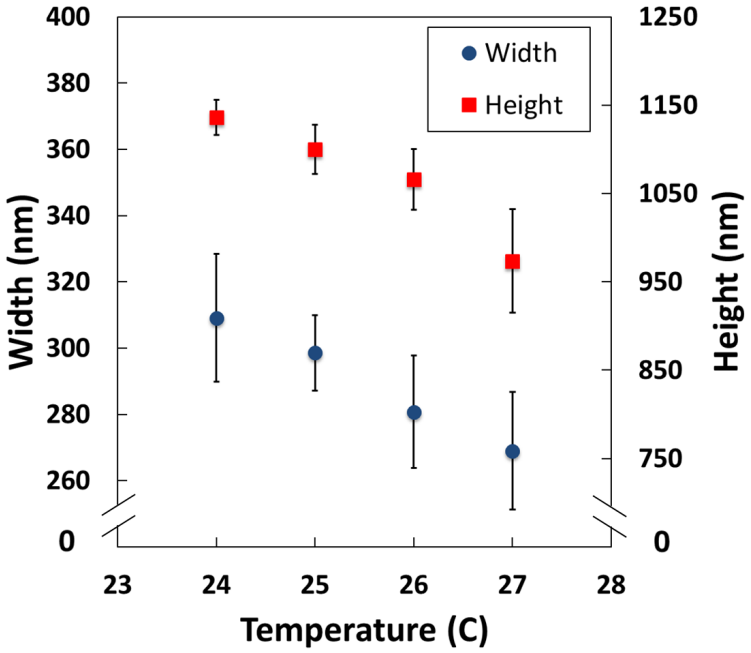

Figure 4.13: Voxel size temperature dependence for sample of 0.05 wt% KL68 in 1:1 SR368/499.

4.3.5 Two beam study

As was mentioned above, for a negative contrast photoresist, an excitation beam that drives polymerization can also deactivate photoinitiator molecules, causing fabrication of smaller features at longer exposure times (or slower fabrication velocities). Because the polymerization rate in photoresists containing KL68 is highly dependent on temperature, a longer exposure time could also be locally heating the photoresist, leading to the creation of smaller features.

Thermal polymerization deactivation was tested by exposing resists containing KL68 to two lasers at various wavelengths, including studies in which we changed the distance between the beams and or introduced exposure delays. Sets of lines were written with two 800 nm ML lasers at various fabrication velocities under two conditions: 1) both beams overlapped in the XY plane; 2) one beam offset along the X axis relative to the center of the other beam (Fig. 4.14).

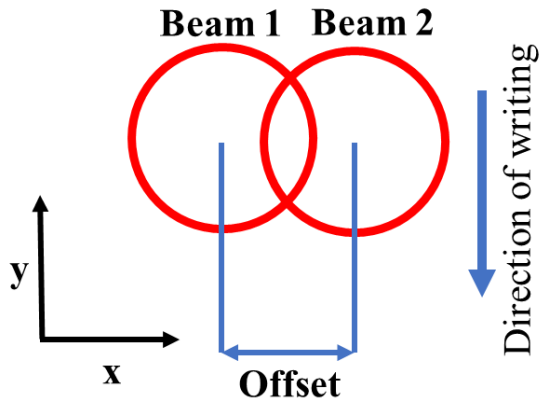

Figure 4.14: Schematic diagram of the two-beam exposure experiment.

In F3.0, the two 800 nm beams were tested at different powers - the first beam was set at 22 mW or 15 mW and the second beam was set at 9 mW, 15 mW or 30 mW. To distinguish the first and second laser beams, a mechanical chopper was used to periodically block and unblock the second beam; the first beam was unblocked at all times. All lines were fabricated at 100 μm/sec. As before, no polymerization was observed below 80 μm/sec with single-beam exposure at 9 mW.

For all tested power combinations, two overlapping 800 nm ML beams created wider lines than did single-beam exposure. The fabricated lines were examined with SEM. The widths of the lines made with the first beam were 340 $\pm$20 nm, compared to 420 $\pm$18 nm when the two beams were overlapped (Fig. 4.15).

For a second test, various offsets of the two lasers were explored. The presence of a second laser focus adjacent to the first focus could create a temperature gradient, and potentially lead to polymerization deactivation. As before, the second laser beam was chopped periodically. For all offsets between the two beams, the widths of the fabricated lines increased (Fig. 4.16).

Overlapping of an 800 nm ML beam and an 800 nm CW beam was used to test for photodeactivation. The sample stage was moved at velocities ranging from 80 μm/sec to 300 μm/sec. The excitation beam power was set at 12 mW at the sample plane. The CW beam power was set at 18, 36, 54, 90, 100 and 120 mW to determine the effect of its power on the polymerization rate. No polymerization was observed under CW exposure at any velocity. However, when the CW beam exposed the sample at the same time as the ML beam, the width of the fabricated lines increased as compared to those fabricated with the ML beam alone. This poly-

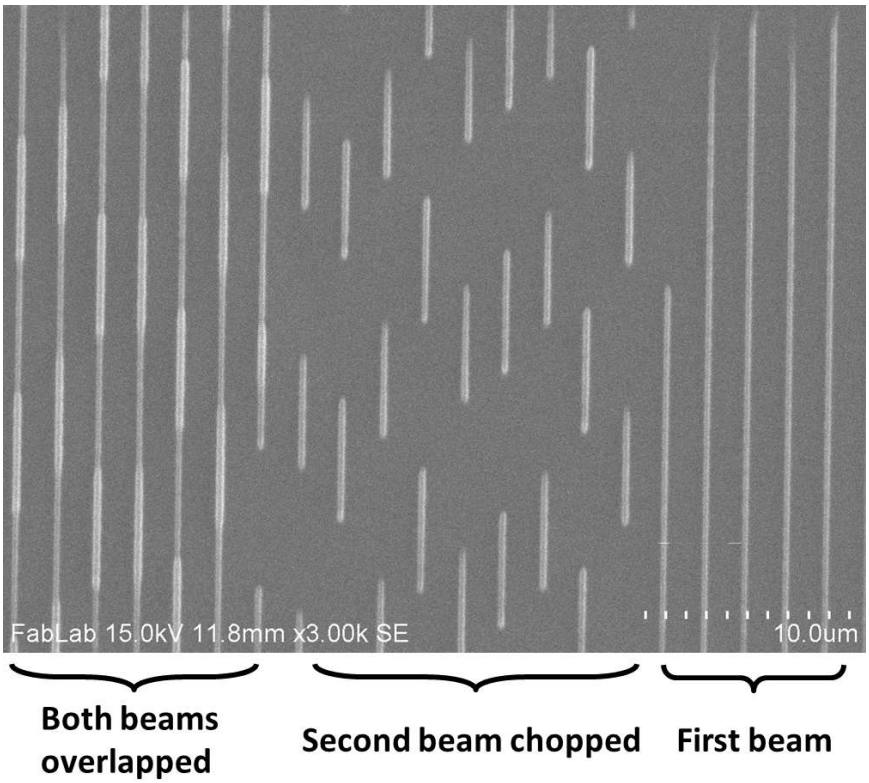

Figure 4.15: SEM image of lines fabricated in F3.0 with two 800 nm ML laser beams. The first beam was unblocked at all times, creating solid lines. The second beam was chopped periodically, leading to fabrication of dashed lines. The two overlapping beams produced wider lines, compared to single-beam exposure.

merization enhancement was observed for all beam powers and fabrication velocities tested. Therefore, addition of 800 nm CW light does not deactivate photoinitiator molecules, but rather enhances polymerization. The results of these experiments are summarized in Table 4.2.

The two-beam deactivation experiment was also performed for F2.5. Mode-locked exposure initiated polymerization at 12 mW, but only at velocities above 200 μm/sec. This was the lowest power that did not cause local burning at the range

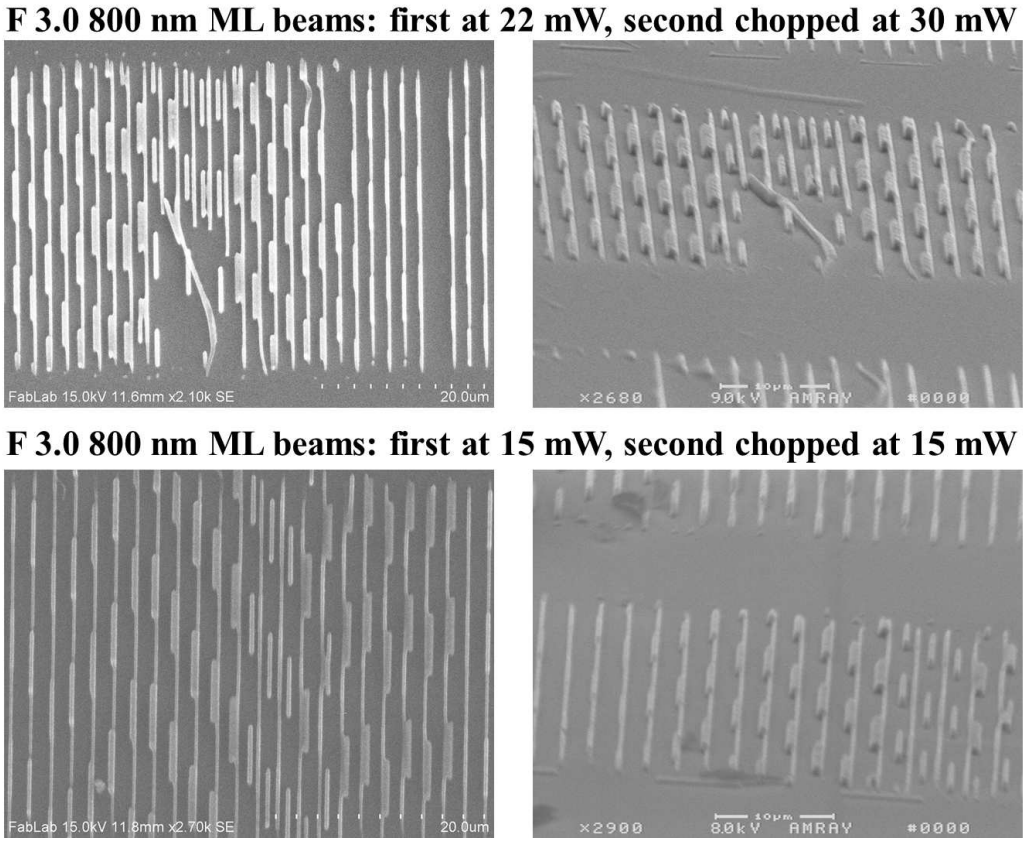

Figure 4.16: SEM images of lines fabricated in F3.0 with two 800 nm ML beams at various offsets. The left panels show top-views and the right panels show side-views of lines fabricated at various offsets between the two laser beams.

of velocities from 200 μm/sec to 450 μm/sec. For dual-beam exposure, one ML beam was set at 12 mW and the other was set at 3 mW, 6 mW or 9 mW. All three combinations led to wider lines.

Similar polymerization enhancement was observed when 800 nm ML and CW beams were combined. Fabrication velocities from 200 μm/sec to 450 μm/sec and CW beam powers at 60, 90, 100, 120, and 150 mW were tested. For all power

<table>
<tr><th>800 nm ML, mW</th><th>800 nm CW, mW</th><th>Velocity, μm/sec</th><th>Result</th></tr>
<tr><td rowspan="2">12</td><td>18, 36, 54, 100, 120, 150</td><td>60, 70, 80, 90, 100, 120, 130, 140, 150, 160, 170, 180, 190, 200, 250, 300</td><td rowspan="2">Linewidth increase when two beams exposing the sample, compared to 800 nm ML alone</td></tr>
<tr><td>18, 120, 140, 180</td><td>80</td></tr>
</table>

Table 4.2: Summary of two-beam exposure parameters for testing deactivation in the F3.0.

combinations and velocities, the lines became wider when CW light was added. The summary of of these experiments is shown in Table 4.3.

Exposure of F2.5 and F3.0 to a combination of two 800 nm ML beams or to 800 nm ML and CW beams yields wider lines compared to single-beam 800 nm ML exposure. For a wide range of tested powers and fabrication velocities polymerization enhancement was observed under both conditions.

Comparison experiments were performed in a resin containing KL68 in 1:1 SR368/499. Dual-beam experiments in this sample were performed by combining

<table>
<tr><th>First beam, 800 nm ML, mW</th><th>Second beam, 800 nm ML, mW</th><th>Second beam, 800 nm CW, mW</th><th>Result</th></tr>
<tr><td rowspan="8">12</td><td>3</td><td rowspan="3"></td><td rowspan="8">Linewidth increases when two beams exposing a sample, compared to a first beam only</td></tr>
<tr><td>6</td></tr>
<tr><td>9</td></tr>
<tr><td rowspan="5"></td><td>60</td></tr>
<tr><td>90</td></tr>
<tr><td>100</td></tr>
<tr><td>120</td></tr>
<tr><td>150</td></tr>
</table>

Table 4.3: Summary of two-beam exposure parameters for testing deactivation in F2.5.

800 nm ML and 880 nm ML beams as well as 800 nm ML and 800 nm CW or 880 nm CW beams.

For 800 nm ML and 880 nm ML excitation, polymerization was initiated at 50 μm/sec at 2 mW and 5 mW, respectively. Combining 800 nm ML and 800 nm CW beams at 2 mW and 110 mW respectively led to wider lines, whereas combining an 800 nm ML beam at 2 mW and an 880 nm CW beam at up at 40 mW did not affect the size of the polymerized lines. A summary of the dual-beam exposure experiments is presented in Table 4.4.

As was described above, increasing the sample temperature leads to a decrease in polymerization. Because an objective heater was used to control the temperature,

	0	800 nm ML	880 nm ML
532 nm CW	Does not polymerize		
800 nm ML	Polymerizes		Enhances polymerization
800 nm CW	Does not polymerize	Enhances polymerization	
880 nm CW	Does not polymerize	No effect	

Table 4.4: Summary of dual-beam exposure experiments in 0.05 wt% KL68 in 1:1 SR368/499.

the entire sample was heated, making it challenging to perform reference experiments within the sample. To heat a sample in a smaller area, the photoresist temperature was increased by exposing a spot in the sample to a CW beam at a wavelength that does not lead to polymerization.

A single 880 nm CW beam was used to expose a spot in the photoresist prior to initiating polymerization with the 800 nm ML beam. The CW beam was first offset with respect to the ML beam. A 40 μm line was scanned with the ML beam blocked. Then the CW beam was blocked and a line was scanned across the same area with the ML beam. Because of the offset, the first 10 μm of the line was not

exposed to the CW beam. A single scan initiated at an offset between the centers of 800 and 880 beams along the direction of fabrication allows us to compare the linewidth in the region not previously exposed to the CW beam to that in the pre-scanned spots.

The widths of lines that were fabricated in the area pre-scanned at 880 nm were the same as those lines in the sample region exposed to 800 nm only. This result suggests that the power of the CW beam was not high enough to generate the desired temperature gradient. Increasing the number of scans with the 880 nm beam led to the formation of finer lines. Ten and twenty scans visibly reduced the width of the lines fabricated with 800 nm ML exposure.

In conclusion, both 800 nm ML and 880 nm ML light can initiate polymerization in the photoresist. Simultaneous exposure to both 800 nm ML and 800 nm ML or 800 nm ML and 800 CW beams increases the linewidth.

Exposure of the sample to an 880 nm CW beam prior to 800 nm ML polymerization leads to narrower lines. Because 880 nm is close to the end of the tuning range of our laser, the available power was not sufficient for spot exposure experiments. Therefore, for thermal deactivation studies 532 nm CW light was used.

4.3.6 Thermal deactivation with a 532 nm CW beam

Because KL68 in toluene has an absorption maximum near 430 nm, polymerization initiation was tested at 800 nm. Individual polymerized lines were created in a sample containing 0.05 wt% of KL68 in a 1:1 SR368/499. Exposure to a combina-

tion of an 800 nm ML beam and an 800 nm CW beam yielded thicker lines than did 800 nm ML exposure alone. This result was also observed for F2.5 (KL68 in AR5 resin). Exposure to a 532 nm CW beam did not lead to polymerization at powers up to 50 mW at velocities from 2 μm/sec to 200 μm/sec. Therefore, 532 nm light was used to heat the sample locally prior to polymerization with 800 nm pulses.

To test the local heating effect of the 532 nm CW beam, the center of 532 nm beam was set 6 μm ahead of the 800 nm ML beam, and exposed a spot for 2 mins. The 532 nm CW beam was then blocked and the 800 nm beam was used to write at a power of 2.5 mW or 3 mW. A diagram of this experiment is presented in Fig. 4.17.

Because KL68 does not absorb at 532 nm, the effect of 532 nm CW heating was not pronounced. To increase absorption at 532 nm and heat the photoresist to a higher temperature, the photoresist was mixed with different dyes, which led to a stronger temperature effect on the polymerization rate.

4.3.7 Thermal deactivation with 532 nm CW beam and various dyes

One of the potential dyes with an absorption band around 532 nm, Sulphorhodamine 101 (SRd101), was first mixed in 1:1 SR368/499. No polymerization was initiated with either an 800 nm ML beam or a 532 nm CW beam. The powers tested were up to 40 mW for the 532 nm CW and up to 40 mW for the 800 nm ML beam, above which the resist burned. These powers are consistent with those at which the monomer mixture burns.

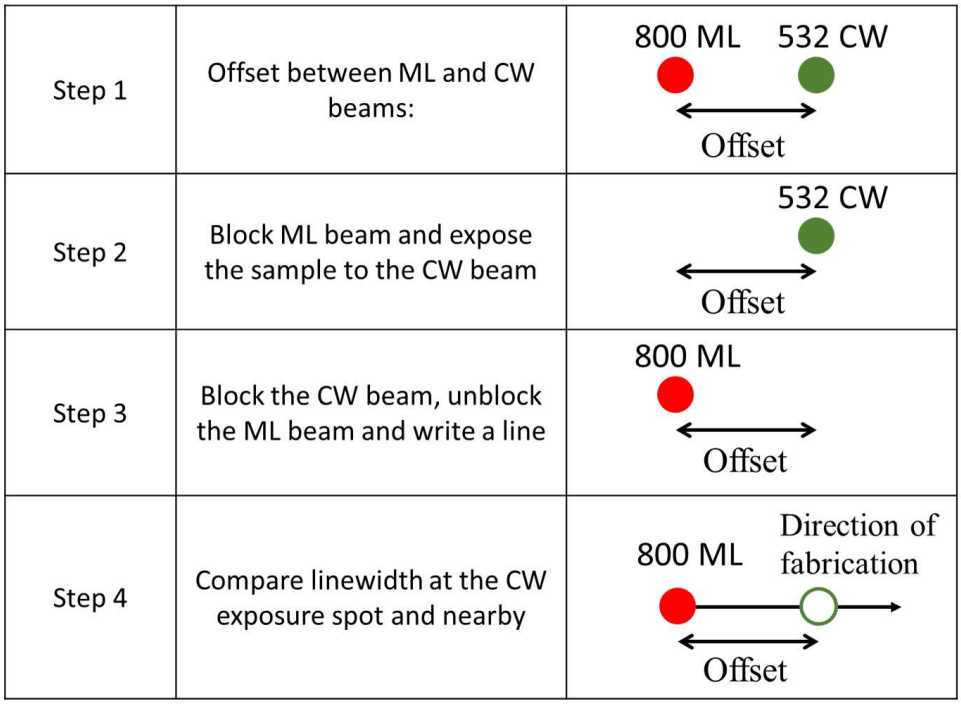

Figure 4.17: Experimental scheme for exploring the effect of spot exposure by a 532 nm CW beam on polymerization initiated by an 800 nm ML beam. The CW beam was focused about 6 μm away from the ML beam along the direction of fabrication. The 532 nm beam was unblocked for a desired time. It was then blocked and a line was fabricated with the 800 nm beam. The grey circle in Step 4 corresponds to the spot exposed to the 532 nm CW beam.

The local heating effect of 532 nm CW spot exposure was tested in a sample containing 0.05 wt% KL68 and 0.5 wt% SRd101 in 1:1 SR368/499. Polymerization was initiated at 800 nm at a constant fabrication velocity. The 532 nm beam focus was set at 6 μm from that of the 800 nm beam in the direction of fabrication, as shown in Fig. 4.18.

The power of the 800 nm beam was set at 3.5 mW and the power of 532 nm beam was set at 5, 13, or 24 mW at the sample plane. The exposure times tested for

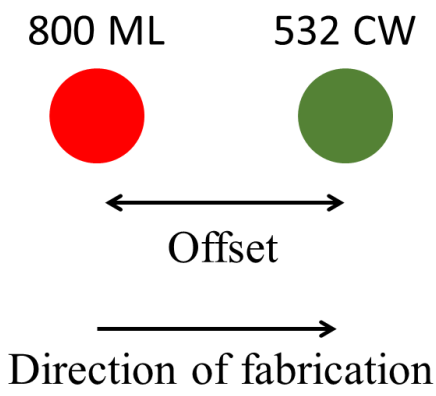

Figure 4.18: Schematic diagram of the spot exposure experiment at 532 nm.

the 532 nm beam included 10 sec, 30 sec and 60 sec. SEM images of the fabricated lines are presented in Figure 4.19.

The red lines in Fig. 4.19 correspond to regions without any 532 nm CW exposure. Green ellipses are drawn around the areas in which the 532 nm beam affected polymerization. The center of each ellipse corresponds approximately to the center of the 532 nm beam. The width of the top line 1 on image Fig. 4.19A, fabricated prior to any exposure to 532 nm, is constant throughout the SEM image. The second line was polymerized with 800 nm ML beam after the 532 nm beam, set at 24 mW, exposed a spot for 60 sec. The following lines were alternating: line 3 was fabricated with the 800 nm beam only, line 4 was fabricated after 532 nm exposure, and line 5 was fabricated with the 800 nm beam only. The lines in Fig. 4.19B-G were made following the same pattern.

The strongest effect of exposure at 532 nm was observed for highest power, 24 mW. Lines in the exposed areas were thinner or absent entirely. Exposure at this

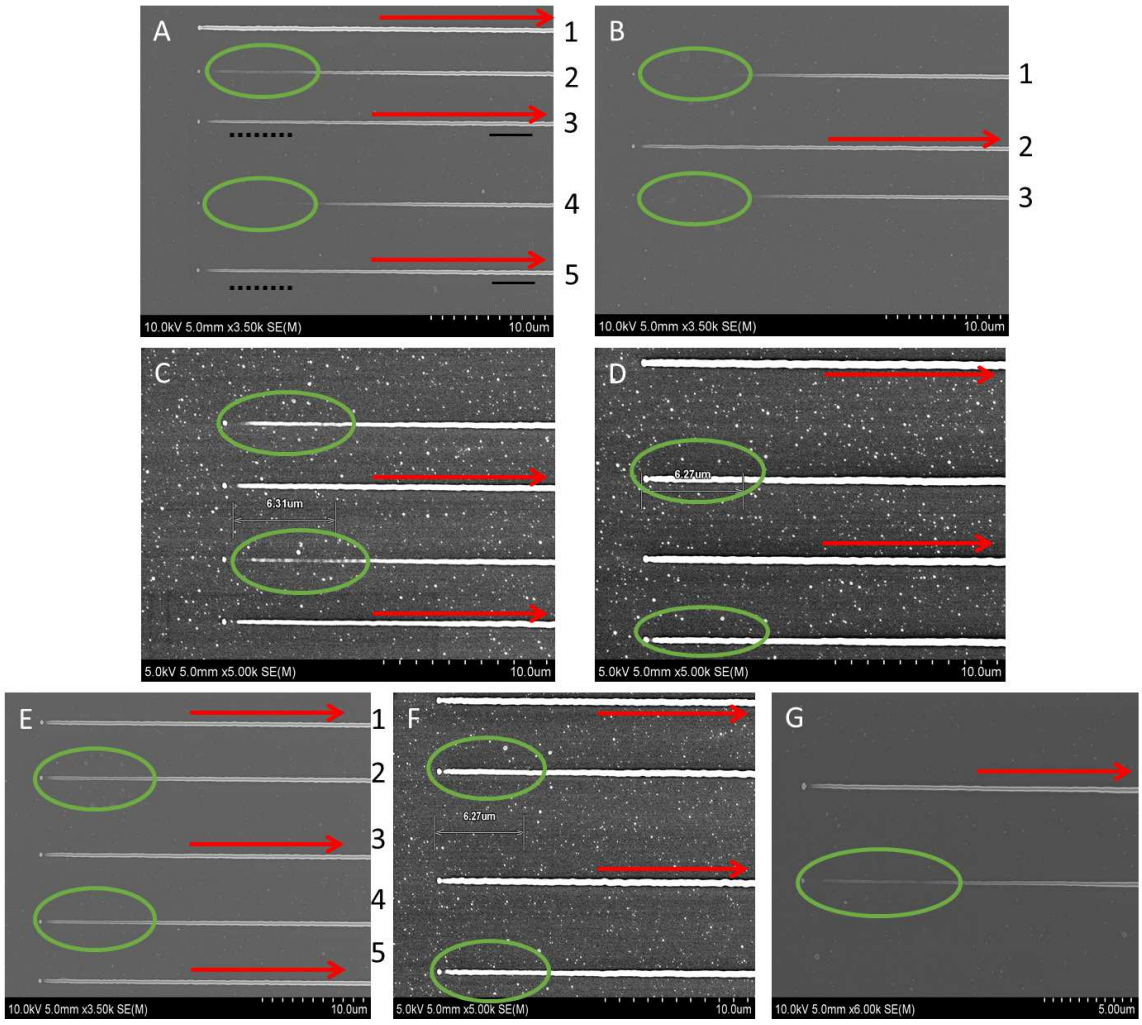

Figure 4.19: SEM images of lines polymerized with 800 nm light following 532 nm spot exposure. The wider lines indicated by red arrows correspond to reference lines fabricated without 532 nm exposure along the line. The green ellipses correspond to lines fabricated in the area exposed to the 532 nm beam. Dashed black lines indicate the lines in the region around 532 nm exposure. The solid black lines indicate lines formed in spots not affected by the 532 nm beam. Powers and exposure times for 532 nm beam were: A) 24 mW for 60 sec; B) 24 mW for 30 sec; C) 13 mW for 60 sec; D) 13 mW for 30 sec; E) 24 mW for 10 sec; F) 13 mW for 10 sec; G) 5 mW for 50 sec.

power for 60 seconds had a stronger effect on surrounding photoresist areas as well.

The dashed lines in Fig. 4.19A indicate a region of line 3 that was not exposed to 532

nm light. However, width of the line in this region is around 140 nm, as compared to 300 nm in the photoresist area not affected by 532 nm beam. Similarly, parts of line 5 in Fig. 4.19A right below the 532 nm exposure spot on line 4 are thinner. The fabrication of each of these lines took about 5 seconds. It is evident that the effect of exposure to 532 nm at higher power for longer time (24 mW for 60 sec) lasted longer and affected a greater photoresist area. The duration of the thermal effect on polymerization was further studied through a set of experiments in which the exposure times and number of scans were varied.

4.3.7.1 Offset 800 nm and 532 nm exposure at various exposure times and delays

Similar to the previous study, a photoresist sample containing 0.05 wt% KL68 and 0.5 wt% SRd101 dyes in 1:1 SR368/499 was tested with two-beam exposure. Polymerization was initiated by an 800 nm ML beam and a 532 nm CW beam was used to heat the sample locally prior to polymerization. An offset of 6.6 μm was introduced between the 800 nm and 532 nm beams. To determine the effect of the 532 nm exposure time on the polymerization rate, four different conditions were tested. First, the 532 nm beam exposed a spot in the sample for 10 sec (short exposure). After additional 10 sec (short wait) later, the 800 nm ML light was then used to fabricate a line across the area that was pre-exposed to the 532 nm beam. For the second test, 532 nm exposed a spot for 10 sec (short exposure). An additional 1 min (long wait) later, the 800 nm ML beam was used to fabricate a

line across the heated area of the sample. Tests 3 and 4 were the same as 1 and 2, respectively, except that the 532 nm exposure time was 1 min (long exposure). These conditions are summarized in the Table 4.5.

532 nm CW beam unblocked	532 nm CW beam blocked	Time periods, sec	Result
Short exposure	Short wait	10 /10	No effect on linewidth
Short exposure	Long wait	10 / 60	No effect on linewidth
Long exposure	Short wait	60 / 10	Linewidth decrease
Long exposure	Long wait	60 / 60	No effect on linewidth
Long exposure	No wait	60 / 0	Complete polymerization deactivation

Table 4.5: Summary of the 532 nm CW spot heating test conditions.

For these experiments, the power of the 800 nm beam was set to 3.5 mW and the power of the 532 nm beam was set to 24 mW at the sample plane. The fabrication velocity was 50 μm/sec. The reference line, fabricated without any 532 nm CW light, was observed through a CCD camera during the experiment, and appeared to be fully polymerized. 1 min exposure with the 532 nm beam followed by immediate exposure to the 800 nm ML beam almost completely turned polymerization off. 1 min exposure to the 532 nm beam with a 10 sec delay prior

to 800 nm ML exposure resulted in thin lines created in the regions of the 532 CW exposure. The linewidth increased in the areas outside of 532 nm beam exposure region. A wait of 1 min after 30 sec or 1 min exposure at 532 nm did not cause narrowing of the fabricated lines within our experimental error, just as 532 nm exposure for 10 sec did not change width of the lines. In summary, longer 532 nm exposure times and short delays are most efficient for deactivating polymerization, and can result in complete polymerization suppression in the exposed areas. To maintain the same rate of polymerization, longer exposure times require a longer delay before initiating polymerization with the 800 nm ML beam.

4.3.7.2 Simultaneous overlapped 800 nm and 532 nm exposure

Exposure to pulsed 800 nm light immediately after 532 nm CW exposure can lead to complete suppression of polymerization. We next tested the effects of overlapping the 800 nm and 532 nm beams in space and time. The sample tested was again composed of 0.05 wt% KL68 and 0.5 wt% SRd101 in 1:1 SR368/499. A chopper was used to block and unblock the 532 nm beam periodically. Sets of lines were also fabricated under single-beam exposure to compare to lines polymerized under dual-beam exposure for an extended period of time.

Because the polymerization efficiency at a constant laser power depends on the fabrication velocity, and slower velocities can lead to the absence of polymerization, polymerization was initiated at speeds ranging from 20 μm/sec to 200 μm/sec with 10 μm/sec steps. The power of the 800 nm beam was set at 2.5 mW or 3 mW, and

the power of the 532 nm beam was set at 50 mW at the sample plane. The SEM images in Fig. 4.20 show almost no polymerization at velocities below 50 μm/sec. At velocities of 60 μm/sec and higher, the difference in the presence of 532 nm light was more pronounced. However, it was difficult to make a definitive conclusion as to whether the presence of 532 nm beam made lines wider or narrower.

Inconclusive results were also obtained from a sample with a higher concentration of SRd101. In a sample with 0.05 wt % KL68 and 1 wt% SRd101 in a 1:1 SR368/499 monomer mixture, fabrication was initiated by an 800 nm ML beam at 1 mW or 3 mW at the sample plane. The power of the 532 nm beam was set at 15, 24 or 50 mW. As in the previous measurements, sets of lines were fabricated at velocities varying from 20 μm/sec to 200 μm/sec in 10 μm/sec steps. Shown in Fig. 4.22 are the SEM measurements of the resultant lines. Lines polymerized under each set of parameters were inconsistent in width, and could be wider or narrower than lines fabricated under exposure to both the 800 nm and 532 nm beams.

Because these experimental results were inconclusive, additional experiments were performed in a sample made with SRd101 from a new bottle.

4.3.7.3 Studies of spot exposure at 532 nm at an offset prior to 800 nm polymerization with new SR101

The first experiments with the new SR101 used a spot exposure of the 532 nm beam at an offset from the 800 nm beam using sample containing 0.05 wt% KL68 and 0.1 wt% SRd101 in 1:1 SR368/499. The power of the 800 nm beam was set at

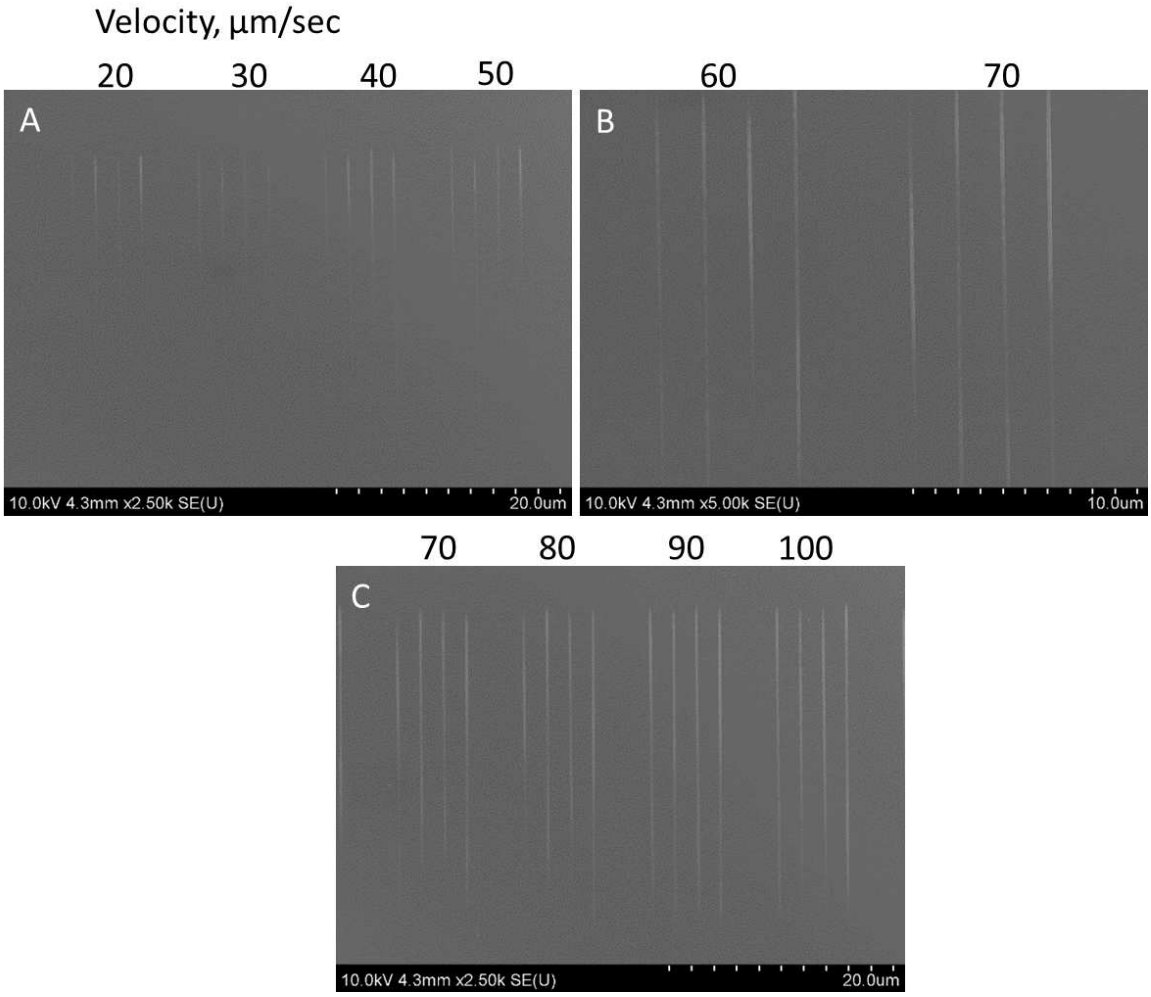

Figure 4.20: SEM images of polymerized lines in a photoresist sample with 0.05 wt% KL68 and 0.5 wt% SRd101 in 1:1 SR368/499. 800 nm ML and 532 nm CW beams were overlapped and exposed the sample simultaneously. The power of the 800 nm beam at the sample plane was 3 mW and the power of the 532 nm beam was 50 mW. Fabrication velocities ranged from 20 m/sec to 200 μm/sec in 10 μm/sec steps. The top left-hand group of 4 lines in A) corresponds to a 20 μm/sec fabrication speed, the next group of four lines was created at 30 μm/sec, etc. The last group at the right corresponds to 50 μm/sec. B) Two groups of four lines fabricates at 60 μm/sec (leftmost) and 70 μm/sec (rightmost). C) Left-hand group of 4 lines corresponds to a 70 μm/sec fabrication speed, the next group of four lines was created at 80 μm/sec, etc. The last group at the right corresponds to 100 μm/sec.

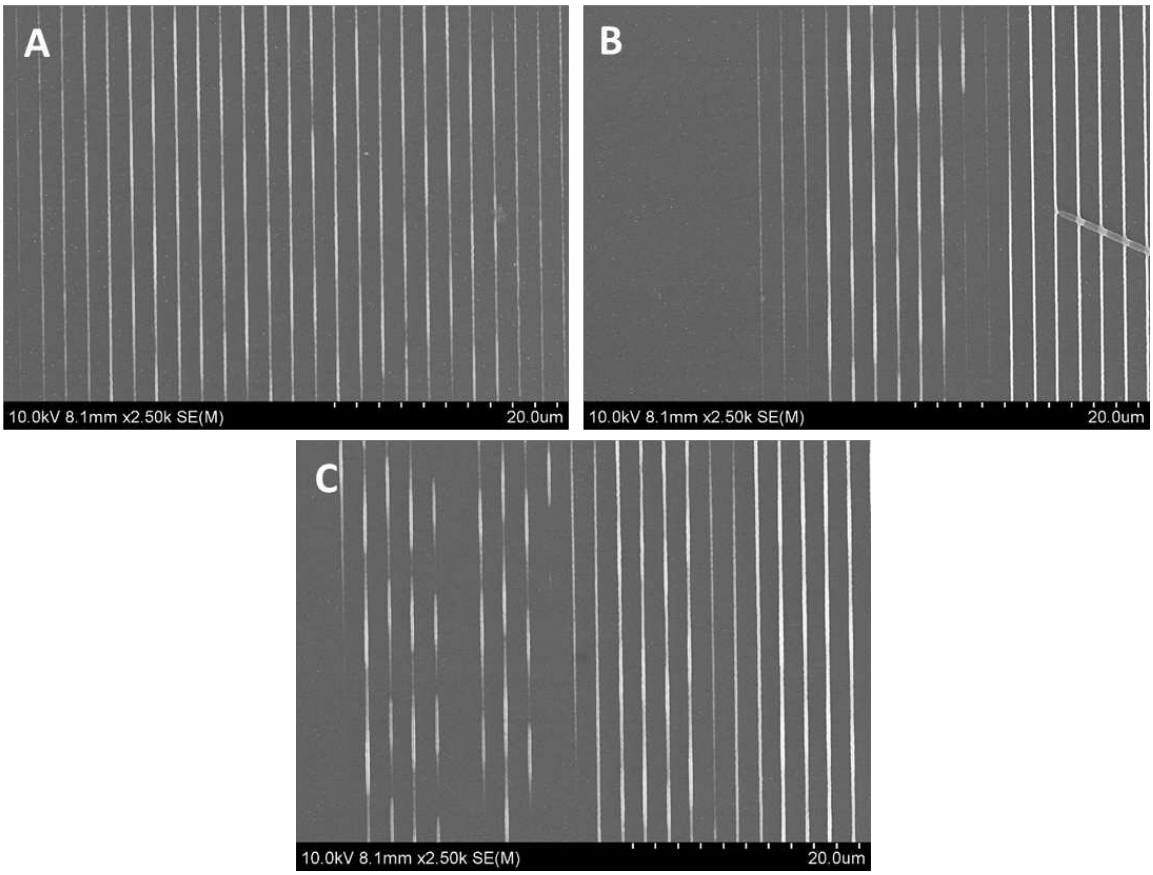

Figure 4.21: SEM images of lines fabricated in a sample with 0.05 wt% KL68 and 1 wt% SRd 101 in 1:1 SR368/499 monomer mixture by writing lines at 50 μm/sec with 800 nm ML at 1 mW and 532 nm CW at A) 15 mW; B) 24 mW; C) 50 mW.

3 mW and the power of the 532 nm beam was set at 24 mW or 50 mW. Sets of lines were fabricated at velocities ranging from 20 μm/sec to 200 μm/sec.

A spot in the photoresist was exposed to the 532 nm beam for 30 sec at an offset from the 800 nm beam along a fabricated line. The 532 nm beam was then blocked and the 800 nm beam was moved across the area. No polymerization was observed in the region exposed to the 532 CW beam. Polymerization was only observed outside the region heated by the 532 nm beam. The widths of the lines

fabricated prior to 532 nm beam exposure or far away from the exposed region did not change along the fabricated line, which is consistent with the previously observed behavior.

4.3.7.4 Simultaneous exposure with offset 800 nm and 532 nm beams with new SR101

Exposure to 532 nm CW light at up to 40 mW power at the sample surface did not cause polymerization. To test the effect of 532 nm exposure on the polymerization efficiency, a set of lines was written with the 800 nm and 532 nm beams at the same time, but with various offsets (Fig. 4.18).

The polymerization under 800 nm exposure was performed at 3 mW at 50 μm/sec or 60 μm/sec. The power of the 532 nm beam was set at 5, 10, 15 or 35 mW at the sample surface. The offset between the laser beams was varied between 2 and 6 μm. A summary of the performed experiments is shown in Table 4.6.

A chopper was used to block and unblock the 532 nm beam periodically. For all laser powers and offsets tested, polymerization was enhanced when the 532 nm beam was unblocked. Fig. 4.22 shows SEM images of the polymerized lines at offsets of 6, 5, and 4 μm and powers of 15 and 30 mW. The faint lines denoted by red arrows correspond to the lines fabricated with 800 nm light only. The thicker lines denoted by green arrows were fabricated with both beams.

The linewidth increase under two-beam exposure was observed visually and confirmed with SEM images. Measurements of lines show a clear trend of the line

800 nm ML, mW	532 nm CW, mW	Offset, μm	Velocity, μm/sec
12	5	2	60
	10	2	60
	15	0	60
		2	60, 50
		3	60, 50
		4	60, 50
		6	60
	35	3	60
		4	60
		5	60

Table 4.6: Summary of parameters for simultaneous exposure with offset 532 nm CW and 800 nm ML beams.

width increasing at higher CW powers. The plots in Fig. 23A show the width measurements. Red crosses represent lines that were fabricated using the 800 nm beam only. Blue dots indicate the lines formed with two-beam exposure. The error bars represent the standard deviation of the measured linewidth. These lines were formed at 60 μm/sec using 3 mW of 800 nm power and 15 mW of 532 nm power with a 2 μm offset. Fig. 23B shows the change in linewidth with the addition of 532 nm CW exposure.

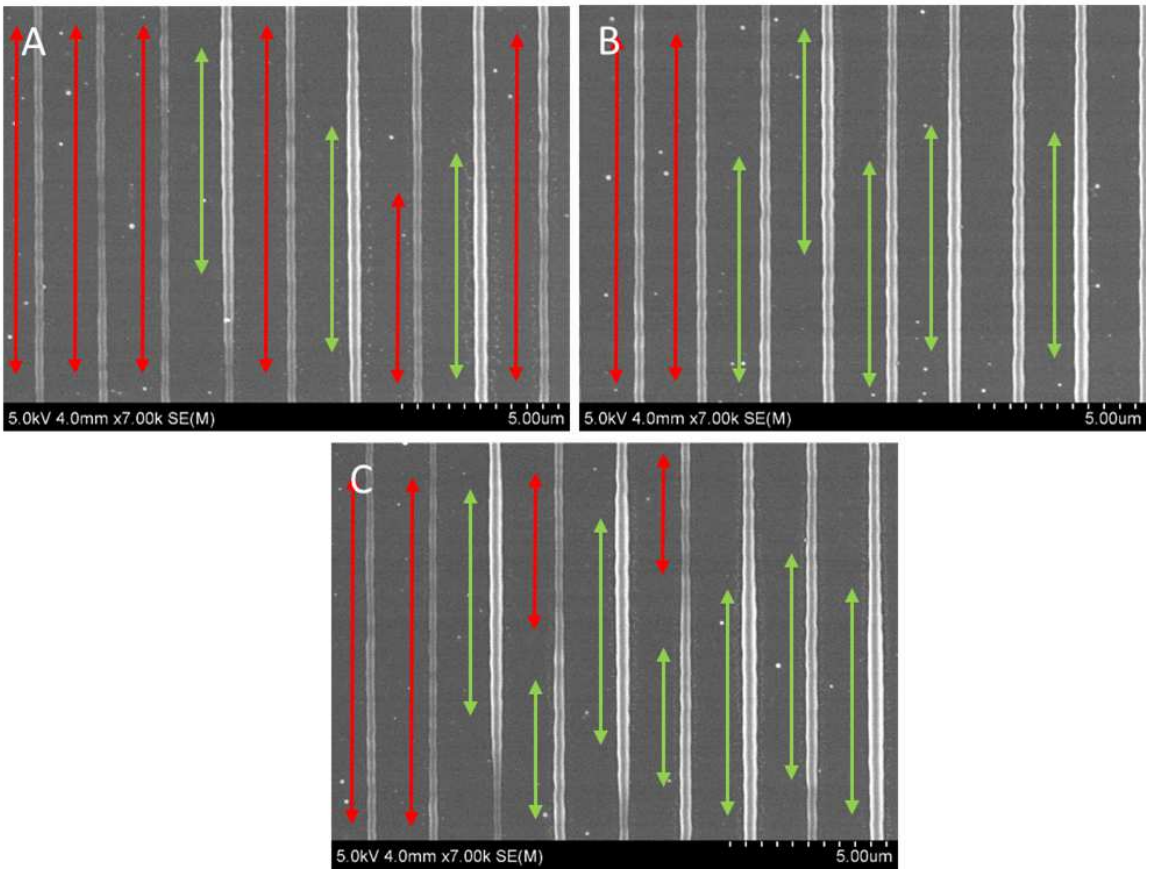

Figure 4.22: SEM images of lines fabricated at 60 μm/sec with the 800 nm ML beam at 3 mW. Red arrows indicate lines polymerized with 800 nm ML only. Green arrows correspond to lines fabricated with both 800 nm and 532 nm beams: A) 6 μm offset and 15 mW 532 nm power; B) 5 μm offset and 30 mW 532 nm power; C) 4 μm offset and 30 mW 532 nm power.

4.3.7.5 Spot heating with a higher concentration of new SR101

The effect of Sulphorhodamine 101 on the polymerization efficiency was next studied in samples containing 0.05 wt% KL68 and 0.7 wt % SRd101 and 0.5 wt% SRd101. For each sample, the fabrication velocity was varied from 20 μm/sec to 200 μm/sec in 10 μm/sec steps. The effect of the 532 nm beam on polymerization

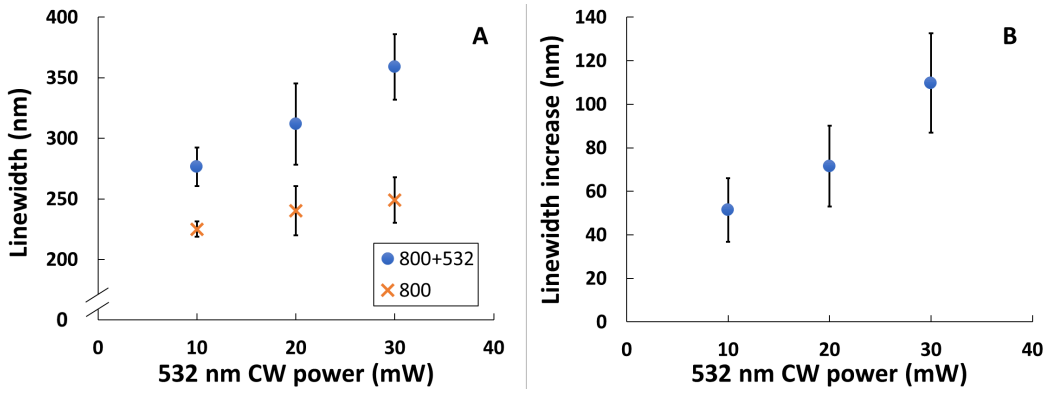

Figure 4.23: A) Linewidth measurements of lines fabricated under 800 nm ML beam exposure (red cross), and both the 800 nm and 532 nm beams (blue circles). B) Difference in linewidths from single-beam and two-beam exposure at 2 μm offset.

initiated at 800 nm was studied by overlapping the two beams in time and space. For each given velocity, sets of perpendicular lines were fabricated at a 2 μm spacing. The power of the 800 nm ML beam was set at 3 mW and the power of the 532 nm CW was set at 50 mW at the sample plane. A mechanical chopper was used to block the 532 nm beam periodically to test the difference between one- and two-beam exposure. At 50 mW, the 532 nm beam did not affect the width of the lines fabricated at speeds above 100 μm/sec. The widths of the lines formed under two-beam exposure were greater than those for a single-beam exposure at velocities below 100 μm/sec. As seen in Fig. 4.24, the width of the lines gradually increased as the fabrication velocity decreased. The red arrows in the Fig. 4.24 indicate exposure to 800 nm only and the green arrows indicate exposure to both beams.

One distinct feature of this positive-contrast photoresist is the absence of polymerization at the turning points of the fabricated lines, where the stage slows down

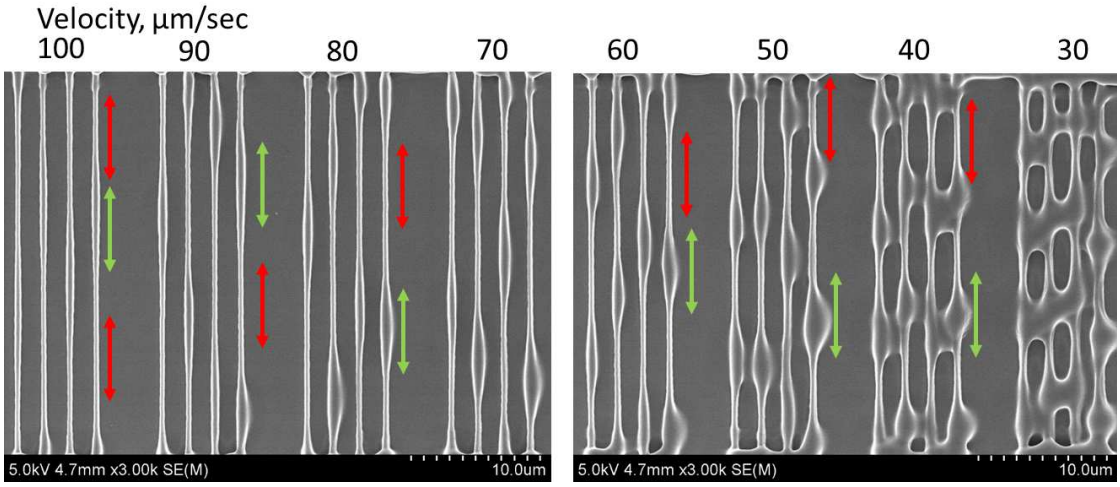

Figure 4.24: SEM images of lines polymerized under 800 nm single-beam exposure (red arrows) and 800 nm and 532 nm dual-beam exposure (green arrows) at fabrication velocities from 30 μm/sec to 100 μm/sec.

and exposure increases. For this experiment, turning points of the stage were fully polymerized under dual-beam exposure, as can be seen in Fig. 4.25. Red lines indicate the absence of polymerized turning points under single-beam exposure, whereas the addition of the 532 nm beam led to wide polymerized corners. A more detailed study of the effect of the 532 nm beam was performed by fabricating longer lines at a constant velocity.

A similar effect of increasing linewidth was observed when lines were fabricated at 50 μm/sec and 70 μm/sec. In Fig. 4.26A and 4.26B, the three lines on the left (indicated by red arrows) were fabricated with single-beam exposure only. Starting from the fourth line, the chopped 532 nm beam was added. The lines became wider (indicated by green arrows). It is clear from the images that the addition of the 532 nm CW beam made the lines wider. The linewidth also increased from left to right

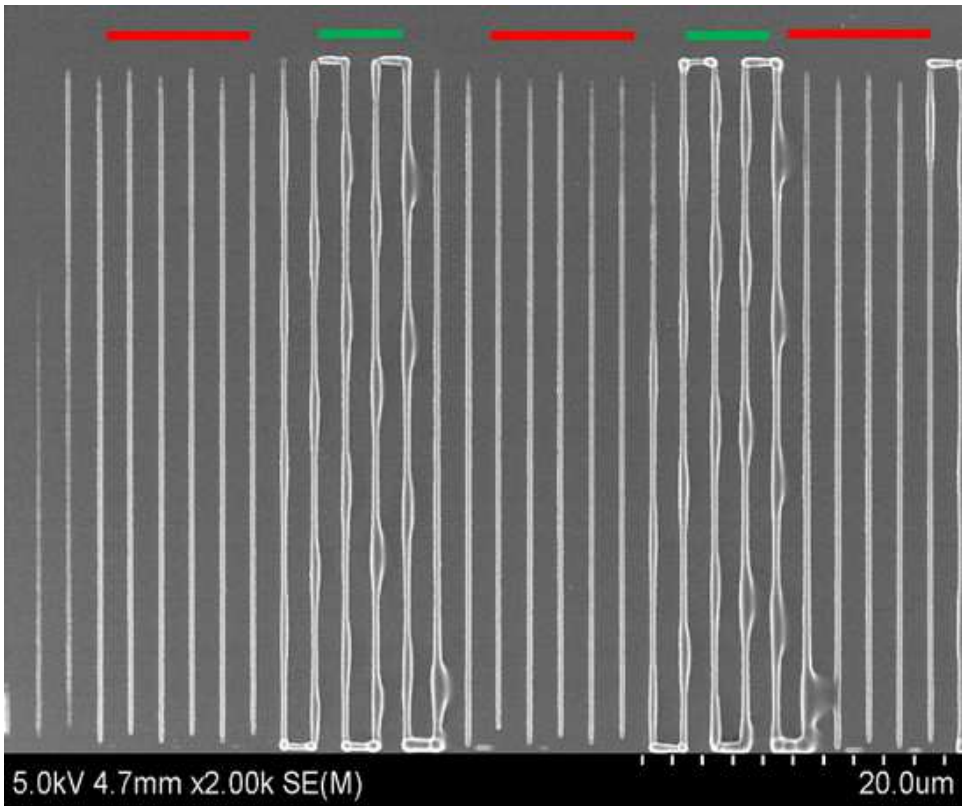

Figure 4.25: SEM images of lines polymerized under single-beam (below red line) and dual-beam exposure (below green line). There is no polymerization at the turning points under single-beam exposure, but there is polymerization at the turning points under dual-beam exposure.

as more lines were fabricated, indicating that the 532 nm exposure had cumulative effect.

To investigate 532 nm exposure build up, a sample with 0.05 wt% KL68 and 0.7 wt% SRd101 was exposed to 532 nm CW only by scanning lines 2 μm apart. In the fabrication process (Fig. 4.27), the focus was first moved 20 μm along the y axis, offset by 2 μm along the x axis, then moved back 20 μm along the y axis, offset by 2 μm along the x axis and so on while chopping the 532 nm beam. Exposure was started on the left side, and the SEM images show no presence of lines or dots at

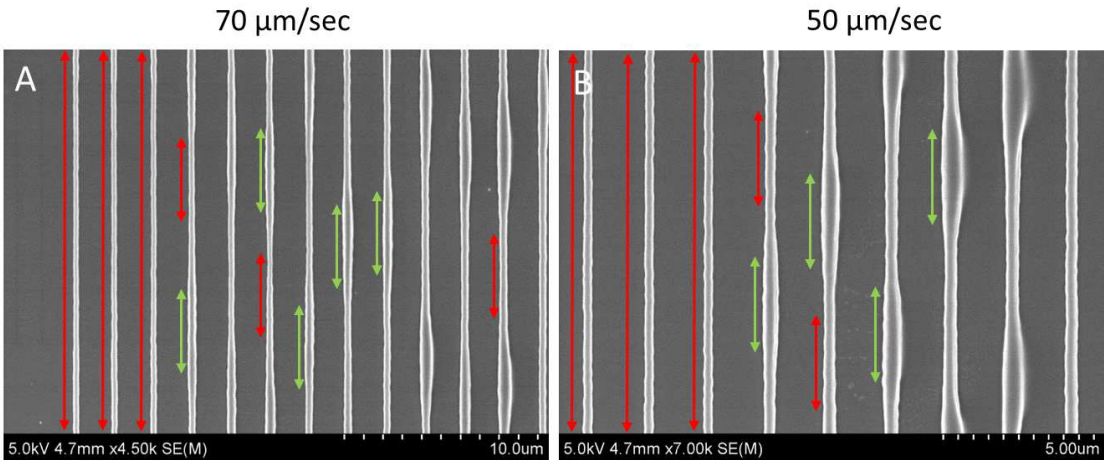

Figure 4.26: SEM images of lines fabricated with an 800 nm ML beam (red arrows) and with two 800 nm and 532 nm beams simultaneously (green arrows).

first. As the beam was moved towards the right side, dots started to appear. The dots then increased in size from one line to the next, until the fabricated features overlapped with one another. This experiment contradicted our initial results with Sulphorhodamine 101. This difference might have been caused by dye degradation over time, as the SRd101 in the initial experiments was from a bottle that was in the laboratory for couple of years. Newly purchased SRd101 demonstrated a different polymerization initiation behavior.

4.3.7.6 Other dyes tested for thermal polymerization deactivation

Because 532 nm light initiated polymerization in the monomer, other potential dyes with an absorption band around 532 nm were tested, including Sulphorhodamine B, Rhodamine 123, Lissamine Rhodamine B sulfonyl chloride and Pyrromethene

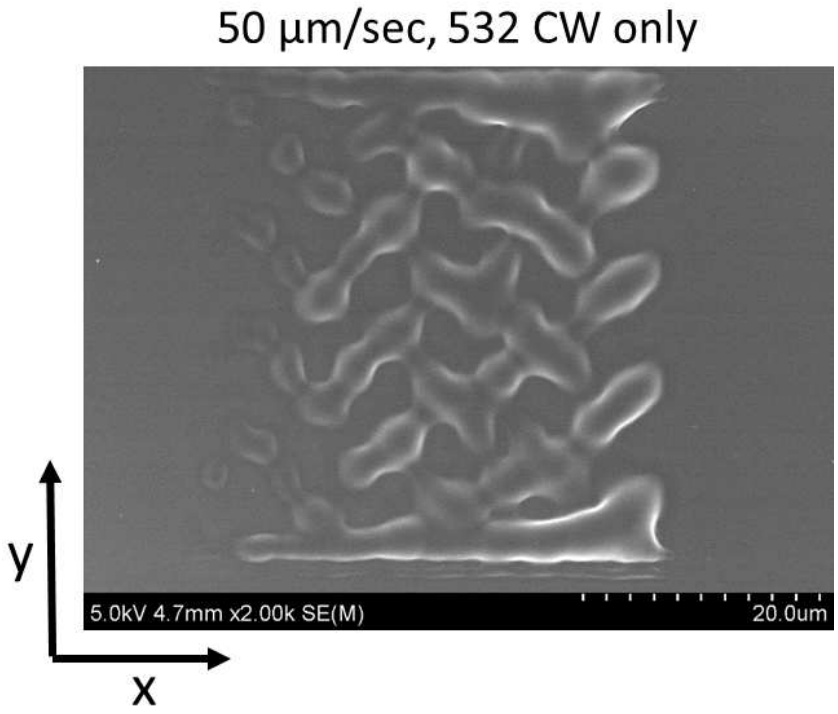

Figure 4.27: EM image of lines formed by a 532 nm CW beam at 50 mW. The chopped 532 nm laser was set on the left side of the image, then moved 20 μm along the y axis, offset by 2 μm along the x axis, then moved back 20 μm along the y axis, offset by 2 μm along the x axis and so on. At first, no polymerization was observed. As the beam scanned towards the right side, first dots appeared, then fabricated features increased in size until they overlapped with one another.

605. All dyes were mixed with the monomer solution and exposed to 532 nm CW and 800 nm ML. 800 nm powers up to 24 mW at the sample were tested (this is the maximum power before local burning and explosions within the focal point starts). 532 nm powers up to 40 mW at the sample were tested (the maximum available power on the day of experiment).

Polymerized lines were observed in the sample with 0.025 wt% of Rhodamine 123 in 1:1 SR368/499 under 532 nm exposure. However, no polymerization was ob-

served under 800 nm exposure. Pyrromethene 605 at 0.032 wt% in 1:1 SR368/499 did not polymerize under 532 nm exposure, but the 800 nm beam led to polymerization.

For two concentrations of Sulphorhodamine B (SRdB), 0.014 wt% and 0.056 wt% no polymerization was observed at 532 nm or 800 nm light at various fabrication velocities from 20 μm/sec to 200 μm/sec. Similar results were observed for Lissamine Rhodamine B Sulfonyl Chloride (LRdB) at 0.074wt% in 1:1 SR368/499. For these reasons, either LRdB or SRdB was mixed with photoresists containing KL68 for the thermal deactivation studies.

4.3.7.7 Thermal deactivation studies with Lissamine Rhodamine B sulfonyl chloride

The next sample tested was composed of 0.05 wt% KL68 and 0.074 wt% Lissamine Rhodamine B sulfonyl chloride (LRdB) (the same number of moles as KL8) in 1:1 SR368/499. The powers tested were 2.1 mW for the 800 nm ML beam and 26 mW for the 532 nm CW beam. No polymerization was observed with 532 nm excitation at various fabrication velocities. The 800 nm exposure initiates polymerization in the resist with KL68 only. When the photoresist containing KL68 and LRdB was exposed to both the 532 nm beam and the 800 nm ML beam, the linewidth increased at a fabrication velocity of 60 μm/sec.

Polymerization initiated at 800 nm was suppressed in the region that was previously heated with the 532 nm beam for 10 sec. Similar results were obtained for lower and higher concentrations of LRdB.

However, these dyes were harder to dissolve in the monomer mixture compared to the other tested dye and KL68, Sulphorhodamine B was therefore used as the dye for majority of following experiments.

4.3.7.8 Thermal deactivation study with Sulphorodamine B

Samples were prepared containeding 0.05 wt% KL 68 and Sulphorhodamine B (SRdB) at 0.014 wt% (half the number of moles of KL8) and 0.056 wt% (twice number of moles of KL68) in 1:1 SR368/499. Polymerization was performed with the 800 nm ML and 532 nm CW beams under two conditions: a) with two beams overlapping and exposing the same sample spot simultaneously; and b) with local spot heating with the 532 nm CW beam at an offset.

In the sample containing 0.05 wt% KL68 and 0.056 wt% SRdB, the two beams were overlapped and sets of lines were fabricated at 60 μm/sec with the 800 nm beam at 2.6 mW and the 532 nm beam set at 40 mW at the sample plane. A chopper was used to block the 532 nm beam periodically. Exposure to the 800 nm beam initiated polymerization at a power of 2.6 mW. No polymerization was observed with 532 nm exposure alone at powers up to the maximum tested, 40 mW. Lines got wider when the two beams exposed the sample at the same time. When the 800 nm power was

lowered to 2 mW, the 532 nm beam had no effect at low powers and caused the lines to broaden at high power.

For a typical experiment with the 800 nm beam set at 2.6 mW and the 532 nm beam set at 30 mW, a set of lines was fabricated with a 2 μm spacing (Fig. 4.28). The lines fabricated with 800 nm ML were 250±10 nm wide. However, when both beams were overlapped the linewidth increased to 380±15 nm. As a control experiment, the 800 nm beam then was blocked, 532 nm exposure alone at 30 mW did not lead to any polymerization, which is consistent with the previous observations.

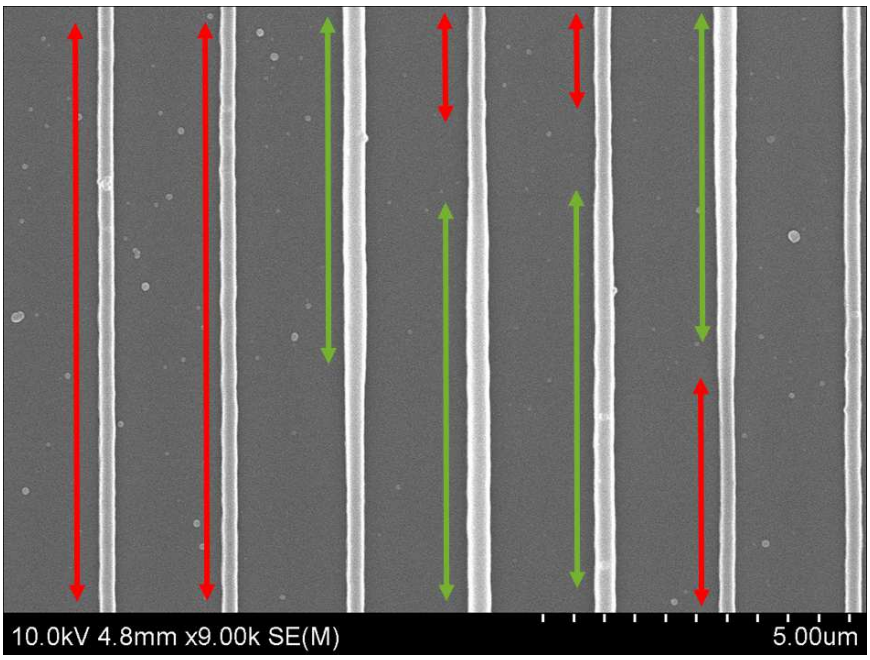

Figure 4.28: SEM images demonstrating polymerization enhancement when 800 nm and 532 nm beams are overlapped and expose the same spot at the same time in 0.05 wt% KL68 and 0.056 wt% SRdB in 1:1 SR368/499. The red lines indicate 800 nm exposure, and the green lines indicate dual-beam exposure.

The sample used for the spot heating experiment contained the same concentrations of KL68 and SRdB, 0.05 wt% and 0.056 wt% respectively. First, lines were fabricated in the Y direction to distinguish sets of lines, fabricated in the X direction that were polymerized by scanning a laser over a heated spot, Fig. 4.29. Line 1 in Fig. 4.29 is a reference line, fabricated prior to 532 nm exposure, and has a thickness of 300±20 nm. For Line 2, the 532 nm beam was focused at the position indicated by the green circle in Fig. 4.29. The size of the circle does not represent the size of the beam. The 532 nm beam was unblocked for 10 sec. After an additional 10 sec delay time, the 800 nm beam exposed the sample along Line 2 at 60 μm/sec. No polymerization was observed in the region exposed to the 532 nm beam. Having the 532 nm beam unblocked for 10 sec has an effect on the surrounding areas as well. For example, Lines 3 and 4 were exposed to the 800 nm beam only. However, in the region right below the spot of the 532 nm exposure, either no polymerization was observed (Line 3) or lines were only partially polymerized (Line 4).

The effect of 532 nm CW heating was further explored though varying the 532 nm power and exposure time, as well as the number of 800 nm scans. These conditions were tested in a sample containing 0.05 wt% KL68 and 0.055 wt% Sulforhodamine B (SRb) in 1:1 SR368/499. The threshold power of the 800 nm beam was at 2.3 mW at a velocity of 50 μm/sec. The power of the 532 nm beam was set to either 17.7 mW, 9 mW, or 4 mW at the sample. The 532 nm beam was offset by 10 μm with respect to the 800 nm beam for a spot exposure. The 532 nm beam exposed the sample for a desired time, followed by a single or multiple scans with

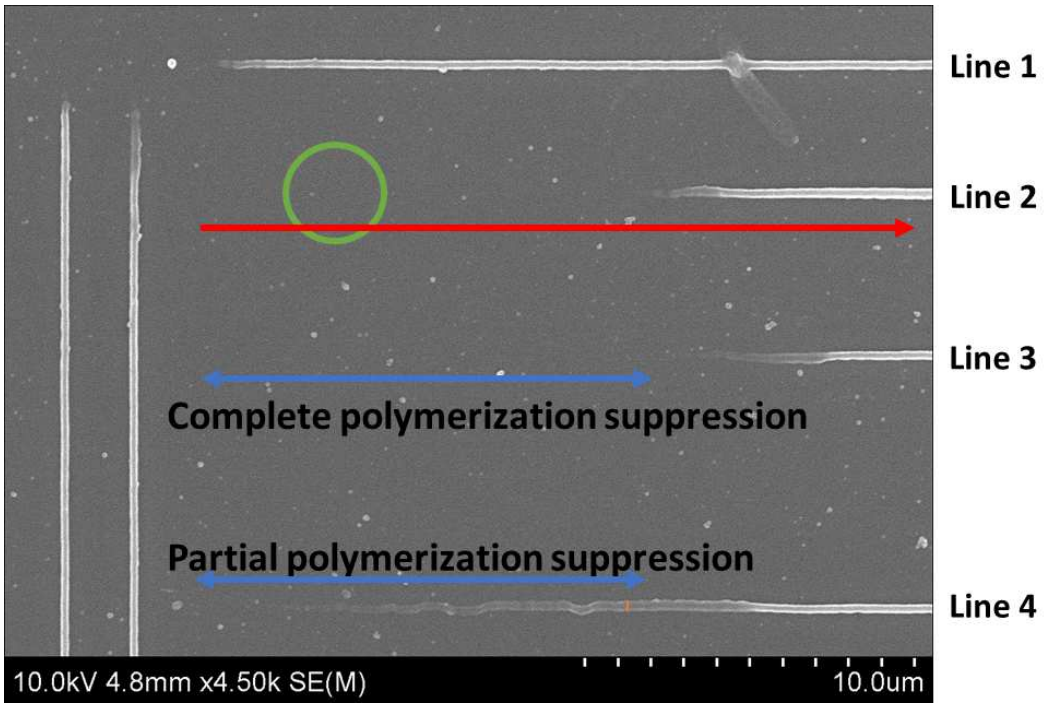

Figure 4.29: Polymerization deactivation with 532 nm spot heating. The green circle indicates the position of the 532 nm exposure. The vertical lines are for reference exposure. The red arrow indicates the direction of 800 nm exposure. The blue arrows highlight the deactivation of polymerization by the 532 nm beam. Line 1 was written prior to 532 nm exposure. Line 2 was fabricated after 10 sec of 532 nm exposure and a 10 sec waiting period. Lines 3 and 4 were written without any additional 532 nm exposure.

the 800 nm only over the areas exposed to the 532 nm beam. Fig. 4.30 shows the results of sample exposure to the highest tested CW power, 17.7 mW.

Perpendicular lines (vertical in Fig. 4.30) and dots were fabricated to indicate the start of the fabricated test lines. Line 1 is a reference, written prior to any 532 nm exposure. After Line 1 was fabricated, the 800 nm ML beam was blocked and a spot 10 μm to the right of the dot on Line 2 was exposed to the 532 nm beam for five seconds, after which sets of horizontal lines were immediately fabricated with

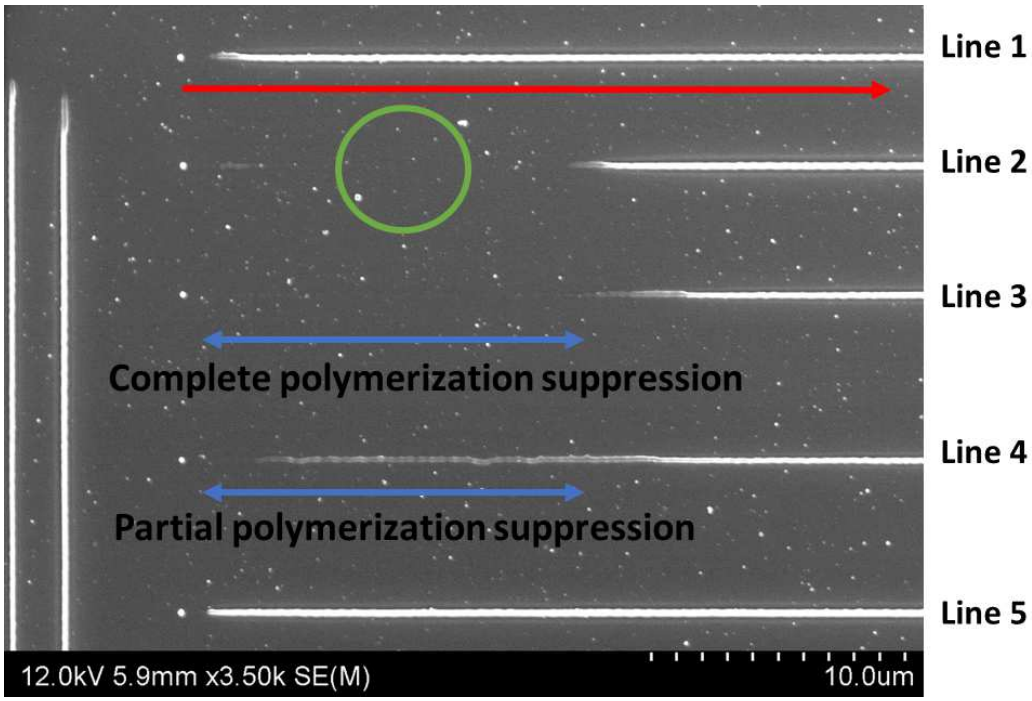

Figure 4.30: Effect of 532 nm spot exposure. The 800 nm power was 2.3 mW, and the 532 nm power was 17.7 mW. Line 1: Reference line, no 532 nm spot exposure, one scan with 800 nm exposure. Line 2: 532 nm exposure for five seconds, followed by one scan with the 800 nm beam. Line 3: No 532 nm exposure, one scan with 800 nm beam. Line 4: No 532 nm exposure, one scan with 800 nm beam. Line 5: No 532 nm exposure, four scans with 800 nm beam.

single 800 nm scans. As evidenced from Lines 2 and 3 in Fig. 4.30, exposure to the 532 nm beam at this power for five seconds prevents any subsequent polymerization in the region.

Polymerization of Line 4, which was outside of the direct 532 nm beam exposure region, was partially diminished. Line 5 was fabricated with four scans of the 800 nm ML beam to test the thermal effect on the polymerization rate. The width of Line 5 in the region nearest to the 532 nm exposure was not different from the width in regions that were further away. This result may be due to the fact that

Line 5 was further away from 532 nm spot and that it was fabricated ten seconds after 532 nm exposure. Therefore, a test with multiple scans of excitation beam over exposed area was repeated immediately after the photoresist was exposed to 532 nm beam.

To test the effect of 532 nm exposure on initiation, the sample was exposed to the 532 nm beam for three seconds and then lines were scanned with the 800 nm beam multiple times. Line 1 in Fig. 4.31A is a reference line, fabricated before the 532 nm exposure.

Lines 2, 3 and 4 were fabricated using four scans of the 800 nm beam following a 532 nm spot exposure for three seconds. Even after four scans, no polymerization was observed in the center of the area of the sample that was exposed to the 532 nm beam for lines 2 and 3. The center of line 4 was clear after the first scan, and only after four scans was partial polymerization observed in this region.

Fig. 4.31B, shows a direct comparison of four scans with the 800 nm ML beam before and after three seconds of 532 nm exposure. Line 5 was fabricated with four scans of the 800 nm beam after heating the center of the line for 3 sec. Fabrication of this line took 8 sec.

The thermal effects were tested at lower powers of the 532 nm beam as well by performing scans with the 800 nm ML beam until polymerization occurred. As shown in Fig. 4.32, a spot along Line 2 was exposed to the 532 nm beam at 8.6 mW for two seconds. The 532 nm beam was then blocked and the 800 nm beam was scanned four times across the spot exposed to 532 nm. Each scan had a duration of 1 sec. Even after four scans with 800 nm beam, polymerization was prevented

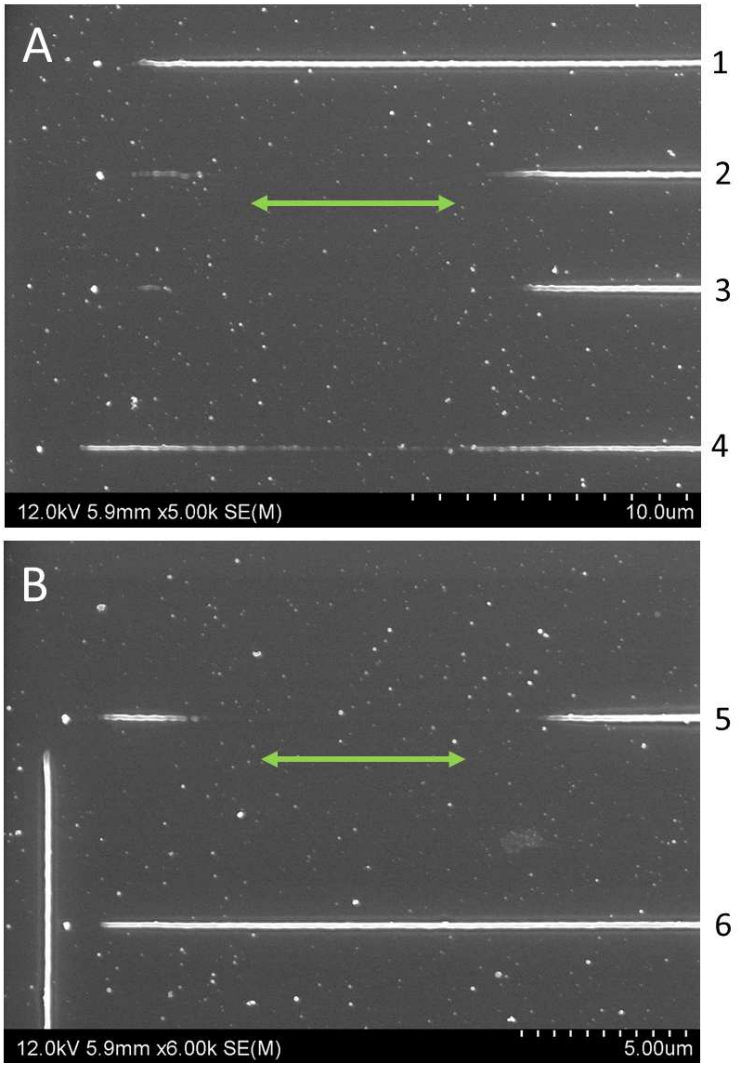

Figure 4.31: Additional tests of thermal deactivation with SRd. The 800 nm power was set at 2.3 mW, and the 532 nm power at 17.7 mW. Line 1: Only 800 nm exposure for one scan. Line 2: 532 nm on for three seconds, followed by four scans of the 800 nm beam. Line 3: No 532 nm exposure, four scans with 800 nm beam. Line 4: No 532 nm exposure, four scans with 800 nm beam. Line 5: 532 nm on for three seconds, followed by four scans of the t800 nm beam. Line 6: No 532 nm, four scans of the 800 nm beam. Each line is 100 μm long. The green arrow indicates the area exposed to the 532 nm CW beam.

completely in the area previously exposed to 532 nm. After no polymerization was observed in the tested area of Line 2, a spot in Line 3 was tested. This spot was

exposed to 532 nm for 2 sec, after which it took 24 scans of the 800 nm beam before faint fabricated lines were visible.

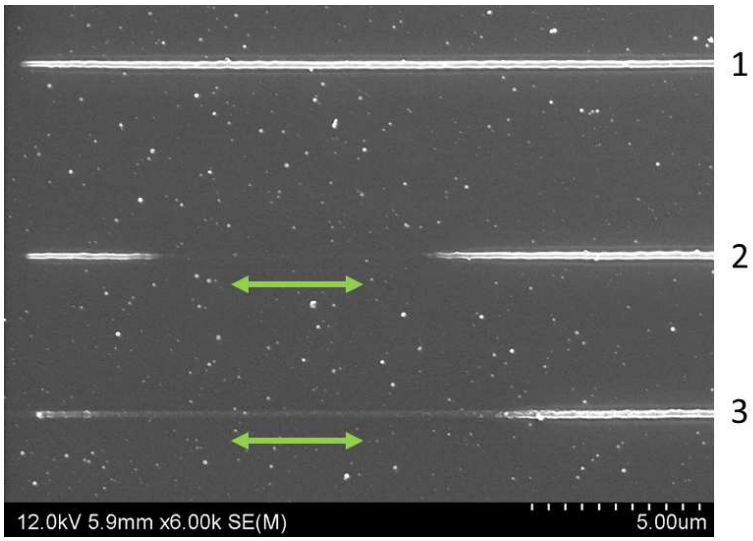

Figure 4.32: Multiple scans of the 800 nm ML beam over the spot exposed to 532 nm. The 800 nm power was set at 2.3 mW, and the 532 nm power at 8.6 mW. Line 1: No 532 nm, four scans with 800 nm. Line 2: 532 nm exposure for two sec, followed by four scans with 800 nm. Line 3: 532 nm CW exposure for two sec, followed by 24 scans of 800 nm ML. Each line is 50 μm long. The green arrows represent the regions exposed to 532 nm.

Next, the combination of a higher power and a shorter duration was tested by exposing a sample to the 532 nm beam for 5 sec at 4 mW. Lines 1, 3 and 6 (Fig. 4.33) were fabricated with single scans without exposure to the 532 nm beam. The widths of these lines are the same, whereas polymerization in the centers of the Lines 2, 4, 5 and 7 was either completely or partially inhibited after this number of scans. Lines 2 and 4, both fabricated with five scans of the 800 nm beam, correspond to 5 and 2 sec of 532 nm exposure, respectively, demonstrating the positive correlation between the duration of exposure and the amount of polymerization inhibition.

SEM examination showed traces of polymerized features in the heated region in the center of Line 4, which was only exposed at 4 mW of 532 nm light for 2 sec. The polymerization inhibition in Line 4 is comparable to that in Line 5, which was exposed to 532 nm for 2 sec, but was fabricated with ten scans of the 800 nm beam. Fabrication of line 4 took 5 sec, whereas fabrication of Line 5 took twice as much time and twice as many laser beam scans. Fabricated lines were observed in the heated region after 36 scans of the 800 nm beam.

4.4 Conclusions

The absorption spectrum of KL68 in toluene was measured at room temperature and had a absorption band at 430 nm. MAP was initiated under pulsed laser exposure at 800 nm in both SR368/499 and AR5 resins containing KL68 as the photoinitiator. Neither 800 nm CW, 880 nm CW or 532 nm CW alone initiated polymerization. Negative contrast was observed for all monomers mixed with KL68.

In samples F2.5 and F3.0, consisting of KL6 and AR5, fabrication was initiated starting from 80 μm/sec and 200 μm/sec respectively. The polymerization threshold was 12 mW for F2.5 and 9 mW for F3.0. Using these threshold levels prevented the samples from undergoing local explosions over the wide range of fabrication velocities tested. This allowed us to perform initial single-beam polymerization studies. For these photoresists, a slower fabrication velocity corresponds to a longer exposure time and leads to a partial or a complete absence of polymerization at a given

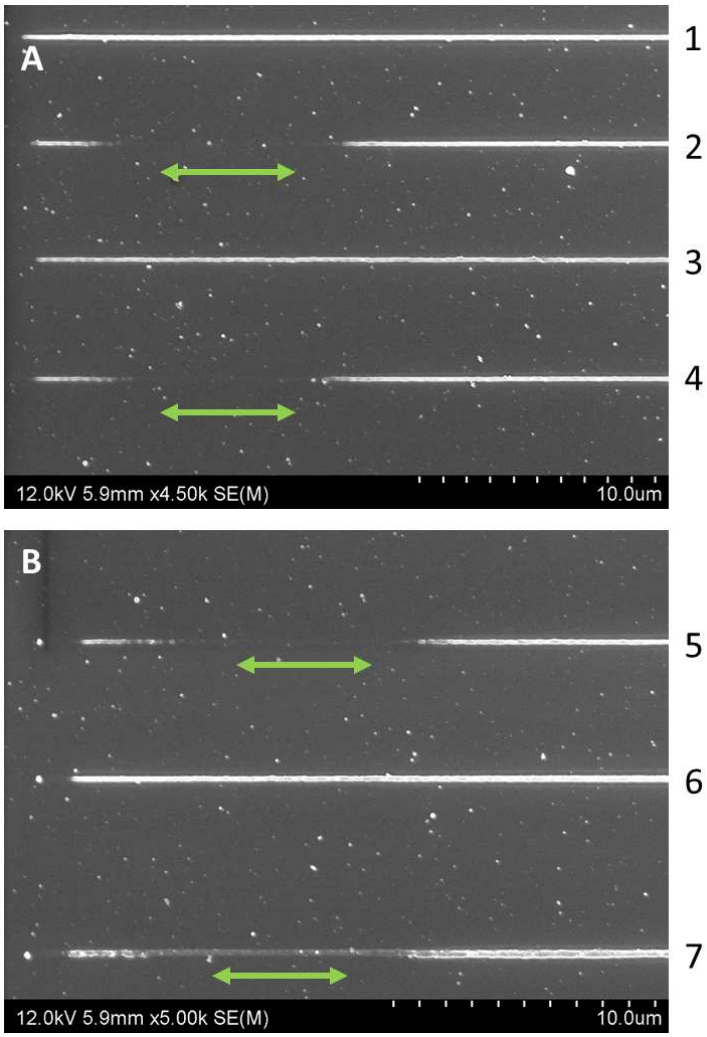

Figure 4.33: Effect of a spot exposure to 532 nm light on multiple scans of the 800 nm beam across the heated spot. The 800 nm power was set at 2.3 mW, and the 532 nm power at 4 mW. Line 1: Reference line 50 m long, from five scans with the 800 nm beam. Line 2: 532 nm exposure for 5 sec, followed by five scans with the 800 nm beam. Line 3: no 532 nm exposure, five scans with the 800 nm beam. Line 4: 532 nm exposure for 2 sec, followed by five scans with the 800 nm beam. Line 5: 532 nm exposure for 2 sec, followed by ten scans with the 800 nm beam. Line 6: No 532 nm exposure, 15 scans with the 800 nm beam. Line 7: 532 nm exposure for 2 sec, followed by 36 scans with the 800 nm beam. Green arrows indicate areas of the photoresist exposed to the 532 nm beam.

fabrication power level. No polymerization was observed below these fabrication velocities, depending on the monomer type and photoinitiator concentration.

Samples with lower concentrations of the photoinitiator required more power to initiate polymerization, which was similar to the positive contrast materials. Polymerization initiation in a photoresist with a lower concentration of KL68 occurred at higher fabrication velocities, which is opposite to the traditional positive-contrast materials. Similar results were found for the photoresists based on SR368/499. Reciprocity curves were measured for three different concentrations of KL68. The polymerization threshold decreased as the concentration of KL68 increased. However, under the same excitation beam power level, the polymerization initiation velocity increased with increased KL68 concentration.

The observed relationship between photoinitiatior concentrations and polymerization thresholds can be explained as follows. Samples with a lower concentration of the photoinitiator create fewer free radicals under the constant specific power level of the exposure beam. Therefore, higher excitation laser power is required to excite a larger number of photoinitiator molecules to create enough radicals to overcome the polymerization threshold and to fabricate features.

Because self-deactivation from the pulses of the excitation beam can result in negative contrast behavior, an increased polymerization rate at higher fabrication velocities can be expected. The faster the laser focus is moved away from the exposed area, the less deactivation takes place in the exposed spot, which leads to wider polymerized lines. It was observed that, when the excitation beam power level was constant, the polymerization initiation velocity increased as the photoinitiator

concentration decreased. In other words, the fewer photoinitiator molecules that were present in the photoresist, the higher the velocityneeded to form the lines. This observation suggests more efficient deactivation at lower concentrations. As the photoinitiation concentration increased, more molecules were exposed to the laser beam, and fewer of the molecules were deactivated, which led to a higher polymerization rate. We will need to test other monomers and photoinitiatiors, including traditional positive-contrast materials, and measure reciprocity curves at different concentrations to determine the dependence of polymerization thresholds and fabrication velocities with regard to photoresist concentrations.

To test if deactivation happens through the recombination of radicals, two 800 nm ML beams were used simultaneously to expose F2.5, F3.0 and KL68 in 1:1 SR368/499 at various beam powers. The distance between beams was gradually decreased until their focal points overlapped. Lines fabricated under simultaneous exposure to both beams were wider when compared to those that were created with a single beam for all tested powers. In F3.0 the linewidth increased from 340±20 nm to 420±18 nm under a single 800 nm ML beam, or two overlapped 800 nm ML beams, exposure respectively. Given this result, it seems that polymerization deactivation, by creating a large number of radicals to recombine to form narrower lines, is unlikely.

Wider lines were also observed when the first laser beam was an 800 nm ML beam and the second beam was either an 800 nm CW or an 880 nm ML beam. Tested velocities ranged from 60 μm/sec to 450 μm/sec. It is possible that exposure to a second 800 nm beam, either ML or CW, can result in excited state

absorption, transitioning molecules to the state that created the radicals. No effect on the polymerization rate was observed when the 880 CW beam was added to the 800 nm ML beam. Exposure to other wavelength combinations might lead to polymerization deactivation, such as the addition of a 445 nm CW or a 400 nm ML beam. Polymerization initiation via linear absorption with a 405 nm CW or a 445 nm CW beam needs to be tested. Because of the absorption spectrum band at 430 nm, a 445 nm CW beam might initiate polymerization.

The initiation process was further explored via 2-BIT measurements of the order of nonlinear absorption in a photoresist that consisted of 0.1 wt% of KL68 and 1:1 SR368/499. Because of the nonlinear nature of the reciprocity curve, the 2-BIT measurements were performed at several velocities. Three chosen fabrication velocities (10 μm/sec, 20 μm/sec, and 40μm/sec) corresponded to parts of the nonlinear relationship between the fabrication velocity and polymerization threshold. At 60 μm/sec and 100 μm/sec, polymerization becomes independent of the fabrication velocity. 2-BIT data were collected at these velocities as well.

The order of the effective nonlinear absorption increased with increasing fabrication velocity. For some of the fabrication velocities corresponding to the nonlinear part of the reciprocity curve, the best-fit exponent was approximately 2, indicating that polymerization was initiated primarily through 2-photon absorption under these exposure conditions. The best-fit exponent to the data collected at the fabrication velocities corresponding to the linear part of the reciprocity curve was greater than 2, which indicates that other nonlinear processes take place during the exposure process, most likely self-deactivation.

More information about initiation can be gathered by performing 2-BIT measurements in photoresists with different concentrations of KL68. We have seen dependence of the power and velocity thresholds on the KL68 concentration. 2-BIT data collected for samples with different photoinitiator concentrations and fabrication velocities would help to map the exposure conditions at which the effective nonlinearity of the material is changing and could reveal more information about initiation.

The effect of iodonium salt on the polymerization rate was tested by performing MAP in a KL68 photoresist mixed with the iodonium salt. The iodonium salt was added at five different concentrations to each of the two photoresists consisting of different concentration of KL68. The polymerization threshold increased in the photoresist containing the lowest concentration of salt compared to one without a salt. However, the polymerization threshold in the photoresists containing higher concentrations of salt was comparable to that of the photoresist with KL68 only. The strongest effect of iodonium salt on initiation was observed at lower concentrations and slower fabrication velocities. Because lower salt concentrations required higher laser power to initiate polymerization, the salt may be contributing to the deactivation processes more efficiently than it does at higher concentrations.

The effective nonlinearity of the photoresist with different concentrations of iodonium salt and KL68 will need to be determined through 2-BIT measurements. Because of the observed nonlinear relationship between the iodonium salt concentration and the fabrication velocity, 2-BIT data collected at different velocities at

each concentration will help determine effective nonlinearity and nonlinear processes for these materials.

The observed nonlinear relationship between the polymerization threshold and the fabrication velocity was in the range of velocities between 1 μm/sec and 200 μm/sec. Because slower fabrication velocities correspond to longer exposure times, the thermal heating from the laser beam can be contributing to the polymerization initiation, leading to observed nonlinear behavior between sample concentration, laser power and fabrication velocity. This nonlinear relationship was tested by performing MAP in the heated photoresist.

Polymerization initiation at different temperatures was performed by using an objective heater to heat the photoresist with KL68 and iodonium salt. The heater was used to increase the temperature of the oil-immersion objective, which in turn heated the photoresist. Contrast curves were measured at three different temperatures, and revealed that the polymerization threshold increased with the temperature. Thus, higher temperatures can contribute to the self-deactivation processes. Thermal effects on initiation were further studied through two sets of experiments that were performed with photoresists containing KL68 and traditional positive contrast photoinitiators. One experiment involved an objective heater, which increased the temperature of the entire photoresist sample. The other heating experiment employed a second laser beam that was offset with respect to the fabrication beam. The laser exposed a spot of the sample for a controlled amount of time at a set power level, and then was turned off. The fabrication beam was then unblocked to initiate polymerization.

In the case of heating with an objective heater, sets of lines and voxels were fabricated at four different temperatures ranging from room temperature to 33 °C. Voxels were fabricated at different heights above the substrate, and the sizes of fallen voxels were compared at each temperature using SEM. In the positive-contrast materials, such as TPO-L and MGCB, the size of the voxels either increased with the temperature or was similar across the measured temperature range. Measurements over a wider range of temperatures might lead to a bigger change in voxel size.

The same temperature range had a stronger effect on voxels fabricated in photoresist composed of KL68 and either AR5 (F2.5) or 1:1 SR368/499. We observed a lower initiation rate as the temperature increased, leading to smaller fabricated lines and voxels. At 33 °C neither lines nor voxels could be fabricated in either of the KL68 photoresists. In comparison, photoresists that contained either MGCB or TPO-L had fully polymerized lines and voxels at this temperature. At a 3 °C temperature increase polymerization was completely terminated in both KL68 photoresists. The exact mechanism of the deactivation process, based on the temperature increase, is not yet clear. Heating the sample might increase the diffusive processes in the photoresist, leading to fewer radicals present per unit volume compared to that which are at room temperature. It is not clear whether change of temperature has an effect on the nonlinear processes. To illuminate that possibility, 2-BIT measurements need to be performed at different temperatures. The effect of the diffusion rate can be traced by measuring reciprocity curves at different temperatures and collecting 2-BIT data at different fabrication velocities at each set temperature.

A second set of thermal deactivation experiments was performed by using two laser beams at different wavelengths, one to heat the target spot of the sample, and the other to initiate polymerization. The heating beam focus was adjacent to the fabrication beam to create a local temperature gradient. The exposure conditions were varied by changing the offset between the beam centers, by changing the time delay between the beam exposure, and by changing the fabrication velocity.

Because simultaneous exposure to an 800 nm ML beam and a 880 nm CW beam did not have an effect on polymerization, the latter beam was used to pre-scan the area of the photoresist before the 800 nm ML beam was used to expose the same area to initiate polymerization. The size of the fabricated lines decreased as the number of scans of the 880 nm CW beam increased. Because the power range of the 880 nm CW beam was limited by the laser cavity alignment, and exposure to a 532 nm CW beam did not initiate polymerization, a 532 nm beam was used to locally heat the sample. Thermal local heating was tested by placing the center of the 532 nm CW beam 6 μm ahead of the 800 nm ML fabrication beam, which was used to write a line across the target spot. The power of the fabrication beam was set at the polymerization threshold. The exposure time and power of the 532 nm CW beam were varied, as was the delay between blocking the 532 nm beam and turning the 800 nm beam on. The width of the polymerized lines outside of the target spot that was exposed to the 532 nm beam was compared to those made within the heated region.

Because KL68 does not have an absorption band at 532 nm, the heating effect of the 532 nm beam was not pronounced. To increase the temperature change

caused by the 532 nm beam exposure, KL68 photoresists were mixed with dyes that absorbed at 532 nm. Various dyes were tested to see if exposure to 800 nm and 532 nm beams could initiate polymerization.

The tested dyes, with an absorption band around 532 nm, included Sulphorhodamine B, Rhodamine 123, Lissamine Rhodamine B sulfonyl chloride and Pyrromethene 605. All dyes were added to the 1:1 SR368/499 mixture and exposed to 800 nm ML and 532 nm CW at various exposure powers.

A photoresist containing 0.025 wt% of Rhodamine 123 polymerized under 532 nm CW exposure. In the sample that contained 0.032 wt% of Pyrromethene 605, which was exposed to the 800 nm ML beam, line formation was observed. No polymerization occurred in the Rhodamine 123 photoresist under 800 nm ML exposure or in the Pyrromethene 605 photoresist under 532 nm CW exposure.

Neither the 800 nm ML nor the 532 nm CW beams initiated polymerization at fabrication velocities ranging from 20 μm/sec to 200 μm/sec in three photoresists containing different dyes. One photoresist contained 0.5 wt% Sulphorodamine 101 (SRd101). The second was Sulphorhodamine B (SRdB) added to 1:1 SR368/499 at two different concentrations (0.014 wt% and 0.056 wt%). The third was Lissamine Rhodamine B Sulfonyl Chloride (LRdB) mixed at 0.074 wt% in 1:1 SR368/499.

Initial exposure experiments using Sulphorhodamine 101 (SRd101) in 1:1 SR368/499 did not show initiation with the 800 nm ML or the 532 nm CW beams at power levels up to 40 mW. Therefore, 0.5 wt% of SRd101 was added to 0.05 wt% KL68 in 1:1 SR368/499 for heating with a 532 nm CW beam set at 5, 13, and 24 mW each for 10 sec, 30 sec, and 60 sec. The exposure to the higher power for the longer

time, with no delay between turning the 532 nm beam off and turning the 800 nm ML beam on, led to either a complete or a partial absence of polymerization. This exposure condition had a stronger effect on the surrounding regions as well.

To test how long the 532 nm spot exposure effect lasts, a set of experiments was performed in which 532 nm beam exposed a spot in the sample for a set time and then was blocked. The 800 nm ML beam was scanned across the heated region for a controlled number of time. Initiation and widths of the formed lines were recorded as a function of the number of scans.

Experiments with overlapped 800 nm and 532 nm beams were performed in a sample consisting of 0.05 wt% KL68 and 0.5 wt% SRd101 or 1 wt% SRd101 in 1:1 SR368/499 at fabrication velocities ranging from 20 μm/sec to 200 μm/sec with 10 μm/sec steps. As the power of the 532 nm CW beam increased from 10 mW to 30 mW, the width of the formed lines increased from about 270 nm to 360 nm in a photoresist consisting of 0.05 wt% KL68 and 0.1 wt% SRd101 in 1:1 SR368/499. The lines formed under both 800 nm ML and 532 nm CW exposure decreased as the fabrication velocity increased, until the linewidth became comparable to that formed under an 800 nm ML exposure alone. These experiments were performed at the highest power of 532 nm laser available, 50 mW.

Similar results were obtained for a photoresist composed of 0.05 wt% KL68 and 0.074 wt% Lissamine Rhodamine B sulfonyl chloride. The 800 nm ML laser was used to fabricate a line across a spot previously exposed to the 532 nm CW beam. Comparing to the lines formed outside of the region exposed to 532 nm beam, those in the heated spot were considerably narrower. However, when two overlapped

lasers simultaneously exposed the sample, the fabricated lines were wider than lines formed with 800 nm ML beam alone at fabrication velocities of either 50 or 60 μm/sec. The tested power of the 532 nm CW beam was 26 mW, which might be too high when two beams are exposing the same spot simultaneously. Dual-beam experiments need to be performed over a wider range of fabrication velocities and lower powers of the 532 nm CW beam.

There might be an exposure condition at which the laser beam powers and fabrication velocities are set at values that partially or completely deactivate polymerization. Employing a phase-shaping element, such as a phase mask for the beam used to heat the photoresists, can create a temperature change on the sides of the fabricated lines, leading to the formation of thinner line .

Overlapped dual-beam experiments were performed in photoresist composed of 0.05 wt% KL 68 and Sulphorhodamine B (SRdB) at 0.014 wt% and 0.056 wt% in 1:1 SR368/499 using 40 mW of the 532 nm laser and 2.6 mW of 800 nm laser. The exposure of two overlapping beams yields wider lines of 380 $\pm$ 15 nm as compared to lines 250 $\pm$ 10 nm wide created with the 800 nm ML beam alone. Dual-beam exposure was tested only under one set of beam powers and one fabrication velocity. Additional measurements under various beam powers and fabrication velocities are required for this photoresist to examine the possibility of fabricating narrower lines with two overlapped beams.

Spot heating experiments were performed in photoresists containing 0.05 wt% KL68 and 0.056 wt% SRdB. The width of lines fabricated prior to the 532 nm CW exposure was 300$\pm$20 nm. In the KL68 photoresist containing SRdB exposure to

the 532 nm CW beam had a much stronger effect than in the photoresist without SRdB. Polymerization was completely prevented when the photoresist was exposed for 10 sec to the 532 nm beam and 10 sec later the 800 nm beam was used to write a line across the heated spot. Moreover, surrounding areas were affected to a greater degree compared to other dyes tested. Complete or partial polymerization deactivation was achieved in regions around the heated spot that were not exposed directly to the 532 nm beam. Sets of lines were fabricated at varying powers of 532 nm beam (17.7 mW, 9 mW, and 4 mW), different exposure times, and different delays between turning the 532 nm beam off and turning the 800 nm beam on.

The effect of heating was further studied by scanning an 800 nm beam multiple times across the pre-heated spot in photoresists containing 0.05 wt% KL68 and 0.056 wt% SRdB in 1:1 SR368/499. The 532 nm beam power was set at 17.7 mW or 8.6 mW. The exposure time was 2, 3 and 5 sec. Lines with an 800 nm beam were scanned once, 4 times, and 24 times. At a 2 sec exposure at 8.6 mW, even after four consecutive scans with the 800 nm beam, no polymerization was observed in the heated region. It took 24 scans for polymerization to occur to some degree. Because each scan took 1 sec, polymerization started to appear 24 sec after the sample was exposed to a 532 nm beam for 2 sec at 8.6 mW. The longer the sample was exposed to a 532 nm beam, the larger the number of scans that were required to initiate polymerization.

Additional studies involving excitation light at different wavelength combinations are required to gather more information about KL68 excitation and initiation at higher temperatures. Excitation pathway is a key part of setting exposure condi-

tions such as laser wavelength and repetition rate. The excitation to different states can be traced by using a pulse-picker to change the repetition rate of the excitation beam. The polymerization threshold should be measured as a function of the laser repetition rate at various fabrication velocities. Polymerization initiation, after local heating, should be tested at different exposure durations and exposure powers for various beam repetition rates. Determining pulsed laser parameters that lead to polymerization, but could be used to locally heat sample, would be of great interest because the local exposure could be controlled by changing timing between pulses, therefore providing more control over heating. This scheme could potentially lead to formation of finer lines using phase elements for the heating beam.

Chapter 5

An overview of three-color photolithography using biacetyl as a representative photoinitiator

Contributors: Zuleykhan Tomova, Nikolaos Liaros, Sandra A. Gutierrez Razo, Samuel Cohen, Steven M. Wolf. Contributions: 2-BIT measurements, polymerization initiation and deactivation experiments were performed by Z.T. and N.L.; samples were prepared by Z.T. and S.G.R.; SEM measurements were performed by Z.T.; Matlab code for the best-fit exponential to 2-BIT data was written by S.C.; absorption spectra and triplet transient absorption spectra were collected by S.W.

5.1 Introduction

In this Chapter we will discuss the principles of 3-color lithography and its potential for resolving the challenges that the lithography industry is currently facing. The use of the extreme UV light was intended to fuel rapid advances in fabrication in the semiconductor industry. However, the cost of production using this technique is quickly increasing, and many technical challenges remain unmet. With the ongoing need to fabricate smaller and smaller features, alternative approaches based on use of the visible light might be more economically preferable. 3-color lithography has the advantages of using inexpensive sources of visible light and promising the ability to create super-resolved structures. In this thesis we use MAP as a first step in performing 3-color lithography by rapidly screening materials and eliminating those that will not satisfy the requirements of the method. Here, the concepts of 3-color lithography are introduced and a promising 3-color initiator, biacetyl, is discussed.

5.2 Theory

An alternative approach to reducing the feature size and increasing the resolution (the distance between these features) in photolithography involves using two lasers. As in conventional lithography, in 2-color lithography an activation beam takes photoinitiator molecules from the ground state to an excited state, which leads to the initiation of polymerization. A second laser beam, called the deactivation beam, is used to deactivate the excited photoinitiator molecules, preventing initiation. A schematic of this process is shown in Fig. 5.1.

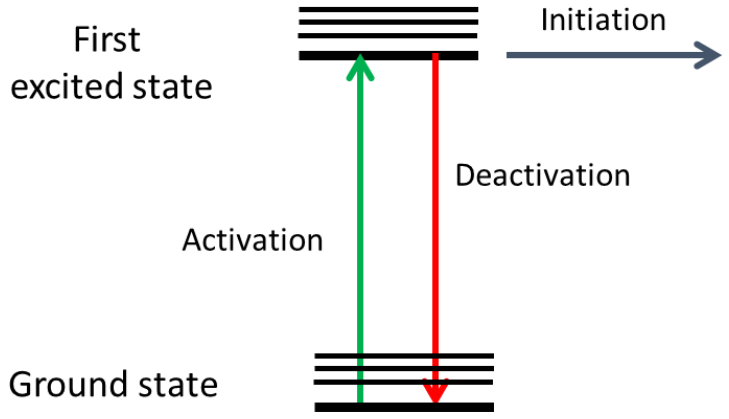

Figure 5.1: Schematic diagram for 2-color lithography. An activation beam transfers photoinitiator molecules an excited state that can generate free radicals, leading to polymerization initiation. A deactivation beam brings molecules back to the ground state before free radicals are formed, preventing initiation.

The spatial intensity distribution of the deactivation beam can be changed by using optical elements, such as phase masks. For example, a phase mask can be used to create a doughnut-shaped point-spread function with a dark region in the center,

as was shown in Section 2.1. If such a beam is overlapped with the activation beam, molecules in the central dark region will remain in the excited state and will initiate polymerization. However, the molecules in the bright region of the doughnut will be deactivated. These latter molecules will not create free radicals, and therefore will not contribute to initiation (Fig. 5.2). Such selective deactivation of the photoinitiator molecules can decrease the feature size and improve resolution.

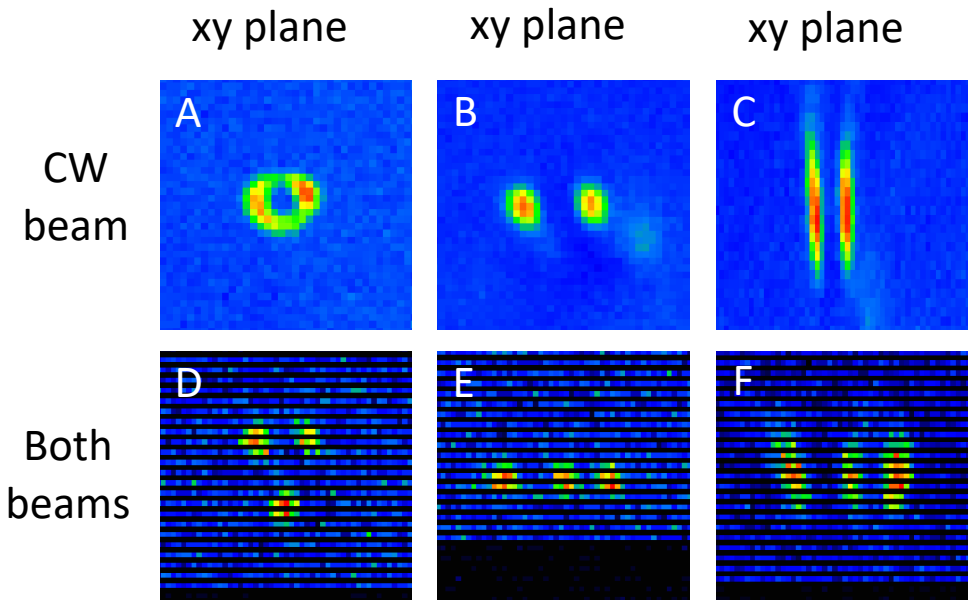

Figure 5.2: Diagram of overlapping two laser beam focal points in X, Y, and Z directions by collecting MAIL from gold nanoparticles by both beams. A) MAIL from the gold nanoparticles generated by the doughnut-shaped beam after the radial polarizer. Point-spread function (PSF) of the deactivation beam after the polarizing beam cube in B) XY plane and C) XZ plane. D) PSF of excitation and deactivation beams with an ofset in the Y-axis. The excitation beam is positioned between the lobes of the deactivation beam, and an ofset is introduced to demonstrate the accuracy of laser beam alignment along the X-axis. E) PSF of excitation and deactivation beams with an ofset in the Y-axis. F) Corresponding MAIL images from gold nanoparticles scanned in the XZ plane.

Because of these nonlinear chemical processes, 2-color lithography allows for fabrication with a considerably improved feature size, as was discussed in Section 1.4. However, the resolution enhancement of 2-color lithography is not as great as had originally been expected.

In 2-color lithography, initiation and deactivation take place from the same state, and therefore compete with one another. Even in the deactivated regions, cross-linking chemistry takes place to some degree. Although residual cross-linking is not a major contributing factor to the size of isolated features, when features are fabricated closely together this phenomenon significantly increases the feature sizes and diminishes resolution. Closely packed features are fabricated through multiple pattering exposure steps. Thus, the higher the feature density required, the worse the feature size and resolution become [111].

This effect of residual cross-linking growth in the multi-step exposure process can be avoided by using 3-color photolithography. A schematic of this approach is presented in Fig. 5.3. First, a pre-activation laser beam takes photoinitiator molecules to a metastable excited state that is not chemically active. Once excited, molecules remain in this state for a considerable time, without creating free radicals or initiating polymerization. Next, in desired regions a deactivation beam brings molecules back to the ground state. Finally, an activation beam can excite any remaining pre-activated molecules to a higher energy state that can initiate polymerization. Thus, in 3-color lithography, polymerization and deactivation do not compete with each other, as these processes happen from different energy states.

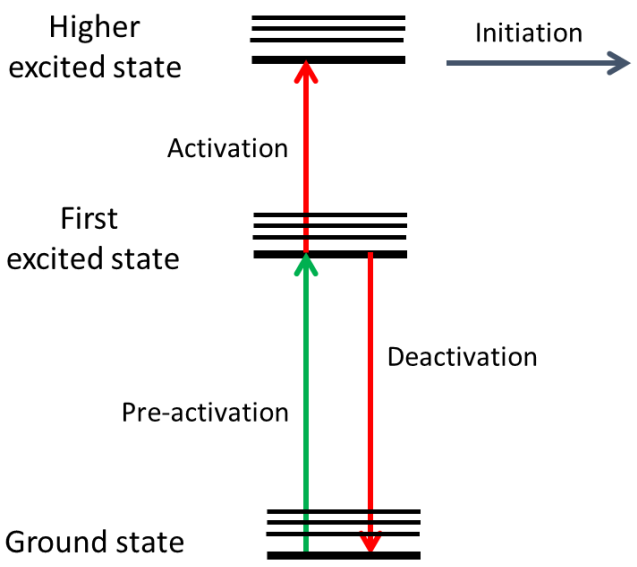

Figure 5.3: Schematic diagram for the 3-color lithographic process. The pre-activation beam brings photoinitiator molecules to the first excited state, which does not produce free radicals. Unless brought back to the ground state by the deactivation beam, molecules can be further excited to the chemically active state, creating free radicals.

The existence of a pre-activated state allows for more efficient deactivation. Because molecules cannot make free radicals in the pre-activated state, no background cross-linking occurs in the deactivated regions.

Three-color photolithography was tested in a resin that contained photosensitizers having a long-lived, non-reactive lowest triplet state. The first candidate we tested with this approach was biacetyl (Fig. 5.4). Biacetyl is a vicinal diketone that has been widely used in the study of photochemical and photophysical processes in various chemical systems. It has been employed as a gas-phase emission standard and also as a triplet energy accepter, because it has a low-energy triplet

state [112–116]. The biacetyl absorption spectrum peaks at 420 nm both in solution and the vapor phase [117, 118].

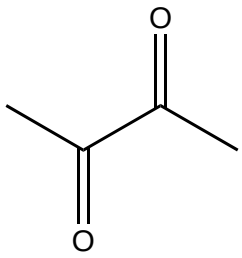

biacetyl

Figure 5.4: Structure of biacetyl

The lifetimes of the first excited singlet state and the lowest triplet state of biacetyl have been determined in solutions and in vapor-phase experiments performed by several groups. Anderson and Parmenter measured a lifetime of $\tau_1 = 10.6 \pm 1.3$ nsec for S_1 by examining the decay of fluorescence in pure biacetyl vapor [119]. Sidebottom *et al.* reported an S_1 lifetime of $\tau_1 = 24 \pm 4$ nsec, and a T_1 lifetime of $\tau_2 = 1.52 \pm 0.26$ msec in biacetyl vapor at an excitation wavelength 383 nm [120]. McClelland *et al.* measured fluorescence decay of biacetyl vapor as a function of excitation wavelength and found that τ_1 changes from $\sim$14 nsec for excitation near 445 nm to $\sim$6 nsec for excitation at 372 nm [121]. With 376 nm excitation they found that $\tau_1 = 11.7 \pm 2$ nsec, in agreement with the work of Anderson [119]. Reported S_1 lifetimes of biacetyl in benzene solutions include $\tau_1 = 10$ nsec [122] and 12.3 ± 1.8 nsec [119].

The T_1 lifetime, $\tau_2 = 1.87$ msec, was measured from the phosphorescence decay of biacetyl at an excitation wavelength 444 nm by Moss *et al.* [123], as compared to $\tau_2 = 1.49 \pm 0.20$ msec at 436 nm [120] and $\tau_2 = 1.65 \pm 0.2$ msec [124] at 440 nm, all determined in biacetyl vapor.

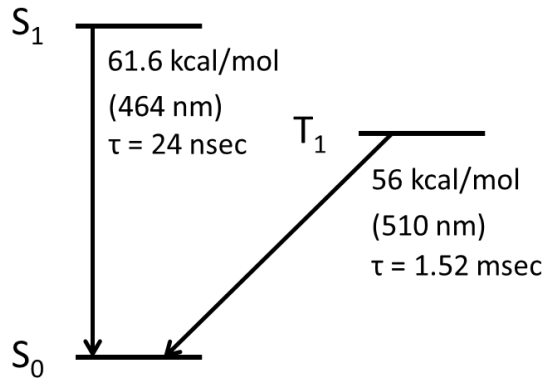

Figure 5.5: Energy level diagram of biacetyl. First-excited singlet state energy reported in [125], energy of the excited triplet state from [126], lifetimes of S_1 and T_1 reported in [120].

The experimentally measured energy difference between S_0 and S_1 corresponds to 464 nm (Fig. 5.5). After excitation to the low vibration levels of the first excited singlet state, biacetyl quickly undergoes intersystem crossing to an excited vibrational level of T_1 [120, 121, 127]. Due to biacetyl's long-lived T_1 state, and biacetyl's potential to be excited through two-photon absorption of 800 nm light, photoresists containing biacetyl as a photoinitiator were studied under various exposure conditions.

5.3 Materials and methods

Initial single-beam MAP experiments were performed with biacetyl obtained from Sigma Aldrich. For MAP and dual-beam exposure experiments, described in Section 5.4.3, biacetyl was added to a mixture of SR368 and SR499 monomers and samples were prepared as described in Section 2.2. For the rest of the experiments discussed in this chapter, biacetyl was distilled before use. The distilled biacetyl was then added to either SR368/499 or SR399 monomers, which were prepared as described in Section 3.3.2. Samples for experiments were prepared by placing a drop of the photoresist on an acrylated #1 coverslip. Two pieces of tape were used to secure the coverslip on top of a microscope slide. A second coverslip was placed on top of the first coverslip, so that the photoresist was set between them. A piece of tape between coverslips was used as a spacer to determine the thickness of the film. Finally, the glass microscope slide was mounted to a sample holder for placement on the microscope stage.

Single- and dual-beam exposure experiments at wavelengths ranging from 720 nm to 900 nm were performed with a tunable Ti:Sapphire oscillator, as described in Section 2.1. Continuous-wave wavelengths tested for polymerization initiation and depletion also included 405 nm, 445 nm and 532 nm. 400 nm ML light was also tested.

Linear photopolymerization experiments at 405 nm were performed using a CW Stradus 405-100 laser diode (Vortran). Linear photopolymerization at 445 nm was initiated by an S3 Arctic Series diode laser (Wicked Lasers). A solid-state,

diode-pumped laser (Coherent Verdi V10) was used as the 532 nm CW source. All of the laser beams were collimated by a set of lenses, and cleaned with a spatial filter prior to entering the microscope. The laser power at the sample was controlled using a half-wave plate and a polarizer. 400 nm ML light was created by second-harmonic generation of 800 nm light with a KDP crystal. 2-BIT experiments were performed with a tunable, pulsed Ti:Sapphire laser, as described in Chapter 3.

5.4 Results and discussion

5.4.1 Single-beam MAP

The UV-visible spectrum of biacetyl measured in benzene (blue line in Fig. 5.6) shows a wide absorption peak at around 410 nm, which suggests the possiblility for two-photon absorption at around 800 nm. Initial experiments with an 800 nm, ML laser demonstrated initiation of polymerization in a sample containing 1 wt% biacetyl in 1:1 SR368/499. The oscillator wavelength was tuned between 730 nm and 860 nm to test the wavelength dependence of the initiation efficiency. The laser power below which no polymerization was observed was defined as the polymerization threshold. The red dots in Fig. 5.6 represent a polymerization action spectrum. Each dot corresponds to the inverse square value of the polymerization threshold at that wavelength. The polymerization action spectrum is blue shifted and narrower than the absorption spectrum. These results suggest that an additional state may be involved in initiation.

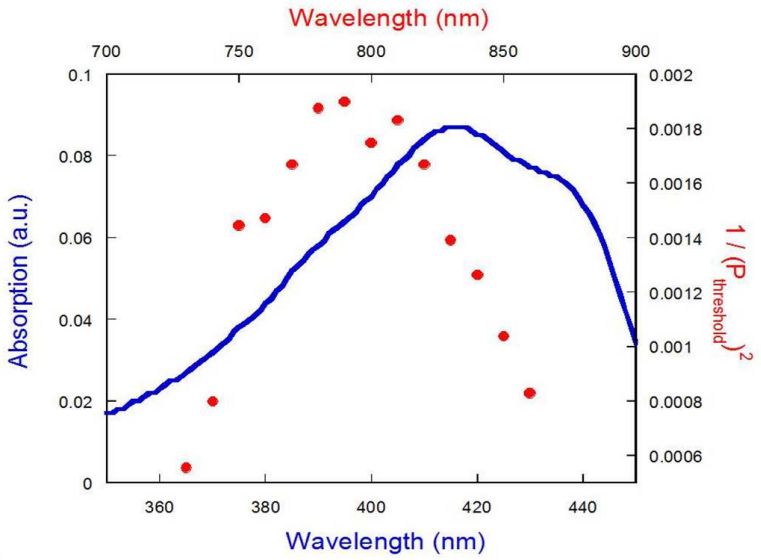

Figure 5.6: Absorption spectrum of biacetyl in benzene (blue line) and polymerization action spectrum of biacetyl in 1:1 SR 368/499 (red dots).

Exposure of the photoresist to CW wavelengths ranging from 730 nm to 860 nm did not cause any initiation. Similarly, no initiation was observed under exposure to a 532 nm CW beam. Exposure to either a 405 nm CW beam or a 445 nm CW beam initiated polymerization, as was expected from the absorption spectrum. The results of the single-beam exposure experiments are summarized in the Table 5.1.

5.4.2 2-BIT measurements of the order of the effective nonlinear absorption of biacetyl in a photoresist

Polymerization in a biacetyl-based photoresist was initiated under exposure to pulsed light at wavelengths in the 730-900 nm range. To understand better the process of initiation, the order of the effective nonlinear absorption was measured as a function of wavelength by 2-BIT measurements, as described in Chapter 3. Each

Polymerization	No polymerization
405 nm CW	
445 nm CW	532 nm CW
750 - 880 nm ML	750 - 880 nm CW

Table 5.1: Summary of single-beam exposure in a 1:1 SR368/499 photoresist containing 1 wt% biacetyl.

laser power value was normalized to the polymerization threshold and the best-fit exponential was determined by nonlinear least-squares fitting of the recorded data to Eq. 3.13. Each data point is an average of at least 5 measurements, and the error bars in figures with 2-BIT data represent plus or minus one standard deviation.

2-BIT data were measured for 1 wt% biacetyl in SR399 monomer. The fabrication velocity was held constant at 20 μm/sec and the polymerization threshold laser powers were recorded at 750, 760, 780, 800, 830, 840 and 850 nm. Shown in Fig. 5.7 are 2-BIT data for 750 nm, 760 nm, and 780 nm exposure with best-fit exponentials of n= 2.0 $\pm$ 0.2, 2.1 $\pm$ 0.1, and 2.08 $\pm$ 0.07 respectively, suggesting that at these wavelengths polymerization initiation occurs primarily through two-photon absorption.

The nonlinearity of the absorption process for biacetyl increased as the wavelength was tuned to the red. Fig. 5.8 shows 2-BIT data measured at 800, 830, 840, and 850 nm with a velocity of 20 μm/sec. The best-fit exponential was 2.4 $\pm$ 0.1

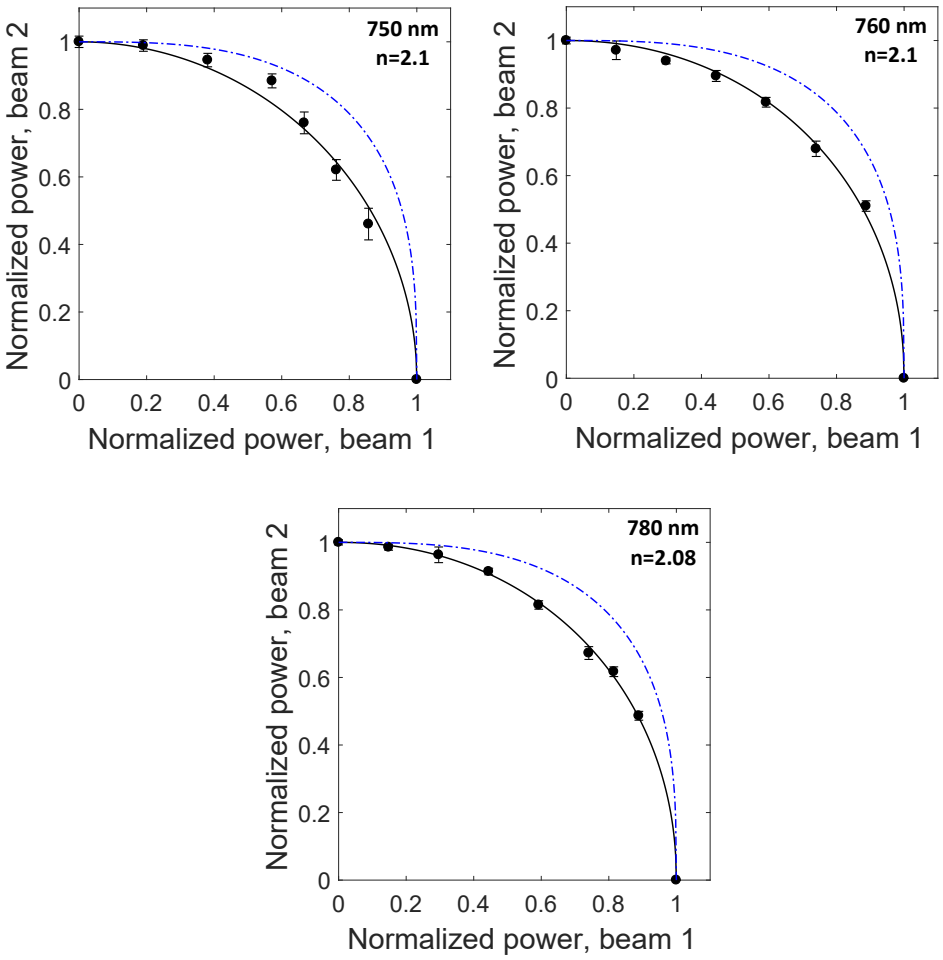

Figure 5.7: 2-BIT data for 1 wt% biacetyl in SR399 at a velocity of 20 μm/sec, at 750 nm, 760 nm, and 780 nm. The black solid lines correspond to best fits to Eq. 3.13. The blue dashed-dotted lines show how the fits would look for a three-photon absorption process for reference.

for 800 nm, 2.4 ± 0.1 for 830 nm, 2.7 ± 0.2 for 840 nm, and 2.53 ± 0.05 for 850 nm. A summary of the best-fit exponents at different wavelengths is presented in Table 5.2.

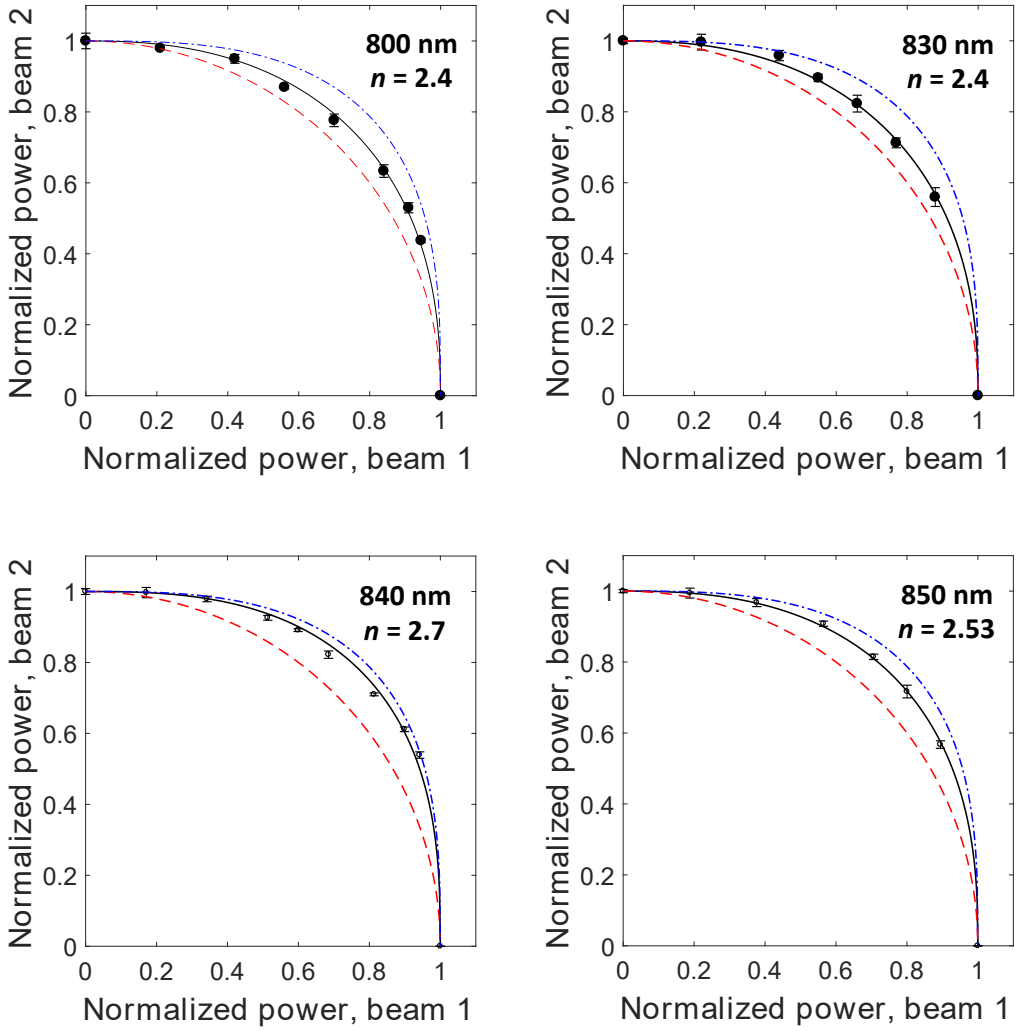

Figure 5.8: 2-BIT data for 1 wt% biacetyl in SR399 at a velocity of 20 μm/sec at 800 nm, 830 nm, 840 nm, and 850 nm. The black solid lines correspond to best fits to Eq. 3.13. For reference, the red dashed lines correspond to 2-photon absorption and blue dashed-dotted correspond to 3-photon absorption.

Exposure wavelength, nm	$P_1^n + P_2^n = P_{th}^n$
750	n= 2.0 ± 0.2
760	n= 2.1 ± 0.1
780	n= 2.08 ± 0.07
800	n= 2.4 ± 0.1
830	n= 2.4 ± 0.1
840	n= 2.7 ± 0.2
850	n= 2.53 ± 0.05

Table 5.2: Summary of best-fit 2-BIT exponents for 1 wt% biacetyl in SR399 at a fabrication velocity of 20 μm/sec.

The 2-BIT data indicate that the order of the effective nonlinearity is greater at longer wavelengths. The values of the best-fit exponent n are between two and three, which suggests that other processes are involved in radical formation process, such as, for example, self-deactivation.

Because the order of the effective nonlinear absorption measured at a constant velocity increases at longer wavelengths, additional data were collected at different fabrication velocities. At each velocity, the laser power was adjusted to the lowest value at which polymerization was visually observed on the monitor. Fabricating at a faster velocity is effectively equivalent to decreasing the exposure dose. This

shorter exposure time can influence processes such as self-deactivation, potentially changing the 2-BIT exponent.

Three wavelengths were chosen for collecting 2-BIT data as a function of a fabrication velocity. The first wavelength was 750 nm, because 2-BIT data collected at 20 μm/sec indicated that the order of the effective nonlinearity at this wavelength is 2. Shown in Fig. 5.9A are 2-BIT data measured at 40 μm/sec with 750 nm excitation. The best-fit exponent in this case is 2.1 $\pm$ 0.1, which is in agreement with the exponent obtained at 20 μm/sec.

At 20 μm/sec with 800 nm excitation, the 2-BIT exponent was 2.4 $\pm$ 0.1. At 40 μm/sec the best-fit exponent was 2.3 $\pm$ 0.2 (Fig. 5.9B). At 80 μm/sec the best-fit exponent was 2.2 $\pm$ 0.1. Thus, with increasing fabrication velocity, the order of the effective nonlinearity at 800 nm appears to decrease slightly, although the differences may not be statistically significant.

2-BIT measurements at 840 nm showed a similar tendency. Shown in Fig. 5.9C are data measured at 40 μm/sec. The best-fit exponent in this case is 2.5 $\pm$ 0.1, as compared to 2.7 $\pm$ 0.2 at 20 μm/sec (Table 5.3). Again, the exponent appears to decrease with increasing velocity.

At shorter wavelength, where the order of the effective nonlinearity is $\sim$2, the 2-BIT exponent is insensitive to velocity, suggesting a pure 2-photon absorption process. At longer wavelengths, n is greater than 2, but decreases with increasing velocity. These results suggest that self-deactivation, which is expected to be less important at higher velocity [83], is present at longer wavelengths.

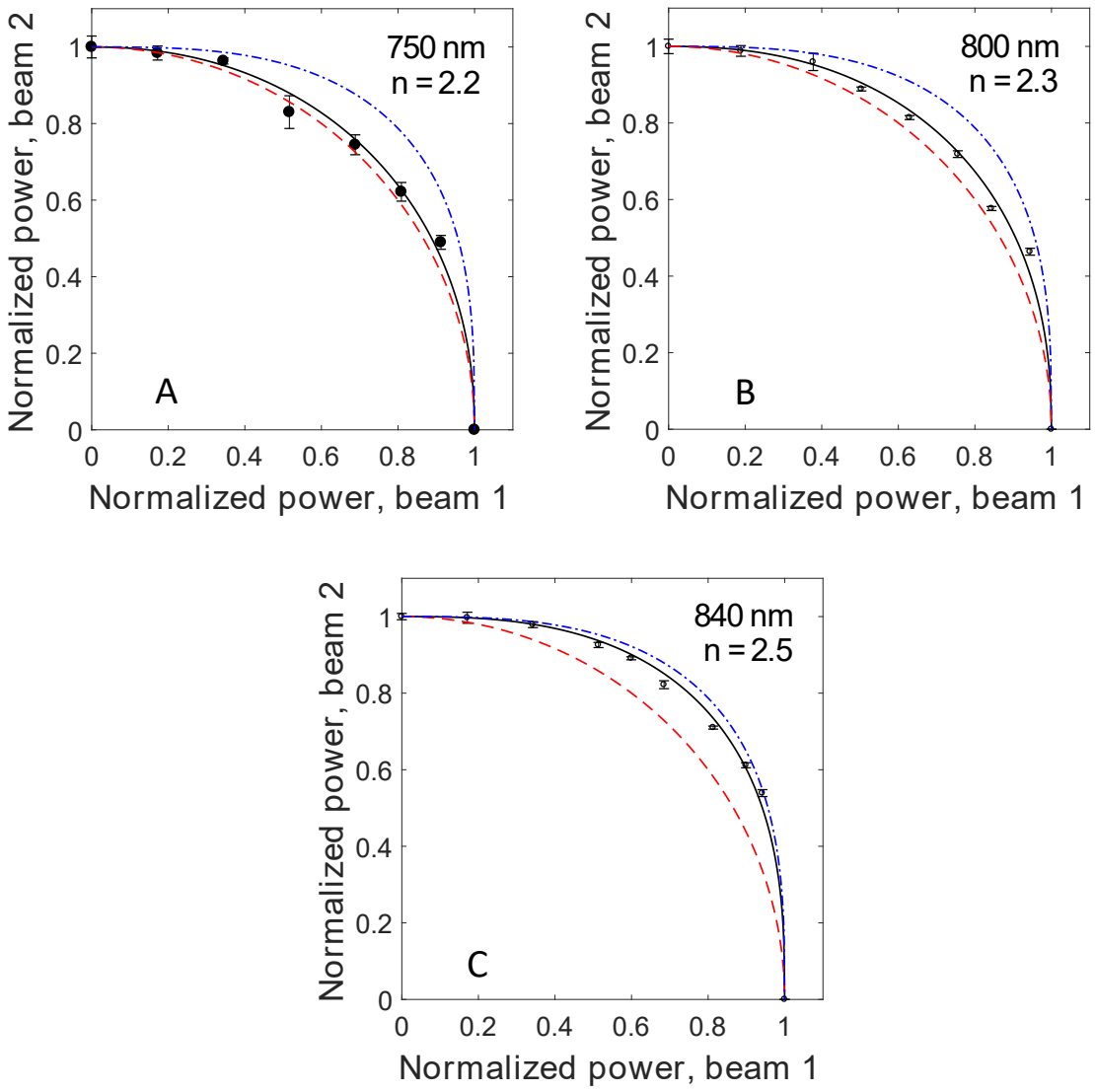

Figure 5.9: 2-BIT data for 1 wt% biacetyl in SR399 at excitation wavelengths of 750 nm (A), 800 nm (B), and 840 nm (C), and a velocity of 40 μm/sec. The black solid lines correspond to best fits to Eq. 3.13. For reference, the red dashed lines correspond to 2-photon absorption and blue dashed-dotted correspond to 3-photon absorption.

5.4.3 Dual-beam exposure

To test for deactivation, experiments were performed with two lasers. An 800 nm ML beam was used to initiate polymerization. Addition of an 800 nm CW

Wavelength, nm	n at 20 μm/sec	n at 40 μm/sec
750	2.0 ± 0.2	2.1 ± 0.1
800	2.4 ± 0.1	2.3 ± 0.2
840	2.7 ± 0.2	2.5 ± 0.1

Table 5.3: Summary of 2-BIT measurements of the order of effective nonlinear absorption in photoresist with in the 1wt% biacetyl in SR399 measured at 40 μm/sec fabrication velocity.

beam at the same spot and at the same time could inhibit polymerization completely. To demonstrate this effect, the 800 nm CW beam was periodically blocked with a mechanical chopper. As shown in Fig. 5.10, lines were formed under exposure to the

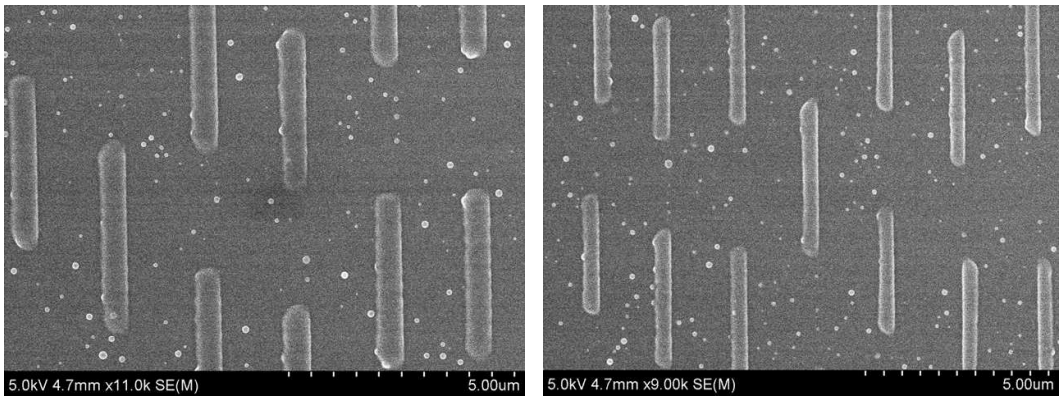

Figure 5.10: SEM images of polymerization deactivation in 1 wt% biacetyl in 1:1 SR368/499. Lines are formed by exposure to the 800 nm ML beam alone. The 800 nm CW beam was periodically blocked. The clear spaces along the lines indicate that the deactivation beam inhibited polymerization completely.

800 nm ML beam alone. Simultaneous exposure to both beams led to deactivation, as indicated by the breaks in the lines. Moreover, thorough examination of the SEM images revealed the absence of any polymerization traces or residual polymerization in the deactivated regions. Typically, SEM images of the lines made with 2-color photolithography show slight residual polymerization in deactivated regions [3]. In the photoresist containing biacetyl, clear spaces between the polymerized parts of the line illustrate more efficient polymerization deactivation.

Polymerization deactivation was further studied at other wavelengths. CW exposure with wavelengths ranging from 730 nm to 900 nm was found to deactivate polymerization that was initiated by ML excitation in the same range of wavelengths. For example, polymerization initiated by a 770 nm ML beam was inhibited by CW exposure at wavelengths ranging from 760 nm to 860 nm. The efficiency of deactivation of the CW beam depended on the wavelength that was used to initiate polymerization, as will be discussed in detail in the following sections.

Exposure to a 405 nm CW beam or a 445 nm CW beam also initiated polymerization. When a second CW laser at any wavelength ranging from 760 nm to 880 nm was added to the 405 nm or 445 nm beams, the width of the polymerized lines increased, indicating enhancement of polymerization rather than deactivation. The same effect was observed when the second beam was mode-locked. Similar linewidth increases were observed when the sample was simultaneously exposed to a 532 nm CW beam and a ML laser at any wavelength between 760 and 880 nm. However, exposure to either 532 nm CW light alone or to a combination of two CW beams, one at 532 nm, and the other between 760 nm and 880 nm, did not cause

polymerization in the sample. The results of the dual-beam exposure experiments are summarized in the Table 5.4 and Fig. 5.11.

Exposure conditions	800 nm ML + 760 - 880 nm CW	400 nm ML + 800 nm CW	405 nm CW + 760 - 880 nm CW or ML	532 nm CW + 760 - 880 nm ML	532 nm CW + 760 - 880 nm CW
Result	Deactivation	Activation	Activation	Activation	No polymerization

Table 5.4: Summary of results of multiple beam exposure experiments in the 1 wt% biacetyl in 1:1 SR368/499.

Exposure to a 400 nm ML beam initiated polymerization even at sub-mW powers. Simultaneous exposure to an 800 nm CW beam enhanced polymerization rather than deactivating it. For comparison, exposure to an 800 nm ML beam at 10 mW initiated polymerization. 800 nm CW deactivation was achieved at a comparable power. These results suggest that different excitation and polymerization channels are available for biacetyl. 800 nm ML excitation leads to a deactivatable state. 400 nm excitation, however, leads to irreversible polymerization. Possible pathways of excitation will be discussed in Section 5.4.5.

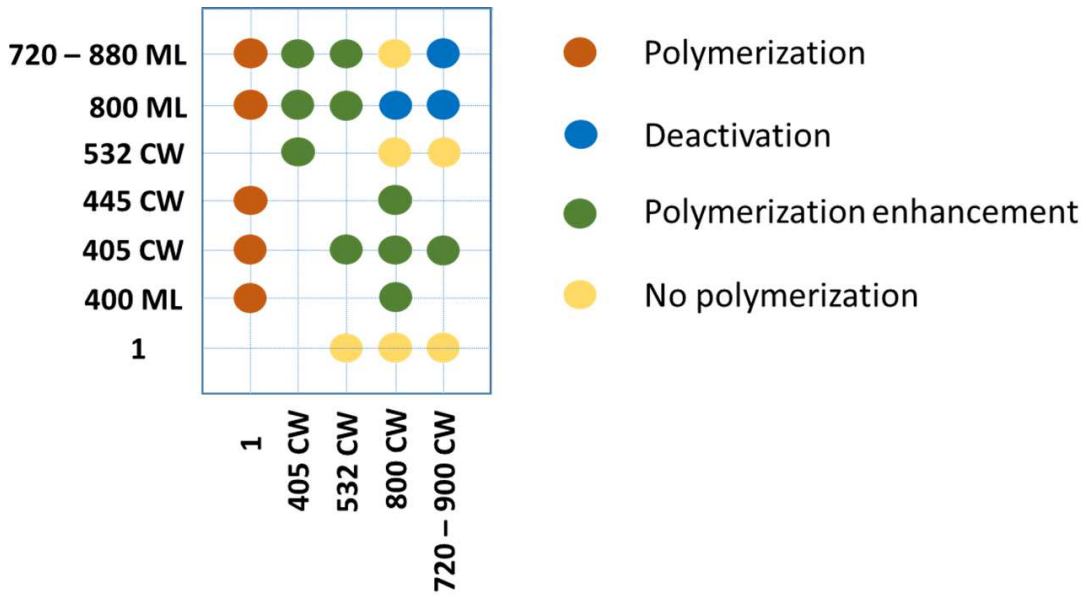

Figure 5.11: Summary of dual-beam exposure experiments for 1 wt% biacetyl in 1:1 SR368/499.

5.4.4 Deactivation

To investigate the deactivation efficiency, measurements were performed with 740 nm, 770 nm, and 800 nm ML excitation. For each of these excitation wavelengths, the CW deactivation wavelength was tuned from 730 nm to 900 nm in 10 nm steps. The power of the excitation beam was set at the polymerization threshold in each experiment. The efficiency of deactivation was defined as an inverse of the minimum power required to inhibit polymerization.

Fig. 5.12 presents deactivation action spectra for each excitation wavelength. The blue data points are for 740 nm excitation, the green data points are for 770 nm excitation and the red data points are for 800 nm excitation. At longer excitation wavelengths the deactivation action spectrum shifts to the red as well.

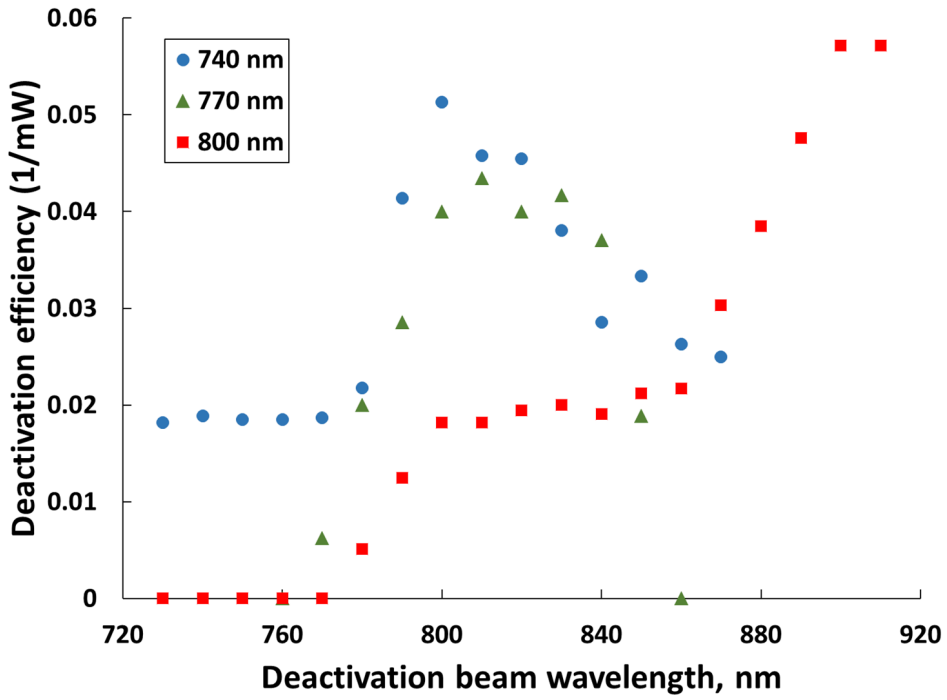

Figure 5.12: Deactivation action spectrum of 1 wt% biacetyl in 1:1 SR368/499. The data points correspond to the minimum power required for deactivating polymerization for excitation at 740 nm (blue), 770 nm (green), or 800 nm (red).

The deactivation action spectrum in Fig. 5.12 was measured for 1 wt% biacetyl in SR368 and SR499 monomers. Deactivation efficiency was also tested in another monomer, SR399. The deactivation action spectrum for biacetyl in SR399 was measured in the same manner as above. The ML excitation wavelengths tested were 750 nm, 770 nm, 800 nm, 830 nm, and 860 nm. For each excitation wavelength the CW deactivation beam was tuned between 730 nm and 940 nm in 10 nm steps. The results are shown in Fig. 5.13.

The data in Fig. 5.13 indicate that it is easier to turn off polymerization when it is initiated at some excitation wavelengths. For example, polymerization initiated

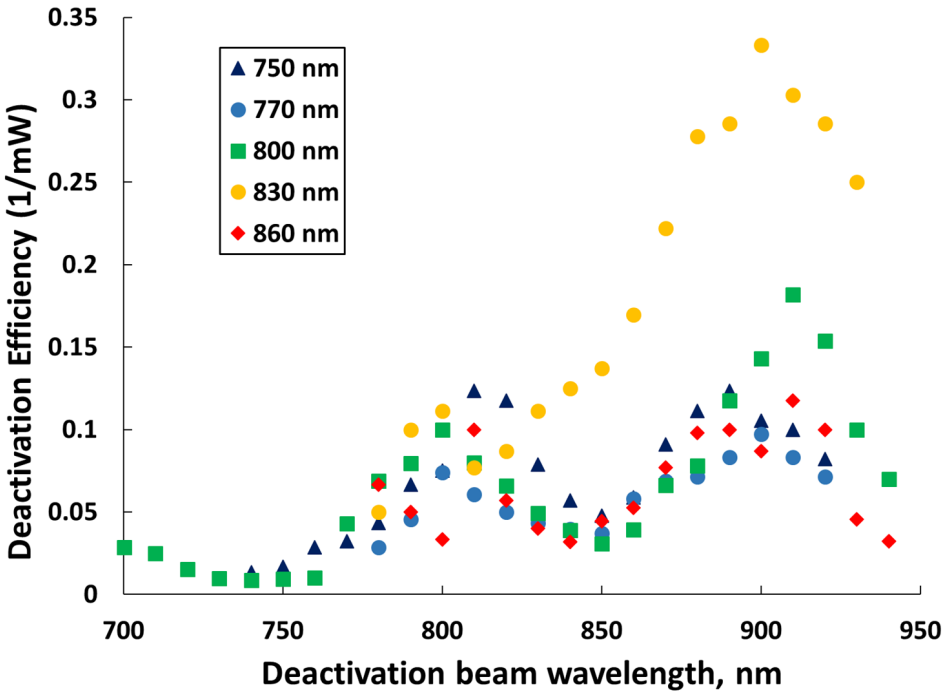

Figure 5.13: Deactivation action spectrum of 1 wt% biacetyl in SR399. The data points correspond to the minimum power required for deactivation for mode-locked excitation at 750 nm, 770 nm, 800 nm, 830 nm, and 860 nm.

at 800 nm is more efficiently deactivated compared to that initiated at 770 nm. These results may be indicative of self-deactivation during excitation.

The relationship between the deactivation efficiency and the wavelengths of the excitation and deactivation beams can be visualized through a 3D deactivation action spectrum (Fig. 5.14). The y axis on this plot is the excitation wavelength, the x axis is the deactivation wavelength, and the colors denote the deactivation efficiency. The powers were measured only for the wavelength combinations in Fig. 5.13. The remaining data values were interpolated. Based on this plot, the most

efficient polymerization deactivation is achieved for excitation wavelengths between 820 nm and 840 nm, and a CW deactivation wavelength of 900 nm.

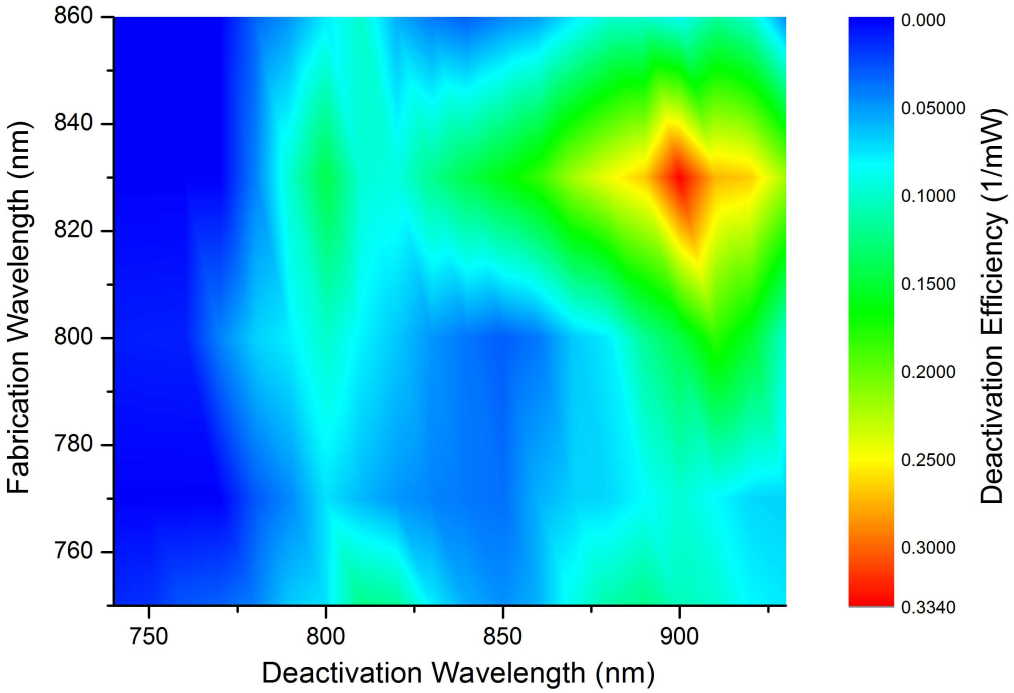

Figure 5.14: The 3D deactivation action spectrum of 1 wt% biacetyl in SR399. The data points are experimentally measured for 750 nm, 770 nm, 800 nm, 830 nm, and 860 nm excitation. The deactivation beam was tuned between 730 nm and 940 nm with a 10 nm step. The remaining data are interpolated from the experimentally measured values.

5.4.5 Interpreting the excitation and deactivation data

As can be seen from Figs. 5.13 and 5.14, the polymerization deactivation efficiency depends on the excitation and deactivation wavelengths. The deactivation action spectrum resembles the transient triplet absorption spectrum of biacetyl, (Fig. 5.15) [128]. This correlation suggests that deactivation involves excitation

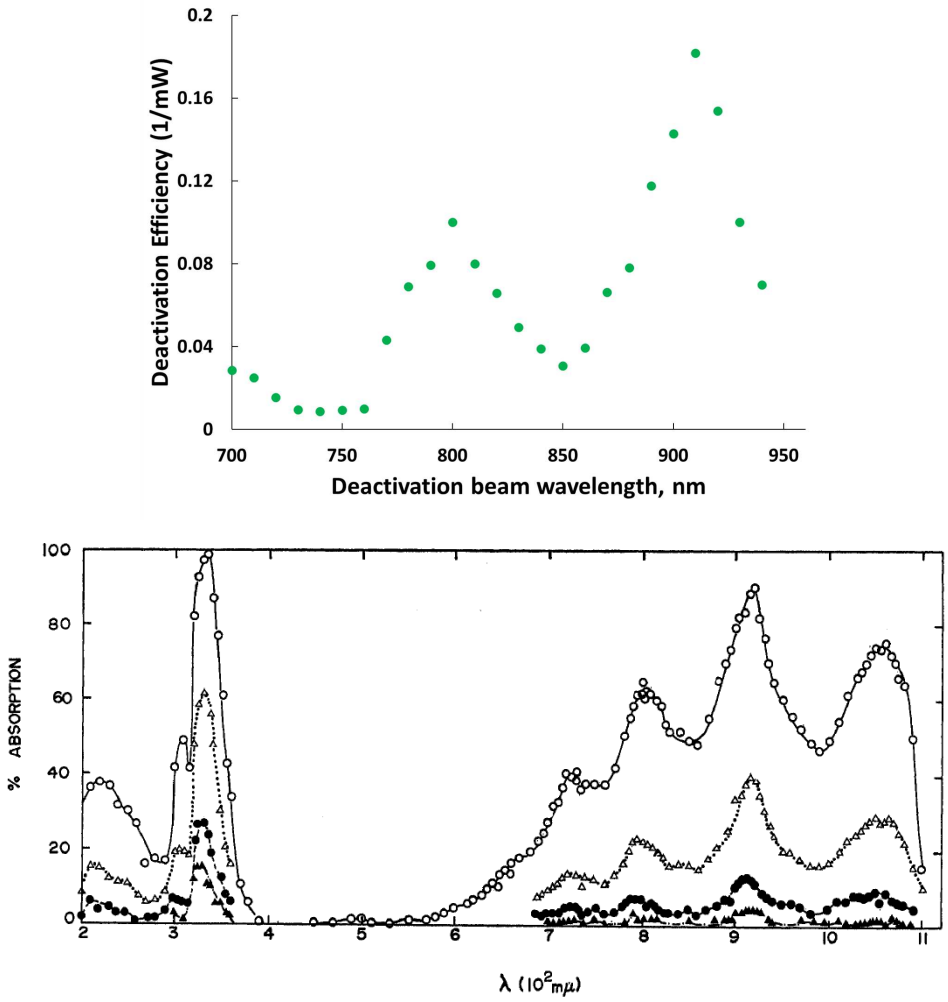

Figure 5.15: Deactivation action spectrum of 1 wt% biacetyl in SR399 at 800 nm excitation (top). Triplet transient absorption spectrum for biacetyl in carbon tetrachloride [128] (bottom).

from T_1. Deactivation may therefore occur from reverse intersystem crossing (RISC) from a higher triplet state. Some photoinitiators have been shown, by performing time-resolved experiments and testing polymerization inhibition for different timing settings, to deactivate via RISC from the excited triplet state [129]. Our collaborator Dr. Daniel Falvey has calculated vertical transition energies in biacetyl using

density functional theory methods. Geometries were optimized at the (u)M062X/6-311G+(d,p) level (Fig. 5.16).

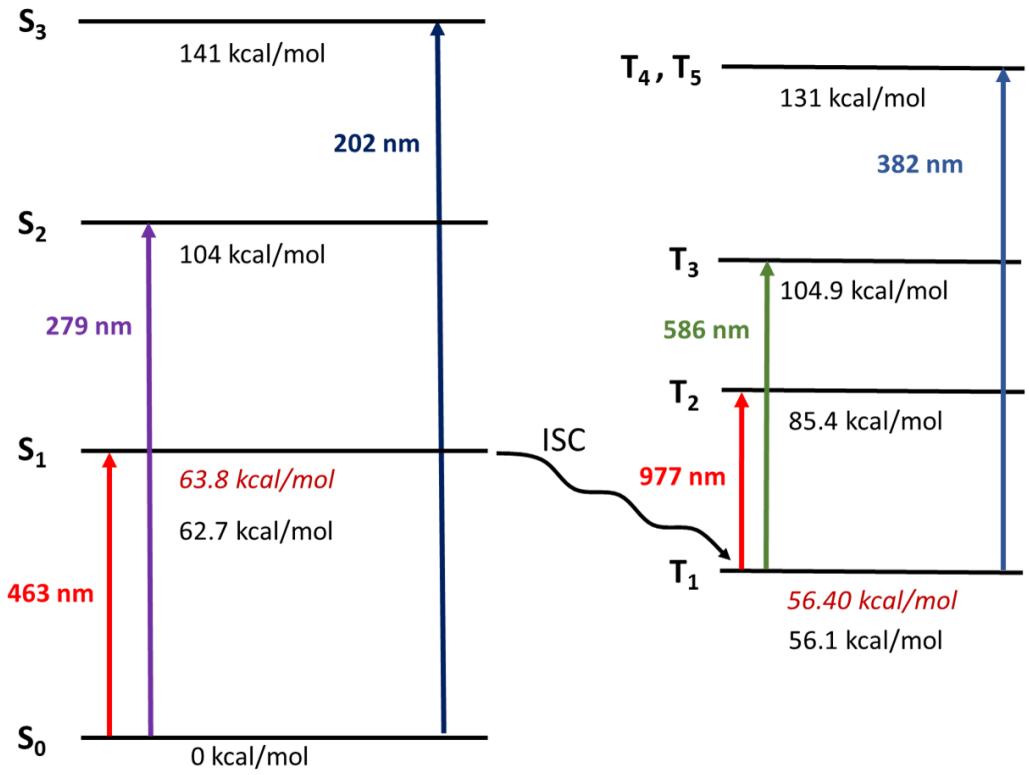

Figure 5.16: Schematic diagram of biacetyl levels, calculated by Dr. Daniel Falvey, unpublished. The energy level values in italic are reported in [125].

Biacetyl is known to have a high quantum yield for ISC [119,120,128], so most excited molecules will end up in T_1. 800 nm photons from the deactivation beam are energetic enough to drive absorption to T_2. From T_2 molecules can undergo RISC to a highly vibrationally excited level of the ground state S_0, thus preventing polymerization. We do not know for sure how polymerization is initiated in molecules

that are not deactivated, but one possibility is excitation to a higher triplet state by a subsequent excitation pulse.

Another possible pathway for initiation is triplet-triplet annihilation (TTA). The triplet transient absorption spectrum of biacetyl was measured in benzene at 355 nm pulsed excitation (Fig. 5.17). The spectrum has bleaching at 450 nm corresponding to strong ground state absorption as compared to the triplet state absorption at this wavelength. Fig. 5.18 shows a transient of triplet biacetyl at 320 nm. The triplet decay at 320 nm was fitted with second-order kinetics, which is consistent with triplet formation through a triplet-triplet annihilation process.

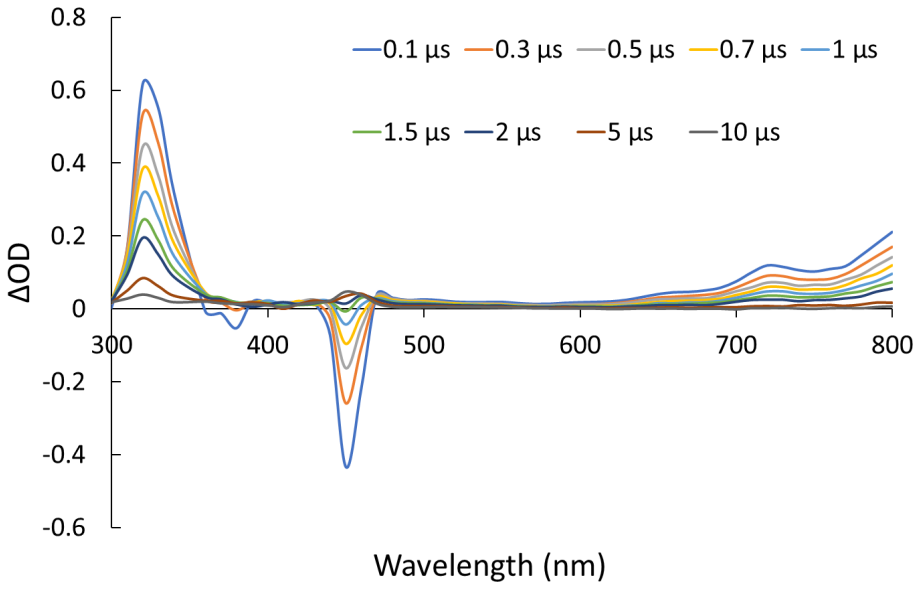

Figure 5.17: Transient absorption spectrum of biacetyl in benzene following 355 nm pulsed excitation.

Biacetyl cannot be deactivated following linear excitation, which suggests that initiation follows a different pathway in this case. One pathway for initiation with

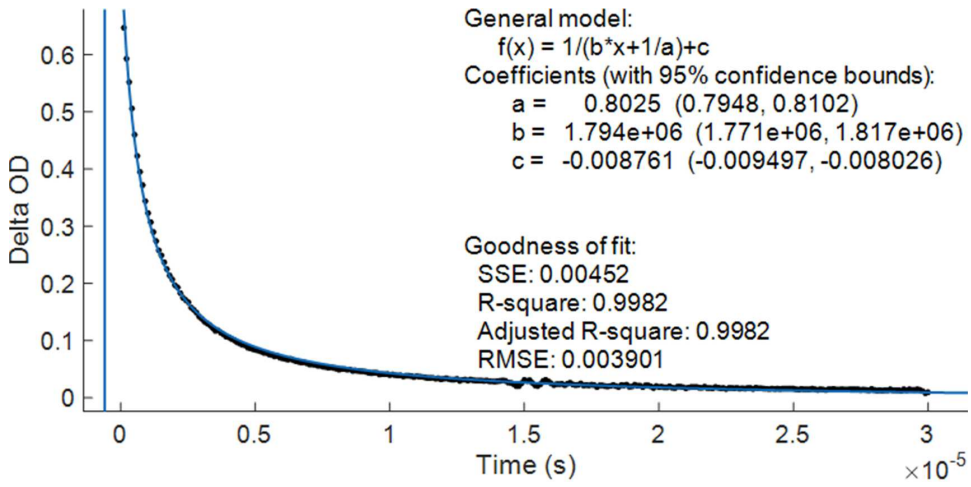

Figure 5.18: Waveform of triplet biacetyl at 320 nm.

biacetyl in the 400 nm wavelength range might involve excited-state absorption from S_1. Because the reported lifetime of the S_1 state of 10.6 nsec [119] is comparable to the repetition rate of the excitation laser (∼13 nsec), a second 400 nm pulse might excite molecules that have not yet undergone ISC. By the same token, 405 nm and 445 nm CW light could also drive this process (Fig. 5.19A).

Another possible pathway could involve triplet states, taking place simultaneously with excited-state absorption from S_1. Some of the molecules from S_1 can undergo ISC to the lowest triplet state. TTA can occur regardless of the mechanism of excitation (Fig. 5.19B). As seen in Fig. 5.15, biacetyl has no triplet absorption at 400 nm, so linear absorption to higher triplet states is unlikely to be involved. However, 800 nm light can take molecules to T_2, from which absorption at 400 nm is expected. Thus, initiation may again occur from higher triplet state if RISC is a slow process (Fig. 5.19C).

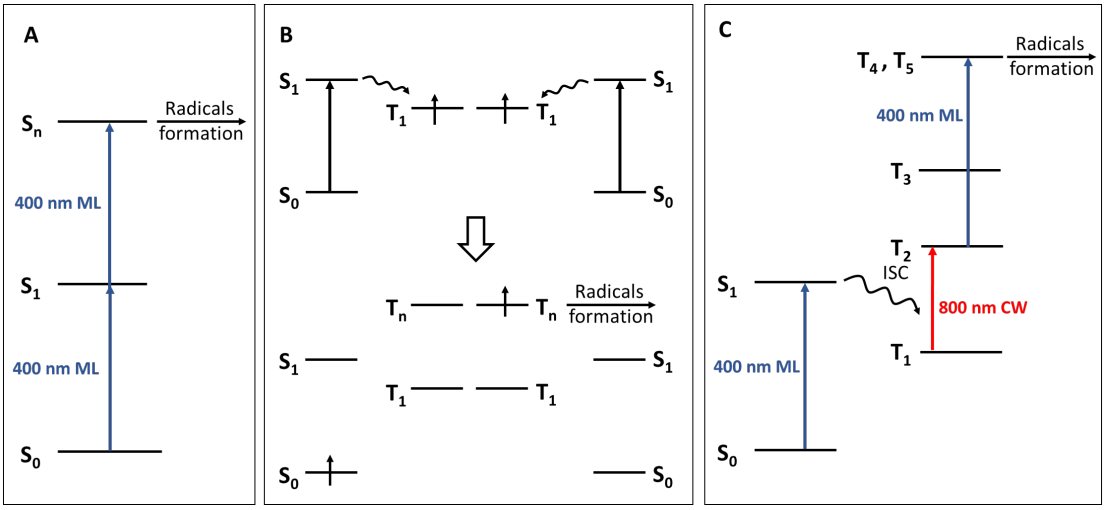

Figure 5.19: Possible excitation pathways of biacetyl: A) excited-singlet state absorption; B) triplet-triplet annihilation. C) triplet state absorption.

To explore the initiation pathways in greater detail, we added stilbene to the photoresist. Stilbene is a triplet quencher that had not been reported to initiate polymerization. When half an equivalent of stilbene was mixed into 1 wt% biacetyl in SR399, the polymerization threshold increased for 800 nm ML excitation, 400 nm ML excitation, and 405 nm CW excitation. The results of these experiments are summarized in Table 5.5. The most important result is that the increase in the threshold was much greater for linear excitation than for nonlinear excitation. The presence of stilbene did not change the effect of adding an 800 nm CW beam. Initiation was enhanced in all cases.

Although it was not a known photoinitiator, control experiments revealed that stilbene alone in the monomer mixture can initiate polymerization with an 800 nm ML beam. Thus, the 800 nm ML data cannot be compared directly with the other

1 wt% biacetyl in SR 399 no quencher		1 wt% biacetyl in SR 399 with half equivalent stilbene	
Laser beam	Powers before periscope, mW	Laser beam	Powers before periscope, mW
800 nm ML	10	800 nm ML	14
400 nm ML	0.3	400 nm ML	6
405 nm CW	4 (laser controller)	405 nm CW	35 (laser controller)

Table 5.5: Effect of stilbene on polymerization threshold the 1wt% biacetyl in SR399 photoresist

data. However, the fact that the polymerization threshold under linear excitation increases in the presence of stilbene confirms that a prevalent initiation pathway involves triplets. Additional studies are required to develop a deeper understanding of initiation with biacetyl. For example, it would be of great interest to measure the T_2 lifetime. Another experiment would be to measure the deactivation efficiency with excitation at a lower repetition rate.

5.4.6 Resolution improvement experiments

Because polymerization can be deactivated completely at different wavelengths, resolution enhancement experiments were performed with two laser beams. To de-

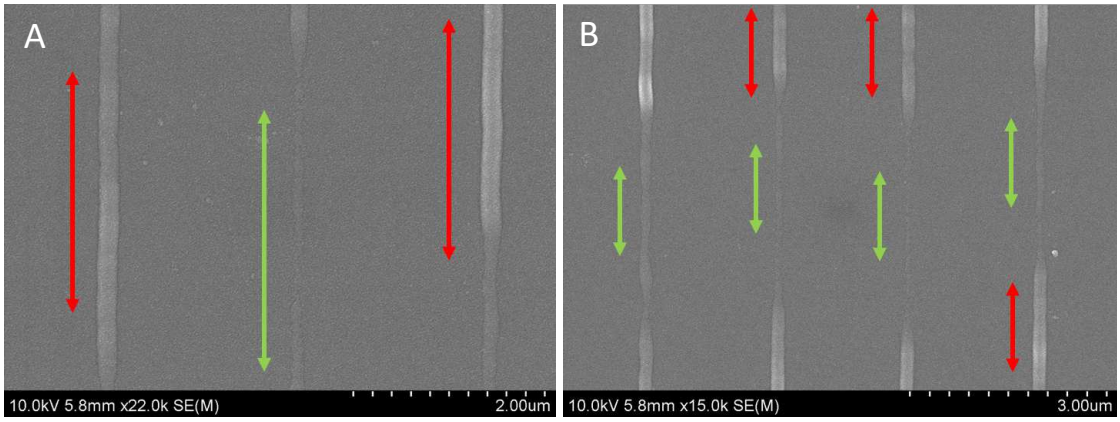

Figure 5.20: (A)-(B) Linewidth decrease with a radially polarized, 800 nm deactivation beam. The red arrows indicate lines fabricated with an excitation beam only, the green arrows indicate lines formed with both excitation and deactivation beams. The linewidth decreased from 200 ± 25 nm to 90 ± 10 nm when two beams were used instead of one.

crease the width of the fabricated lines, the intensity distribution of the deactivation beam was changed. The deactivation beam was sent through a radial polarizer and aligned with the fabrication beam using luminescence from the gold nanoparticles, as described in Section 2.1. In Fig. 5.20 the red arrows indicate lines that were fabricated with only the 800 nm ML beam at 13 mW. The green arrows indicate lines polymerized under simultaneous exposure to 800 nm ML and 800 nm CW beams. With the deactivation beam set at 36 mW, the width of the lines was 90 ± 10 nm, compared to 200 ± 25 nm with 800 nm ML only. These two wavelengths were chosen as the center wavelengths of the femtosecond laser, with more power available as compared to other wavelengths.

Lines with approximately 90 nm width were fabricated at a 2 μm pitch, meaning that for each fabricated line, the laser beam focus was moved 2 μm away from

the previously fabricated line to create the next one. 2 μm is far enough apart to consider features to be isolated, without the impact of exposure building up for each laser pass to fabricate the next line.

To establish the resolution for the biacetyl-based photoresist, a series of lines was fabricated at a decreasing pitch. Lines were first made at a 400 nm pitch. The pitch then was decreased in 10 nm steps. The polymerized structures were analyzed with SEM to determine the minimum pitch at which line were still separate. This experiment was repeated for various sets of the excitation and deactivation laser beam powers.

Shown in Fig. 5.21 are examples of lines with minimum pitch and linewidth values. For the deactivation beam set at 60 mW (Fig. 5.21A), the closest distance at which the lines were fabricated before merging was 70 $\pm$ 5 nm, with a linewidth of 190 $\pm$ 8 nm, corresponding to a 250 nm pitch. A deactivation beam power of 18 mW (Fig. 5.21B) gave lines with comparable size (200 $\pm$ 10 nm), but at finer pitch (220 nm).

The resolution enhancement experiments used a CW deactivation beam with a power of up to 60 mW. The resultant linewidth and resolution were not as good as initially expected. It was later found that, at high powers, the CW beam does not deactivate polymerization. Instead, it leads to the formation of wider lines. A CW beam at lower powers than the 60 mW used might result in a finer pitch.

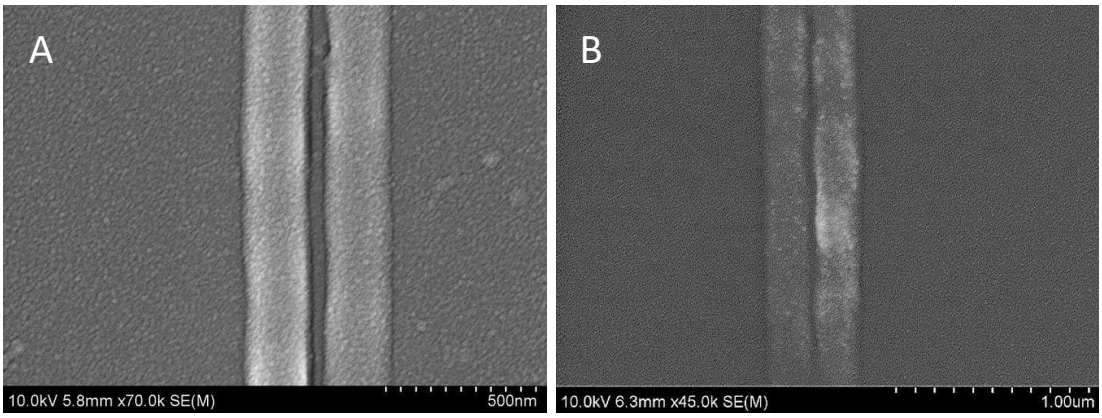

Figure 5.21: A) Polymerization deactivation with overlapped excitation and radially polarized, 800 nm deactivation beams at 15 mW and 60 mW respectively. The width of the lines was 190 ± 8 nm at 250 nm pitch. B) Polymerization deactivation with overlapped excitation and radially polarized, 800 nm deactivation beams at 15 mW and 18 mW respectively. The linewidth was 200 ± 20 nm at 220 nm pitch.

5.5 Conclusions

It has been shown that biacetyl, a vicinal diketone, can be used as a radical photoinitiator in an acrylate-monomer-based photoresist. Polymerization initiation was observed under pulsed exposure at wavelengths ranging from 730 nm to 870 nm. Polymerization was also initiated by 400 nm pulsed light, as well as by CW 405 nm and 445 nm light. The measured polymerization action spectrum of biacetyl in SR368/499 shows that MAP is most efficiently initiated at 790 nm.

The order of the effective nonlinear absorption in the photoresist was measured with 2-BIT. The effective number of absorbed photons necessary to initiate polymerization changed from two to almost three as the exposure wavelength increased. This result indicates that, at these wavelengths, other processes are involved, result-

ing in more highly nonlinear behavior. In the experiments with varied fabrication velocity, the nonlinear order decreased as the fabrication velocity increased.

Additional experiments with more control parameters would allow further exploration into the effect of the fabrication wavelength and the fabrication velocity on the order of nonlinear absorption. For example, combining two separate lasers with the ability to vary the delay between pulses would provide information about how fast biacetyl molecules are excited to the state that creates radicals. In addition, 2-BIT data, collected by exposing a sample to two beams at different wavelengths, could reveal information about different states involved in the polymerization reaction.

Exposure of the photoresist to a combination of available wavelengths revealed that certain dual-beam exposure conditions inhibit polymerization. Polymerization initiated by a mode-locked laser at a wavelength ranging from 750 nm to 860 nm can be completely prevented by a second CW laser at a wavelength in the 730 nm to 940 nm range. The most efficient deactivation was achieved when the excitation beam was between 820 nm and 840 nm and the deactivation beam was at 900 nm. The agreement of the measured deactivation action spectrum with the transient absorption spectrum suggests that deactivation takes place from the second excited state of biacetyl through reverse intersystem crossing.

When polymerization was initiated by any other wavelength, e.g. mode-locked 400 nm, or CW 405 nm, or CW 445 nm, no deactivation was observed at any power. This phenomenon might result from excitation of the molecules to the singlet state by any of the previously mentioned wavelengths. The addition of a second CW

beam enhances polymerization. We have presented unambiguous evidence that at least some initiation follows intersystem crossing to T_1. The idea that deactivation occurs through T_2 needs to be tested by measuring the polymerization deactivation with the excitation beam at a varied repetition rate and varied pulse delay. Although the polymerization initiation process can take place through triplet-triplet annihilation, higher resolution might be achieved by linking biacetyl molecules to the acrylate monomers to prevent TTA through inhibiting diffusion and providing steric hindrance.

Linewidth and resolution improvement experiments were performed with 800 nm ML and 800 nm CW beams. The width of the isolated lines decreased from 200 $\pm$ 25 nm when only the 800 nm ML beam was used to 90 $\pm$ 10 nm with the addition of the phase-shaped deactivation beam. The smallest pitch at which lines were still separate was 240 nm, with lines of width of 200 $\pm$ 10 nm separated by about 40 nm. The experiments on resolution improvement used a deactivation beam with CW powers up to 60 mW. High deactivation powers resulted in wider lines and lower resolution than were initially expected. This result could be improved upon employing more appropriate deactivation powers. Additional experiments that focus on lower deactivation powers are likely to yield a better resolution and smaller pitch. Additionally, more efficient deactivation, resulting in more closely placed features, could be achieved by reconfiguring the optical setup for the deactivation beam to include the option of varying the distance between the deactivating lobes of the beam.

Chapter 6

Study of potential molecules for 3-color photolithography

Contributors: Zuleykhan Tomova, Nikolaos Liaros, Sandra A. Gutierrez Razo, Ryan Dempsey, Samuel Cohen, Steven M. Wolf, Matthew Thum.

Contributions: 2-BIT measurements of benzil were performed by Z.T. and N.L.; polymerization initiation and deactivation experiments of benzil and pyridil were performed by Z.T.; polymerization action spectrum of benzil and β-naphthil, 2-BIT measurements of β-naphthil were performed by R.D.; samples were prepared by Z.T., S.G.R. and R.D.; SEM measurements were performed by Z.T.; Matlab code for the best-fit exponential to 2-BIT data was written by S.C.; UV-visible and transient absorption spectra were collected by S.W. and M.T.; α-naphthil and β-naphthil were synthesized by S.W.

6.1 Introduction

Benzil, α-naphthil, β-naphthil and pyridil (Fig. 6.1) are additional vicinal diketones that were tested as potential photoinitiators for three-color photolithography. This chapter describes our preliminary experiments with these compounds.

Benzil is a compound that includes two carbonyl and two phenyl groups, and has been used as a radical photoinitiator [14, 130–134]. The literature contains conflicting reports on the photophysics of benzil. Upon irradiation at 308 - 355 nm benzil is excited to the S_1 state. Benzil has been found to undergo fast ISC to the T_1 state in solvents including benzene [135], deoxygenated carbon tetrachloride [136], cyclohexane [137], acetonitrile [138], and liquid paraffin [139].

The maximum of the absorption spectrum of benzil in acetonitrile was reported to be at 378 nm by Malval *et al.* [138]. Fluorescence was measured by exciting

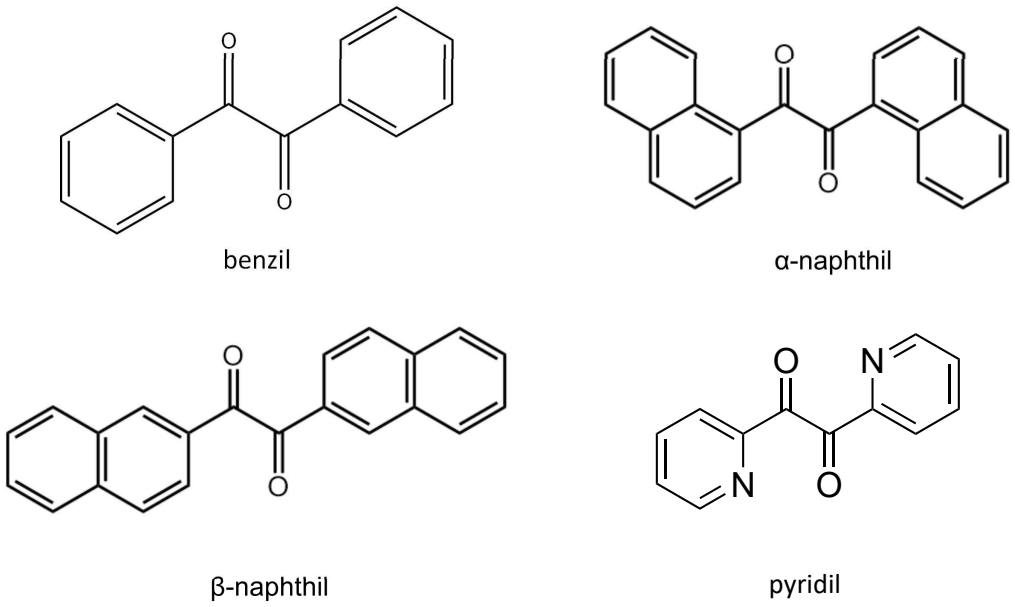

Figure 6.1: Structure of photoinitiators studied.

benzil in cyclohexane and in acetonitrile with a 372 nm pulsed laser [138]. The fluorescence bands of benzil were found to reach a maximum at around 500 nm in both solvents. The phosphorescence spectrum was measured in a glassy matrix at 77 K, and showed a peak at 560 nm that was assigned to a triplet state. The triplet-state energy in acetonitrile was determined to be $E_T = 50.9$ kcal/mol, as compared to the 53.0 kcal/mol measured in a solution of ethylether-isopentane-ethanol by Evans *et al.* [140]. The triplet state absorption band maximum was found to lie at 480 nm by measuring the transient absorption spectrum in deaerated acetonitrile [138].

The absorption maximum of the excited benzil singlet state was reported to be at 525 nm for solution in cyclohexane by Ikeda *et al.* [137]. This peak decays within 3 ns, in agreement with the expected singlet lifetime. A peak in the tran-

sient spectrum at 490 nm was assigned to triplet-state absorption, as compared to the transient absorption peak at 505 nm, reported by Morris and Yoshihara [141] for benzil crystals, and to a peak of the triplet absorption spectrum at ∼480 nm measured in liquid paraffin by Porter *et al.* [139].

Benzil's singlet lifetime ($\tau_1 = 2.6$ ns) was determined by time-correlated single-photon counting in cyclohexane at 293 K, as reported by McGimpsey *et al.* [135]. Fluorescence lifetimes of $\tau_1 = 1.95 \pm 0.05$ ns in cyclohexane and 2.1 ± 0.05 ns in benzene were reported by Flamigni *et al.* [142], and a lifetime of 2.2 ns in cyclohexane was reported by Ikeda *et al.* [137].

According to Bhattacharya *et al.* [143] the S_1 lifetime of benzil varies between 1.35 ± 0.1 ns and 2.35 ± 0.2 ns in methyl cyclohexane and between 1.28 ± 0.1 ns and 2.22 ± 0.2 ns in ethanol, when the excitation wavelength changes from 295 nm to 370 nm. They observed two absorption bands in the 360 - 440 nm range and a stronger absorption band below 350 nm. Upon photoexcitation at 370 nm in both methyl cyclohexane and ethanol, emission bands were observed at 505 nm and 415-430 nm. Under exposure at 320 nm, an additional broad band was observed at 360 nm. These bands were assigned to different electronic states with different conformations. Emission at 505 nm was assigned to fluorescence from the relaxed transplanar geometry of the S_1 state, with a lifetime of 2.2 ± 0.2 ns, in both methyl hexane and ethanol under exposure at 370 nm. Exposure to 296 nm light resulted in lifetimes of 2.4 ± 0.2 ns and 2.1 ± 0.2 ns in methyl cyclohexane and ethanol, respectively. Emission at 360 nm was assigned to fluorescence from the S_2 state, which has a skew geometry, similar to the conformation of the ground state of benzil.

The lifetime of this state was determined to be 1.4 ± 0.1 ns and 1.3 ± 0.1 ns in methyl cyclohexane and ethanol, respectively. Emission at 420 nm was assigned to fluorescence from the S_1 geometry with the skew form. However, fluorescence at 420 nm showed a biexponential decay, with the major component lifetime of about 0.23 ns and a minor component of 2.2 ± 0.2 ns in ethanol. These components were assigned to the relaxed skew and transplannar forms, respectively.

McGimpsey and Scaiano observed a nonlinear dependence of the triplet state yield on the laser dose, which they explained as a contribution from sequential absorption process occurring during the 308 nm pulsed laser excitation [135]. They observed depletion of the lowest triplet state of benzil in benzene solution via 308 nm pulsed laser excitation followed by 517 nm pulsed laser excitation, and proposed that radical formation takes place from an excited triplet state. They concluded that the absorption of the first photon leads to creation of the T_1 state and absorption of the second photon leads to a Norrish type I cleavage of benzil into benzoyl radicals.

Mukai *et al.* [144] reported formation of benzil ketyl and benzoyl radicals in isopropyl alcohol and the benzil anion radical in benzene-triethylamine (TEA) by performing time-resolved electron paramagnetic resonance (TREPR) measurements. According to this study, the radicals observed are produced from different excited triplet states of benzil. Because the benzil anion radical absorption signal in the benzene-TEA mixed solvent was directly proportional to the laser intensity, it was assumed that this radical is produced through single-photon absorption from T_1. The benzil ketyl and benzoyl radical intensities depended on the square of the laser intensity and were produced from a higher excited triplet state of benzil, T_n, through

sequential absorption. They also found that increasing the concentration of amines in the TEA solvent led to an increase in the anion radicals and a decrease in the ketyl and benzoyl radicals, indicating that the formation pathways of different radicals compete with one another.

Mukai *et al.* [145] discussed the excitation mechanisms leading to the formation of benzil ketyl and benzoyl radicals, as well as to the benzil anion radical. The two mechanisms of T_n formation through sequential absorption are 1) direct $T_1 \rightarrow T_n$ excitation and 2) excited singlet state absorption $S_1 \rightarrow S_n$, followed by the ISC to the T_n state. According to Mukai *et al.* [145] the sequential absorption process that leads to the formation of T_n takes place through the singlet state absorption pathway.

The observed results are summarized in Fig. 6.2A, which shows the potential benzil excitation pathway suggested by Mukai *et al.*, reproduced from [145]. Fig. 6.2B shows the benzil excitation pathway proposed by McGimpsey and Scaiano [135].

Mizuno *et al.* [136] measured time-resolved infrared spectrum of benzil following excitation in deoxygenated carbon tetrachloride with a 262 nm pulsed laser. Upon photoexcitation, the formation of the T_1 state was observed. This state had a lifetime of $\sim$10 μsec. Because the measured T_1 decay rates could not be fit with first-order kinetics, and because the addition of oxygen resulted in a shorter lifetime, the decay of T_1 was assumed to arise from triplet-triplet annihilation.

Flamigni *et al.* [142] measured the decay times of the fluorescence and phosphorescence of benzil in cyclohexane and benzene solutions at low concentration at

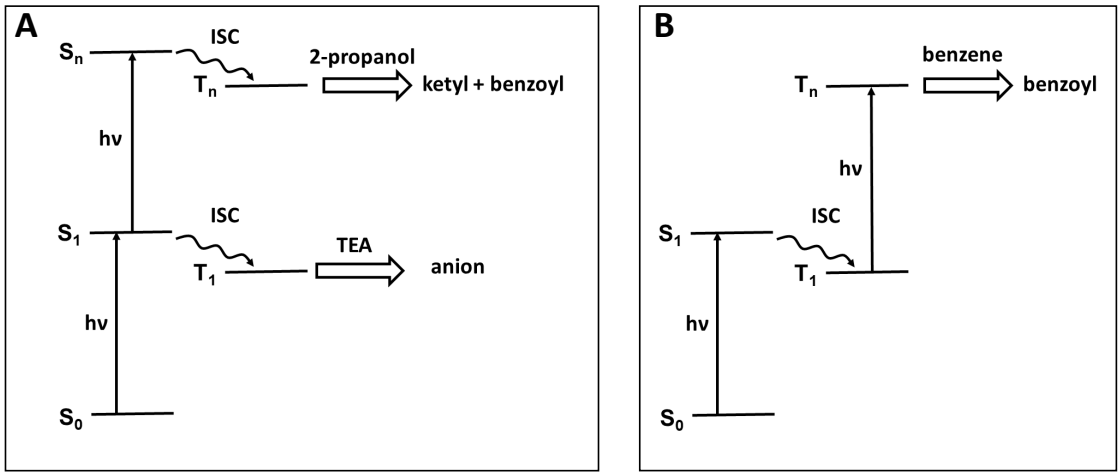

Figure 6.2: A) Benzil excitation and radical formation pathways proposed by Mukai *et al.* in benzene-TEA and isopropyl alcohol solutions (reproduced from [145]). B) Benzil excitation and radical formation pathway proposed by McGimpsey and Scaiano in benzene solution [135].

temperatures ranging from 20 °C to 69 °C. The phosphoresce decay was fitted with first-order kinetics, and triplet-triplet annihilation was not considered significant. According to the study of Flamini *et al.*, the decay of T_1 is due to phosphoresce.

The lifetime of T_1 measured by Mukai *et al.* in 2-propanol at room temperature was about 3 μs [145]. However, at -10 °C it was reported to be 9 μs in absence of oxygen. Mukai *et al.* reported triplet-state quenching by oxygen, leading to a shortening of the triplet lifetime to 0.2 μs at -10 °C and 0.4 μs at -40 °C. Malval reported a triplet state lifetime of 0.45 μs in deaerated acetonitrile at 300 K [138].

Benzil was studied as a 3-color photoinitiator based on these photophysical and phochemical properties. Upon photoexcitation at a wavelength in the vicinity of 400 nm, benzil transitions to the S_1 state and undergoes efficient intersystem crossing to T_1 [146–148]. The position of the absorption spectrum suggests possibility of

benzil excitation through two-photon absorption with 800 nm light. The triplet-state absorption at ∼480 nm measured in liquid paraffin [139] makes benzil a potential candidate for performing three-color photolithorgaphy, because exposure of benzil in the T_1 state can transfer molecules to higher triplet states that create free radicals. Some of the key benzil properties reported in literature are summarized in Table 6.1.

Absorption band	360 - 440 nm [143]
Singlet S_1 state lifetime	2.1 ± 0.05 ns in benzene [142]
Triplet T_1 state lifetime	∼3 μs in 2-propanol [145]
Singlet S_1 state energy	59.03 kcal/mol [125]
Triplet T_1 state energy	53 kcal/mol [140]

Table 6.1: Summary of reported properties of benzil.

α-naphthil, and β-naphthil are other vicinal diketones that were tested as potential 3-color photoinitiators (Fig. 6.1). These compounds, which were reported previously [149, 150], consist of two carbonyl groups and two conjugate naphthyl groups. Pyridil was also tested as a photoinitiator for 3-color photolithography. The absorption bands of pyridil in cyclohexane lie in the 200 - 300 nm and the 320 - 450 nm wavelength regions (Fig.6.3) [151–153].

In a study reported by Yamada *et al.* [154], changes in the absorption spectrum of pyridil were observed under steady light irradiation in deoxygenated ethanol, Fig.

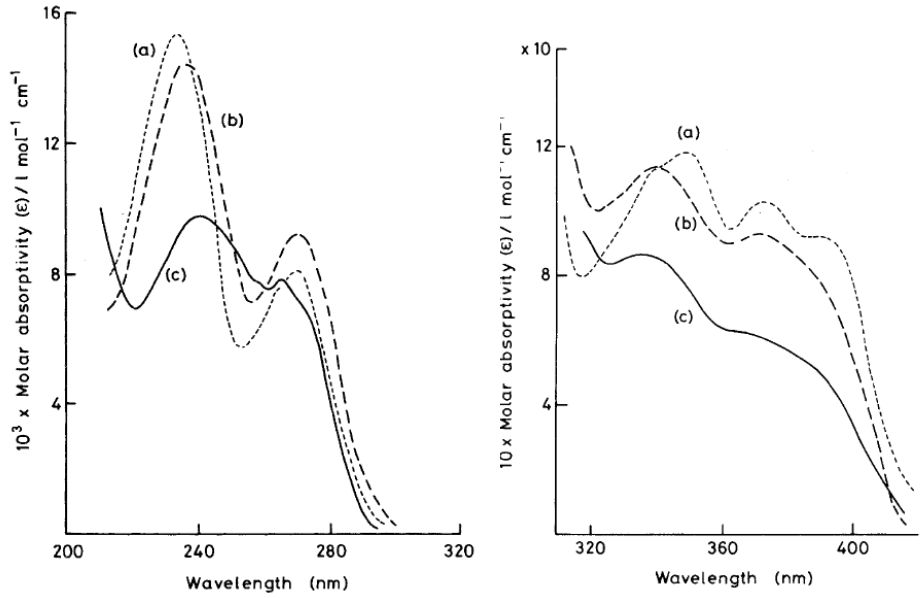

Figure 6.3: Absorption spectra of pyridil in cyclohexane (a), ethanol (b), and ethylene glycol (c) [152].

6.4. Similar to benzil, the ground state of pyridil takes skewed structure and the excited states are planar. Time-resolved transient absorption spectra showed bands at 552 nm and 445 nm that were assigned to a skewed triplet species [154].

6.2 Materials and method

Benzil was obtained from Sigma Aldrich and was used without further purification. α-naphthil and β-naphthil were synthesized by our collaborator, Steven Wolf, following procedures described previously [149,150]. Each photoinitiator was mixed with monomers SR368 and SR499 and the samples were prepared as described in Section 2.2. Single- and dual-beam exposures to wavelengths ranging from 720 nm

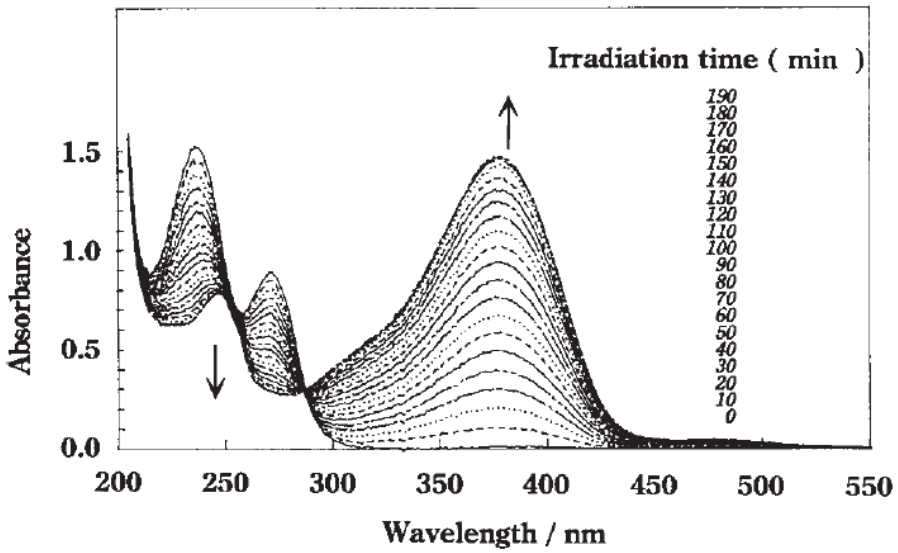

Figure 6.4: Absorption spectra of pyridil in deoxygenated ethanol [154].

to 900 nm were performed with a tunable Ti:Sapphire oscillator, as described in Section 2.1.

6.3 Benzil results

6.3.1 Polymerization initiation

The absorption spectrum of benzil in benzene (the blue line in Fig. 6.5), has a peak at approximately 390 nm, which suggests the possibility for two-photon absorption polymerization using a laser at a wavelength in the near-IR region. It was found that exposure of a photoresist containing benzil to an 800 nm ML beam initiates polymerization. Mode-locked light at wavelengths between 730 nm and 850 nm was also tested. Polymerization was observed over this entire wavelength range.

Because light at different wavelengths initiated polymerization at different powers, a polymerization action spectrum was measured to determine the wavelength dependence of the polymerization initiation efficiency. The red symbols in Fig. 6.5 correspond to the polymerization action spectrum of 1 wt% benzil in 1:1 SR368/499. The dots correspond to $1/P^2$ at the polymerization threshold for each wavelengths tested.

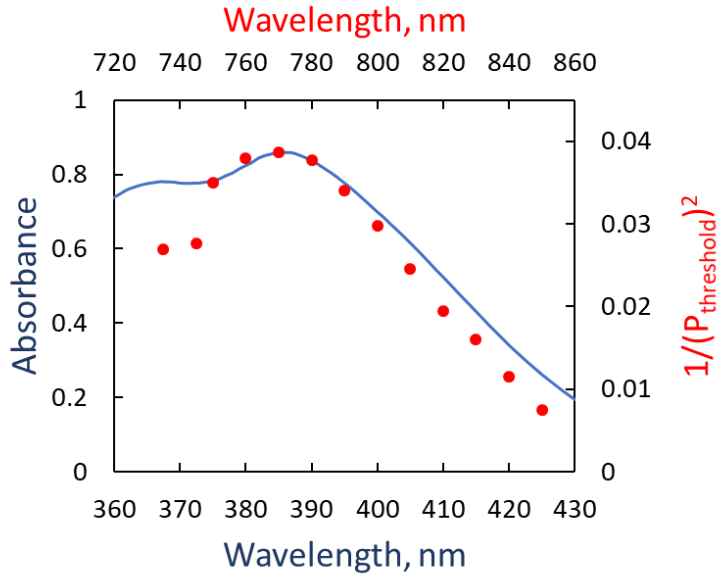

Figure 6.5: Absorption spectrum of benzil in benzene, 53 mM, (blue line) and polymerization action spectrum of benzil in 1:1 SR368/499 (red dots).

The shape and the position of the polymerization action spectrum match those of the absorption spectrum, suggesting that the first step in initiation is excitation to S_1. MAP was most efficiently initiated at 770 nm, i.e. it required the least amount of power to start the reaction at this wavelength. However, it is worth noting that

the polymerization threshold at the wavelengths ranging from 750 nm to 810 nm only by varied by about 1 mW out of 7 mW .

According to the spectrum in Fig. 6.5, benzil absorbs light at 405 nm. Therefore, MAP was tested by exposing a photoresist sample to a CW laser at this wavelength. Polymerization was observed under these circumstances, resulting in the formation of much wider lines than those made via two-photon absorption. These results suggest that initiation is a one-photon process at 405 nm. CW beams at wavelengths ranging from 750 nm to 850 nm, as well as at 532 nm, did not cause any polymerization in the benzil photoresist. A summary of these exposure studies is shown in Table 6.2.

Polymerization	No polymerization
405 nm CW	532 nm CW
750 - 850 nm ML	750 - 860 nm CW

Table 6.2: Summary of single beam exposure studied in a 1:1 SR368/499 photoresist containing 1 wt% benzil.

6.3.2 Polymerization deactivation

Once the ability to initiate polymerization was demonstrated, the photoresist was tested for deactivation. Two lasers at 800 nm were combined at the sample surface, and were overlapped in the X, Y, and Z directions. A mode-locked beam

initiated polymerization. The other beam, which was in CW mode, was able to turn the polymerization off. Similar to the deactivation study of biacetyl, the 800 nm CW beam was periodically blocked using a mechanical chopper, so that the benzil sample was periodically exposed to either one beam or both beams.

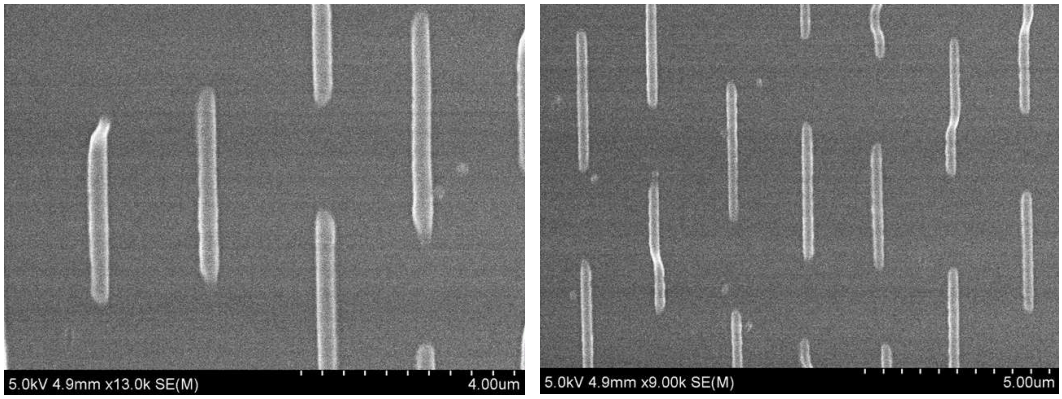

Figure 6.6: SEM images of polymerization deactivation in 1 wt% benzil in 1:1 SR368/499. Lines are formed by an 800 nm ML beam. An 800 nm, CW deactivation beam was periodically turned on and off. The clear spaces along the lines correspond to the deactivation beam exposing the sample and turning polymerization off.

Fig. 6.6 shows SEM images of lines fabricated with the 800 nm ML beam alone. The clear spaces between the end points of the lines were exposed to both the ML and CW beams, which led to a complete deactivation in these regions. As in case of the biacetyl, no residual cross-linking or traces of polymerization were observed in the deactivated regions.

The deactivation efficiency was measured at different deactivation wavelengths. Polymerization was initiated by a ML beam tuned to 800 nm. The minimum power required for complete polymerization deactivation was recorded for wavelengths

ranging from 740 nm to 870 nm. The deactivation action spectrum is shown in Fig. 6.7A.

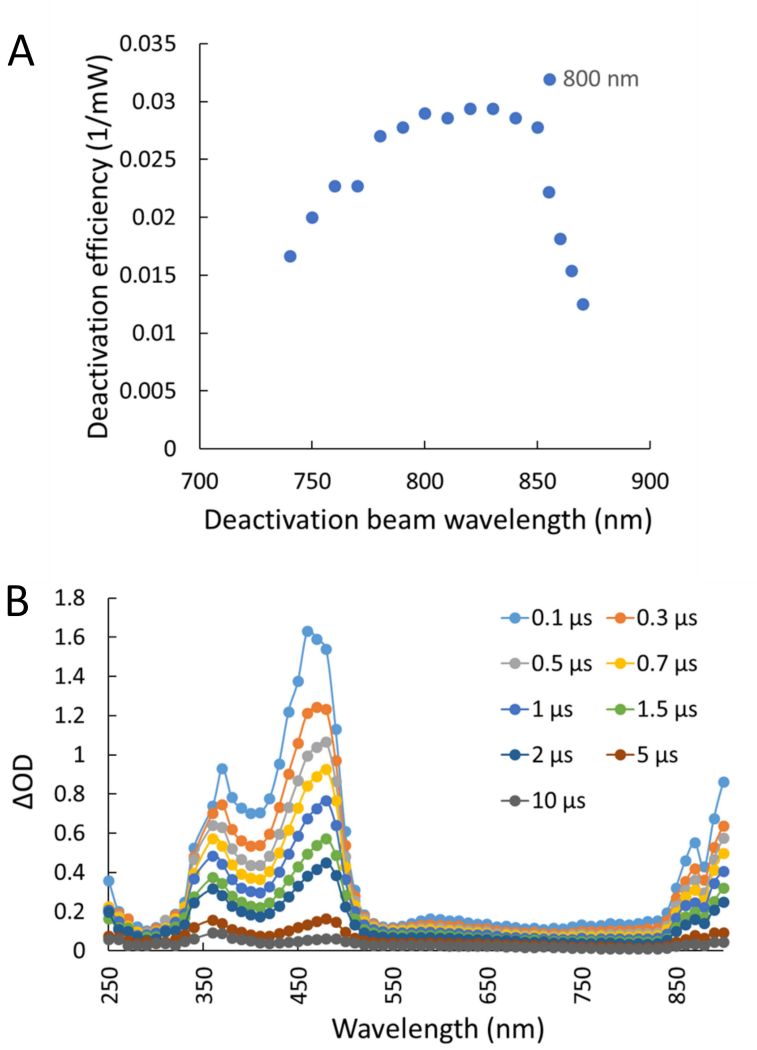

Figure 6.7: A) Deactivation action spectrum of 1 wt% benzil in SR368/499. Data points correspond to the minimum power required for polymerization depletion of 800 nm ML excitation wavelength. The CW deactivation beam power was measured for wavelengths from 740 nm to 870 nm with a 10 nm step. B) Triplet transient absorption spectrum of benzil in acetonitrile.

In contrast to the deactivation action spectrum of biacetyl, the deactivation efficiency of benzil does not show sharp peaks. Polymerization deactivation between

800 nm and 830 nm was achieved at comparable powers. The deactivation efficiency drops off to the red and blue of this range. The triplet transient absorption spectrum measured in acetonitrile is shown in Fig. 6.7B for comparison. The triplet transient absorption spectrum peak is located at 870 nm and is red-shifted as compared to the deactivation action spectrum, which monotonically decreases starting from 850 nm.

Results of multiple-beam exposure at other wavelengths are presented in Table 6.3. Lines polymerized with a 405 nm CW beam increased in size when a second CW laser beam at 800 nm was added, indicating polymerization enhancement. This result was observed when the 800 nm beam was either mode-locked or continuous-wave. Among the tested wavelengths, only polymerization initiated by the 800 nm ML beam was deactivated by the wavelengths in the 740 - 870 nm CW range. A

Deactivation	Enhancement	No polymerization
800 nm ML	405 nm CW	532 nm CW
+	+	+
760 - 880 nm CW	800 nm CW or ML	800 nm CW or ML

Table 6.3: Summary of multiple-beam exposure experiments in the 1 wt% benzil in 1:1 SR368/499.

532 nm CW beam alone did not cause polymerization. Combining this beam with an 800 nm CW beam also did not initiate polymerization. In contrast to biacetyl,

when polymerization was initiated using the 800 nm ML beam, the addition of a 532 nm CW beam did not make a visible difference, i.e. the polymerized lines did not became wider or narrower.

6.3.3 2-BIT measurements

The polymerization initiation process was explored by measuring the order of the effective nonlinear absorption in the benzil photoresist using 2-BIT. The measurements was performed as described in Chapter 3, by combining two mode-locked beams at a wavelength of 800 nm. The best-fit exponential was determined by non-linear least-square fitting of the recorded data to Eq. 3.2. 2-BIT data were collected for 2 wt% benzil in 1:1 SR368/499 exposed at a velocity of at 20 μm/sec (Fig. 6.8). The best-fit exponential n was 1.9 ± 0.2, suggesting that at 800 nm ML polymerization is initiated via two-photon absorption.

6.3.4 Resolution enhancement

Because 800 nm was the most efficient wavelength range for initiating polymerization, and was also one of the most efficient for deactivating polymerization, two beams at this wavelength were used for the resolution enhancement experiments. The 800 nm CW deactivation beam was sent through the radial polarizer and overlapped with the 800 nm ML excitation beam in the X, Y, and Z directions, as described in Section 2.1.

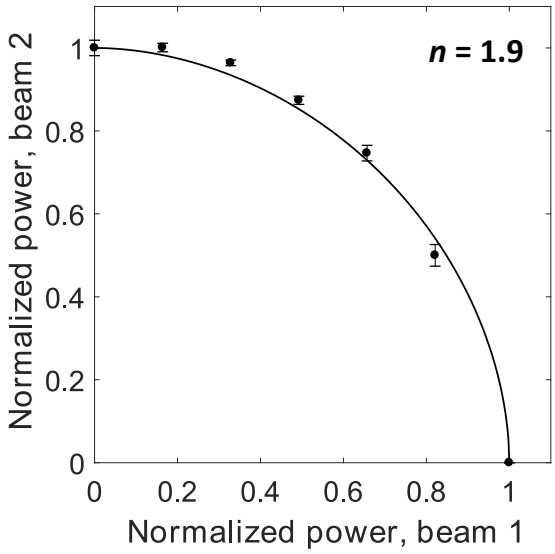

Figure 6.8: 2-BIT measurements of the order of the nonlinear absorption for 2 wt% benzil in 1:1 SR368/499. Mode-locked excitation was at 800 nm and the stage velocity was 20 μm/sec.

Line pairs were fabricated at a decreasing pitch until the two lines were no longer separable. The best results were obtained for a photoresist composed of 0.5 wt% benzil and SR368/499. The lines were polymerized with a width of 145 $\pm$ 10 nm and were separated by 65 $\pm$ 8 nm. The best pitch attained was 210 nm (Fig. 6.9).

6.4 Naphthil results

6.4.1 Polymerization action spectrum

The absorption spectrum of β-naphthil in acetonitrile (the blue line in Fig. 6.10) peaks at 350 nm, with no visible absorption at 400 nm. However, exposure to

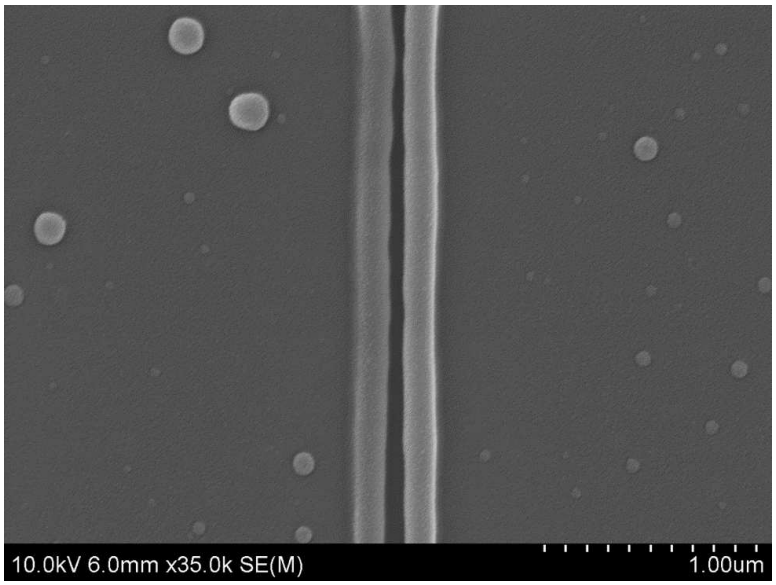

Figure 6.9: Polymerization deactivation in 0.5 wt% benzil in SR368/499 with overlapped excitation and phase-shaped deactivation beams. The width of the lines is 145 ± 7 nm and the separation is 66 ± 8 nm at a 210 nm pitch.

a mode-locked 800 nm beam initiated polymerization in a photoresist composed of β-naphthil and SR368/499.

MAP was observed at the other wavelengths as well. Due to the laser cavity alignment, the tuning range of the oscillator was limited to 745 - 850 nm range when these experiments were performed. The polymerization threshold was recorded every 10 nm in this wavelength range, and a polymerization action spectrum was constructed under the assumption that polymerization was initiated through two-photon absorption. The red dots in Fig. 6.10 correspond to the polymerization action spectrum. The measured action spectrum does not align well with the absorption spectrum. This might be caused by the transition of β-naphthil to a different energy level under 2-photon exposure.

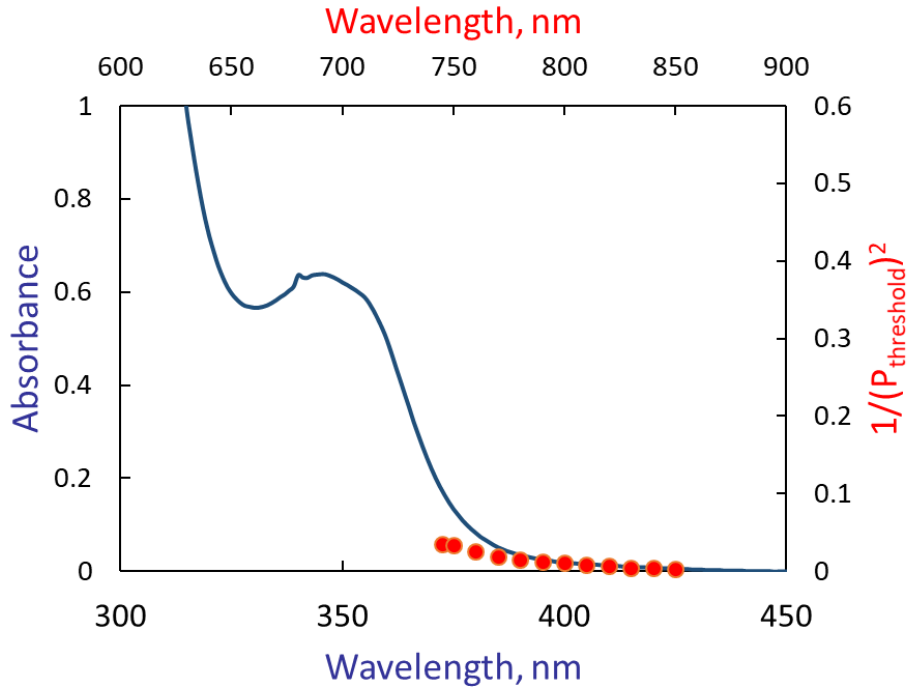

Figure 6.10: Absorption spectrum of β-naphthil in acetonitrile (blue line) and polymerization action spectrum of 1 wt% β-naphthil in 1:1 SR368/499 (red dots).

It may also be the case that exposure involves the absorption of more than two photons. 2-BIT measurements were performed to assess this possibility.

6.4.2 2-BIT characterization of β-naphthil

2-BIT measurements of the order of the effective nonlinear absorption were performed at a 20 μm/sec fabrication speed in photoresists containing β-naphthil at two concentrations, 0.5 wt% and 1 wt%. 2-BIT data for the 0.5 wt% sample are presented in Fig. 6.11. The best fit exponential is $n = 3.0 \pm 0.2$. The data collected for the photoresist composed of 1 wt% β-napthil and SR368/499 were best fit with

an exponential 3.1 ± 0.2 (Fig. 6.12). The best-fit exponentials of ∼3 suggest that polymerization is initiated through three-photon absorption at 800 nm.

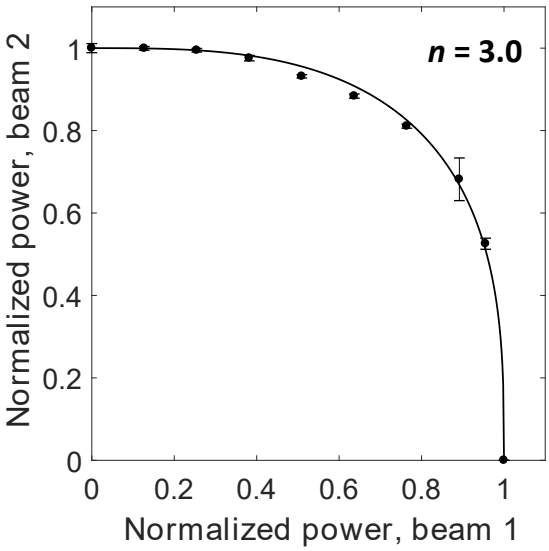

Figure 6.11: 2-BIT measurements of the order of the nonlinear absorption for 0.5 wt% β-naphthil in 1:1 SR368/499 collected with an 800 nm ML beam at a fabrication velocity of 20 μm/sec.

The yellow triangles in Fig. 6.13 correspond to the $1/P^3$ at polymerization threshold for each wavelength tested. The comparison between the absorption spectrum and the polymerization action spectrum is plotted assuming three-photon absorption at the excitation wavelength. This is a counter-intuitive representation, as the absorption order was determined via 2-BIT for only one wavelength, 800 nm. We have observed that for other photoinitiators that exhibit self-deactivation behavior, for example ITX, the order of effective nonlinearity changes with the wavelength. In this case the deactivation efficiency is wavelength dependent. When deactivation is independent of the wavelength, the order of the effective nonlinear absorption is

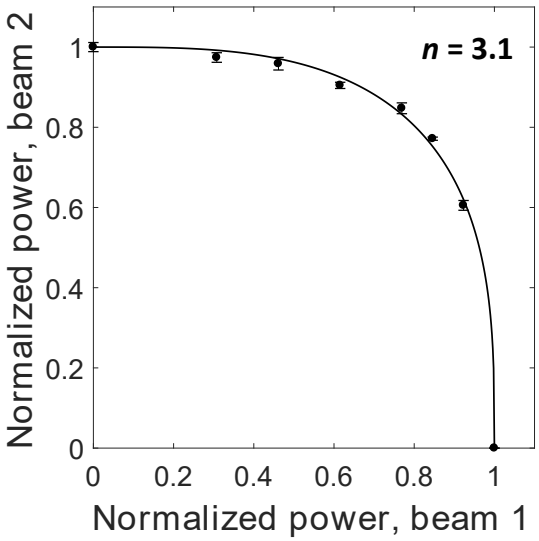

Figure 6.12: 2-BIT measurement of order of effective nonlinear absorption for 1 wt% β-naphthil in 1:1 SR368/499 collected with an 800 nm ML beam at a fabrication velocity of 20 μm/sec.

closer to 2. However, when deactivation starts contributing to the initiation process, the 2-BIT exponent increases. This nonlinearity affects the polymerization action spectrum measurements. For the correct comparison between absorption spectrum and polymerization action spectrum, the order of the nonlinear absorption should be determined at each wavelength via 2-BIT measurements and the deactivation efficiency should be plotted as a function of wavelength with the absorption order adjusted for this wavelength. The photoresist containing β-naphthil was not tested for the polymerization deactivation.

Another photoresist tested included α-naphthil mixed with either SR368/499 or SR499 at concentrations of 0.3 wt% and 1 wt% respectively. The absorption spectrum of α-naphthil in acetonitrile is presented in Fig. 6.14. α-naphthil was difficult to dissolve in the monomer mixture than were other photoinitiators tested,

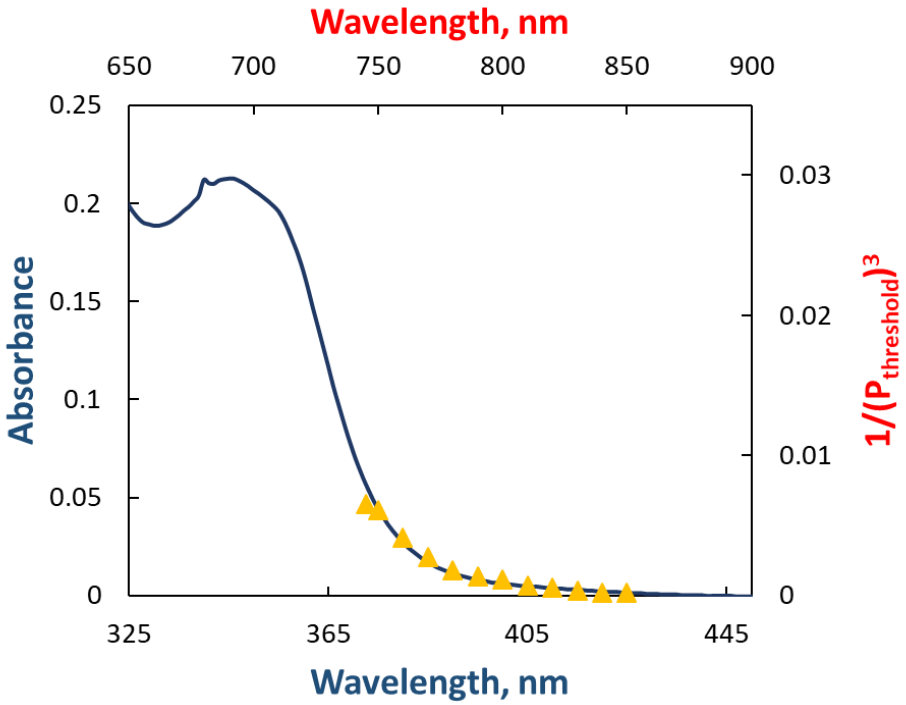

Figure 6.13: Absorption spectrum of β-naphthil in acetonitrile (blue line) and three-photon polymerization action spectrum of 1 wt% β-naphthil in 1:1 SR368/499 (yellow triangles).

such as benzil, biacetyl, and β-naphthil. After a week of dissolution, the photoresist containing α-naphthil was exposed to 750 nm, 800 nm, or 860 nm ML light. No polymerization was observed with laser powers up to 30 mW. At this power, the sample burned within laser focal point. The same effect is observed in the monomer mixture alone at such exposure powers.

The excitation beam wavelengths of 750 nm, 800 nm, and 860 nm correspond to linear absorption at 375 nm, 400 nm, and 430 nm, assuming two-photon absorption. The corresponding three-photon absorption wavelengths are 250 nm, 266 nm, and 286 nm.

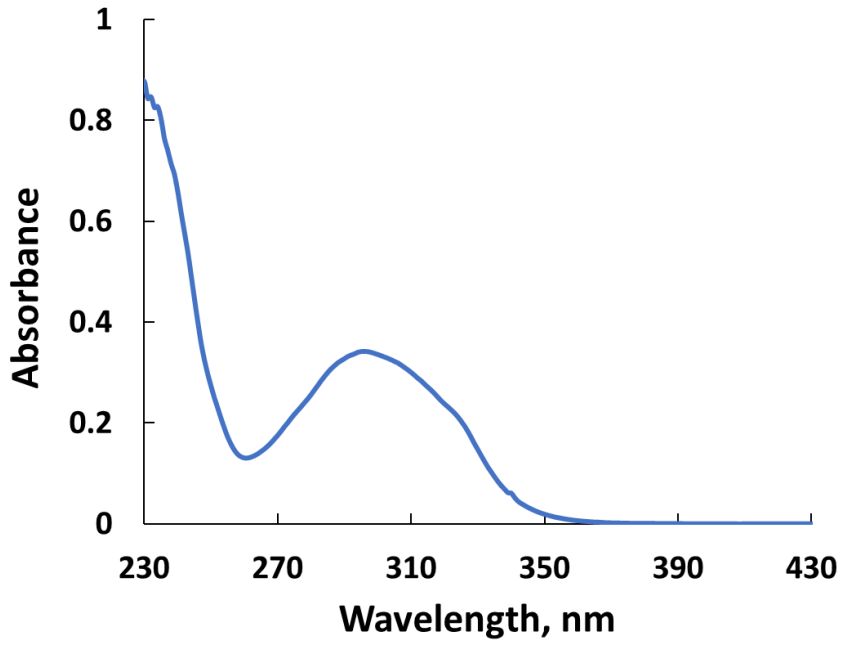

Figure 6.14: Absorption spectrum of α-naphthil in acetonitrile

There are no absorption bands in the UV-visible spectrum between 375 nm and 430 nm. α-naphthil in acetonitrile has strong absorption at 286 nm, so if the polymerization were initiated via three-photon absorption, exposure to 860 nm would result in some polymerization. The theory that α-naphthil initiates polymerization through two-photon absorption could be tested by exposing the photoresist to a mode-locked beam at wavelengths ranging from 540 nm to 680 nm.

It is also possible that exposure to 750 nm, 800 nm or 860 nm does not bring α-naphthil to a state that can create radicals. The transient absorption spectra of α-naphthil and β-naphthil were measured in acetonitrile with an excitation beam set at 266 nm. The transient absorption spectrum of α-naphthil (Fig. 6.15A) has week absorption at 400 nm, but stronger absorption at 490 nm. In comparison, the

transient absorption spectrum of β-naphthil (Fig. 6.15B) has a peak at 420 and has much stronger absorption than 1-naphthil. Photoresists containing α-naphthil will need to be exposed to a combination of different wavelengths, one including 447 nm, that together might transition molecules to a chemically active state that leads to polymerization.

Polymerization initiation in photoresists with α-naphthil was tested only at 20 μm/sec. At the 750 nm exposure light polymerization was observed at 13 mW, however this process was accompanied with often sample burning. We have seen negative contrast behavior in other photoinitiators, in which linewidth increases with the increasing fabrication velocity. The exact nature of this behavior is not quite clear yet. It might be possible that α-naphthil follows the same pattern and polymerization might be observed at higher fabrication velocities. For each of the tested monomers and concentrations the polymerization should be tested at velocities ranging from 1 μm/sec to at least 250 μm/sec to completely exclude polymerization initiation in this sample.

6.5 Pyridil results

MAP was tested in a resin consisting of pyridyl in SR399. Pulsed 800 nm light initiated polymerization. However, even at the lowest tested powers, the sample exhibited burning within the laser focal point. Polymerization was also initiated at other wavelengths. The polymerization action spectrum was measured for 2 wt% pyridyl in SR399, Fig. 6.16. The polymerization efficiency increased as the

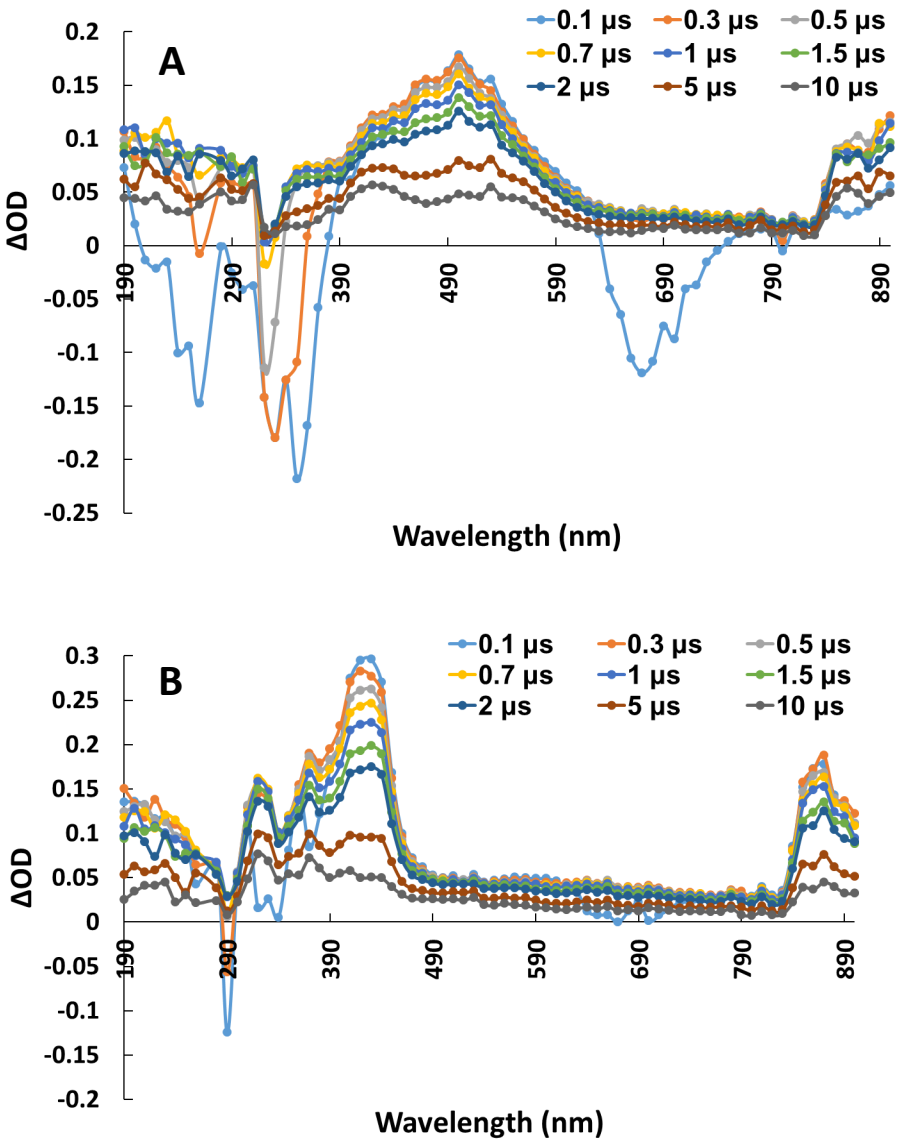

Figure 6.15: Transient absorption spectra of α-naphthil (A) and β-naphthil (B) in acetonitrile following excitation at 266 nm.

wavelength decreased. MAP was observed at wavelengths as short as 730 nm, which was the limit of the laser on the day the experiments were performed. Additional studies will need to be performed to gather further information about excitation and deactivation.

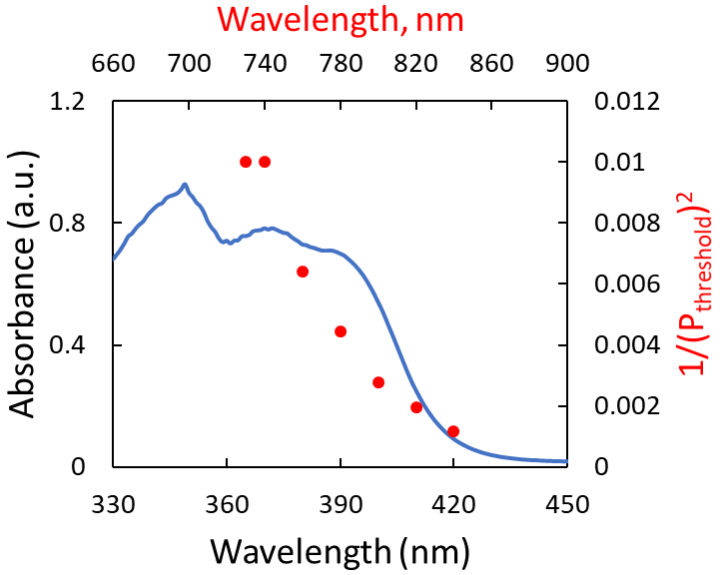

Figure 6.16: Absorption spectrum of pyridil in benzene (blue line) and polymerization action spectrum of 2 wt% pyridyl in SR399 (red dots).

6.6 Conclusions

Four compounds were tested as potential photoinitiators for three-color photolithography in acrylate-based resists: benzil, α-naphthil, β-naphthil and pyridil. In photoresists with benzil, polymerization was initiated with a mode-locked laser at wavelengths ranging from 730 nm to 850 nm. Polymerization was also observed under exposure to a 405 nm CW beam. A CW laser at 532 nm did not initiate polymerization. According to the measured polymerization action spectrum of benzil in SR368/499, the 770 nm pulsed beam initiated polymerization more efficiently than ML beams tuned to other wavelengths.

The order of the effective nonlinear absorption in this photoresist was measured with 2-BIT. 2-BIT data were collected at a 20 μm/sec fabrication velocity at 800 nm ML exposure. Under these conditions, the effective number of photons required to initiate polymerization was two.

Additional 2-BIT experiments at different wavelengths and fabrication velocities should be performed to determine whether these parameters influence the order of the effective nonlinearity changes. At some wavelengths or velocities, the best-fit exponential to 2-BIT data might change from 2 to a higher value. This would indicate exposure conditions in which other nonlinear processes affect polymerization initiation, and would help to determine the set of exposure parameters that achieve the best resolution.

Polymerization initiated by an 800 nm pulsed laser beam was deactivated by addition of a second CW laser at wavelengths ranging from 740 nm to 880 nm. The deactivation action spectrum is broad, monotonically increasing from 740 nm to 800 nm and monotonically declining from about 850 nm to 880 nm. The spectrum has a plateau at wavelengths between 800 nm and 840 nm.

The deactivation action spectrum was measured only using 800 nm excitation. No peaks in the spectrum were observed across the tested deactivation wavelength range. For other excitation wavelengths, for example 770 nm, deactivation might be more efficient at an exposure wavelength outside of the 800 nm to 840 nm range. Measuring the deactivation action spectrum for a range of the excitation wavelengths would provide insight into how efficiently these processes take place and would reveal information about molecule transitions to different excitation states.

Neither pulsed nor CW exposure at 800 nm deactivated polymerization initiated with a 405 nm CW beam. Dual-beam exposure experiments at these wavelengths led to enhancement of polymerization. This effect might be caused by the excitation of benzil to a higher singlet state that cannot be deactivated, implying that there are different excitation pathways for linear excitation at 405 nm and two-photon excitation at 800 nm.

The linewidth and resolution enhancement experiments were performed using 800 nm ML and 800 nm CW beams, as these two wavelengths were efficient for initiation and deactivation. Sets of line pairs were fabricated at a decreasing pitch until the two lines were no longer separable. The smallest pitch at which two lines were separate was 210 nm, with a linewidth of 145 $\pm$ 10 nm, separated by 65 $\pm$ 8 nm. It is possible that other wavelengths for polymerization initiation and deactivation, as well different fabrication velocities, will result in narrower lines and a finer pitch. After the 2-BIT data for different exposure conditions have been collected and the 3D polymerization action spectrum has been measured, the best resolution enhancement parameters will be revealed.

Polymerization initiatation was observed in photoresists containing β-naphthil as photoinitiator under exposure to a pulsed laser at wavelengths ranging from 745 nm to 850 nm. The measured polymerization action spectrum rises monotonically from 850 nm to 745 nm. Shorter wavelengths may be even more efficient in initiating polymerization.

2-BIT data were used to determine the order of the effective nonlinear absorption of β-naphthil in 1:1 SR368/499 at 0.5 wt% and 1 wt%. The measurements were

performed with 800 nm excitation. Even though 800 nm was not the most efficient polymerization initiation wavelength, it provided enough power for the beam to be split into two parts that could initiate polymerization on their own. The best-fit exponentials to the 2-BIT data were 3.0 ± 0.2 and 3.1 ± 0.2 for 0.5 wt% and 1 wt % of β-naphthil, respectively.

The 2-BIT data will need to be measured at different excitation wavelengths within the 730 nm to 850 nm range. The order of nonlinear absorption obtained at each excitation wavelengths will need to be taken into account when plotting the polymerization action spectrum. It will determine the exponent of the deactivation efficiency at each tested excitation wavelength and represent accurate comparison between the polymerization action spectrum and the absorption spectrum.

The photoresist was not tested for polymerization deactivation. The next steps in this study will be testing deactivation with excitation at different wavelengths and determining the wavelength or range of wavelengths that deactivate polymerization. Then, measuring the deactivation efficiency at each of these wavelengths will provide the optimal exposure conditions for resolution enhancement. The widths of the isolated lines should be compared to those made with the addition of the phase-shaped deactivation beam at various powers. The linewidth and smallest pitch should be analyzed with SEM or AFM. Polymerization initiation and deactivation should be tested using lasers at other wavelengths as well, such as 405 nm CW, 445 nm CW, and 532 nm CW.

No polymerization was observed in a photoresist composed of α-naphthil in either 1:1 SR368/499 or SR499 at a fabrication velocity of 20 μm/sec using pulsed

excitation at 750 nm, 800 nm or 860 nm. Because no polymerization initiation was observed, no 2-BIT data were collected.

Only the polymerization action spectrum was measured for the pyridil photoresist. The most efficient wavelengths for initiating polymerization was 730 and 740 nm. Polymerization at other wavelengths needs to be tested, including CW light at 405 nm, 445 nm, and 532 nm. Polymerization deactivation experiments are the next step in testing pyridil as photoinitiator.

Chapter 7

Conclusions and future work

7.1 Conclusions

The size of the structures fabricated with conventional lithographic methods is restricted by the Abbe criterion and is typically in the order of $\lambda/4$, where λ is the wavelength of light used. Currently employed manufacturing methods in the semiconductor industry overcome this limit with the use of short wavelengths. However, this approach is facing increasing costs and extreme technological challenges.

One alternative way to satisfy the demand of for ever-smaller features and decreased manufacturing costs is to use a photolithographic technique based on light in the visible or near-IR. The combination of two-colors of light has shown promising results for fabrication of sub-100 nm features. One color is used to initiate polymerization and the second color is used to deactivate the process, leading to a creation of isolated features with size on the order of $\lambda/40$. However, for applications requiring multiple patterning steps, the size of the features increases, as compared to that of isolated ones. This loss of resolution arises from the build-up of the exposure tails at each exposure step.

The 2-color approach can be improved by adding a third color. In 3-color lithography initiation and deactivation take place from different chemical states, thus avoiding competition between the polymerization and deactivation processes.

One color excites photoinitiator molecules to a chemically inert state. From this state the second color deactivates molecules. The third color brings any remaining molecules from the chemically inert state to one that can produce ree radicals and initiate polymerization. This approach allows us to avoid the exposure tail build-up, and therefore to achieve better resolution.

Understanding photoinitiator properties and selecting the right candidates is crucial for performing 3-color lithography. In Chapter 3 we introduced the 2-beam initiation threshold (2-BIT) method for *in situ* measurements of the order of effective nonlinear absorption in the photoresist. Photoinitiators tested were Lucirin TPO-L, Irgacure 369, Irgacure 651, Irgacure 819, and crystal violet lactone. The order of effective nonlinear absorption was determined for each one of them. It was shown that conventional techniques of measuring the order of nonlinear absorption in solvents are not sufficient, as the photoinitiator behaves differently when it is immersed in the monomer mixture.

Chapter 4 focused on the study of a negative-contrast photoinitiator bis-[4-(diphenylamino) stryl]-1-(2-ethylhexyloxy), 4-(methoxy)benzene (KL-68). This type of photoinitiator exhibits efficient deactivation, so that it can undergo self-deactivation from the excitation laser pulses. Negative-contrast photoinitoators, such as KL68, have a proportional velocity (PROVE) dependence, i.e. the size of the fabricated features decreases with exposure. Polymerization initiation in a KL68-based photoresist was demonstrated to depend nonlinearly on the fabrication velocity. It was shown that increasing the temperature of the sample can lead to complete suppression of polymerization. Temperature dependence studies were per-

formed using either an objective heater or a second laser to induce local temperature change. 532 nm CW light on its own did not initiate polymerization. However, exposure of the photoresist sample to 532 nm prior to polymerization initiation with pulsed 800 nm light prevented polymerization in the exposed regions. A variety of dyes were tested in the photoresist for enhancing the temperature change.

The 3-color lithography principles were discussed in detail in Chapter 5. It has been shown that biacetyl, a vicinal diketone, can be used as a radical photoinitiator. Polymerization was initiated under pulsed exposure at various wavelengths ranging from 730 nm to 870 nm, with pulsed 400 nm light, and with CW 405 nm and 445 nm light. The order of effective nonlinear absorption, determined via 2-BIT, increased from two to almost three as the exposure wavelength increased. This result indicates that other processes are involved, and affect the nonlinearity. The most efficient wavelength for polymerization initiation was 790 nm, as determined from the polymerization action spectrum. The deactivation action spectrum was measured for a combination of excitation and deactivation wavelengths, ranging between 730 nm and 940 nm. The most efficient deactivation was achieved when the excitation beam was set between 820 nm and 840 nm and the deactivation beam was at 900 nm. The width of the isolated lines was 200 $\pm$ 20 nm under pulsed exposure to 800 nm alone. Addition of a phase-shaped deactivation beam at 800 nm CW decreased the linewidth to 90 $\pm$ 10 nm. The smallest pitch at which lines were still separate was 240 nm with the corresponding linewidth of 200 $\pm$ 10 nm. It was found that polymerization initiated by pulsed 400 nm, or CW 405 nm light, or CW 445 light nm was not deactivated by any other wavelength tested at any power.

Studies of additional potential 3-color photoinitiators were discussed in Chapter 6. The other vicinal diketones tested were benzil, α-naphthil, β-naphthil, and pyridil. Three of the tested molecules, benzil, β-naphthil, and pyridil were shown to act as photoinitiators in an acrylate-monomer-based photoresist. Polymerization initiation was detected under exposure to pulsed light at wavelength ranging from 730 nm to 850 nm in all three photoresists. Polymerization was deactivated in the photoresist containing benzil under exposure to a second CW laser at wavelengths ranging from 740 nm to 880 nm. Resolution enhancement was tested under exposure to pulsed 800 nm light to initiate polymerization, and CW 800 nm to deactivate polymerization. The best pitch at which two lines were separated was 210 nm, with a linewidth of 145 $\pm$ 10 nm. The order of the effective nonlinear absorption was measured with 2-BIT. It was found that the effective number of photons required to initiate polymerization in the benzil-based photoresist is two under exposure to pulsed 800 nm light. 2-BIT experiments were performed in photoresist containing β-naphthil and the best-fit exponentials to 2-BIT data were 3.

7.2 Future work

7.2.1 Advancing the 2-BIT technique

The 2-BIT method for *in situ* measurements of the order of effective nonlinear absorption can be further advanced beyond the approach discussed in Chapter 3. Results presented in this thesis were obtained using a single beam divided into two parts and recombined at the sample. Therefore, the wavelength of both beams

was the same and the timing between pulses of the two beams was limited by the repetition rate of the oscillator. If two separate beams were involved, the wavelength of each of two beams could be changed independently, allowing us to gather data about photoinitiator excitation pathways. In addition, changing the repetition rate of the separate beams using a pulse picker and adjusting the timing between beam pulses would allow to measure excited state transitions of the photoinitiator in the monomer matrix.

7.2.2 Refining the experimental setup

The resolution improvement experiments were performed using a radial polarizer to change phase of the deactivation beam and to produce two lobes along a lateral direction. The distance between the maxima of the deactivation beam in this case cannot be varied. If the initiation beam was set at the polymerization threshold value, the size of the beam might be much smaller than the distance between the points of the maximum intensity of the deactivation beam and, therefore, deactivation might be insufficient (Fig. 7.1A). One way to overcome the gap between focal points of the initiation and deactivation beam is to increase the size of the deactivation beam focal volume via raising the beam intensity (Fig. 7.1B). Unfortunately, as we saw in case of biacetyl, when the deactivation beam power surpasses a certain threshold the deactivation efficiency decreases, polymerization can even be promoted. Precise overlapping of the polymerization and deactivation beams is not enough for most optimal deactivation conditions. The ability to vary the size

of the deactivation beam other than by changing the beam intensity will allow us to reach higher pitch and smaller feature sizes (Fig. 7.1C). One way to do so is to separate the deactivation beam into two parts and recombine them at the sample. The distance between two deactivation beams can be changed using sets of prisms and translation stage or by using a beam splitter and a mirror to control position of one part of the deactivation beam with respect to the other.

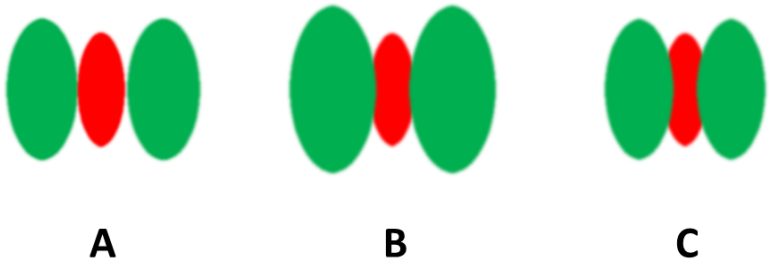

Figure 7.1: Schematics of possible alignments of initiation and deactivation beams. A) Deactivation beam (green) is overlapped with the initiation beam (red); however there is a present gap between deactivation beam lobes and the focal point of the fabrication beam. B) Deactivation beam focal volume is increased by adjusting the laser intensity to assure more precise overlap of the two initiation and deactivation beams. C) The position of the deactivation beam maxima is changed without raising the intensity of the deactivation beam, allowing for more efficient deactivation.

7.2.3 Customize materials

We have shown in Chapter 5 that polymerization initiation in a phototresist containing biacetyl can take place through triplet-triplet annihilation (TTA). Eliminating TTA during the excitation and deactivation processes would allow us to attain higher resolution. This goal could be achieved by customizing the photoresist

by linking the photoinitiator molecules to acrylate monomers to inhibit diffusion. The steric hindrance of such molecules would make them less likely to undergo TTA. One of the challenges of producing a photoinitiator-lined-monomer resin is to provide high enough concentration of the photoinitiators to overcome the radical formation threshold to initiate polymerization. The photoinitiators also should be evenly distributed in the resin to assure a uniform polymerization rate under constant exposure. Some of the parameters that need to be tested are polymerization initiation in the phototoresist consisting completely of photoitiator-linked-monomers versus a mixture of free photoinitiator added to the linked monomers. The exact ratio of free photoinitiators versus those linked to monomers in the resin will need to be established through polymerization and deactivation efficiency experiments.

7.2.4 Single photon polymerization in thin films

In this thesis we have tested materials suitable for 3-color lithography using MAP for rapid screening of molecules for their potential applications as 3-color photoinitiators. In the long term, 3-color lithography will be performed using a single-photon excitation sources. CW light is easier and less expensive to produce than pulsed laser light, and will be easier to incorporate in the existing industrial lithography setups. Typically, in MAP the size of the laser focal volume limits the fabrication area. The height of the fabricated structures can be limited with the use of the phase mask, as in the 2-color approach. However, with the use of thin films, the necessity of limiting the height of the resultant features with phase-

shaping elements is no longer needed. Instead, the height will be determined by the thickness of the photoresist film. The photoresist suitable for 3-color lithogrpahy will be spin-coated into thin films. Polymerization initiation and deactivation will be performed by combining CW 405 nm, or 445 nm and 800 nm or 532 nm light. Because the axial resolution will be determined by the thickness of the thin film, the phase-shaping elements will be used to control the transverse resolution.

Bibliography

[1] G. E. Moore, "Progress in digital integrated electronics [Technical literaiture, Copyright 1975 IEEE. Reprinted, with permission. Technical Digest. International Electron Devices Meeting, IEEE, 1975, pp. 11-13.]," *IEEE Solid-State Circuits Society Newsletter*, vol. 20, pp. 36–37, Sept. 2006.

[2] "Intel®'s 22 nm Technology Moves Transistor Into the 3rd Dimension."

[3] L. Li, R. R. Gattass, E. Gershgoren, H. Hwang, and J. T. Fourkas, "Achieving $\lambda/20$ Resolution by One-Color Initiation and Deactivation of Polymerization," *Science*, vol. 324, pp. 910–913, May 2009.

[4] T. F. Scott, B. A. Kowalski, A. C. Sullivan, C. N. Bowman, and R. R. McLeod, "Two-Color Single-Photon Photoinitiation and Photoinhibition for Subdiffraction Photolithography," *Science*, vol. 324, pp. 913–917, May 2009.

[5] Z. Gan, Y. Cao, R. A. Evans, and M. Gu, "Three-dimensional deep sub-diffraction optical beam lithography with 9 nm feature size," *Nat Commun*, vol. 4, June 2013.

[6] J. Fischer, J. B. Mueller, J. Kaschke, T. J. A. Wolf, A.-N. Unterreiner, and M. Wegener, "Three-dimensional multi-photon direct laser writing with variable repetition rate," *Opt. Express, OE*, vol. 21, pp. 26244–26260, Nov. 2013.

[7] M. Göppert-Mayer, "Über Elementarakte mit zwei Quantensprüngen," *Ann. Phys.*, vol. 401, pp. 273–294, Jan. 1931.

[8] M. Göppert-Mayer, "Elementary processes with two quantum transitions," *Ann. Phys.*, vol. 18, pp. 466–479, Aug. 2009.

[9] C. N. LaFratta, J. T. Fourkas, T. Baldacchini, and R. A. Farrer, "Multiphoton Fabrication," *Angewandte Chemie International Edition*, vol. 46, no. 33, pp. 6238–6258, 2007.

[10] M. Gu, B. Jia, J. Li, and M. Ventura, "Fabrication of three-dimensional photonic crystals in quantum-dot-based materials," *Laser & Photon. Rev.*, vol. 4, pp. 414–431, Apr. 2010.

[11] L. Li, G. Kumi, R. R. Gattass, E. Gershgoren, W.-Y. Chen, P.-T. Ho, W. N. Herman, and J. T. Fourkas, "Fabrication of High-Performance Optical Devices Using Multiphoton Absorption Polymerization," in *Organic Thin Films for Photonic Applications*, vol. 1039 of *ACS Symposium Series*, pp. 129–137, American Chemical Society, Jan. 2010.

[12] C. E. Olson, M. J. R. Previte, and J. T. Fourkas, "Efficient and robust multiphoton data storage in molecular glasses and highly crosslinked polymers," *Nat Mater*, vol. 1, pp. 225–228, Dec. 2002.

[13] D. A. Parthenopoulos and P. M. Rentzepis, "Three-Dimensional Optical Storage Memory," *Science*, vol. 245, pp. 843–845, Aug. 1989.

[14] B. H. Cumpston, S. P. Ananthavel, S. Barlow, D. L. Dyer, J. E. Ehrlich, L. L. Erskine, A. A. Heikal, S. M. Kuebler, I.-Y. S. Lee, D. McCord-Maughon, J. Qin, H. Röckel, M. Rumi, X.-L. Wu, S. R. Marder, and J. W. Perry, "Two-photon polymerization initiators for three-dimensional optical data storage and microfabrication," *Nature*, vol. 398, pp. 51–54, Mar. 1999.

[15] W. Denk, J. H. Strickler, and W. W. Webb, "Two-Photon Laser Scanning Fluorescence Microscopy," *Science*, vol. 248, pp. 73–76, Apr. 1990.

[16] D. R. Larson, W. R. Zipfel, R. M. Williams, S. W. Clark, M. P. Bruchez, F. W. Wise, and W. W. Webb, "Water-Soluble Quantum Dots for Multiphoton Fluorescence Imaging in Vivo," *Science*, vol. 300, pp. 1434–1436, May 2003.

[17] S.-W. Teng, H.-Y. Tan, J.-L. Peng, H.-H. Lin, K. H. Kim, W. Lo, Y. Sun, W.-C. Lin, S.-J. Lin, S.-H. Jee, P. T. C. So, and C.-Y. Dong, "Multiphoton Autofluorescence and Second-Harmonic Generation Imaging of the Ex Vivo Porcine Eye," *IOVS*, vol. 47, pp. 1216–1224, Mar. 2006.

[18] C. Soeller and M. B. Cannell, "Two-photon microscopy: imaging in scattering samples and three-dimensionally resolved flash photolysis," *Microsc. Res. Tech.*, vol. 47, pp. 182–195, Nov. 1999.

[19] H.-S. Lee, Y. Liu, H.-C. Chen, L.-L. Chiou, G.-T. Huang, W. Lo, and C.-Y. Dong, "Optical biopsy of liver fibrosis by use of multiphoton microscopy," *Opt. Lett.*, vol. 29, pp. 2614–2616, Nov. 2004.

[20] C. Xu and W. W. Webb, "Multiphoton Excitation of Molecular Fluorophores and Nonlinear Laser Microscopy," in *Topics in Fluorescence Spectroscopy* (J. R. Lakowicz, ed.), no. 5 in Topics in Fluorescence Spectroscopy, pp. 471–540, Springer US, 2002. DOI: 10.1007/0-306-47070-5_11.

[21] E. Collini, C. Ferrante, and R. Bozio, "Strong Enhancement of the Two-Photon Absorption of Tetrakis(4-sulfonatophenyl)porphyrin Diacid in Water upon Aggregation," *J. Phys. Chem. B*, vol. 109, pp. 2–5, Jan. 2005.

[22] D. A. Fishman, C. M. Cirloganu, S. Webster, L. A. Padilha, M. Monroe, D. J. Hagan, and E. W. V. Stryland, "Sensitive mid-infrared detection in wide-bandgap semiconductors using extreme non-degenerate two-photon absorption," *Nat Photon*, vol. 5, pp. 561–565, Sept. 2011.

[23] K. D. Belfield, D. J. Hagan, E. W. Van Stryland, K. J. Schafer, and R. A. Negres, "New Two-Photon Absorbing Fluorene Derivatives: Synthesis and Nonlinear Optical Characterization," *Org. Lett.*, vol. 1, pp. 1575–1578, Nov. 1999.

[24] B. Xue, C. Katan, J. A. Bjorgaard, and T. Kobayashi, "Non-degenerate two photon absorption enhancement for laser dyes by precise lock-in detection," *AIP Advances*, vol. 5, p. 127138, Dec. 2015.

[25] T. Baldacchini, C. N. LaFratta, R. A. Farrer, M. C. Teich, B. E. A. Saleh, M. J. Naughton, and J. T. Fourkas, "Acrylic-based resin with favorable properties for three-dimensional two-photon polymerization," *Journal of Applied Physics*, vol. 95, pp. 6072–6076, May 2004.

[26] C. Martineau, R. Anémian, C. Andraud, I. Wang, M. Bouriau, and P. L. Baldeck, "Efficient initiators for two-photon induced polymerization in the visible range," *Chemical Physics Letters*, vol. 362, pp. 291–295, Aug. 2002.

[27] M. Malinauskas, A. Žukauskas, G. Bičkauskaitė, R. Gadonas, and S. Juodkazis, "Mechanisms of three-dimensional structuring of photo-polymers by tightly focussed femtosecond laser pulses," *Opt. Express, OE*, vol. 18, pp. 10209–10221, May 2010.

[28] S. Maruo, O. Nakamura, and S. Kawata, "Three-dimensional microfabrication with two-photon-absorbed photopolymerization," *Opt. Lett., OL*, vol. 22, pp. 132–134, Jan. 1997.

[29] H.-B. Sun and S. Kawata, "Two-Photon Photopolymerization and 3d Lithographic Microfabrication," pp. 169–273, 2004.

[30] W. H. Teh, U. Dürig, G. Salis, R. Harbers, U. Drechsler, R. F. Mahrt, C. G. Smith, and H.-J. Güntherodt, "SU-8 for real three-dimensional subdiffraction-limit two-photon microfabrication," *Applied Physics Letters*, vol. 84, pp. 4095–4097, May 2004.

[31] X. Yin, N. Fang, X. Zhang, I. B. Martini, and B. J. Schwartz, "Near-field two-photon nanolithography using an apertureless optical probe," *Applied Physics Letters*, vol. 81, pp. 3663–3665, Nov. 2002.

[32] L. Li and J. T. Fourkas, "Multiphoton polymerization," *Materials Today*, vol. 10, pp. 30–37, June 2007.

[33] Y. Liu, D. D. Nolte, and L. J. Pyrak-Nolte, "Large-format fabrication by two-photon polymerization in SU-8," *Appl. Phys. A*, vol. 100, pp. 181–191, July 2010.

[34] W. H. Teh, U. Dürig, U. Drechsler, C. G. Smith, and H.-J. Güntherodt, "Effect of low numerical-aperture femtosecond two-photon absorption on (SU-8) resist for ultrahigh-aspect-ratio microstereolithography," *Journal of Applied Physics*, vol. 97, p. 054907, Mar. 2005.

[35] A. d. Campo and C. Greiner, "SU-8: a photoresist for high-aspect-ratio and 3d submicron lithography," *J. Micromech. Microeng.*, vol. 17, no. 6, p. R81, 2007.

[36] C. Li, L. Luo, S. Wang, W. Huang, Q. Gong, Y. Yang, and S. Feng, "Two-photon microstructure-polymerization initiated by a coumarin derivative/iodonium salt system," *Chemical Physics Letters*, vol. 340, pp. 444–448, June 2001.

[37] Y. Murakami, C. A. Coenjarts, and C. K. Ober, "Preparation and Two-Photon Lithography of a Sulfur Containing Resin with High Refractive Index," *Journal of Photopolymer Science and Technology*, vol. 17, no. 1, pp. 115–118, 2004.

[38] W. Zhou, S. M. Kuebler, K. L. Braun, T. Yu, J. K. Cammack, C. K. Ober, J. W. Perry, and S. R. Marder, "An Efficient Two-Photon-Generated Photoacid Applied to Positive-Tone 3d Microfabrication," *Science*, vol. 296, pp. 1106–1109, May 2002.

[39] A. S. Dvornikov, E. P. Walker, and P. M. Rentzepis, "Two-photon three-dimensional optical storage memory," *J Phys Chem A*, vol. 113, pp. 13633–13644, Dec. 2009.

[40] U. Stute, J. Serbin, C. Kulik, and B. Chichkov, "Three-dimensional micro- and nanostructuring with two-photon polymerisation," *International Journal of Materials and Product Technology*, vol. 21, pp. 273–284, Jan. 2004.

[41] T. Ikegami, M. P. Stocker, K. Monaco, J. T. Fourkas, and S. Maruo, "Fabrication of Three-Dimensional Metalized Movable Microstructures by the Combination of Two-Photon Microfabrication and Electroless Plating," *Japanese Journal of Applied Physics*, vol. 51, p. 06FL17, 2012.

[42] F. Burmeister, S. Steenhusen, R. Houbertz, U. D. Zeitner, S. Nolte, and A. Tünnermann, "Materials and technologies for fabrication of three-dimensional microstructures with sub-100 nm feature sizes by two-photon polymerization," *Journal of Laser Applications*, vol. 24, p. 042014, July 2012.

[43] W. Haske, V. W. Chen, J. M. Hales, W. Dong, S. Barlow, S. R. Marder, and J. W. Perry, "65 nm feature sizes using visible wavelength 3-D multiphoton lithography," *Opt. Express*, vol. 15, pp. 3426–3436, Mar. 2007.

[44] D. Psaltis, S. R. Quake, and C. Yang, "Developing optofluidic technology through the fusion of microfluidics and optics," *Nature*, vol. 442, pp. 381–386, July 2006.

[45] L. Mazutis, J. Gilbert, W. L. Ung, D. A. Weitz, A. D. Griffiths, and J. A. Heyman, "Single-cell analysis and sorting using droplet-based microfluidics," *Nat. Protocols*, vol. 8, pp. 870–891, May 2013.

[46] A. A. Sikorsky, J. T. Fourkas, and D. Ross, "Gradient Elution Moving Boundary Electrophoresis with Field-Amplified Continuous Sample Injection," *Anal. Chem.*, vol. 86, pp. 3625–3632, Apr. 2014.

[47] J. H. Strickler and W. W. Webb, "Three-dimensional optical data storage in refractive media by two-photon point excitation," *Opt. Lett., OL*, vol. 16, pp. 1780–1782, Nov. 1991.

[48] M. H. Hong, B. Luk'yanchuk, S. M. Huang, T. S. Ong, L. H. Van, and T. C. Chong, "Femtosecond laser application for high capacity optical data storage," *Appl. Phys. A*, vol. 79, pp. 791–794, Sept. 2004.

[49] D. Wu, S.-Z. Wu, L.-G. Niu, Q.-D. Chen, R. Wang, J.-F. Song, H.-H. Fang, and H.-B. Sun, "High numerical aperture microlens arrays of close packing," *Applied Physics Letters*, vol. 97, p. 031109, July 2010.

[50] S. Kawata, H.-B. Sun, T. Tanaka, and K. Takada, "Finer features for functional microdevices," *Nature*, vol. 412, pp. 697–698, Aug. 2001.

[51] C. N. LaFratta, D. Lim, K. O'Malley, T. Baldacchini, and J. T. Fourkas, "Direct Laser Patterning of Conductive Wires on Three-Dimensional Polymeric Microstructures," *Chem. Mater.*, vol. 18, pp. 2038–2042, Apr. 2006.

[52] V. F. Paz, M. Emons, K. Obata, A. Ovsianikov, S. Peterhänsel, K. Frenner, C. Reinhardt, B. Chichkov, U. Morgner, and W. Osten, "Development of functional sub-100 nm structures with 3d two-photon polymerization technique and optical methods for characterization," *Journal of Laser Applications*, vol. 24, p. 042004, July 2012.

[53] A. R. Wu, T. L. A. Kawahara, N. A. Rapicavoli, J. v. Riggelen, E. H. Shroff, L. Xu, D. W. Felsher, H. Y. Chang, and S. R. Quake, "High throughput automated chromatin immunoprecipitation as a platform for drug screening and antibody validation," *Lab Chip*, vol. 12, pp. 2190–2198, May 2012.

[54] R. Marie, J. N. Pedersen, D. L. V. Bauer, K. H. Rasmussen, M. Yusuf, E. Volpi, H. Flyvbjerg, A. Kristensen, and K. U. Mir, "Integrated view of genome structure and sequence of a single DNA molecule in a nanofluidic device," *PNAS*, vol. 110, pp. 4893–4898, Mar. 2013.

[55] R. Guo, S. Xiao, X. Zhai, J. Li, A. Xia, and W. Huang, "Micro lens fabrication by means of femtosecond two photon photopolymerization," *Opt. Express*, vol. 14, pp. 810–816, Jan. 2006.

[56] S. Bichler, S. Feldbacher, R. Woods, V. Satzinger, V. Schmidt, G. Jakopic, G. Langer, and W. Kern, "Functional flexible organic–inorganic hybrid polymer for two photon patterning of optical waveguides," *Optical Materials*, vol. 34, pp. 772–780, Mar. 2012.

[57] R. Woods, S. Feldbacher, D. Zidar, G. Langer, V. Satzinger, G. Schmid, W. Leeb, and W. Kern, "Development and characterization of optoelectronic circuit boards produced by two-photon polymerization using a polysiloxane containing acrylate functional groups," *Appl. Opt.*, vol. 52, pp. 388–393, Jan. 2013.

[58] C. Reinhardt, S. Passinger, B. N. Chichkov, C. Marquart, I. P. Radko, and S. I. Bozhevolnyi, "Laser-fabricated dielectric optical components for surface plasmon polaritons," *Opt. Lett.*, vol. 31, pp. 1307–1309, May 2006.

[59] S. Klein, A. Barsella, H. Leblond, H. Bulou, A. Fort, C. Andraud, G. Lemercier, J. C. Mulatier, and K. Dorkenoo, "One-step waveguide and optical circuit writing in photopolymerizable materials processed by two-photon absorption," *Applied Physics Letters*, vol. 86, p. 211118, May 2005.

[60] M. Malinauskas, A. Žukauskas, V. Purlys, K. Belazaras, A. Momot, D. Paipulas, R. Gadonas, A. Piskarskas, H. Gilbergs, A. Gaidukevičiūtė, I. Sakellari, M. Farsari, and S. Juodkazis, "Femtosecond laser polymerization of hybrid/integrated micro-optical elements and their characterization," *J. Opt.*, vol. 12, p. 124010, Dec. 2010.

[61] Y. Huang, Y. Xu, and A. Yariv, "Fabrication of functional microstructured optical fibers through a selective-filling technique," *Applied Physics Letters*, vol. 85, pp. 5182–5184, Nov. 2004.

[62] M. Malinauskas, M. Farsari, A. Piskarskas, and S. Juodkazis, "Ultrafast laser nanostructuring of photopolymers: A decade of advances," *Physics Reports*, vol. 533, pp. 1–31, Dec. 2013.

[63] T. Sherwood, A. Young, J. Takayesu, A. K. Y. Jen, L. R. Dalton, and A. Chen, "Microring resonators on side-polished optical fiber," *IEEE Photonics Technology Letters*, vol. 17, pp. 2107–2109, Oct. 2005.

[64] L. Li, E. Gershgoren, G. Kumi, W.-Y. Chen, P.-T. Ho, W. N. Herman, and J. T. Fourkas, "High-Performance Microring Resonators Fabricated with Multiphoton Absorption Polymerization," *Advanced Materials*, vol. 20, no. 19, pp. 3668–3671, 2008.

[65] H.-B. Sun, S. Matsuo, and H. Misawa, "Three-dimensional photonic crystal structures achieved with two-photon-absorption photopolymerization of resin," *Applied Physics Letters*, vol. 74, pp. 786–788, Feb. 1999.

[66] M. Straub and M. Gu, "Near-infrared photonic crystals with higher-order bandgaps generated by two-photon photopolymerization," *Opt. Lett.*, vol. 27, pp. 1824–1826, Oct. 2002.

[67] M. Deubel, G. von Freymann, M. Wegener, S. Pereira, K. Busch, and C. M. Soukoulis, "Direct laser writing of three-dimensional photonic-crystal templates for telecommunications," *Nat Mater*, vol. 3, pp. 444–447, July 2004.

[68] N. Tétreault, G. von Freymann, M. Deubel, M. Hermatschweiler, F. Pérez-Willard, S. John, M. Wegener, and G. A. Ozin, "New Route to Three-Dimensional Photonic Bandgap Materials: Silicon Double Inversion of Polymer Templates," *Adv. Mater.*, vol. 18, pp. 457–460, Feb. 2006.

[69] K. K. Seet, V. Mizeikis, S. Matsuo, S. Juodkazis, and H. Misawa, "Three-Dimensional Spiral-Architecture Photonic Crystals Obtained By Direct Laser Writing," *Adv. Mater.*, vol. 17, pp. 541–545, Mar. 2005.

[70] J. Serbin, A. Ovsianikov, and B. Chichkov, "Fabrication of woodpile structures bytwo-photon polymerization and investigation of their optical properties," *Opt. Express*, vol. 12, pp. 5221–5228, Oct. 2004.

[71] K. Kaneko, H.-B. Sun, X.-M. Duan, and S. Kawata, "Submicron diamond-lattice photonic crystals produced by two-photon laser nanofabrication," *Appl. Phys. Lett.*, vol. 83, pp. 2091–2093, Sept. 2003.

[72] X.-Z. Dong, Q. Ya, X.-Z. Sheng, Z.-Y. Li, Z.-S. Zhao, and X.-M. Duan, "Photonic bandgap of gradient quasidiamond lattice photonic crystal," *Appl. Phys. Lett.*, vol. 92, p. 231103, June 2008.

[73] S. Maruo and T. Saeki, "Femtosecond laser direct writing of metallicmicrostructures by photoreduction of silvernitrate in a polymer matrix," *Opt. Express*, vol. 16, pp. 1174–1179, Jan. 2008.

[74] R. A. Farrer, C. N. LaFratta, L. Li, J. Praino, M. J. Naughton, B. E. A. Saleh, M. C. Teich, and J. T. Fourkas, "Selective Functionalization of 3-D Polymer Microstructures," *J. Am. Chem. Soc.*, vol. 128, pp. 1796–1797, Feb. 2006.

[75] J.-F. Xing, X.-Z. Dong, W.-Q. Chen, X.-M. Duan, N. Takeyasu, T. Tanaka, and S. Kawata, "Improving spatial resolution of two-photon microfabrication by using photoinitiator with high initiating efficiency," *Applied Physics Letters*, vol. 90, pp. 131106–131106–3, Mar. 2007.

[76] M. Campbell, D. N. Sharp, M. T. Harrison, R. G. Denning, and A. J. Turberfield, "Fabrication of photonic crystals for the visible spectrum by holographic lithography," *Nature*, vol. 404, pp. 53–56, Mar. 2000.

[77] S. W. Hell, "Improvement of lateral resolution in far-field fluorescence light microscopy by using two-photon excitation with offset beams," *Optics Communications*, vol. 106, pp. 19–24, Mar. 1994.

[78] S. W. Hell, "Far-Field Optical Nanoscopy," *Science*, vol. 316, pp. 1153–1158, May 2007.

[79] T. A. Klar, S. Jakobs, M. Dyba, A. Egner, and S. W. Hell, "Fluorescence microscopy with diffraction resolution barrier broken by stimulated emission," *PNAS*, vol. 97, pp. 8206–8210, July 2000.

[80] Y. Cao, Z. Gan, B. Jia, R. A. Evans, and M. Gu, "High-photosensitive resin for super-resolution direct-laser-writing based on photoinhibited polymerization," *Opt. Express*, vol. 19, pp. 19486–19494, Sept. 2011.

[81] J. Fischer, G. von Freymann, and M. Wegener, "The Materials Challenge in Diffraction-Unlimited Direct-Laser-Writing Optical Lithography," *Adv. Mater.*, vol. 22, pp. 3578–3582, Aug. 2010.

[82] J. Fischer and M. Wegener, "Three-dimensional direct laser writing inspired by stimulated-emission-depletion microscopy [Invited]," *Opt. Mater. Express*, vol. 1, pp. 614–624, Aug. 2011.

[83] M. P. Stocker, L. Li, R. R. Gattass, and J. T. Fourkas, "Multiphoton photoresists giving nanoscale resolution that is inversely dependent on exposure time," *Nat Chem*, vol. 3, pp. 223–227, Mar. 2011.

[84] R. A. Farrer, F. L. Butterfield, V. W. Chen, and J. T. Fourkas, "Highly Efficient Multiphoton-Absorption-Induced Luminescence from Gold Nanoparticles," *Nano Lett.*, vol. 5, pp. 1139–1142, June 2005.

[85] "Radial Polarization."

[86] K. J. Schafer, J. M. Hales, M. Balu, K. D. Belfield, E. W. Van Stryland, and D. J. Hagan, "Two-photon absorption cross-sections of common photoinitiators," *Journal of Photochemistry and Photobiology A: Chemistry*, vol. 162, pp. 497–502, Mar. 2004.

[87] L. W. Tutt and T. F. Boggess, "A review of optical limiting mechanisms and devices using organics, fullerenes, semiconductors and other materials," *Progress in Quantum Electronics*, vol. 17, no. 4, pp. 299–338, 1993.

[88] B. A. Reinhardt, L. L. Brott, S. J. Clarson, A. G. Dillard, J. C. Bhatt, R. Kannan, L. Yuan, G. S. He, and P. N. Prasad, "Highly Active Two-Photon Dyes: Design, Synthesis, and Characterization toward Application," *Chem. Mater.*, vol. 10, pp. 1863–1874, July 1998.

[89] G. S. He, L. Yuan, N. Cheng, J. D. Bhawalkar, P. N. Prasad, L. L. Brott, S. J. Clarson, and B. A. Reinhardt, "Nonlinear optical properties of a new chromophore," *J. Opt. Soc. Am. B, JOSAB*, vol. 14, pp. 1079–1087, May 1997.

[90] M. Sheik-bahae, A. A. Said, and E. W. V. Stryland, "High-sensitivity, single-beam n_2 measurements," *Opt. Lett., OL*, vol. 14, pp. 955–957, Sept. 1989.

[91] M. Sheik-Bahae, A. A. Said, T. H. Wei, D. J. Hagan, and E. W. V. Stryland, "Sensitive measurement of optical nonlinearities using a single beam," *IEEE Journal of Quantum Electronics*, vol. 26, pp. 760–769, Apr. 1990.

[92] M. G. Kuzyk, 1958, C. W. Dirk, and 1954, *Characterization techniques and tabulations for organic nonlinear optical materials*. Marcel Dekker, 1998.

[93] B. R. Cho, K. H. Son, S. H. Lee, Y.-S. Song, Y.-K. Lee, S.-J. Jeon, J. H. Choi, H. Lee, and M. Cho, "Two Photon Absorption Properties of 1,3,5-Tricyano-2,4,6-tris(styryl)benzene Derivatives," *J. Am. Chem. Soc.*, vol. 123, pp. 10039–10045, Oct. 2001.

[94] M. A. Albota, C. Xu, and W. W. Webb, "Two-photon fluorescence excitation cross sections of biomolecular probes from 690 to 960 nm," *Appl. Opt., AO*, vol. 37, pp. 7352–7356, Nov. 1998.

[95] C. Xu and W. W. Webb, "Measurement of two-photon excitation cross sections of molecular fluorophores with data from 690 to 1050 nm," *J. Opt. Soc. Am. B, JOSAB*, vol. 13, pp. 481–491, Mar. 1996.

[96] L. Singer, Z. Baram, A. Ron, and S. Kimel, "The two-photon phosphorescence excitation spectrum of triphenylene," *Chemical Physics Letters*, vol. 47, pp. 372–376, Apr. 1977.

[97] P. Esherick, P. Zinsli, and M. A. El-Sayed, "The low energy two-photon spectrum of pyrazine using the phosphorescence photoexcitation method," *Chemical Physics*, vol. 10, pp. 415–432, Sept. 1975.

[98] D. S. Kliger, "Thermal lensing: a new spectroscopic tool," *Acc. Chem. Res.*, vol. 13, pp. 129–134, May 1980.

[99] H. L. Fang, T. L. Gustafson, and R. L. Swofford, "Two-photon absorption photothermal spectroscopy using a synchronously pumped picosecond dye laser. Thermal lensing spectra of naphthalene and diphenylbutadiene," *The Journal of Chemical Physics*, vol. 78, pp. 1663–1669, Feb. 1983.

[100] C. V. Bindhu, S. S. Harilal, V. P. N. Nampoori, and C. P. G. Vallabhan, "Investigation of nonlinear absorption and aggregation in aqueous solutions of rhodamine B using thermal lens technique," *Pramana - J Phys*, vol. 52, pp. 435–442, Apr. 1999.

[101] J. Fischer, J. B. Mueller, A. S. Quick, J. Kaschke, C. Barner-Kowollik, and M. Wegener, "Exploring the Mechanisms in STED-Enhanced Direct Laser Writing," *Advanced Optical Materials*, vol. 3, pp. 221–232, Feb. 2015.

[102] C. B. d. Araújo, A. S. L. Gomes, and G. Boudebs, "Techniques for nonlinear optical characterization of materials: a review," *Rep. Prog. Phys.*, vol. 79, no. 3, p. 036401, 2016.

[103] J. B. Mueller, J. Fischer, F. Mayer, M. Kadic, and M. Wegener, "Polymerization Kinetics in Three-Dimensional Direct Laser Writing," *Adv. Mater.*, vol. 26, pp. 6566–6571, Oct. 2014.

[104] C. S. Colley, D. C. Grills, N. A. Besley, S. Jockusch, P. Matousek, A. W. Parker, M. Towrie, N. J. Turro, P. M. W. Gill, and M. W. George, "Probing the Reactivity of Photoinitiators for Free Radical Polymerization: Time-Resolved Infrared Spectroscopic Study of Benzoyl Radicals," *J. Am. Chem. Soc.*, vol. 124, pp. 14952–14958, Dec. 2002.

[105] S. Wu, M. Straub, and M. Gu, "Single-monomer acrylate-based resin for three-dimensional photonic crystal fabrication," *Polymer*, vol. 46, pp. 10246–10255, Nov. 2005.

[106] C. R. Mendonca, D. S. Correa, T. Baldacchini, P. Tayalia, and E. Mazur, "Two-photon absorption spectrum of the photoinitiator Lucirin TPO-L," *Appl. Phys. A*, vol. 90, pp. 633–636, Mar. 2008.

[107] J. Serbin, A. Egbert, A. Ostendorf, B. N. Chichkov, R. Houbertz, G. Domann, J. Schulz, C. Cronauer, L. Fröhlich, and M. Popall, "Femtosecond laser-induced two-photon polymerization of inorganic–organic hybrid materials for applications in photonics," *Opt. Lett., OL*, vol. 28, pp. 301–303, Mar. 2003.

[108] S. J. Jhaveri, J. D. McMullen, R. Sijbesma, L.-S. Tan, W. Zipfel, and C. K. Ober, "Direct Three-Dimensional Microfabrication of Hydrogels via Two-Photon Lithography in Aqueous Solution," *Chem. Mater.*, vol. 21, pp. 2003–2006, May 2009.

[109] R. J. DeVoe, T.-C. Lee, and B. J. Gates, "Negative Contrast Curves for Two-photon Free Radical Polymerization Systems and Their Potential Applications in Sub-diffraction Limited Two-photon Photolithography," vol. 1499, Cambridge University Press, 2013.

[110] F. D. Lewis and R. J. DeVoe, "Exciplex and radical ion intermediates in the photochemical reaction of 9-cyanophenanthrene with 2,3-dimethyl-2-butene," *Tetrahedron*, vol. 38, no. 8, pp. 1069–1077, 1982.

[111] J. T. Fourkas and J. S. Petersen, "2-Colour photolithography," *Phys. Chem. Chem. Phys.*, vol. 16, pp. 8731–8750, Apr. 2014.

[112] H. Ishikawa and W. A. Noyes, "Photosensitization by Benzene Vapor: Biacetyl. The Triplet State of Benzene," *The Journal of Chemical Physics*, vol. 37, pp. 583–591, Aug. 1962.

[113] C. S. Parmenter and B. L. Ring, "Energy Transfer between Benzene and Biacetyl and the Lifetime of Triplet Benzene in the Gas Phase," *The Journal of Chemical Physics*, vol. 46, pp. 1998–1999, Mar. 1967.

[114] U. Brühlmann and J. R. Huber, "Self-quenching and electronic energy transfer of triplet molecules. The benzaldehyde-biacetyl system in the vapor phase," *Chemical Physics Letters*, vol. 66, pp. 353–357, Oct. 1979.

[115] M. Schuh, "Orientation and distance requirements for energy transfer between triplet alkylbenzenes and biacetyl and cis-piperylene vapors," *Journal of Photochemistry*, vol. 9, pp. 243–245, Jan. 1978.

[116] K. Aizawa, H. Igarashi, and K. Kaya, "Radiationless transitions of pyridine, pyrazine and pyrimidine studied by intermolecular energy transfer to biacetyl," *Chemical Physics*, vol. 23, pp. 273–280, July 1977.

[117] G. M. Almy, H. Q. Fuller, and G. D. Kinzer, "The Fluorescence of Diacetyl," *The Journal of Chemical Physics*, vol. 8, pp. 37–45, Jan. 1940.

[118] E. Drent, R. P. van der Werf, and J. Kommandeur, "Small molecule behavior and the 3bg state of biacetyl," *The Journal of Chemical Physics*, vol. 59, pp. 2061–2067, Aug. 1973.

[119] L. G. Anderson and C. S. Parmenter, "Effect of Phase on the Fluorescence Lifetime and on the Intersystem Crossing Rate in Biacetyl," *The Journal of Chemical Physics*, vol. 52, pp. 466–468, Jan. 1970.

[120] H. W. Sidebottom, C. C. Badcock, J. G. Calvert, B. R. Rabe, and E. K. Damon, "Lifetime studies of the biacetyl excited singlet and triplet states in the gas phase at 25.deg.," *J. Am. Chem. Soc.*, vol. 94, pp. 13–19, Jan. 1972.

[121] G. M. McClelland and J. T. Yardley, "Electronic and vibrational relaxation in biacetyl vapor," *The Journal of Chemical Physics*, vol. 58, pp. 4368–4373, May 1973.

[122] N. J. Turro and R. Engel, "Molecular photochemistry. VII. Enhancement of biacetyl luminescence by deuteration," *J. Am. Chem. Soc.*, vol. 90, pp. 2989–2990, May 1968.

[123] A. Z. Moss and J. T. Yardley, "Radiationless decay from triplet state biacetyl molecules with selected vibrational energies," *The Journal of Chemical Physics*, vol. 61, pp. 2883–2889, Oct. 1974.

[124] G. M. Almy and S. Anderson, "Lifetime of Fluorescence in Diacetyl and Acetone," *The Journal of Chemical Physics*, vol. 8, pp. 805–814, Oct. 1940.

[125] "Handbook of Photochemistry, Second Edition," Aug. 1993.

[126] G. N. Lewis and M. Kasha, "Phosphorescence and the Triplet State," *J. Am. Chem. Soc.*, vol. 66, pp. 2100–2116, Dec. 1944.

[127] K. Kaya, W. R. Harshbarger, and M. B. Robin, "Triplet states of biacetyl and energy transfer as revealed by opto-acoustic spectroscopy," *The Journal of Chemical Physics*, vol. 60, pp. 4231–4236, June 1974.

[128] A. Singh, A. R. Scott, and F. Sopchyshyn, "Flash photolysis of camphorquinone and biacetyl," *J. Phys. Chem.*, vol. 73, pp. 2633–2643, Aug. 1969.

[129] B. Harke, P. Bianchini, F. Brandi, and A. Diaspro, "Photopolymerization Inhibition Dynamics for Sub-Diffraction Direct Laser Writing Lithography," *ChemPhysChem*, vol. 13, pp. 1429–1434, Apr. 2012.

[130] H. Simbürger, W. Kern, K. Hummel, and C. Hagg, "Photoreactions in polymers containing benzil units: a comparative study under excimer laser and Hg-lamp irradiation," *Polymer*, vol. 41, pp. 7883–7897, Oct. 2000.

[131] B. R. Chinmayanandam and H. W. Melville, "Photosensitization of polymerization reactions," *Trans. Faraday Soc.*, vol. 50, pp. 73–82, Jan. 1954.

[132] J. Hutchison and A. Ledwith, "Mechanisms and relative efficiencies in radical polymerization photoinitiated by benzoin, benzoin methyl ether and benzil," *Polymer*, vol. 14, pp. 405–408, Sept. 1973.

[133] I. Lukáč and C. Kósa, "The formation of dibenzoyl peroxide by photooxidation of benzil in a polymer film," *Macromol. Rapid Commun.*, vol. 15, pp. 929–934, Dec. 1994.

[134] B. Husár and I. Lukáč, "Synthesis, photoperoxidation and crosslinking of styrene copolymer with pendant benzil moieties," *Journal of Photochemistry and Photobiology A: Chemistry*, vol. 195, pp. 191–197, Apr. 2008.

[135] W. G. McGimpsey and J. C. Scaiano, "A two-photon study of the "reluctant" Norrish type I reaction of benzil," *J. Am. Chem. Soc.*, vol. 109, pp. 2179–2181, Apr. 1987.

[136] M. Mizuno, K. Iwata, and H. Takahashi, "Time-resolved infrared and resonance Raman studies of benzil. Vibrational analysis and structures of the excited states," *Journal of Molecular Structure*, vol. 661, pp. 3–10, Dec. 2003.

[137] N. Ikeda, M. Koshioka, H. Masuhara, and K. Yoshihara, "Picosecond dynamics of excited singlet states in organic microcrystals: Diffuse reflectance laser photolysis study," *Chemical Physics Letters*, vol. 150, pp. 452–456, Sept. 1988.

[138] J.-P. Malval, C. Dietlin, X. Allonas, and J.-P. Fouassier, "Sterically tuned photoreactivity of an aromatic α-diketone family," *Journal of Photochemistry and Photobiology A: Chemistry*, vol. 192, pp. 66–73, Nov. 2007.

[139] G. Porter and M. W. Windsor, "The Triplet State in Fluid Media," *Proceedings of the Royal Society of London A: Mathematical, Physical and Engineering Sciences*, vol. 245, pp. 238–258, June 1958.

[140] T. R. Evans and P. A. Leermakers, "Emission spectra and excited-state geometry of .alpha.-diketones," *J. Am. Chem. Soc.*, vol. 89, pp. 4380–4382, Aug. 1967.

[141] J. M. Morris and K. Yoshihara, "Interband transitions in molecular crystals," *Molecular Physics*, vol. 36, pp. 993–1003, Oct. 1978.

[142] L. Flamigni, F. Barigelletti, S. Dellonte, and G. Orlandi, "Photophysical properties of benzil in solution: triplet state deactivation pathways," *Journal of Photochemistry*, vol. 21, pp. 237–244, Jan. 1983.

[143] B. Bhattacharya, B. Jana, D. Bose, and N. Chattopadhyay, "Multiple emissions of benzil at room temperature and 77 K and their assignments from ab initio quantum chemical calculations," *J Chem Phys*, vol. 134, p. 044535, Jan. 2011.

[144] M. Mukai, S. Yamauchi, and N. Hirota, "A time-resolved EPR study of one- and two-photon processes in the photochemical reactions of benzil," *J. Phys. Chem.*, vol. 93, pp. 4411–4413, June 1989.

[145] M. Mukai, S. Yamauchi, and N. Hirota, "Time-resolved EPR study on the photochemical reactions of benzil," *J. Phys. Chem.*, vol. 96, pp. 3305–3311, Apr. 1992.

[146] D. S. Roy, K. Bhattacharyya, S. C. Bera, and M. Chowdhury, "Conformational relaxation in the excited electronic states of benzil and naphthyl," *Chemical Physics Letters*, vol. 69, pp. 134–140, Jan. 1980.

[147] K. K. Das and D. Majumdar, "Ground and excited states of benzil: A theoretical study," *Journal of Molecular Structure: THEOCHEM*, vol. 288, pp. 55–61, Nov. 1993.

[148] Z. Pawelka, A. Koll, and T. Zeegers-Huyskens, "Solvent effect on the conformation of Benzil," *Journal of Molecular Structure*, vol. 597, pp. 57–66, Oct. 2001.

[149] M. Gomberg and F. J. V. Natta, "REDUCTION OF AROMATIC 1,2-DIKETONES BY THE BINARY SYSTEM MAGNESIUM IODIDE (OR BROMIDE) + MAGNESIUM," *J. Am. Chem. Soc.*, vol. 51, pp. 2238–2245, July 1929.

[150] Q. Miao, J. Gao, Z. Wang, H. Yu, Y. Luo, and T. Ma, "Syntheses and characterization of several nickel bis(dithiolene) complexes with strong and broad Near-IR absorption," *Inorganica Chimica Acta*, vol. 376, pp. 619–627, Oct. 2011.

[151] S. C. Bera, R. K. Mukherjee, D. Mukherjee, and M. Chowdhury, "n→π Transition of 2, 2'-Pyridil," *The Journal of Chemical Physics*, vol. 55, pp. 5826–5828, Dec. 1971.

[152] H. Inoue and K. Nagaya, "Hydrogen bonding and conformational change of 2,2'-pyridil in polyhydric solvents," *Journal of the Chemical Society, Perkin Transactions 2*, vol. 0, no. 9, pp. 1581–1583, 1983.

[153] A. Sarkar and S. Chakravorti, "Photo-rotamerism of 2,2'-pyridil in different environments: A quest for geometry in excited states," *Journal of Luminescence*, vol. 69, pp. 161–168, Nov. 1996.

[154] N. Yamada, M. Hasegawa, K.-i. Kumagai, S. Enomoto, H. Horiuchi, T. Yoshinaga, H. Hiratsuka, M. Kobayashi, and T. Hoshi, "Photochemical Reaction Mechanism of 2,2'-Pyridil in Alcoholic Media," *BCSJ*, vol. 78, pp. 1018–1025, June 2005.